

**EVALUATION AND CRITICALITY ASSESSMENT OF RADIOLOGICAL SOURCE
TERMS TO BE USED FOR FIRE RISK STUDIES AT ACCELERATOR FACILITIES.**

Thesis by
Francisco Ogallar Ruiz

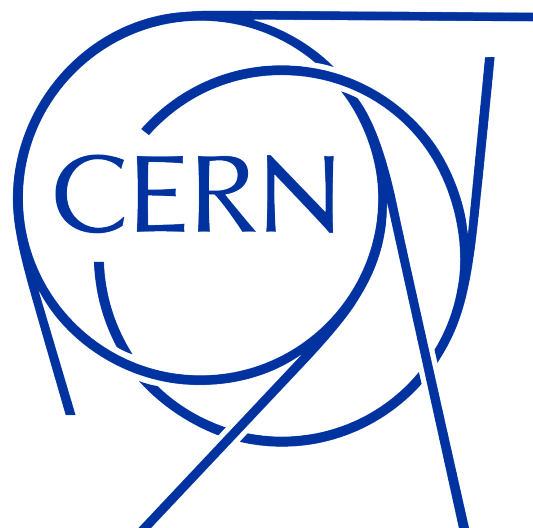
In partial fulfillment of the requirements for the degree of
Doctor of Philosophy



Ph.D. Programme in Physics and Space Sciences
UNIVERSIDAD DE GRANADA
Granada, Spain

Submitted in November of 2021
To be defended in January of 2022

Editor: Universidad de Granada. Tesis Doctorales
Autor: Francisco Ogállar Ruiz
ISBN: 978-84-1117-231-8
URI: <http://hdl.handle.net/10481/72879>



Occupational Health & Safety and Environmental Protection Unit
EUROPEAN ORGANIZATION FOR NUCLEAR RESEARCH
Geneva, Switzerland

Doctoral Student Programme

Acknowledgements

ALTHOUGH these are the first pages of the manuscript, I write them to conclude it and embrace the opportunity to acknowledge the numerous and crucial contributions that shape this thesis and my personal background. I take the liberty of switching between English and Spanish depending on the interlocutor I am addressing.

I would like to start by thanking CERN as a whole and the Radiation Protection group and the FIRIA project in particular for providing the opportunity and means to carry out this thesis in such an interesting topic. I would also like to thank the University of Granada, its International Postgraduate School and the PhD Programme in Physics and Space Sciences for accepting my application to perform my doctoral studies under their academic supervision.

Me gustaría dar las gracias a Ignacio Porras, director de esta tesis y mi mentor desde que Francisco Gálvez me acompañó hasta su despacho un día a principios de 2015. Gracias por tu cercanía, tu confianza, tu buena voluntad y, sobre todo, tu pasión. De cada visita a tu despacho salí siempre con más ganas de trabajar que con las que entré, consecuencia de tu talento natural para contagiar las ganas de hacer ciencia. Esta es probablemente una de las mayores virtudes a las que un profesor puede aspirar y en gran medida responsable de que yo esté hoy depositando esta tesis doctoral. Muchas gracias por aquella primera oportunidad, así como por todas las que han venido después.

Thanks to Helmut Vincke, co-director of the present thesis and my supervisor at CERN, for giving me the opportunity to start it in the very first place. Thank you for your very valuable supervision and contributions along the way, as well as for your willingness to help. Thank you for your trusting and friendly demeanor, which made everything easier to handle. Thanks to Chris Theis, also co-director of this thesis. Thank you for all your efforts during the past years, for the invariably enriching discussions and for being able to find the time even in the busiest moments. Thank you for your always astonishing effectiveness and for everything you have taught me. Thank you also for acknowledging whatever you believe to be a good piece of work. It is a seemingly simple quality, but rare and very often underrated. Dankeschön!

Thanks also to Heinz Vincke, section leader of the Accelerators and Sites section of the Radiation Protection group, for suffering my technical notes stoically.

A large number of CERN colleagues has contributed directly or indirectly to the completion of this thesis. In particular I would like to thank Saverio La Mendola, Stefan Roesler, Guilherme Correia,

Sebastian Rothe, Jochen Ballof, Alexandre Dorsival, Nabil Mena, Oriol Rios, Giordana Gai, Berta Rubio Pascual, Juliana Schell, Karl Jhonston, Thierry Stora, Joachim Vollaire, Reiner Geyer, Yann Pira, Lucie Vitkova, Aurore Boscher, Giuseppe Prete, Renaud Charousset, Miranda Van Stenis, Julia Trummer, Dejan Pramberger, Elzbieta Nowak and Alessio Mereghetti. Merci! Dankeschön! Grazie! Thank you! ¡Gracias! Obrigado! Dziękuję! Děkuji!

Por supuesto, quiero dar las gracias a cada uno de los miembros de mi familia, por estar siempre ahí independientemente de todo lo demás. Esta tesis les pertenece a ellos. La familia no se elige, pero yo elegiría la que me ha tocado una y mil veces. Gracias a mi padre por ser día tras día un ejemplo de superación, de serenidad, de entereza y de trabajo. Eres una fuerza de la naturaleza. Cada vez que huelo tomillo, su olor me transporta al campo en una mañana fresca y soleada, con los perros pasando a mi lado y contigo unos pasos por delante de mí. Automáticamente se dibuja en mi cara una sonrisa, gracias también por eso. Infinitas gracias a mi queridísima madre, que ha visto parte de lo bueno y sufrido todo lo malo. Gracias porque eres la sal de la Tierra. Gracias por apoyarme siempre, por tu voluntad, pasión, esfuerzo y sacrificio. Pero sobre todo, gracias por no rendirte nunca ante nada ni ante nadie. Gracias a mi hermana Encarni. Gracias por tu ayuda incondicional. Gracias por estar ahí cuando pintaban bastos, por tu atención y por tu enorme generosidad. Gracias porque siempre te he sentido y te siento cerca, al alcance de la mano, a pesar de la distancia. Gracias a mi hermano y amigo Pedro. He crecido mirándote y soy como soy en gran medida por tí. Gracias por todo lo que me has enseñado, intencionadamente o no, que es mucho más de lo que imaginas. Gracias por ese "si quieres quemarlo llámame a mí", que nunca olvidaré y que te resume magistralmente. Gracias porque, aunque hay pocas certezas en la vida, saber que tú estarás ahí es una de ellas. Gracias a mi tercer hermano, Adrián, que lleva en mi vida desde que el que escribe pensaba que Cartagena era parte del antiguo Estado de Cartago. Gracias por haberme tratado siempre tan bien. Gracias a mis sobrinas Julia y Nora, porque son extraordinarias y contagian alegría. Gracias también a mis abuelos, que siempre me hicieron sentir querido y a quienes recuerdo con inmenso cariño.

Gracias a mis amigos Seba y Fran, que me acompañan desde mucho antes de que esto comenzara. Gracias por la inmutabilidad de nuestra amistad y por vuestro a menudo insultante cariño. Gracias a Pepe, Nandy, Pedro, Javi, David, Martin, Apaco, Ramón, Andrea, Juanpe, Nuria, María Salud, Alex, Nico, Trini y tantos otros. Gracias a mis amigos y compañeros de carrera, que hicieron ameno lo que no lo era y con quienes me reí hasta no poder más, en especial a Jalito, Aurelio, Ibáñez, Víctor, Guillermo y Nahual.

Thanks to all the new friends that my stay at CERN has brought me. Thanks in particular to José, João, Riccardo, Marta, Berto, Cristina, Charlotte, Carlos, Mercedes, Alessia, Andreas, Matthias, Francesca, Matteo, Nouridine and Stathis.

Reservo mis últimas líneas para Lucía, la guinda del pastel. Gracias por ser la mejor compañera de vida. Gracias por tu cariño, tu sinceridad, tu ímpetu, tu complicidad y nuestras tonterías. Gracias por tu apoyo y sobre todo, gracias por tu amor.

Dicen que hay gente con suerte, y es verdad. Yo soy uno de ellos.

Abstract

THE EUROPEAN Organisation for Nuclear Research (CERN) is one of the largest scientific laboratories worldwide. Nowadays, mainly focused on high energy particle physics, it provides the scientific community with a unique range of particle accelerator facilities that are used by over 600 institutes and universities around the world. In such particle accelerator facilities, high energy particles end up almost inevitably impinging onto the surrounding material, inducing nuclear reactions. This often results in activation, which is the artificial induction of radioactivity in otherwise non-radioactive materials. Particles ejected in radioactive decays are part of the so-called ionising radiation, and their interaction with living biological tissue can have harmful and eventually lethal results. The CERN Radiation Protection group ensures that the personnel of the laboratory, the public and the environment are protected from potentially harmful effects of ionizing radiation linked to the organization's activities. CERN is also a unique laboratory with respect to challenges related to fire protection. The complexity of the facilities and their radiological hazards often require dedicated studies to successfully prevent, mitigate and face potential accidental fires. To carry out these studies, the Occupational Health & Safety and Environmental Protection Unit of CERN launched the FIRIA project. Its aim is to develop an integrated approach to quantitatively assess potential discharges of radioactive substances induced by a fire accident. The accurate determination of the inventory of radionuclides released from activated materials as a consequence of fire is of the utmost importance in order to estimate the potential radiological consequences derived from such an event. This has revealed the need to evaluate the contribution of the thermally promoted *out-diffusion* of radionuclides. We refer as out-diffused to those radionuclides initially placed in the matrix of a solid, which due to thermally promoted diffusion reach the surface of the object that contains them and manage to escape from it, subsequently being released to the environment. The work presented here aims to meet the need for an accurate assessment of this phenomenon by designing, implementing and benchmarking a simulation software to realistically estimate the contribution of radioisotope out-diffusion for a wide range of possible fire scenarios.

In general, atomic migration in solids is the result of successive jumps of fixed lengths, and the success rate of the jumps follows an exponential dependence of the medium's temperature. From a phenomenological perspective, the equations governing diffusion are known as Fick's laws. The evolution of our radionuclide inventory in case of fire is described by Fick's second law, also called the diffusion equation: $\partial C(\vec{r}, t) / \partial t = D \nabla^2 C(\vec{r}, t)$. This is a linear second-order partial differential equation relating the time evolution of the particle concentration $C(\vec{r}, t)$ with its gradient divergence. The diffusion coefficient D is the proportionality constant in the diffusion

equation and it tells us how fast a given species can diffuse within a host material at a certain temperature.

It can be shown that, under certain assumptions, random walks emulate the diffusion process. This is important because it suggests that we can simulate diffusion processes using stochastic methods, avoiding the need for deterministic solutions of the diffusion equation, which for us would pose a number of difficulties. Based on this, we deem the development of a Monte Carlo based diffusion model internally linked to the general purpose Monte Carlo code FLUKA as the best strategy to tackle our problem. It can be proven that the probability of finding an atom in a given position after numerous atomic jumps converges towards the result obtained from a normal distribution centered on the atom's initial position, whose variance is proportional to the diffusion coefficient and the diffusion time. This result is not surprising, since the aforementioned distribution is a fundamental solution of the diffusion equation. In the light of that, we make use of a standard *Wiener process* to simulate diffusion employing a mathematically well-defined tool. It is a real valued continuous-time stochastic process with normally distributed and independent increments. In practice, this means that one can sample the position of a radionuclide after a given diffusion time using a multivariate normal distribution. This would overlook the presence of boundaries, but we can solve this problem by splitting the total diffusion time into a suitable number of sub-steps to be sampled in sequence. The position of the radionuclide is therefore checked after each sub-step, detecting if it has reached a surface during its trajectory through the host material. Following this strategy, we created a simple and reliable software named SOLIDUSS, mainly written in C++. The code takes advantage of the FLUKA geometry kernel to perform out-diffusion calculations for arbitrarily complex geometries. It allows for the determination of the amount of radionuclides out-diffused from a given source material into an arbitrary number of target materials in any area of interest of our geometry. This is done for a set of diffusion periods as defined by the user and, in addition, the software provides a 3-D map of the radionuclide concentration for each of them. It offers the possibility of performing multiple diffusion calculations while running a single FLUKA simulation, and can simulate the diffusion of radionuclides according to a user-defined 3-D map of temperatures. The initial position of the radionuclides created as a result of the radiation-matter interaction simulation performed by FLUKA is internally passed to SOLIDUSS. In order to perform a simulation, the user needs to provide a so-called diffusion input file, which will include all the information needed to simulate diffusion according to the user preferences (radionuclide of interest, host-material, activation parameters, diffusion times, temperature maps, concentration mesh boundaries, *etc.*). If requested by the user, online optimization operations aimed at cutting down the computational time spent in the radioisotope tracking are executed by SOLIDUSS without undermining the correctness of its results.

The fraction of radionuclides out-diffused from a given object, what we call the out-diffusion fraction (ODF), will always be underestimated when calculated using simulated step lengths greater than the real atomic jump lengths of the atoms in the solid lattice. Note that if a radionuclide reached the surface of an object N_R times during its real path inside of it, its simulation using normal distributions to aggregate a number of atomic jumps in a single simulation step would be able to identify only $N_S < N_R$. In the limit of simulated steps of the size of real atomic jumps, we say that the simulation is performed with a *perfect path resolution*. However, this type of

simulation is unpractical or even impossible for bulky objects, due to its high consumption of CPU resources. The discrepancy between the estimator N_S and the accurate result N_R is therefore influenced by the chosen size of the step lengths, which directly influences the reliability of the final result. A dedicated study showed that the ODF follows a well-defined function of the time step Δt used to sample the radioisotopes paths: $\text{ODF}(\Delta t) = a \cdot \text{erfc}(b \cdot \sqrt{\Delta t}) + c$, where a , b and c are fit parameters and erfc is the complementary error function. The extrapolation of this function for $\Delta t \rightarrow 0$ could be used to obtain a more accurate estimation of the ODF. Tests involving different combinations of radionuclide - host material, geometries, temperature gradients and non-uniform initial distributions were performed to verify the generality of this behaviour, which proved to remain unaltered in all of them. This allows us to estimate the ODF whenever we have several calculated values for different time steps, even if these values are far from the real out-diffusion fraction. As a consequence, the CPU time needed to estimate an ODF is largely reduced, and we obtain a much better approximation of the real fraction. The post-processing of SOLIDUSS results and the calculations and fits outlined here have been automatized by means of C++ and Python scripts in order to perform accurate estimations of the ODF in an efficient way.

If we ignore chemical reactions with surrounding substances, a radionuclide reaching an object's surface can either diffuse back into the object's bulk matrix or desorb (*i.e.* escape) from it. Let us imagine a surface with a given number of adsorbed atoms, θ_0 . If we assume that the only process these atoms can undergo is first-order *desorption*, the number of atoms on the surface will vary with time t as follows: $d\theta/dt = -\theta\nu_0 \exp[-E_{des}/(k_B T)]$, where E_{des} is the activation energy of desorption, ν_0 the vibration frequency of the atom, T is the absolute temperature and k_B the Boltzmann's constant. The activation energy of desorption can be interpreted as the energy needed to completely break the bounds of an atom on an object's surface with those surrounding it. Using the previous equation, the desorption rate can be calculated and compared with the diffusion rate whenever there is a competition between both processes, whose outcome can be determined by sampling a random number ξ from a uniform distribution. SOLIDUSS simulates the radionuclides' paths through solids at a given scale above the atomic level. It uses adaptive time steps, which condense multiple microscopic steps into a single one. Therefore, the comparison between diffusion and desorption rates explained above is not directly applicable. Nonetheless, it can be adapted to be implemented on top of SOLIDUSS diffusion treatment. The key would be to find out the number of times that a given radionuclide would reach an object's surface during one simulation time step, provided that it does not desorb in any of them. With this data, we can obtain the probability for a radionuclide to desorb in one simulation step. In order to do this, once we know that the atom would cross a boundary in the current step, we estimate the distance to the boundary. It is later used to sample the time at which the first hit to the surface takes place, which follows a Lévy Distribution. Once the atom reaches a boundary for the first time, the average number of times that it will encounter the boundary again N_{enc} is a function of the number of jumps N it performs: $\langle N_{enc} \rangle = a \cdot N^b$, where a and b are parameters that depend on the lattice structure and its orientation with respect to the boundary. The actual number of encounters follows a half-normal distribution characterized by the average $\langle N_{enc} \rangle$. After sampling such a quantity when a radionuclide is found to reach a surface, we can obtain the desorption probability and sample if the radionuclide would desorb or not during the time step under consideration. If the outcome of the sampling determines that the radionuclide did not desorb, we continue tracking its diffusion in the solid.

An *experimental campaign* was carried out aiming to provide data on the out-diffusion of radionuclides from activated materials when exposed to high temperatures. The central element of the performed experiments is the heating up of radioactive samples, which are carried out in a controlled oxygen-free atmosphere in order to avoid combustion. Further tests in an air atmosphere using non radioactive samples were also performed, to simulate conditions more similar to those of a real fire. To guarantee a smooth execution of the experiments involving radioactive isotopes, few tests using non radioactive samples were performed ahead. After the selection of suitable radioactive samples, the procedure followed for each experiment consisted of performing a gamma-ray spectrometry measurement to accurately determine the radionuclides present in the sample and their activities, followed by heating the sample up to very high temperatures during a certain period of time. This has been done using a furnace able to reach temperatures well beyond 1000 °C. The temperature was set to maximize the ODF while keeping it sufficiently low to avoid melting. Finally, a second gamma-ray spectrometry of the samples is performed under the same experimental conditions as the first one. Subtraction of both results allows to estimate the ODF. We used two 11.0 cm × 4.8 cm metallic activated foils in the experiments. The first one was made out of Cu, 49 μm thick, and with 0.6 Bq of ⁶⁰Co. The second one was made out of Al, 94 μm thick, and with 17.8 Bq of ²²Na. The furnace temperature profile was characterised, and the samples placed in its most uniform region. We obtained an ODF for ⁶⁰Co from Cu of 1.6 ± 11.0 % after 5 h of heating at approximately 1000 °C. As a consequence, we cannot assume that any ⁶⁰Co isotopes escaped from the sample; but we can say that the amount that escaped was less than 12.6 % with 1σ certainty. For ²²Na from Al, the ODF obtained was 14.6 ± 7.3 % after 2 h and up to 40.4 ± 7.0 % after approximately 6 h at 600 °C. We carried out two different tests in order to assess what would happen to a Cu piece in the event of a fire. We are particularly interested in understanding whether a part of it and its potential radioactive content could be released to the environment or not. In the first one we used a 35 μm thick Cu foil, and in the second one 150 μm diameter Cu filaments from a standard power cable. The Cu foil, which was very thin, is representative of the typical Cu foils used as cable shielding. After 20 minutes at 800 °C, it was completely oxidized and breaking apart when manipulated. Even for thicker objects, we expect a very similar oxidation effect (at least) on their surfaces, which could easily result in the release of material flakes to the environment. After the exposure of the filaments to similar conditions, a significant amount of powder came off as a consequence of a brief manipulation bending them. The conclusion of this test support that of the previous one: in the event of a fire, the outermost part of Cu objects (and probably other metals) would burn and may be partially released to the environment in the form of powder or flakes due to fire turbulence.

As part of SOLIDUSS' *benchmarking*, we carried out a number of calculations to check the implementation of its numerical treatment of diffusion. When simulating the diffusion of radionuclides, one of the most important inputs that needs to be provided to the code is the diffusion coefficient. A typical procedure to experimentally obtain this quantity is the so-called tracer diffusion experiments. We can emulate this procedure by replacing the diffusion experiment with a diffusion simulation. Using SOLIDUSS' results for problems whose boundary conditions allow for the analytical solution of the diffusion equation, we could determine the diffusion coefficient for different species and temperatures. If the resulting values are compatible with the diffusion coefficients provided to the software in the first place, we can be fairly confident about the correctness of SOLIDUSS' diffusion

implementation and underlying method. The results of such numerical experiments showed a good compatibility of input and calculated values within the error bars. Therefore, we conclude that the software implementation and the numerical treatment of diffusion in which it is based work as intended to the best of our knowledge. Note that SOLIDUSS does not make explicit use of the diffusion equation, yet the results of the two are in excellent agreement.

The experimental campaign summarized above provided data for the benchmarking of the code against experimental data. Few simulations were performed using SOLIDUSS with the aim of reproducing the experiments' results. We used three different sets of data in order to obtain a mean for the ODF as well as lower and upper limits to it taking into account the uncertainties of the different parameters employed. For ^{60}Co from Cu we obtained an ODF of $7.7^{+1.7}_{-3.4} \cdot 10^{-2}$ % after 5 h of heating. For ^{22}Na from Al, the results were $34.7^{+55.5}_{-24.2}$ % after 2 h and $59.7^{+39.6}_{-41.3}$ after approximately 6 h. When looking at ODF results, the reader is advised to think in terms of logarithmic scale, rather than linearly. At a first glance, a result like the one for ^{22}Na in Al after 2 h may seem to be covering almost the whole range of values and therefore may be misinterpreted as a poor result when thinking linearly on the [0% – 100%] range. To better understand the reason, let us imagine we are dealing with an activity of 10 TBq, then to say that few TBq would escape if the sample is exposed to a given temperature (case of Na in Al) may be radically different in terms of radiation protection than an ODF of few MBq (case of Co in Cu), which is still far from zero and could be important, even if the relative amount escaping may be considered as low. The results from the experiments and the simulations are in good agreement within error bars. They clearly support the importance of the implemented desorption model. The ODF simulation results for Co would have been definitely off without it. We have also learned that the calculations can be extremely sensitive to variations of the parameters provided by the user (*e.g.* activation energies, frequency factors, temperature, *etc.*), which are often estimations with significant uncertainties. Given the tests performed so far and in absence of further supporting experimental data, the author consider it as prudent to take SOLIDUSS' results as order-of-magnitude estimations, while encouraging the user to perform accompanying sensitivity analyses.

In the course of this work, we have identified few *analytical expressions* that can be used to easily estimate the ODF for simplified scenarios. In particular, we can make use of them in cases in which it is reasonable to assume a uniform temperature within the object of interest as well as a uniform concentration of radionuclides. In order to calculate the ODF, we will need to estimate two quantities: the Fraction of atoms Reaching an object's Surface (FRS) and their Global Desorption Probability (GDP). If N_A is the total number of radionuclides inside our object, the total number of radionuclides reaching the object's surface will be given by $N_A \cdot \text{FRS}$. And the fraction of them that will manage to escape the object would be given by the GDP. The FRS can be approximated as $\text{FRS} \simeq \text{erf}(\sqrt{Dt_T} \cdot S/V)$, where erf is the error function, S is the surface of the object and V its volume, D is the diffusion coefficient of interest and t_T is the total diffusion time in consideration. It seems intuitive that the radionuclide's chances of reaching the object's surface increase with the ratio S/V and with the factor $\sqrt{Dt_T}$, which is a measure of how far can the radionuclide travel within the object. A significant amount of calculations have been performed to compare the results provided by the software and the formula. We could observe that, for low FRS fractions (below 10 %), formula and simulation agree within a 5 % of relative error. Outside this region,

the agreement evolves differently for different geometries, but in all cases we have tested, the relative error does not surpass 15 %. In this respect, it is important to mention that for most cases of interest from the radiation protection point of view, the FRS will fall below a few percent, where we find the best agreement between formula and simulations. Although the FRS can be used to set a conservative upper limit for the ODF, there may be cases in which a more accurate estimation is sought. We can get such an estimation by taking the desorption phenomenon into account. We know that the probability of desorption of a particular radionuclide must be calculated taking into account several parameters and, among them, the time when it reached the surface of the object for the first time. We can assume that every radionuclide reached the surface at t_0 , the beginning of the fire. This will allow us to estimate a GDP that, although overestimated, allows us to assess the impact of desorption:

$$\text{GDP} = 1 - \left[1 - \frac{1}{1 + \exp\left(\frac{E_{des} - Q}{k_B T}\right)} \right] a \left(\frac{6Dt_T}{\text{DNN}^2}\right)^b,$$

where E_{des} is the desorption activation energy, Q is the diffusion activation energy, T is the temperature, k_B is the Boltzmann's constant, DNN is the distance between nearest atomic neighbours in the host material lattice, and a and b are the aforementioned parameters that depend on the lattice structure and its orientation with respect to the boundary, but for which default values have been selected. The ODF can then be estimated as $\text{ODF} = \text{FRS} \cdot \text{GDP}$. Provided the input parameters are accurate, the equation will overestimate the out-diffused fraction, as previously discussed. Nonetheless, it may be of great help since there are many cases in which the desorption probability is very low and therefore only a small fraction of the radionuclides reaching an object's surface manage to escape. To assume total desorption in such cases could imply overestimations of several orders of magnitude, while this equation should limit them to a factor of a few according to our experience so far.

With the aim of providing some quantitative data on the potential *impact of out-diffusion*, we took a look at one scenario of interest. For this we relied on the ActiWiz code, which was initially developed to facilitate the optimization—from a radiation protection standpoint—of the chemical composition of materials used in the accelerator equipment at CERN. To this end, ActiWiz uses some generic radiation scenarios that are representative of radiation environments often encountered along the accelerator chain. For our calculation, we benefit from some of these scenarios to simulate the radiation environment in which exemplary fictitious accelerator components are placed. This allowed us to estimate the contribution of out-diffusion to effective inhalation doses following an accidental fire affecting the following components: cables typically placed next to the LHC tunnel wall (side-cables), an LHC warm quadrupole magnet and an LHC collimator. We focused on the global committed effective dose E_{50} corresponding to the whole source terms for each material in case of fire. In order to calculate the fraction of the radionuclide inventory escaping, we have assumed a 1 h long fire and different temperatures: 800 °C, 900 °C and 1000 °C. Combining the ODF results with the radionuclide inventories, we could obtain quantitative data on the contribution of out-diffusion to the radiological hazard posed by such fire scenario. The collimator vessel presents the highest radiological hazard due to out-diffusion per cm^3 exposed to fire, closely followed by magnet coils conductor. If we consider a single quadrupole at 900 °C and we exclude the ^3H

contribution, the radiological hazard posed by the out-diffused radionuclides from the quadrupole is equivalent to the combustion of approximately 8.2 m³ of side-cable insulation (polyethylene), this is 7708 kg of cable insulation. If we consider all the ³H to be inside the different components at the time of fire, this value rises to 33 044 kg. We can therefore conclude that the contribution of out-diffusion to radiological source terms may be of considerable significance. The reason is that, even if out-diffused fractions are typically low, releases can be important in absolute terms since fire may affect highly radioactive noncombustible materials.

Resumen

LA ORGANIZACIÓN Europea para la Investigación Nuclear (CERN) es uno de los laboratorios científicos más grandes del mundo. Actualmente, sus actividades se focalizan principalmente en la física de partículas de altas energías y proporciona a la comunidad científica una gama única de aceleradores de partículas que son utilizados por más de 600 institutos de investigación y universidades de todo el mundo. En estos aceleradores, partículas de alta energía colisionan casi inevitablemente con el material circundante, dando lugar a reacciones nucleares. Como consecuencia de dichas reacciones, materiales previamente estables pasan a ser radiactivos: a este fenómeno se le conoce como activación. Las partículas emitidas durante una desintegración radioactiva forman parte de la denominada radiación ionizante, y su interacción con tejido biológico vivo puede tener resultados dañinos e incluso letales. El grupo de Protección Radiológica del CERN se asegura de que el personal del laboratorio, así como el público y el medio ambiente estén protegidos de los efectos nocivos de las radiaciones ionizantes vinculadas a las actividades de la organización. En lo que respecta a la protección contra incendios, el CERN es también un entorno único. La complejidad de sus instalaciones y los peligros radiológicos asociados a ellas a menudo requieren de estudios específicos para prevenir, mitigar y hacer frente con éxito a posibles incendios. Para llevar a cabo estos estudios, la Unidad de Seguridad, Salud Laboral y Protección del Medio Ambiente del CERN lanzó el proyecto FIRIA, que tiene como objetivo desarrollar una metodología integral para evaluar cuantitativamente la posible liberación de sustancias radiactivas derivadas de incendios accidentales. La determinación precisa del tipo y cantidad (inventario) de radioisótopos provenientes de materiales activados que se podría liberar al medio ambiente como consecuencia de un evento de estas características es de suma importancia para estimar sus posibles consecuencias radiológicas. Es por esta razón que se ha hecho patente la necesidad de evaluar la contribución de la llamada *liberación de radioisótopos por difusión*. Denominamos como liberados por difusión a aquellos radioisótopos inicialmente ubicados en la matriz de un sólido, que debido a su difusión potenciada térmicamente a través del mismo, llegan a la superficie del objeto que los contiene y logran escapar de él, siendo liberados al medio ambiente. El trabajo que aquí se presenta tiene como objetivo el diseño, implementación y evaluación de un código de simulación que se pueda utilizar para estimar de manera realista la contribución de este fenómeno de acuerdo a las características concretas de cada incendio e instalación.

Los átomos que componen un sólido son capaces de migrar dentro de él, realizando en general saltos sucesivos de longitudes fijas, exponencialmente más probables cuanto mayor es la temperatura del medio. La longitud de estos saltos es típicamente similar a la distancia que separa dos posiciones

atómicas en la estructura del sólido. Desde una perspectiva fenomenológica, las ecuaciones que gobiernan la difusión se conocen como *leyes de Fick* y, en particular, es la segunda ley de Fick (también conocida como ecuación de difusión) la que describe la evolución de la posición de nuestro inventario de radionucleidos en caso de incendio: $C(\vec{r}, t)/t = D\nabla^2 C(\vec{r}, t)$. Esta es una ecuación en derivadas parciales de segundo orden que relaciona la evolución en el tiempo de la concentración de partículas $C(\vec{r}, t)$ con la divergencia de su gradiente. El coeficiente de difusión D es la constante de proporcionalidad en la ecuación, y nos dice cómo de rápido una especie atómica puede difundirse dentro de un material a una determinada temperatura.

Se puede demostrar que, bajo ciertos supuestos, los denominados caminos aleatorios emulan los procesos de difusión. Esto sugiere que podemos simular difusión utilizando métodos estocásticos, evitando así la necesidad de soluciones deterministas de la ecuación de difusión que para nosotros plantearía importantes dificultades. En este sentido, consideramos que el desarrollo de un modelo de difusión basado en métodos Monte Carlo e internamente vinculado al código de simulación FLUKA es la mejor estrategia para afrontar nuestro problema. Se puede demostrar que la probabilidad de encontrar un átomo en cierta posición después de numerosos saltos atómicos converge hacia la que se obtiene de una distribución normal centrada en la posición inicial del átomo y cuya varianza es proporcional al coeficiente de difusión y el tiempo transcurrido. Este resultado no es sorprendente, ya que dicha distribución es una solución fundamental de la ecuación de difusión. De acuerdo con esto, podemos emplear un *proceso de Wiener* estándar para simular la difusión de radioisótopos a través de nuestros materiales. Este es un proceso estocástico a tiempo continuo, de valores reales y con incrementos independientes y normalmente distribuidos. En la práctica, esto significa que se puede muestrear la posición de un radionucleido después de un tiempo de difusión determinado utilizando una distribución normal multivariada. Sin embargo, esto pasaría por alto la presencia de límites geométricos en el sólido en cuestión, lo cual se puede resolver fragmentando el tiempo total de difusión en un número adecuado de pequeños pasos muestreados secuencialmente. De esta manera podemos comprobar la posición del radionucleido después de cada paso, detectando si ha alcanzado alguna superficie durante su trayectoria a través del material. Siguiendo esta estrategia, hemos desarrollado un código de simulación robusto y fiable llamado SOLIDUSS, que está mayoritariamente escrito en C++. El código está internamente ligado a FLUKA y utiliza sus rutinas de navegación geométrica para realizar cálculos de difusión en geometrías arbitrariamente complejas. Permite la obtención de la cantidad de radionucleidos que se liberan desde un material determinado en cualquier área de interés de nuestra geometría. Esto se hace para un conjunto de períodos de difusión definidos por el usuario y, además, el programa proporciona un mapa tridimensional de la concentración de radionucleidos para cada uno de estos periodos. A su vez, ofrece la posibilidad de realizar múltiples cálculos de difusión al tiempo que ejecutamos una única simulación de FLUKA, y puede hacerlo de acuerdo a diferentes mapas de temperaturas definidos por el usuario. La posición inicial de los radionucleidos creados como resultado de la interacción radiación-materia simulada por FLUKA se pasa automática e internamente a SOLIDUSS sin intervención humana. Para llevar a cabo una simulación, el usuario debe proporcionar un archivo de texto en el que incluirá toda la información necesaria para simular difusión de acuerdo con sus preferencias. Este archivo deberá contener información relativa al radionucleido de interés, el material activado, los llamados parámetros de activación de difusión, tiempos de difusión, mapas de temperatura, *etc.* Si es solicitado, SOLIDUSS ejecuta operaciones de optimización destinadas

a reducir el tiempo de computación empleado en el seguimiento de radioisótopos sin socavar la exactitud de sus resultados.

La fracción de isótopos radiactivos que se liberan por difusión desde un objeto dado, lo que llamamos la fracción liberada por difusión (ODF), siempre se subestima cuando se calcula simulando longitudes de paso mayores que las longitudes reales de los saltos atómicos en el sólido. Tenga en cuenta que si un radionucleido alcanza la superficie de un objeto N_R veces durante su trayectoria real dentro de él, la simulación utilizando distribuciones normales que agregan un elevado número de saltos atómicos en un único paso de simulación podrá identificar solo $N_S < N_R$. En el límite en el que los pasos simulados son del tamaño de los saltos atómicos reales, decimos que la simulación se realiza con una *resolución perfecta de la trayectoria*. Sin embargo, este tipo de simulación no es práctico o es incluso imposible si consideramos objetos voluminosos, debido a su alto consumo de recursos computacionales. Por lo tanto, la discrepancia entre el estimador N_S y el resultado exacto N_R se ve influenciada por el tamaño elegido de la longitud de los pasos, lo que impacta directamente en la fiabilidad del resultado final. Tras la realización de un estudio específico, advertimos que la manera en que la ODF depende de la duración del paso temporal Δt de la simulación está determinada por la siguiente expresión: $ODF(\Delta t) = a \cdot \operatorname{erfc}(b \cdot \sqrt{\Delta t}) + c$, donde a , b y c son parámetros de ajuste y erfc es la función error complementaria. La extrapolación de esta función para $\Delta t \rightarrow 0$ podría usarse para obtener una estimación más precisa de la ODF. Para escrutar la generalidad de este comportamiento se realizaron pruebas que involucraron diferentes geometrías, distintas combinaciones de especies atómicas y materiales, así como gradientes de temperatura y distribuciones iniciales no uniformes: en todas ellas se mantuvo inalterado. Esto nos permite estimar de manera muy precisa la ODF mediante su cálculo aproximado para diferentes pasos de tiempo, incluso si estos resultados están lejos de la fracción liberada por difusión real. Como consecuencia, el tiempo de cómputo necesario para estimar una ODF se reduce en gran medida, a la vez que obtenemos una aproximación mucho mejor de la fracción real. El procesado de los resultados de SOLIDUSS y los cálculos y ajustes descritos aquí se han automatizado mediante la creación de pequeños programas de C++ y Python para poder realizar estimaciones precisas de la ODF de forma eficiente.

Si ignoramos las reacciones químicas con las sustancias circundantes, un átomo que llega a la superficie de un sólido puede volver a difundirse hacia el interior del mismo o, por el contrario, escapar por *desorción*. Imaginemos una superficie con un número θ_0 de átomos adsorbidos, si asumimos que el único proceso que pueden experimentar estos átomos es desorción de primer orden, el número de átomos θ en la superficie variará con el tiempo t de la siguiente manera: $d\theta/dt = -\theta\nu_0 \exp[-E_{des}/(k_B T)]$, donde E_{des} es la energía de activación de desorción, ν_0 la frecuencia de vibración del átomo, T es la temperatura absoluta y k_B la constante de Boltzmann. La energía de activación de desorción se puede interpretar como la energía necesaria para romper por completo las ligaduras de un átomo en la superficie de un objeto con los átomos que lo rodean. Usando la ecuación anterior, se puede calcular la tasa de desorción y comparar con la de difusión siempre que exista una competición entre ambos procesos, para poder así determinar su resultado mediante el uso de números aleatorios. SOLIDUSS utiliza pasos de tiempo adaptativos, que condensan múltiples pasos saltos atómicos. Por esta razón, la comparación entre las tasas de difusión y desorción explicada anteriormente no es directamente aplicable. No obstante, el método se puede

modificar para poder ser implementado en nuestro código. La clave es obtener el número de veces que un radionucleido alcanza la superficie del objeto que lo contiene durante un paso de simulación, suponiendo que no se escapa en ninguna de las ocasiones. Con este dato, podríamos obtener la probabilidad total de que se escape en un paso de simulación determinado. Para hacer esto, una vez que sabemos que el isótopo llegará a la superficie del objeto en el paso actual, estimamos la distancia que lo separa de dicha superficie. Posteriormente, la utilizamos para muestrear el instante en el que llega a la superficie por primera vez, que sabemos que sigue una distribución de Lévy. Una vez aquí, el número promedio de veces que encontrará la superficie nuevamente N_{enc} es una función del número de saltos N que realiza: $\langle N_{enc} \rangle = a \cdot N^b$, donde a y b son parámetros que dependen de la estructura del sólido y su orientación con respecto a la superficie. Una vez conocemos el número de veces que nuestro isótopo ha llegado a la superficie del objeto que lo contiene, podemos obtener la probabilidad de desorción y utilizar un número aleatorio para determinar si se escaparía o no durante el intervalo de tiempo del paso considerado. En caso negativo, deberemos continuar simulando su difusión en el sólido. Este proceso se repetirá cada vez que un isótopo alcance la superficie del sólido en cuestión.

Con el objetivo de obtener datos sobre la liberación de radionucleidos por difusión, se llevó a cabo una *campana experimental* sometiendo materiales activados a muy altas temperaturas. El elemento central de los experimentos fue el calentamiento de muestras radiactivas, llevado a cabo en una atmósfera controlada y libre de oxígeno para evitar su combustión. También se realizaron pruebas en una atmósfera de aire normal, utilizando muestras no radiactivas, simulando condiciones similares a las de un incendio real. Para garantizar una ejecución segura de los experimentos con isótopos radiactivos, se realizaron con antelación ensayos utilizando materiales no radiactivos. Después de la selección de las muestras de material activado, el procedimiento llevado a cabo para cada experimento comenzó con la determinación del contenido radiactivo de cada una de ellas mediante espectrometría de rayos gamma. Después, las muestras se sometieron a muy altas temperaturas durante un periodo determinado utilizando un horno capaz de calentar a más de 1000 °C. Las temperaturas se eligieron de manera que maximizaban la ODF y a su vez eran lo suficientemente bajas como para evitar la fusión de nuestros materiales. Finalmente, se realizó una segunda espectrometría de rayos gamma de las muestras en las mismas condiciones experimentales que la primera. La substracción de ambos resultados nos permitió estimar la ODF. Las muestras utilizadas fueron dos láminas metálicas activadas de 11.0 cm × 4.8 cm. La primera era de Cu de 49 μm de espesor, con 0.6 Bq de ^{60}Co en su interior. La segunda era de Al, de 94 μm de espesor, y con 17.8 Bq de ^{22}Na . El perfil de temperatura del horno fue caracterizado de manera que las muestras se pudieron colocar en su región más uniforme. Obtuvimos una ODF para ^{60}Co en Cu de $1.6 \pm 11.0\%$ tras 5 h a aproximadamente 1000 °C. A la vista de este resultado, no podemos determinar si parte del ^{60}Co escapó de la muestra o no; pero sí que podemos afirmar que, en caso de que lo hiciera, la cantidad que escapó fue menos del 12.6 % con 1σ de certeza. Para ^{22}Na en Al, la ODF obtenida fue $14.6 \pm 7.3\%$ después de 2 h y subió hasta $40.4 \pm 7.0\%$ después de aproximadamente 6 h a 600 °C. Dos experimentos diferentes fueron realizados para evaluar los efectos de las altas temperaturas en Cu. En particular, nos interesaba comprender si una parte del mismo y su contenido radiactivo podrían liberarse al medio ambiente en caso de accidente. En la primera prueba utilizamos una lámina de Cu de 35 μm de espesor, y en la segunda filamentos de Cu de 150 μm de diámetro de un cable de alimentación estándar. La fina lámina de Cu es

representativa de las láminas de Cu utilizadas para el blindaje de cables eléctricos. Después de 20 minutos a 800 °C, se oxidó por completo y se hizo añicos tras una ligera manipulación. Incluso para objetos más gruesos, esperamos un efecto de oxidación muy similar en sus superficies, lo que fácilmente podría resultar en la liberación de escamas de material al medio ambiente. Tras la exposición de los filamentos a condiciones similares, se desprendió una cantidad significativa de polvo como consecuencia de una breve manipulación. La conclusión de este experimento respalda la del anterior: en caso de incendio, la parte más externa de los objetos de Cu (y probablemente otros metales) se deteriorará dando lugar a material quebradizo que podría liberarse con facilidad debido a la turbulencia del fuego.

Tras finalizar la campaña experimental y como parte de la *evaluación de SOLIDUSS*, llevamos a cabo una serie de cálculos para comprobar la implementación del tratamiento numérico de difusión. Cuando se simula la difusión de radionucleidos, uno de los parámetros más importantes que debe proporcionarse al código es el coeficiente de difusión. Un procedimiento típico para obtener experimentalmente esta cantidad son los denominados experimentos de difusión de trazadores, que podemos imitar utilizando una simulación. Usando los resultados de SOLIDUSS como si se tratara de resultados experimentales, podemos resolver problemas cuyas condiciones de contorno permiten la solución analítica de la ecuación de difusión. Comparando ambos resultados podemos determinar el coeficiente de difusión para diferentes especies y temperaturas. Si los valores resultantes son compatibles con los coeficientes de difusión proporcionados al código en primer lugar, podemos estar razonablemente seguros de que la implementación del modelo de difusión de SOLIDUSS es correcta. Los resultados de tales experimentos numéricos mostraron un buen acuerdo entre valores introducidos y valores calculados, siempre dentro de las barras de error. Por lo tanto, concluimos que la implementación del software y el tratamiento numérico de difusión en el que se basa funcionan según lo previsto. Tenga en cuenta que SOLIDUSS no hace un uso explícito de la ecuación de difusión, sin embargo, los resultados de ambos coinciden a la perfección.

Con los datos obtenidos en la campaña experimental resumida anteriormente procedimos a la evaluación comparativa del código. Con la intención de reproducir los resultados de los experimentos, se realizaron una serie de simulaciones utilizando SOLIDUSS recreando las condiciones experimentales. Tres conjuntos de parámetros diferentes fueron utilizados para tener en cuenta las incertidumbres asociadas a los mismos. De esta manera pudimos obtener un valor medio para la ODF, así como límites superior e inferior. Para el ^{60}Co del Cu obtuvimos una ODF de $7.7^{+1.7}_{-3.4} \cdot 10^{-2} \%$ después de 5 h de difusión. Para el ^{22}Na del Al, los resultados fueron $34.7^{+55.5}_{-24.2} \%$ después de 2 h y $59.7^{+39.6}_{-41.3} \%$ después de aproximadamente 6 h. Para analizar resultados de la ODF se recomienda al lector pensar en términos logarítmicos, en lugar de linealmente. A primera vista, un resultado como el de ^{22}Na en Al después de 2 h puede parecer que cubre casi todo el rango de valores y, por lo tanto, puede malinterpretarse como un resultado deficiente cuando se piensa linealmente en el rango [0 % - 100 %]. Para entender mejor por qué no lo es veamos un ejemplo: imaginemos una muestra con una actividad de 10 TBq, si obtenemos que unos pocos TBq escaparían de nuestra muestra en caso de incendio (caso de Na en Al) el escenario puede ser radicalmente diferente en términos de protección radiológica de si obtenemos unos pocos MBq (caso de Co en Cu), que todavía es considerable y podría ser importante, incluso si la cantidad relativa que se libera puede parecer baja. Los resultados de los experimentos y las simulaciones concuerdan bien dentro de las

barras de error y apoyan claramente la importancia del modelo de desorción implementado. Los resultados de la simulación obtenidos para Co habrían sido radicalmente erróneos sin él. También hemos aprendido que los cálculos pueden ser extremadamente sensibles a las variaciones de los parámetros proporcionados por el usuario (*e.g.* energías de activación, factores de frecuencia, temperatura, *etc.*), que a menudo son estimaciones con incertidumbres importantes. Dadas las pruebas realizadas hasta ahora y en ausencia de más datos experimentales, el autor considera prudente tomar los resultados de SOLIDUSS como estimaciones de orden de magnitud, al tiempo que anima al usuario a realizar análisis de sensibilidad.

En el curso de este trabajo, hemos identificado varias *expresiones analíticas* que se pueden usar para estimar fácilmente la ODF cuando consideramos escenarios simplificados. En particular, podemos hacer uso de ellas en aquellos casos en los que sea razonable asumir una temperatura uniforme dentro del objeto de interés así como una concentración uniforme de radionucleidos. Para calcular la ODF, necesitaremos estimar dos cantidades: la fracción de átomos que llegan a la superficie de un objeto (FRS) y su probabilidad de desorción global (GDP). Si N_A es el número total de radionucleidos dentro de nuestro objeto, el número total que llegará a la superficie vendrá dado por $N_A \cdot \text{FRS}$. Y la fracción de estos que logrará escapar del objeto la determinará la GDP. La FRS se puede aproximar como $\text{FRS} \simeq \text{erf}(\sqrt{Dt_T} \cdot S/V)$, donde erf es la función error, S es la superficie del objeto y V su volumen, D es el coeficiente de difusión y t_T es el tiempo total de difusión considerado. Parece intuitivo que las probabilidades de que un radionucleido alcance la superficie del objeto aumenten con la relación S/V y con el factor $\sqrt{Dt_T}$, que nos da una idea de la distancia que puede recorrer el radionucleido dentro del objeto. Se han realizado numerosos cálculos para comparar los resultados proporcionados por el código y la fórmula, y hemos observado que, para bajas FRS (por debajo del 10 %), la fórmula y las simulaciones concuerdan con menos de un 5 % de error relativo. Fuera de esta región, la concordancia evoluciona de manera diferente para diferentes geometrías, pero en todos los casos que hemos probado, el error relativo no supera el 15 %. En este sentido, es importante mencionar que para la mayoría de los casos de interés desde el punto de vista de la protección radiológica, la FRS caerá por debajo de un pequeño porcentaje, donde encontramos la mejor concordancia entre fórmula y simulaciones. Aunque la FRS se puede utilizar para establecer un límite superior conservativo para la ODF, puede haber casos en los que se busque una estimación más precisa. Podemos obtener tal estimación teniendo en cuenta el fenómeno de desorción. Sabemos que la probabilidad de desorción de un determinado radionucleido debe calcularse teniendo en cuenta varios parámetros y, entre ellos, el momento en que alcanzó la superficie del objeto por primera vez. Si suponemos que cada radionucleido alcanzó la superficie en t_0 (*i.e* el comienzo del incendio), podemos calcular una GDP que, aunque sobreestimada, nos permitirá evaluar el impacto de la desorción:

$$\text{GDP} = 1 - \left[1 - \frac{1}{1 + \exp\left(\frac{E_{des} - Q}{k_B T}\right)} \right]^{a \left(\frac{6Dt_T}{\text{DNN}^2}\right)^b},$$

donde E_{des} es la energía de activación de desorción, Q es la energía de activación de difusión, T es la temperatura, k_B es la constante de Boltzmann, DNN es la distancia atómica entre vecinos más próximos en el sólido, D es el coeficiente de difusión, t_T es el tiempo total de difusión y a y b son los

parámetros previamente mencionados que dependen de la estructura del sólido y su orientación con respecto a su superficie, pero para los cuales se han seleccionado valores por defecto. La ODF se puede estimar entonces como $ODF = FRS \cdot GDP$. Siempre que los parámetros introducidos sean precisos, la ecuación sobrestimaré la fracción que se libera, como se discutió anteriormente. No obstante, puede ser de gran ayuda ya que hay muchos casos en los que la probabilidad de desorción es muy baja y, por tanto, solo una pequeña fracción de los radionucleidos que llegan a la superficie de un objeto logra escapar. Asumir desorción total en tales casos podría implicar sobreestimaciones de varios órdenes de magnitud, mientras que esta ecuación las limita a un factor 2 o 3 de acuerdo con nuestra experiencia hasta la fecha.

Con el objetivo de proporcionar algunos datos cuantitativos sobre el *impacto potencial de la liberación de radioisótopos por difusión*, analizamos un escenario de interés. Para ello nos apoyamos en ActiWiz, que se desarrolló inicialmente para facilitar la optimización —desde el punto de vista de la protección radiológica— de la composición química de los materiales utilizados en los componentes de los aceleradores del CERN. Con este fin, ActiWiz hace uso de algunos escenarios de radiación genéricos que son representativos de los que se encuentran a menudo en diferentes lugares del complejo de aceleradores. Para nuestro cálculo utilizamos varios de estos escenarios para simular el campo de radiación al que se exponen ciertos componentes ficticios de los aceleradores que nos sirven de ejemplo. De esta manera, pudimos estimar la contribución de los radionucleidos liberados por difusión a la dosis global efectiva por inhalación como consecuencia de un incendio accidental que afectase a los siguientes componentes del LHC: cables laterales comúnmente colocados junto a la pared del túnel, un imán cuadrupolar no superconductor y un colimador del haz de partículas. Con la ayuda de ActiWiz obtuvimos la dosis efectiva comprometida E_{50} correspondiente al inventario completo de radioisótopos alojados en cada material. Posteriormente, calculamos la fracción de cada especie que escaparé de cada componente en caso de un incendio de 1 h considerando diferentes temperaturas: 800 °C, 900 °C y 1000 °C. Combinando los resultados de las ODF y los inventarios de radionucleidos, obtuvimos la contribución de la liberación por difusión al peligro radiológico planteado por dicho incendio. La cubierta del colimador es el componente que presenta el mayor riesgo radiológico debido a liberación por difusión por cm^3 expuesto al fuego, seguido de cerca por el conductor eléctrico de las bobinas del imán. Si consideramos un solo imán expuesto a 900 °C y excluimos la contribución del ^3H , el peligro radiológico que plantean los radionucleidos liberados desde este es equivalente a la combustión de aproximadamente 8.2 m^3 de aislante eléctrico de los cables laterales (polietileno), o lo que es lo mismo, 7708 kg de este material. Si consideramos que todo el ^3H sigue contenido en los diferentes componentes en el momento del incendio, este valor se eleva a 33 044 kg. Por lo tanto, podemos concluir que la contribución de la liberación por difusión al peligro radiológico generado por un incendio en una instalación con material activado puede tener una importancia considerable. La razón es que, incluso si las fracciones de liberación por difusión son bajas en general, las emisiones pueden ser importantes en términos absolutos, ya que el fuego puede afectar a materiales altamente radiactivos.

Table of contents

Acknowledgements	iv
Abstract	vi
Resumen	xiii
Table of contents	xx
1 Introduction	1
1.1 Radioactivity and activation	1
1.2 Monte Carlo methods	3
1.3 CERN	5
1.3.1 Radiation Protection	6
1.3.2 The FIRIA project	7
1.4 The need for this work	9
2 Diffusion and random walks	11
2.1 Diffusion	11
2.1.1 Microscopic perspective	11
2.1.2 Phenomenological perspective	14
2.2 Connection between diffusion and random walks	15
2.3 Diffusion coefficient	16
3 The code SOLIDUSS	20
3.1 Numerical treatment	21
3.1.1 Wiener process	21
3.1.2 The meaning of $n \rightarrow \infty$ in our problem	24
3.2 Implementation	26
3.2.1 How to use SOLIDUSS	27
3.2.2 Internal structure	27
3.3 Further considerations	30
3.4 Isotope tracking optimization	31

3.5	Statistical uncertainties calculation	33
3.6	Nonphysical tests	34
3.6.1	^{60}Co from an irradiated Cu cylinder	34
3.6.2	^{54}Mn from a quadrupole yoke	35
4	Perfect path resolutions	38
4.1	Random walk: out-diffusion fraction as a function of the time interval between consecutive position checks	39
4.2	Fitting SOLIDUSS results	40
4.2.1	Different pairs radionuclide - host material	43
4.2.2	Different geometries	44
4.2.3	Different initial distributions	45
4.2.4	Different temperature gradients	46
4.3	Confidence intervals for out-diffusion fraction estimations	47
4.4	Simulation example	48
5	Modelling desorption	51
5.1	Theoretical summary	51
5.2	Monte Carlo desorption model at atomic level	54
5.3	Desorption model for SOLIDUSS	55
5.3.1	Distance to boundary	56
5.3.2	First hitting time	57
5.3.3	Number of atomic jumps	58
5.3.4	Number of surface encounters	59
5.3.5	New position if not desorbed	65
6	Experimental campaign	66
6.1	Methodology	67
6.2	Experimental setup	68
6.2.1	Gas circuit	68
6.2.2	Furnace	71
6.3	Samples	71
6.4	Results and discussion	74
6.4.1	Temperature inside the furnace	74
6.4.2	Non-radioactive Cu in N_2 atmosphere	79
6.4.3	Radioactive Cu in N_2 atmosphere	80
6.4.4	Non-radioactive Al in N_2 atmosphere	82
6.4.5	Radioactive Al in N_2 atmosphere	82
6.4.6	Non-radioactive Cu in Air: foil and filaments	84
6.5	Acknowledgments	86
7	SOLIDUSS benchmarking	88

7.1	Numerical validation of the diffusion treatment	88
7.2	Experimental benchmarking	93
7.2.1	Simulations	93
7.2.2	Experimental data	98
7.2.3	Discussion	98
8	Out-diffusion fraction for simplified scenarios	101
8.1	Fraction of atoms Reaching an object's Surface (FRS)	101
8.1.1	Uniform concentration of radionuclides	102
8.1.2	Non-uniform concentration of radionuclides	105
8.2	Global Desorption Probability (GDP)	106
8.3	Out-Diffusion Fraction (ODF)	106
9	The impact of out-diffusion	111
9.1	ActiWiz and the generic irradiation scenarios	111
9.2	Radionuclide inventories in few accelerator components	112
9.3	The potential impact of out-diffusion	117
9.3.1	Calculation parameters	118
9.3.2	Results	121
9.3.3	Discussion	125
	Conclusion and outlook	128
	Bibliography	131
	Appendices	136
A	Diffusion in anisotropic media	137
B	Diffusion input file	138
C	Diffusion outputs	143
D	Experimental data: temperature profiles	146
E	Diffusion input files of benchmarking simulations	148
F	Temperature profiles for benchmarking simulations	149
G	Out-diffused radionuclide inventories for IR7 objects	151
	List of Figures	154
	List of Tables	156
	List of Abbreviations	157
	List of Terms	159

Introduction

Contents

1.1	Radioactivity and activation	1
1.2	Monte Carlo methods	3
1.3	CERN	5
1.3.1	Radiation Protection	6
1.3.2	The FIRIA project	7
1.4	The need for this work	9

THE CONTENT of this chapter is intended to provide the reader with a brief introduction to a handful of concepts that shall facilitate the understanding of subsequent chapters, as well as to give an overview of the framework within which the activities described in this manuscript take place. We will begin by recalling the concept of radioactivity and Monte Carlo methods. Then, we will introduce CERN and the FIRIA project. We finish the chapter by explaining the motivation of the work reported in this manuscript.

1.1 Radioactivity and activation

Radioactivity or *radioactive decay* is a natural process that unstable atomic nuclei undergo to release energy and gain stability. It results in the ejection of particles carrying some of the released energy and often also in the transmutation of the nucleus —its number of protons and/or neutrons changes. Radioactive decay is an *stochastic process*; the moment at which a particular nuclide will decay cannot be predicted and its decay probability is constant in time. Given a number N of identical and unstable nuclei, the number of decays in a small time interval dt would be proportional to N . The proportionality constant is the so called *decay constant*, λ , which is different for each radionuclide

species:

$$-\frac{dN}{dt} = \lambda N \quad \Rightarrow \quad -\frac{dN}{N} = \lambda dt. \quad (1.1)$$

The result of this differential equation is:

$$N(t) = N_0 e^{-\lambda t}, \quad (1.2)$$

where N_0 is the initial amount of radionuclides at $t = 0$. The decay constant is often provided as a function of the radionuclide's *half-life* $t_{1/2}$, which is the required time period for half of the radionuclides in a given sample to decay:

$$\frac{N_0}{2} = N_0 e^{-\lambda t_{1/2}} \quad \Rightarrow \quad t_{1/2} = \frac{\ln 2}{\lambda}. \quad (1.3)$$

The range of half-lives is vast, from virtually zero ($\sim 10^{-24}$ s) to virtually infinite ($\sim 10^{31}$ s). The *radioactive activity* A , which is a measure of the rate at which radioactive decay takes place, is given by:

$$A = -\frac{dN}{dt} = \lambda N. \quad (1.4)$$

The unit of A in the International System of Units (SI) is the becquerel (Bq), which is defined as one decay per second.

Radioactivity can be artificially induced in otherwise non-radioactive materials. This is typically known as *activation* and can be done by transforming some of its stable nuclei into unstable ones. These transformations are the result of different types of nuclear reactions induced by the interaction of particles (*e.g.* protons, neutrons, photons, *etc.*) with the atomic nuclei of the material. The chart of nuclides is shown in Fig. 1.1, where the reader can observe the stable nuclides as well as the decay mode of the unstable ones.

Once a material has been activated, it will continue to decay even if the initial source of radiation that activated it in the first place is gone. This is often referred to as *residual activation*. The decay rate will of course depend on the half-life of the created radionuclides and their abundance. Therefore, an activated piece of material could remain radioactive from less than one second to virtually forever.

The energetic particles ejected as result of a radioactive decay are part of the so-called *ionising radiation*, which comprises particles and electromagnetic waves sufficiently energetic to ionise atoms or molecules. That is, pulling electrons from them. The interaction of this type of radiation with living biological tissue can have harmful and eventually lethal results. Ionising radiation can also damage any other type of material and could provoke, for instance, the failure of electronic devices. The severity of the damage depends on the type, energy and amount of radiation.

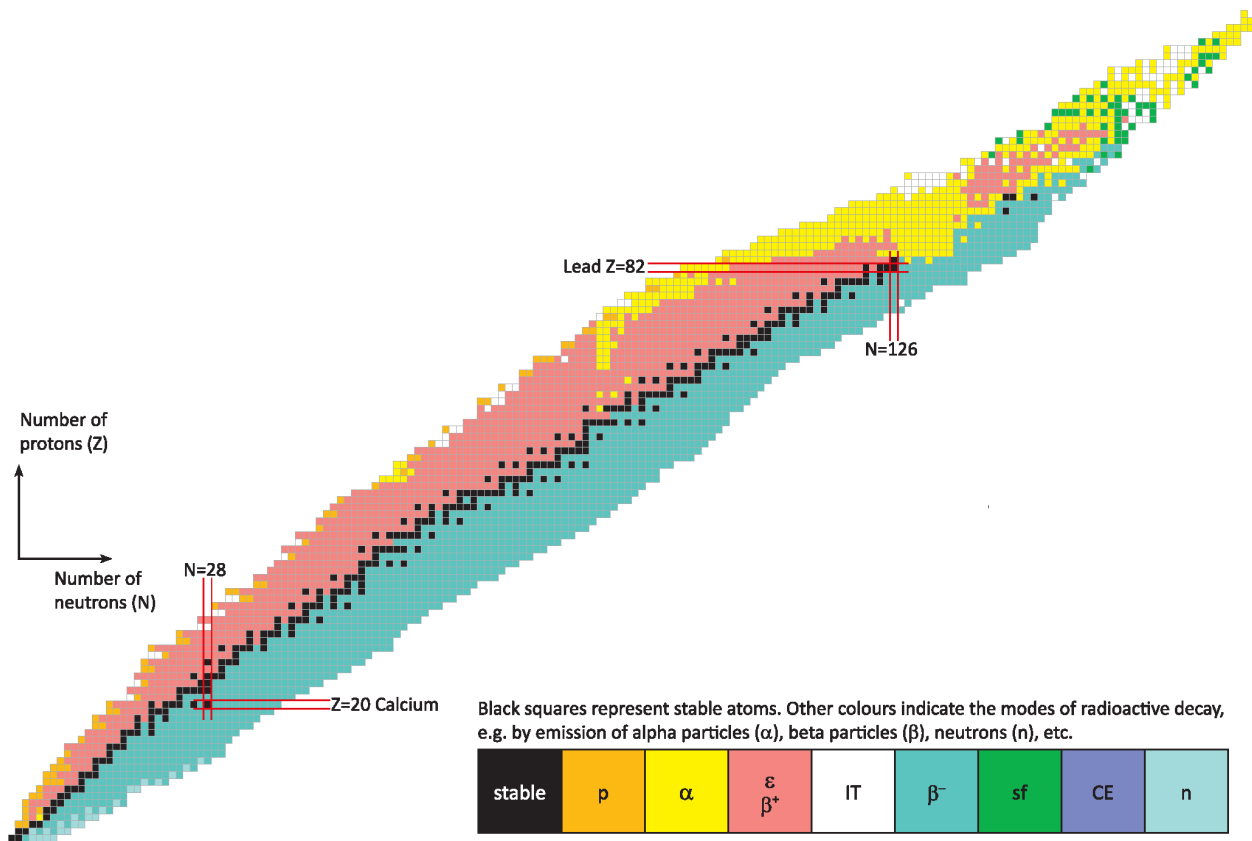


Figure 1.1: The chart of nuclides. Adapted from Ref. [1].

1.2 Monte Carlo methods

The *Monte Carlo methods* (MC) encompass a wide range of numerical techniques based on the use of random numbers to solve mathematical problems. They were developed during the 20th century and nowadays are of major importance for many different fields due to their remarkable versatility. Their use extends to many different domains such as physics, economics, engineering and other interdisciplinary fields. Calculating the number π , characterizing the radiation field in a particle accelerator, modeling the evolution of galaxies, achieving photorealistic computer graphics or evaluating the risks of a financial investment are only few examples of problems that can be tackled using MC methods. These are sometimes the only feasible approach to solve complex problems. Please take a look to Ref. [2] for a formal introduction.

The tremendous increase of the calculation power of computers achieved in the last decades empowered us to perform very demanding MC simulations, which are typically based on the repetitive, independent and realistic sampling of a system's evolution—or history—according to a set of rules and probability distributions, followed by a statistical analysis of the results, which yields to the estimation of the quantities of interest and the associated statistical errors. It can be seen as the repetitive realization of a theoretical experiment (so called histories) and the posterior analysis of its results. The statistical error is inherent to the method due to its stochastic nature, but can be reduced by increasing the number of simulated histories and therefore the calculation time.

The uncertainty of the result of a MC calculation is not limited to errors of a statistical nature. On the contrary, there are numerous sources of systematic errors that may impact the simulation result such as inaccuracies in the models and input data employed, oversimplification of the problem, errors in the implemented algorithms, incomplete knowledge on the system to be simulated, *etc.* For this reason, benchmarks are usually required to assess the reliability of MC codes.

Example: estimating π

One of the simplest and more illustrative applications of the use of MC techniques is the estimation of π . Let us consider a circumference of radius R inscribed in a square with a side length equal to $2R$. The ratio between the area of both geometric objects is given by:

$$\frac{A_c}{A_s} = \frac{\pi R^2}{4R^2} = \frac{\pi}{4}, \quad (1.5)$$

where A_c and A_s are the areas of the circumference and the square, respectively. Now, we sample N_s uniformly distributed random points within the square and keep track of how many of them fall within the circumference: N_c . When $N_s \rightarrow \infty$, the ratio of both quantities will converge towards the ratio of the objects' areas, and therefore:

$$\frac{A_c}{A_s} = \frac{N_c}{N_s} \Rightarrow \pi = \frac{4N_c}{N_s}. \quad (1.6)$$

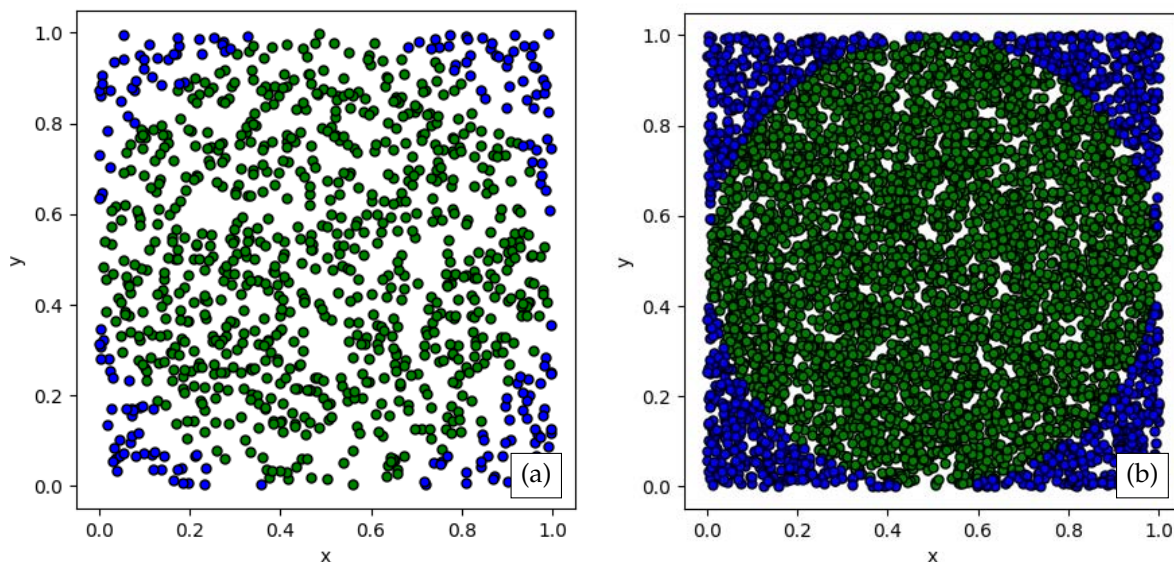


Figure 1.2: Illustration of the random sampling used to calculate π with 1000 simulated points in (a), and 5000 points in (b). In green the points inside the circumference and in blue those outside it. Note that in this case $R = 0.5$.

This way, π can be estimated using random numbers. The estimation will be more accurate the larger the number of sampled points. See Fig. 1.2 for an illustration of the sampled points and the discrimination of those falling within the circumference.

Table 1.1: MC estimation of π (π_{est}) for different number of sampled points together with its statistical uncertainty.

N	π_{est}	Unc.
10000	3.138	0.017
40000	3.139	0.008
160000	3.143	0.004
640000	3.142	0.002
2560000	3.1432	0.0010
10240000	3.1418	0.0005
40960000	3.1418	0.0003
163840000	3.14156	0.00014
655360000	3.14154	0.00006

Few results obtained for π using different number of points are shown in Tab. 1.1. The total number of sampled points was divided in 50 sets, which were used to obtain 50 estimates of π . Later, these results were combined to obtain an average estimation and its statistical uncertainty, calculated using the dispersion of the different estimates. As we can see in Fig. 1.3, the uncertainty of the estimation reduces as $1/\sqrt{N}$, where N is the total number of sampled points —more generally, histories. This dependence of the uncertainty with the number of histories is independent of this particular problem and true for every estimator obtained via MC.

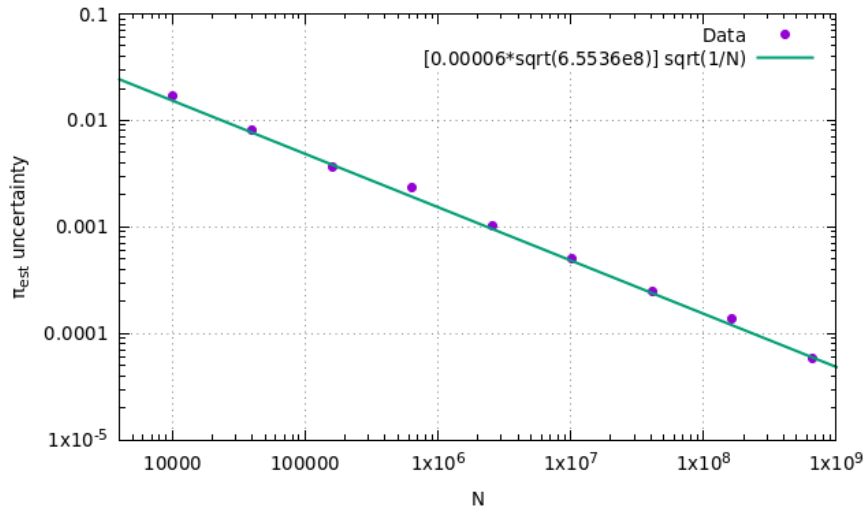


Figure 1.3: Statistical uncertainty of the π estimation as a function of the number of sampled points (Data). The solid curve is used to show the $1/\sqrt{N}$ dependence of the estimation uncertainty, and it is scaled using the the uncertainty obtained for $N = 6.5536 \cdot 10^8$.

1.3 CERN

The European Organisation for Nuclear Research (CERN) [3] is one of the largest scientific laboratories. Nowadays mainly focused on high energy particle physics, it provides the scientific

community with a unique range of particle accelerator facilities that are used by over 600 institutes and universities around the world. CERN was created after the signature of the CERN convention in 1953 by the 12 founding states and, as of today, it has 23 member states, 10 associate member states and few others with observer status. See [4] for a short introduction to CERN's history and origins. There are about 2500 CERN's staff members, and more than 12000 scientist of over 100 nationalities are involved in CERN activities.

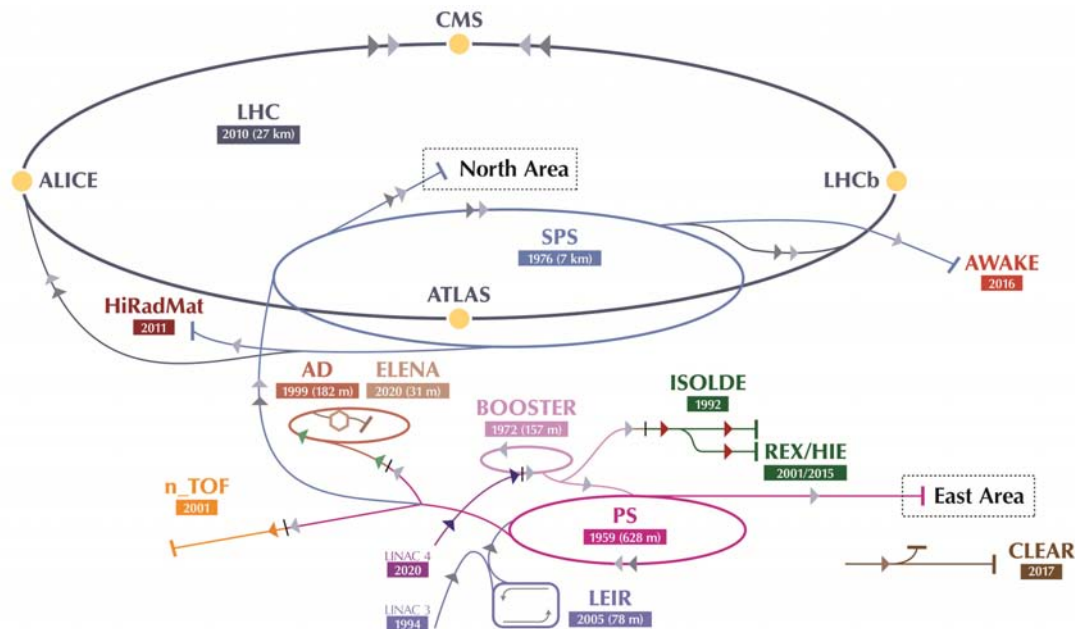


Figure 1.4: Layout of CERN's accelerators and experiments. Source: CERN.

CERN hosts a large complex of accelerators and experiments devoted to push the frontiers of knowledge in multiple fields. A schematic of the complex is shown in Fig. 1.4. Please visit Refs. [5,6] for an introduction to each of the facilities.

1.3.1 Radiation Protection

In particle accelerator facilities, high energy particles end up almost inevitably impinging onto the surrounding material inducing nuclear reactions that often result in its activation. The main reactions contributing to this are neutron capture, photonuclear reactions, spallation and other inelastic hadronic interactions. In hadron and ion accelerators, the radionuclide production rate is particularly high. In addition to this, the highly energetic particles used at CERN and the wide variety of materials employed in the accelerator components give rise to a very diverse and abundant radionuclide inventory. As a consequence, there are numerous highly activated areas at CERN which pose a potential hazard to life even when particle beams are not circulating. If we combine this with the large number of people working on site every day, and the continuous upgrades and interventions that are conducted in the accelerator complex and experiments, we can easily realize that *radiation protection* at CERN can pose significant challenges. The Radiation Protection group (RP) at CERN, whose mandate is quoted below [7], is there to meet these challenges.

“The Radiation Protection group of the occupational Health & Safety and Environmental protection unit (HSE unit) ensures that personnel on the CERN sites and the public are protected from potentially harmful effects of ionizing radiation linked to CERN activities. The RP group fulfils its mandate in collaboration with the CERN departments owning or operating sources of ionizing radiation and having the responsibility for Radiation Safety of these sources.”

The general principles in which the RP group bases its activity [8] and that were specified by the International Commission on Radiological Protection (ICRP) on its Recommendation 60 [9] are the following:

- Justification: any practice involving exposure to radiation should be properly justified.
- Limitation: exposure of workers and members of the public to radiation must not exceed legal limits.
- Optimization: individual and collective doses must be kept As Low As Reasonably Achievable (ALARA).

Among the duties of the RP group we shall highlight the followings:

- Assessment of radiological hazards all along the laboratory and define and implement the appropriate protective measures.
- Monitor radiation levels and ambient and personal radiation doses.
- Ensure the implementation of the ALARA principle in the design, operation and decommissioning of CERN facilities.
- Supervise and guarantee compliance with regulations.
- Characterization and disposal of radioactive material and waste.
- Classification of work places in radiation zones as function of the potential external and internal exposure to radiation. Fig. 1.5 shows how the different radiation areas are signaled at CERN.
- Develop and maintain the tools, instruments and methods necessary for the assessment of radiation hazards at CERN.

1.3.2 The FIRIA project

CERN is also a unique laboratory with respect to challenges related to fire protection. The accelerator complex is placed in very long and often non-compartmentalized tunnels (example in Fig. 1.6). They contain large quantities of combustible material such as cables and are typically underground, up to 100 meters deep [11]. Immense electrical currents circulate along the complex powering the


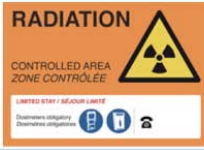


	Supervised Area	Simple Controlled Area	Limited Stay Controlled Area	High Radiation Controlled Area	Prohibited Controlled Area
RADIATION	 <p>RADIATION SUPERVISED AREA ZONE SURVEILLÉE</p> <p>Documents obligatoires Documents obligatoires</p>	 <p>RADIATION CONTROLLED AREA ZONE CONTRÔLÉE</p> <p>Documents obligatoires Documents obligatoires</p>	 <p>RADIATION CONTROLLED AREA ZONE CONTRÔLÉE</p> <p>LIMITED STAY / SÉJOUR LIMITÉ</p> <p>Documents obligatoires Documents obligatoires</p>	 <p>RADIATION CONTROLLED AREA ZONE CONTRÔLÉE</p> <p>HIGH RADIATION / HAUTE RADIATION</p> <p>Documents obligatoires Documents obligatoires</p>	 <p>RADIATION PROHIBITED AREA ZONE INTERDITE</p> <p>NO ENTRY DÉFENSE D'ENTRER</p>
RADIATION / CONTAMINATION		 <p>RADIATION CONTAMINATION CONTROLLED AREA ZONE CONTRÔLÉE</p> <p>Documents obligatoires Documents obligatoires</p>	 <p>RADIATION CONTAMINATION CONTROLLED AREA ZONE CONTRÔLÉE</p> <p>LIMITED STAY / SÉJOUR LIMITÉ</p> <p>Documents obligatoires Documents obligatoires</p>	 <p>RADIATION CONTAMINATION CONTROLLED AREA ZONE CONTRÔLÉE</p> <p>HIGH RADIATION / HAUTE RADIATION</p> <p>Documents obligatoires Documents obligatoires</p>	

Figure 1.5: Radiation signage at CERN as function of the radiological hazard. Adapted from Ref. [10].

accelerator magnets and frequent interventions are performed to carry out technical work *in situ* to upgrade and maintain the different components of the accelerators. If we combine this with the radiological hazards present in many areas of the laboratory premises, it can be seen that the assessment of fire risks and potential consequences, the definition and implementation of protocols and mitigation measures, as well as firefighting, can be remarkably challenging.



Figure 1.6: Large Hadron Collider (LHC) tunnel at CERN. Source: CERN.

CERN has a specialised fire brigade, familiarized with the laboratory premises and prepared to intervene around the clock when the need arises. Nonetheless, the complexity of the facilities and their radiological hazards often require dedicated studies to successfully prevent, mitigate and face potential accidental fires. To carry out these studies, the HSE unit of CERN launched the FIRIA project [12, 13]: a Fire Induced Radiological Integrated Assessment for facilities facing fire and radiological risks. Its aim is to develop an integrated approach to quantitatively assess potential discharges of radioactive substances induced by a fire accident in particle physics' experimental facilities using

state-of-the-art tools and methods to study the radioactive source term, fire dynamics, evacuation, intervention time, environmental dispersion and dose assessment. Prior to the initialization of the FIRIA project, the radiological risk induced by a fire was evaluated by using envelop cases that often grossly overestimated its impact [14]. The facilities that are object of an assessment in the framework of this project usually have one of the following characteristics:

- High fire risk due to the amount and type of combustible materials, complexity of the evacuation routes, difficult firefighting intervention, *etc.*
- High radiological risk in terms of activation or contamination of combustible materials and absence of emergency retention systems for critical radionuclides.
- Strategic importance for CERN and lack of a recent fire risk assessment.

The ultimate goals pursued by each assessment can be summarized as below:

- The life safety of the occupants of the affected facility and the firefighters.
- Protection of the public, members of the CERN personnel and the environment against the harmful effects of ionising radiation.
- Protection of property and continuity of operations.

As it is used in the present document, the *radiological source term* of an accidental fire is defined as the inventory of radionuclides —species and quantities— that is released from activated materials as a consequence of fire. Its accurate determination is of the utmost importance in order to estimate the potential radiological consequences derived from such an event.

1.4 The need for this work

In the past the combustion of activated material (*e.g.* cable insulation) was considered as the only radionuclide release mechanism due to fire in most studies. Yet, the requirement of exhaustive radiological source terms for this type of scenarios in the context of the FIRIA project has revealed the need to evaluate the contribution of a second mechanism: the *out-diffusion* of radionuclides due to the high temperatures reached in the fire and surroundings. We refer as out-diffused to those radionuclides initially placed in the matrix of a solid, which due to thermally promoted diffusion reach the surface of the object that contains them and manage to escape from it, subsequently being released to the environment. It is common in the accelerator complex to find substantially activated components, often made out of metallic materials that one would not expect to be incinerated in a typical fire. Nonetheless, given the absolute activity of such pieces, even a very small relative amount of radionuclides escaping from them could have a significant impact on the radiological source term. Therefore, a complete neglect of this phenomenon would probably underestimate the radiological hazard of a fire. On the contrary, assume a release scenario of 100 % could be

grossly over-conservative, suggesting the implementation of exaggerated mitigation measures with serious economic and operational consequences.

The work presented in this manuscript aims at meeting the need for an accurate assessment of this phenomenon by designing, implementing and benchmarking a simulation software to be used to realistically estimate the contribution of radioisotope out-diffusion to radiological source terms for a vast variety of possible fire scenarios. In particular, this tool will allow the future user to evaluate the out-diffusion of an arbitrary number of different radionuclides from arbitrarily complex geometries according to arbitrary 3-D temperatures maps.

Diffusion and random walks

Contents

2.1	Diffusion	11
2.1.1	Microscopic perspective	11
2.1.2	Phenomenological perspective	14
2.2	Connection between diffusion and random walks	15
2.3	Diffusion coefficient	16

UNDERSTANDING diffusion in solids is key to eventually meet the goals of this thesis. The present chapter aims to give a general but not exhaustive view of this phenomenon. In particular, we will approach it from two different perspectives, the microscopic and the phenomenological, to later reconcile both visions by exemplifying how they are connected. We will then take a closer look to an important and recursive parameter: the diffusion coefficient. The content presented here is mostly based in Refs. [15–17].

2.1 Diffusion

2.1.1 Microscopic perspective

First, we will approach the diffusion phenomenon from a microscopic point of view. From this perspective, diffusion is nothing other than *Brownian motion* of atoms or molecules. Everything spins around one simple fact: atoms can move even through solids. They move due to their thermal energy, which makes them vibrate frenetically around their equilibrium position following a Maxwell–Boltzmann distribution of the velocities.

In this work, we are interested in solids and, particularly, in crystalline ones. These solids can be imagined as perfectly ordered atomic networks with their subsequent inter-atomic potential. Most hops of the vibrating atoms will find the potential well driving the atoms back to their equilibrium position. Nonetheless, sometimes their energy will be sufficient to overcome it, ending up in a different location. This is true for every diffusion mechanism, but let us briefly explain the most important ones before we continue (the reader may want to take a look to Chapter 6 of Ref. [15] for a more exhaustive explanation). Consider a solute atomic species inside a host lattice formed by a different atomic species, the solvent. Then, one can typically find the following mechanisms:

- **Interstitial mechanism:** one could imagine that if the solute atoms are considerably smaller than the solvents, they could stay in normally unoccupied locations of the host lattice. These locations are called interstitial sites and can be used for the solute atoms to diffuse moving from one to another. This mechanism is illustrated in the picture (a) of Fig. 2.1.
- **Collective mechanisms:** they involve the simultaneous movement of more than one atom and are common in amorphous systems. See picture (b) of Fig. 2.1.
- **Vacancy mechanism:** a substitutional solution is created when the solvent and solute atoms are similar in size and therefore, both species are part of the crystal lattice. As you can observe in image (c) of Fig. 2.1, the vacancy mechanism is defect-mediated since it needs a vacancy to be available in the crystal lattice to allow the diffusion of matrix and substitutional atoms. This mechanism is recognised as the dominant one for the diffusion of this type of atoms in metals.
- **Divacancy mechanism:** diffusion can also occur via vacancy agglomerates, as shown in the picture (d) of Fig. 2.1. This mechanism can become important at high temperatures, especially for some crystal structures. The contribution of agglomerates of more than two vacancies is usually negligible.
- **Interstitialcy mechanism:** if an interstitial atom has a similar size than the solvent atoms, diffusion may occur when this atom pushes a matrix atom out of its position in the lattice to take its place. Then, the previous lattice atom will become an interstitial that can also push other atoms out of their position. Note that this is a defect mediated collective diffusion mechanism (illustrated in image (e) of Fig. 2.1), since it requires interstitial sites to be occupied and involve motion of more than one atom.
- **Interstitial-substitutional exchange mechanism:** there are solute atoms that could occupy interstitial and substitutional sites in the host lattice and therefore, they can diffuse in a hybrid way as in the picture (f) of Fig. 2.1. Normally, the proportion of substitutional atoms is greater than that of the interstitials, although the latter generally move much faster through the host lattice.

In general, atomic migration in a solid is the result of successive (typically single-atom) jumps of fixed lengths. The success rate of the jumps follows an exponential dependence of the medium's temperature. To put the impact of temperature into perspective let us consider the vacancy

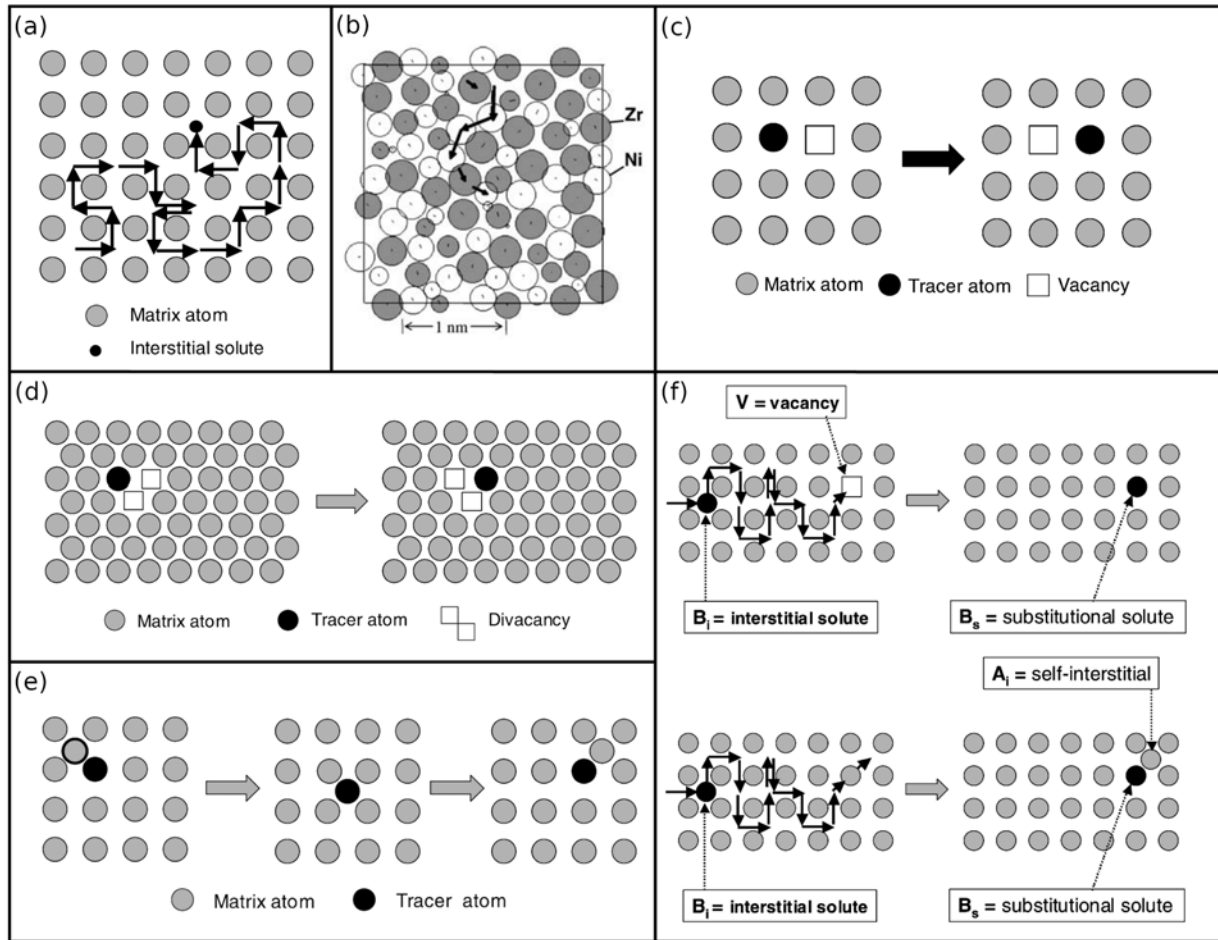


Figure 2.1: Different diffusion mechanisms in solids such as (a) interstitial, (b) collective (atomic chain motion in an amorphous Ni-Zr alloy), (c) monovacancy, (d) divacancy, (e) interstitialcy and (f) interstitial-substitutional (top: dissociative mechanism, bottom: kick-out mechanism). Source: Refs. [15, 18].

mechanism and imagine each atom of the lattice vibrating with a frequency ν of around 10^{13} Hz, and a *migration energy* —energy needed to overcome the potential well— of the order of 1 eV. The probability for an atom to be found with a thermal energy above E [J] is given by $\exp [(-E)/(k_B T)]$, with k_B [J K⁻¹] the Boltzmann's constant and T [K] the absolute temperature. Knowing this, the jumping rate r for an atom would be given by:

$$r = \nu \exp [(-E)/(k_B T)], \quad (2.1)$$

leading us to a jump rate of about 10 successful jumps per day at 25°C, in contrast with the 10^9 jumps per second obtained considering a temperature of 1000°C. Be aware this does not mean that each single atom would jump so many times per second, simply because normally there will be no vacancies available next to it. This is why it is sometimes simpler to think in terms of jumping vacancies, since each atom filling a vacancy will leave a new one after it, and we can easily imagine a vacancy jumping 10^9 times in one second while there will be a similar number of atoms involved.

2.1.2 Phenomenological perspective

From the phenomenological perspective, the equations governing diffusion are known as *Fick's laws* [19, 20], named after their discoverer, Adolf Fick. These laws describe the macroscopic manifestation of the microscopic processes outlined above, and had a purely empirical origin until Albert Einstein derived them from the microscopic theory of diffusion [21].

Fick's laws as they will be shown here are applicable to isotropic media, which is not a major constraint for us since we are mostly interested in solid-state diffusion in cubic metals, where it is isotropic. The extension of the formalism for anisotropic media can be found in appendix A.

Fick's first law relates the diffusion particle flux $\vec{J}(\vec{r}, t)$ to the particle concentration gradient $\nabla C(\vec{r}, t)$ in a point \vec{r} for a given time t as shown below:

$$\vec{J}(\vec{r}, t) = -D\nabla C(\vec{r}, t). \quad (2.2)$$

The factor D is known as the *diffusion coefficient* and it will depend, in general, on the diffusing particles, the host material and the temperature in a way that will be detailed later. Note that this equation is analogous to *Fourier's law of heat flow*¹ and to *Ohm's law*². If we consider now the number of particles to be conserved during the diffusion process, we will end up with a continuity equation such as:

$$\nabla \cdot \vec{J}(\vec{r}, t) = -\frac{\partial C(\vec{r}, t)}{\partial t}. \quad (2.3)$$

Combining both, Fick's first law and the continuity equation, we derive Fick's second law, also called *diffusion equation*:

$$\frac{\partial C(\vec{r}, t)}{\partial t} = D\nabla^2 C(\vec{r}, t), \quad (2.4)$$

where we have assumed a concentration-independent diffusion coefficient, giving rise to a linear second-order partial differential equation relating the particle concentration evolution to its gradient divergence. The trained eye will recognise similarities with other important equations in physics, as the *time-dependant Schrödinger equation* for free particles³. Eq. (2.4) is the one to be solved in order to calculate the evolution of our radionuclide concentrations in case of fire.

To summarise the phenomenological view, we could state that concentration gradients are a driving force for particle currents, eventually leading to an equalisation of the concentration in the absence of particle sinks and sources.

1 $\vec{J}_q(\vec{r}, t) = -\kappa\nabla T$.

2 $\vec{J}_e(\vec{r}, t) = -\sigma\nabla V$.

3 $\frac{\partial \Psi(\vec{r}, t)}{\partial t} = \frac{i}{\hbar} \left(-\frac{\hbar^2}{2m}\right) \nabla^2 \Psi(\vec{r}, t)$.

2.2 Connection between diffusion and random walks

The use of *random walks* is a very pedagogical way of showing the connection between the microscopic and the phenomenological visions. Let us start by considering a single atom that can jump a distance Δx to the left or to the right (we constrain ourselves to 1-D for simplicity) each time interval Δt , with probability $1/2$ for both directions (here we are assuming isotropic media). Let us then define $P(m, n)$ as the probability of finding the particle at a position $m\Delta x$ at a time $n\Delta t$ with $\{m = 0, \pm 1, \pm 2, \dots, \pm n; n = 0, 1, 2, \dots\}$. Then, considering $P(0, 0) = 1$ (we place the atom initially at the origin), we can see that:

$$P(m, n + 1) = \frac{1}{2}P(m - 1, n) + \frac{1}{2}P(m + 1, n). \quad (2.5)$$

In plain words: the probability of being at a given position at a given time is the probability of being next to it just before $[P(m - 1, n) + P(m + 1, n)]$ multiplied by the probability of jumping to it ($1/2$).

We can now add $-P(m, n)$ to both sides of the equation, getting the following:

$$P(m, n + 1) - P(m, n) = \frac{1}{2}[P(m - 1, n) + P(m + 1, n) - 2P(m, n)], \quad (2.6)$$

We can similarly multiply both sides by $(\Delta x)^2/\Delta t$:

$$\frac{P(m, n + 1) - P(m, n)}{\Delta t} = \frac{(\Delta x)^2}{2\Delta t} \frac{P(m - 1, n) + P(m + 1, n) - 2P(m, n)}{(\Delta x)^2}, \quad (2.7)$$

We would like now to move from our discrete description to a continuous one. This can be done by means of the *continuous limit* considering very small Δx and Δt , which means $\Delta x \rightarrow 0$ and $\Delta t \rightarrow 0$. In this case, $n\Delta t \rightarrow t$, $m\Delta x \rightarrow x$ and $P(m, n) \rightarrow \phi(x, t)$, where $\phi(x, t)$ is the continuous probability density function of finding the atom in a position x , at a time t .

The definition of derivative tells us that:

$$\frac{\partial \phi(x, t)}{\partial t} = \lim_{\Delta t \rightarrow 0} \frac{\phi(x, t + \Delta t) - \phi(x, t)}{\Delta t}, \quad (2.8)$$

and

$$\frac{\partial^2 \phi(x, t)}{\partial x^2} = \lim_{\Delta x \rightarrow 0} \frac{\phi(x + \Delta x, t) + \phi(x - \Delta x, t) - 2\phi(x, t)}{(\Delta x)^2}. \quad (2.9)$$

Taking all of this into account, eq. (2.7) becomes:

$$\frac{\partial \phi(x, t)}{\partial t} = \lim_{\substack{\Delta x \rightarrow 0 \\ \Delta t \rightarrow 0}} \left(\frac{(\Delta x)^2}{2\Delta t} \right) \frac{\partial^2 \phi(x, t)}{\partial x^2}. \quad (2.10)$$

The similarities between Fick's second law [eq. (2.4)] and eq. (2.10) are now clear.

We can define a positive constant D such as:

$$D := \lim_{\substack{\Delta x \rightarrow 0 \\ \Delta t \rightarrow 0}} \left(\frac{(\Delta x)^2}{2\Delta t} \right). \quad (2.11)$$

And therefore we find that:

$$\frac{\partial \phi(x, t)}{\partial t} = D \frac{\partial^2 \phi(x, t)}{\partial x^2}. \quad (2.12)$$

Identifying $\phi(x, t)$ as the concentration $C(x, t)$ we obtain the diffusion equation in 1-D:

$$\frac{\partial C(x, t)}{\partial t} = D \frac{\partial^2 C(x, t)}{\partial x^2}. \quad (2.13)$$

If we finally move to 3-D, we would trivially obtain eq. (2.4). The approach presented here is one of the many variants that can be used to show the link between microscopic and phenomenological descriptions of diffusion. One of the main differences between how Einstein did it for the first time is that he worked using the continuum from the beginning, avoiding the discretization we have considered. Discretization is important for us since it is in the center of how the diffusion problem is faced in our particular case. A similar derivation is also described in Ref. [22].

2.3 Diffusion coefficient

As we advanced before, the diffusion coefficient is the proportionality constant in the diffusion equation and will basically tell us how fast a given species can diffuse within a host material at a certain temperature. It has dimensions of [length²/time] and is commonly expressed in [cm²s⁻¹]. Typically, for metals it is a function of temperature following the Arrhenius formula as we can see below:

$$D = A \exp \left(-\frac{Q}{RT} \right), \quad (2.14)$$

where A [cm²s⁻¹] is the so-called the *frequency factor*, Q [J mol⁻¹] is the *diffusion activation energy*, T [K] is the absolute temperature and R [J K⁻¹ mol⁻¹] is the *gas constant*.⁴ The exact physical meaning of the activation parameters A and Q depends on the acting diffusion mechanisms and the lattice geometry (crystal structure) among other parameters. With some simplification one can generally think of A being related to how the atoms of the lattice vibrate and of Q representing the energy required by them to successfully jump. Depending on the medium of consideration, the diffusion coefficient may not follow a simple Arrhenius behaviour, but should rather be expressed as a superposition of several of them⁵. This is normally related to the presence of various relevant diffusion mechanisms⁶.

4 Depending on the units of Q , it is common to find eq. (2.14) written in terms of k_B , since $R = N_A k_B$, with N_A the Avogadro number.

5 Therefore, a more general expression is $D = \sum_{i=1}^l A_i \exp \left(-\frac{Q_i}{RT} \right)$, where l is the number of terms.

6 It can also be the result of impurities and/or microstructural features in the host material, as grain boundaries or dislocations.

The *diffusion activation parameters* A and Q will depend on the host materials and the diffusing species. Most of the available data comes from experiments so we will need to rely on literature values to perform our calculations. A large compilation of these data pairs can be found in chapter 13 of Ref. [23]. Few examples are compiled in Tab. 2.1 and the resulting diffusion coefficient plotted in the left picture of Fig. 2.2 as a function of the temperature.

Table 2.1: Some experimentally obtained data on the diffusion activation parameters for few elements diffusing in Cu and Al. Source: Ref. [23].

Material	Element	A [$\text{cm}^2 \text{s}^{-1}$]	Q [kJ mol^{-1}]	T. range [K]
Cu	Mn	1.42	204.3	773–976
	V	2.48	215	995–1342
Al	Mg	1.24	130.4	667–928
	Na	$6.7 \cdot 10^{-4}$	97.1	719–863

Allotropy

The material structure is of great relevance for the diffusion coefficient and, accordingly, if one chemical element is ordered following different structures —*allotropy*—, D will be different. Allotropy is common in nature and one of the most well-known examples is Carbon, whose atoms can be ordered following different crystal lattices giving rise to diamond or graphite, among many others. We must keep this in mind as it will be important if we have host materials following different structures (*i.e.* we have different allotropes). This will be the case for iron, whose structure is different depending on its temperature because of few structural phase transitions —having an important impact on the diffusion coefficient. Some examples in Tab. 2.2 and the right picture of Fig. 2.2.

Table 2.2: Some experimentally obtained data on the diffusion activation parameters for few elements diffusing in Fe for different temperature ranges. The Fe phase in which the temperature range is enclosed is also provided. Note the very different activation parameters for the different phases. Source: Ref. [23].

Material	Element	A [$\text{cm}^2 \text{s}^{-1}$]	Q [kJ mol^{-1}]	T. range [K]	Phase
Fe	Co	7.19	260.4	956-1000	α -f
	Co	6.38	257.1	1081-1157	α -p
	Co	1.0	301.9	1409-1633	γ
	Co	6.38	257.1	1702-1794	δ
	Mn	1.49	233.6	973-1033	α -f
	Mn	0.35	219.8	1073-1173	α -p
	Mn	0.16	261.7	1193-1553	γ
	P	$2.87 \cdot 10^2$	271	1078-1153	α -p
	P	$6.3 \cdot 10^{-2}$	193.4	1223-1573	γ

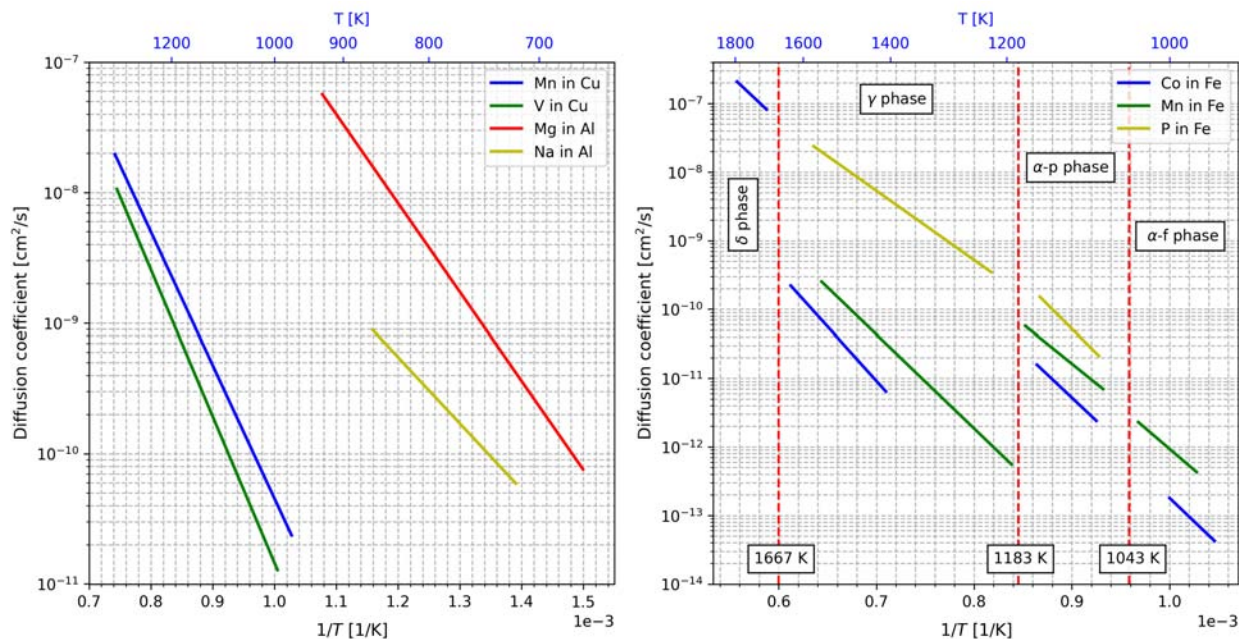


Figure 2.2: Diffusion coefficients as a function of the inverse of temperature for different species and materials. On the right picture we can observe the effect of allotropy in the diffusion coefficient: the different structural phase transitions of Fe occurring at certain temperatures can have a significant impact on it.

Isotope effect

Two isotopes of the same element do not diffuse in exactly the same manner in a given host material. The diffusion coefficient in both cases would be different because of their different isotopic masses. This difference influences only the frequency factor A and not the activation energy Q , since the interatomic potential is determined by the electronic interaction and hence should remain identical for both isotopes (this may not be the case for light nuclei, where mass-dependant quantum effects are not negligible and could influence Q). Considering the frequency factor to be proportional to the vibration frequency of the atoms of the crystal and using the Einstein's model describing them as a set of independent harmonic oscillators⁷, we can calculate the relative impact of the different masses on the diffusion coefficient. From the harmonic oscillator theory we know that for a given kinetic energy in a defined potential, the vibration frequency is inversely proportional to the square root of the mass, meaning that for two isotopes α and β of the same element, we have the following:

$$\frac{D_{\alpha}}{D_{\beta}} = \sqrt{\frac{m_{\beta}}{m_{\alpha}}}. \quad (2.15)$$

From this relation it follows that the difference would be within few percent (at most) for our cases of interest, and it would be shadowed by the experimental uncertainties of the diffusion coefficients. Due to this modest impact, the quantification of the isotope effect on diffusion generally cannot be

⁷ This assumption is not exactly true, since it has been shown later that coupling between atomic vibrations can be important, but this simplified picture is sufficient for our purposes.

deduced from the determination of the diffusion coefficients of both isotopes separately. Please take a look to the chapter 9 of Ref. [\[15\]](#) for further information.

The code SOLIDUSS

Contents

3.1	Numerical treatment	21
3.1.1	Wiener process	21
3.1.2	The meaning of $n \rightarrow \infty$ in our problem	24
3.2	Implementation	26
3.2.1	How to use SOLIDUSS	27
3.2.2	Internal structure	27
3.3	Further considerations	30
3.4	Isotope tracking optimization	31
3.5	Statistical uncertainties calculation	33
3.6	Nonphysical tests	34
3.6.1	^{60}Co from an irradiated Cu cylinder	34
3.6.2	^{54}Mn from a quadrupole yoke	35

NOW THAT we have briefly introduced the diffusion phenomenon, we will focus on our particular problem. In the present chapter we will introduce SOLIDUSS, the Monte Carlo simulation software that we have developed to provide a versatile solution to simulate the out-diffusion of radionuclides in a wide variate of scenarios. We will explain the numerical treatment on which it is based as well as outline the key aspects of its implementation. The reader's attention will be drawn to several considerations that should be kept in mind when using the software. Then, we will explain the online optimization we have put in place to improve its performance and how to calculate the statistical uncertainties associated to simulation results. Finally, a couple of examples of the code's usage will be shown. From this chapter on, we will repeatedly mention the general purpose Monte Carlo code CERN-FLUKA, which we will simply refer to as FLUKA for conciseness.

3.1 Numerical treatment

In section 2.2 it was shown that random walks emulate the diffusion process under certain assumptions. This well known result suggests that we can simulate diffusion processes using stochastic methods, avoiding the need for deterministic solutions of the diffusion equation often based on the use of Finite Elements Methods that for us would pose a number of difficulties—especially considering diffusion of radionuclides produced in an arbitrary geometry following the interaction of the primary particle beam with material— such as:

- The simulated geometry used to obtain the radionuclide inventory and its spatial distribution via particle physics simulation packages such as FLUKA [24–26] would need to be recreated from scratch as the input format is not compatible. Finite Element packages generally create their meshes from standard CAD (Computer-Aided Design) models that are usually surface-based boundary representation models, whereas particle transport codes require a full volumetric description and typically use boolean Constructive Solid Geometry (CSG) to describe complex objects.
- Results are susceptible to meshing quality, boundary conditions and step sizes of the implemented solver. Therefore, the results need to be accompanied by sensitivity studies assessing the impact of these parameters. For general studies, it would require users with experience in the handling of these tools, which is not common within the radiation protection community.
- Simulations have to be carried out with different packages, one for obtaining the radionuclide inventory and another one for simulating its diffusion, which requires data handling and a perfect duplicate of the simulated system, making the whole process more prone to errors.

Considering all the above, we deem the development of a Monte Carlo based diffusion model internally linked to FLUKA as the best strategy to overcome these difficulties. To do this we need to infer a numerical treatment to be coded in such a tool, and this is why we will come back to the previously discussed random walks.

3.1.1 Wiener process

To simply use random walks to simulate each single atomic jump of the radionuclides would obviously be straightforward but very cumbersome for reasons of computational effort. At the same time, it will not be necessary since we can infer a more suitable numerical treatment to be implemented in our tool. Let us have a look at the probability distribution associated to the radionuclide's position after $n \rightarrow \infty$ atomic jumps [17,22,27]. Consider then the already mentioned atom that could jump to the right or to the left with the same probability. Its position after n jumps would be $X(t) = S_n \Delta x$, with $S_n = \sum_{i=1}^{i=n} \epsilon_i$ and $\epsilon_i = \pm 1$ (both values with probability 1/2). From this we can see that:

$$\mu(\epsilon_i) = 0, \quad (3.1a) \quad \sigma^2(\epsilon_i) = 1. \quad (3.1b)$$

Where $\mu(\epsilon_i)$ is the mean of the distribution associated to ϵ_i and $\sigma^2(\epsilon_i)$ its variance. Since ϵ_i are real, independent and identically distributed variables, and $\sigma^2(\epsilon_i)$ is positive, we know because of the *Central Limit Theorem*, that the following is true for all $-\infty < a < b < +\infty$:

$$\lim_{n \rightarrow \infty} P \left(a < \frac{S_n - n\mu(\epsilon_i)}{\sqrt{n}\sigma(\epsilon_i)} < b \right) = \frac{1}{\sqrt{2\pi}} \int_a^b e^{-\frac{x^2}{2}} dx. \quad (3.2)$$

Where $P \left(a < \frac{S_n - n\mu(\epsilon_i)}{\sqrt{n}\sigma(\epsilon_i)} < b \right)$ is the probability of finding $\frac{S_n - n\mu(\epsilon_i)}{\sqrt{n}\sigma(\epsilon_i)}$ between a and b . In order to use eq. (3.2), we can express the position of our atom after n jumps as follows:

$$X(t) = S_n \Delta x = \left(\frac{S_n - n\mu(\epsilon_i)}{\sqrt{n}\sigma(\epsilon_i)} \right) \sqrt{n}\sigma(\epsilon_i) \Delta x, \quad (3.3)$$

where we have used that $\mu(\epsilon_i) = 0$. We can see that:

$$\begin{aligned} \lim_{\substack{n \rightarrow \infty \\ t = n\Delta t}} P(a < X(t) < b) &= \lim_{\substack{n \rightarrow \infty \\ t = n\Delta t}} P \left(a < \left(\frac{S_n - n\mu(\epsilon_i)}{\sqrt{n}\sigma(\epsilon_i)} \right) \sqrt{n}\sigma(\epsilon_i) \Delta x < b \right) \\ &= \lim_{\substack{n \rightarrow \infty \\ t = n\Delta t}} P \left(\frac{a}{\sqrt{n}\sigma(\epsilon_i) \Delta x} < \frac{S_n - n\mu(\epsilon_i)}{\sqrt{n}\sigma(\epsilon_i)} < \frac{b}{\sqrt{n}\sigma(\epsilon_i) \Delta x} \right). \end{aligned} \quad (3.4)$$

If we substitute $n = t/\Delta t$ and apply eqs. (3.1b) and (3.2):

$$\begin{aligned} \lim_{\substack{n \rightarrow \infty \\ t = n\Delta t}} P(a < X(t) < b) &= \lim_{n \rightarrow \infty} P \left(\frac{a}{\sqrt{\frac{t}{\Delta t}} \sigma(\epsilon_i) \Delta x} < \frac{S_n - n\mu(\epsilon_i)}{\sqrt{n}\sigma(\epsilon_i)} < \frac{b}{\sqrt{\frac{t}{\Delta t}} \sigma(\epsilon_i) \Delta x} \right) \\ &= \frac{1}{\sqrt{2\pi}} \int_{\frac{a}{\Delta x \sqrt{\frac{t}{\Delta t}}}}^{\frac{b}{\Delta x \sqrt{\frac{t}{\Delta t}}}} e^{-\frac{x^2}{2}} dx. \end{aligned} \quad (3.5)$$

After a simple variable substitution we obtain¹:

$$\frac{1}{\sqrt{2\pi}} \int_{\frac{a}{\Delta x \sqrt{\frac{t}{\Delta t}}}}^{\frac{b}{\Delta x \sqrt{\frac{t}{\Delta t}}}} e^{-\frac{x^2}{2}} dx = \frac{1}{\Delta x \sqrt{\frac{2\pi t}{\Delta t}}} \int_a^b e^{-\frac{x^2}{2t(\Delta x)^2/\Delta t}} dx, \quad (3.6)$$

and therefore:

$$\lim_{\substack{n \rightarrow \infty \\ t = n\Delta t}} P(a < X(t) < b) = \frac{1}{\Delta x \sqrt{\frac{2\pi t}{\Delta t}}} \int_a^b e^{-\frac{x^2}{2t(\Delta x)^2/\Delta t}} dx. \quad (3.7)$$

1 The equivalence of both sides of eq. (3.6) can be shown using, for instance, the change of variable $y = x \cdot \Delta x \sqrt{\frac{t}{\Delta t}}$ and modifying accordingly the integration limits.

As we assumed in the previous chapter, $\Delta t \rightarrow 0$ and $\Delta x \rightarrow 0$, so we can apply once more eq. (2.11) to finally obtain:

$$\lim_{\substack{n \rightarrow \infty \\ t = n\Delta t \\ \Delta x \rightarrow 0, \Delta t \rightarrow 0}} P(a < X(t) < b) = \frac{1}{\sqrt{4\pi Dt}} \int_a^b e^{-\frac{x^2}{4Dt}} dx = \int_a^b \phi(x, t) dx, \quad (3.8)$$

where $\phi(x, t) = \frac{1}{\sqrt{4\pi Dt}} e^{-\frac{x^2}{4Dt}}$ is the probability density function (PDF) of a normal distribution² with $\mu = 0$ and $\sigma^2 = 2Dt$. This equation demonstrates that the probability of finding an atom in a given position after a large number of jumps converges towards the result obtained from a normal distribution centered on the atom's initial position whose variance is proportional to the diffusion coefficient and the diffusion time. This is not surprising, since one could imagine that for a larger time period, the atom would be able to diffuse further. The appropriateness of the assumption $n \rightarrow \infty$ is discussed in section 3.1.2.

It is easy to prove, via simple substitution, that the aforementioned distribution is a fundamental solution of the 1-D diffusion equation. To fully prove it, we would need to assume the radionuclide distribution to be initially collapsed at the origin, meaning $\phi(x, 0) = \phi_0 \delta(x)$, with $\delta(x)$ denoting the *Dirac delta* function. This follows from the fact that we have also used it in the derivation of eq. (3.8) by means of considering one single atom initially placed at the origin.

In light of the previous derivation, we can make use of a standard *Wiener process* (also called Brownian motion) to simulate diffusion employing a mathematically well-defined tool. This process is a real valued continuous-time stochastic process with normally distributed and independent increments and can be understood as the *scaling limit* of random walks (*Donsker's theorem* [28]). This type of stochastic processes $\{W_t\}_{t \in \mathbb{R}, t \geq 0+}$ are characterized by the following properties:

1. $W_0 = 0$.
2. The function $t \rightarrow W_t$ is continuous in t .
3. The process $\{W_t\}$ has stationary and independent increments³.
4. The increment $W_{t+s} - W_s$ follows a normal distribution $\mathcal{N}(0, t)$.

In practice this means that if the diffusion coefficient is known, one can sample the position of a radionuclide after a given diffusion time (big enough to accommodate a large number of atomic jumps) using a multivariate normal distribution. Of course, by doing this we would overlook the presence of boundaries during this step, which are of major importance to us because we

2 The general PDF of a normal distribution with mean μ and standard deviation σ is $\frac{1}{\sigma\sqrt{2\pi}} e^{-\frac{1}{2}\left(\frac{x-\mu}{\sigma}\right)^2}$. In the rest of the document we will use the more compact notation $\mathcal{N}(\mu, \sigma^2)$ to refer to this distribution.

3 Therefore, the Wiener process is a stationary Markov chain and in the absence of drift, which we assumed, a Martingale. Yet, these two properties are simplifications with respect to reality. Short-term memory effects are involved in diffusion as it is mentioned in section 3.3 and imperfections in the solid lattice could lead to local drifts. However, these imperfections are expected to have a very minor or no impact in our estimations and in addition they are *a priori* unknown as they depend on the specific piece of material. Thus, we stick to our model.

are interested in the number of radionuclides reaching an object's surface. In order to resolve this problem, we can split the total diffusion time into a suitable number of sub-steps that are sampled in sequence. This allows for checking the position of the radionuclide after each of them, as schematically shown in Figs. 3.1 and 3.2, and therefore detecting if a given radionuclide reached a surface during its trajectory through the host material.

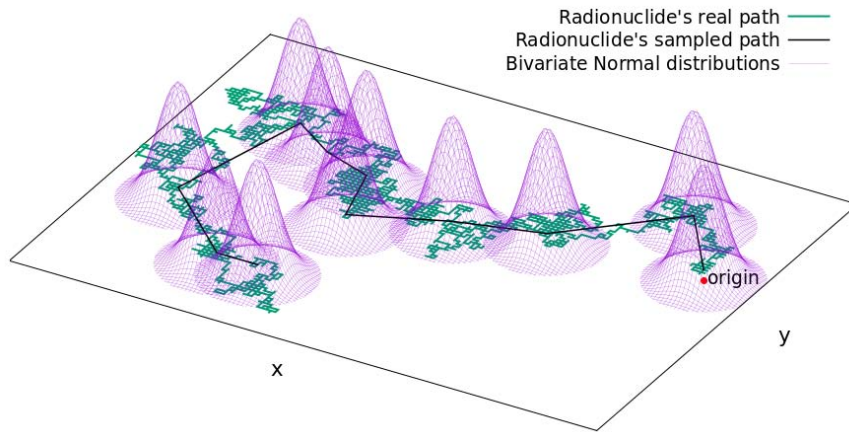


Figure 3.1: Schematic example of the 2-D path followed by a radionuclide and the path that would be obtained by sampling multivariate normal distributions for a given number of time steps. Note that the variances of the normal distributions have been reduced here for illustration purposes, normally these distributions would present a significant overlap.

3.1.2 The meaning of $n \rightarrow \infty$ in our problem

Strictly speaking, what is induced from the example described in section 3.1.1, where we considered a single jumping atom in 1-D is that, after n jumps, the number of jumps to the right (or to the left) follow a *Binomial* distribution. But thanks to the *De Moivre–Laplace theorem* (a special case of the Central Limit Theorem), we know that if n is sufficiently large, the discrete Binomial distribution can be approximated by a Normal one⁴ with:

$$\mu_R = np, \quad (3.9a)$$

$$\sigma_R = \sqrt{np(1-p)}, \quad (3.9b)$$

where n is the total number of trials —jumps in our case—, and p is the probability of success —for instance, the probability of jumping to the right. The natural question that arises now is how large should n be to find the Binomial distribution to be well approximated by the Normal one.

From the discrete point of view (Binomial distribution), the maximum number of successes (*i.e.* jumps to the right) that one can obtain after n trials is clearly n , and the minimum number is 0. If we intend to approximate this behaviour with a continuous approach using the Normal distribution,

⁴ This is what was done in section 3.1.1 in an implicit way, without mentioning the Binomial distribution for the sake of simplicity.

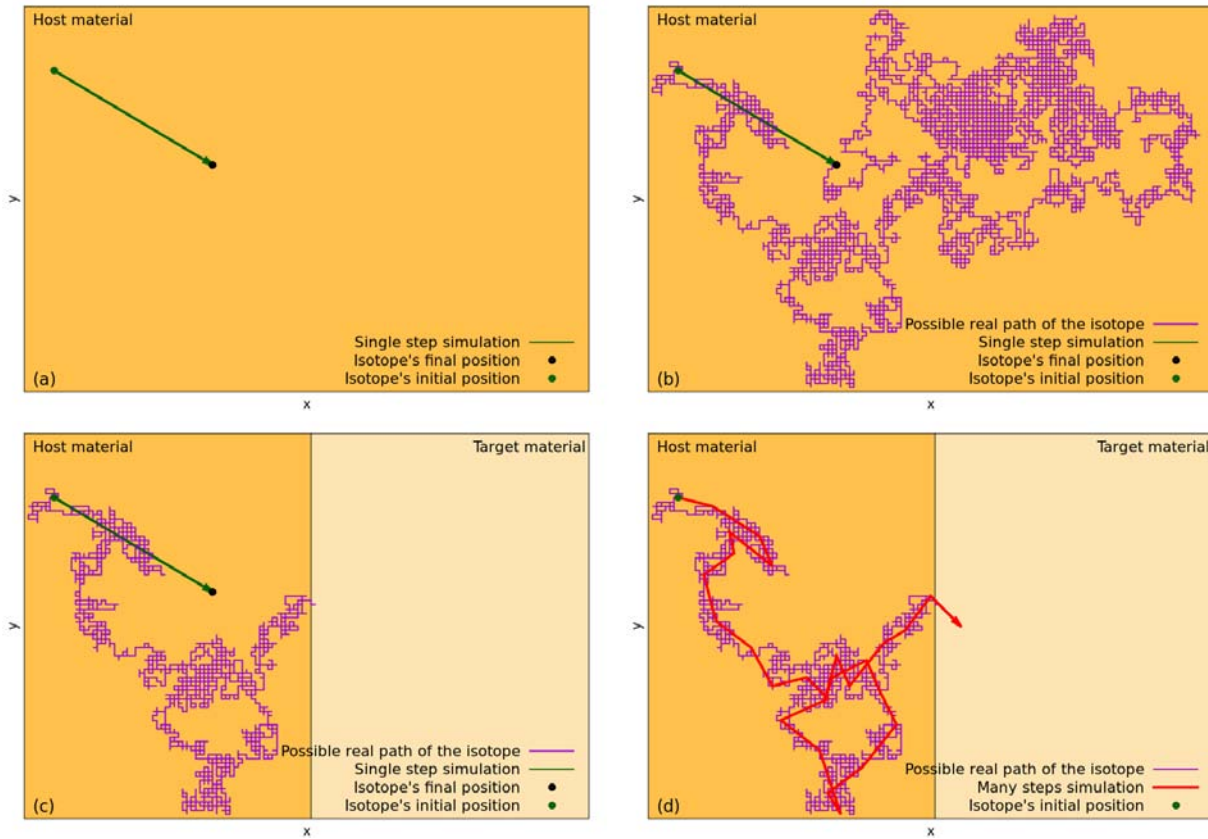


Figure 3.2: Schematic example of the 2-D path followed by a radionuclide used to point out the importance of using small time steps when simulating diffusion near material boundaries. In the images (a) and (b) we can see that a single step is suitable in the absence of boundaries. On the contrary, (c) shows why this approach could lead to wrong results if applied in the neighborhood of material boundaries, assuming as not out-diffused isotopes that actually reached the material surface in their path through the solid lattice. Here it becomes transparent the need of using small time steps to limit the appearance of these events, as shown in the sub-figure (d).

one should seek to minimize the probability of those events with a number of successes above n or below 0. Remember that any value is accessible for the Normal distribution PDF, and it would make no sense to obtain that, after n jumps, a radionuclide performed a negative number of jumps to the right or even more jumps to the right than the total number of jumps. In order to avoid this, one could require the mean to be five standard deviations away from n and 0 (reducing the probability of such an event to a negligible value):

$$0 \leq \mu_R - 5\sigma_R, \quad (3.10a)$$

$$\mu_R - 5\sigma_R \leq n. \quad (3.10b)$$

By simply substituting eqs. (3.9) in the previous expressions, and applying that $p = 1/2$ in our case of interest (same probability of jumping to the right as to the left), one can see that both of them lead to a single condition to be satisfied:

$$n \geq 25. \quad (3.11)$$

Therefore, according to our requirements, a number of jumps equal to 25 is sufficient to meet the condition of a large n in 1-D.

3.2 Implementation

The pursued aim of this thesis is the creation of a simple and reliable software that could be used in the context of radiation protection studies whenever it is important to evaluate the potential out-diffusion of radionuclides from arbitrarily complex geometries in case of fire. The developed diffusion software has been named SOLIDUSS [29], which stands for SOLID-state diffUSion Software, and it is mainly written in C++ (following the guidelines in Ref. [30]). This tool takes advantage of the FLUKA geometry kernel to perform out-diffusion calculations in arbitrarily complex geometries. This way, we can obtain the amount of radionuclides out-diffused from a given *source material* into an arbitrary number of *target materials* in any area of interest of our geometry. This is done for a set of diffusion periods as defined by the user⁵ and, in addition, the software will also provide a 3-D map of the radionuclide concentration for each of them. It also offers the possibility of performing multiple diffusion calculations while running a single FLUKA simulation, which is especially useful if we need to assess the out-diffusion of multiple radionuclide species, or if we need to perform a sensitivity analysis over a certain parameter. In addition, SOLIDUSS can make use of a 3-D map of temperatures provided by the user to track the radionuclides accordingly, allowing the user to evaluate out-diffusion based on more realistic scenarios where the temperature is not found to be the same all over the area of interest. To make this possible, SOLIDUSS is linked to FLUKA at two different levels:

- We make use of FLUKA user routines to trigger different actions of the diffusion software (please take a look to the FLUKA manual if you are not familiar with the structure of its input file):
 - USRINI: when provided the USRICALL card in its input file, FLUKA will call the USRINI routine at the beginning of the simulation. From this routine, the creation of the diffusion machinery will be triggered, passing the control to SOLIDUSS until it is fully set up.
 - USRRNC: if requested by means of the USERWEIG card, FLUKA will call the USRRNC routine every time a residual nuclide is stopped⁶, if it is found to be in a region of interest (ROI), a hook into SOLIDUSS is activated which then takes care of the actual diffusion calculation. At the end of it, the simulation control returns to FLUKA.
 - USROUT: including the USROCALL card in the FLUKA input file will provoke a call to the USROUT routine at the end of the simulation, and this will lead to the export of the diffusion simulation results.

⁵ For instance, we could be interested in studying how out-diffusion evolves during a fire, so we would need to request different diffusion times such as 10 min, 30 min, 60 min, etc.

⁶ The initial radionuclide concentration is thus provided by FLUKA and any inaccuracy will have an impact in the diffusion output. The user is advised to pay attention to the correctness of the FLUKA simulation prior analysis of the diffusion results.

- For the actual tracking of radionuclides, SOLIDUSS calls back into the geometry kernel of the Monte Carlo software, which allows for reusing the identical geometry model already used for simulating the creation of radionuclides.

3.2.1 How to use SOLIDUSS

In order to use the software to simulate diffusion in addition to the standard FLUKA calculations, one must carry out the following actions:

- Create the so-called *diffusion input file*, which will include all the information needed to simulate diffusion according to the user preferences (radionuclide of interest, host material, activation parameters, diffusion times, temperature maps, concentration mesh boundaries, etc.). The diffusion input file format is detailed in appendix B.
- Make sure the FLUKA input file includes:
 - The necessary cards to simulate radioactive decays according to the user's needs (e.g. RADDECAY, IRRPROFI and DCYTIMES). Without them, the user routine USRRNC will never be called and there will be no diffusion simulation.
 - Cards USRICALL, USERWEIG with WHAT(5) > 0.0, and USROCALL as it was pointed out before. The SDUM parameter of USRICALL should include the path to the diffusion input file⁷.
- Compile SOLIDUSS and link it against FLUKA to create a combined executable.

Once this setup is accomplished, the procedure to run the simulation is identical to that of a standard FLUKA simulation.

3.2.2 Internal structure

SOLIDUSS is mainly structured as a C++ class that we refer to as *CDiffEngine*, which groups several important classes to meet the different needs of the diffusion procedure. Below you can find a description of the most representative ones:

- *CParameters*: this class groups all the parameters provided by the user and is in charge of feeding the rest of the program with all the information derived from them when necessary.
- *CTracker*: deals with the radioisotope tracking through the geometry. The numerical treatment detailed in section 3.1 is implemented here, using FLUKA functions as GEOREG and GEOFAR to identify the region where the radioisotope is located at any time and determine whether it out-diffused from its host material or not.

⁷ One must remember the eight characters limit for the strings in FLUKA.

- *COptimizer*: this class is designed to perform online optimization operations (if requested by the user) to reduce the computation time consumed by the diffusion simulation whenever it is possible to do so. You can find the basics of the procedure in section 3.4.
- *CExporter*: responsible for exporting the diffusion simulation results in accordance with the output formats described in appendix C.

The 3-D maps created during the diffusion calculations (either for radionuclide concentrations or temperatures) are stored in another important class called *CMeshGrid*, which helps us organize and access these data optimally.

Now that we have outlined the internal structure of the program, please refer to Fig. 3.3 to get a taste of how the diffusion simulation process started by a call to `USRRNC` works.

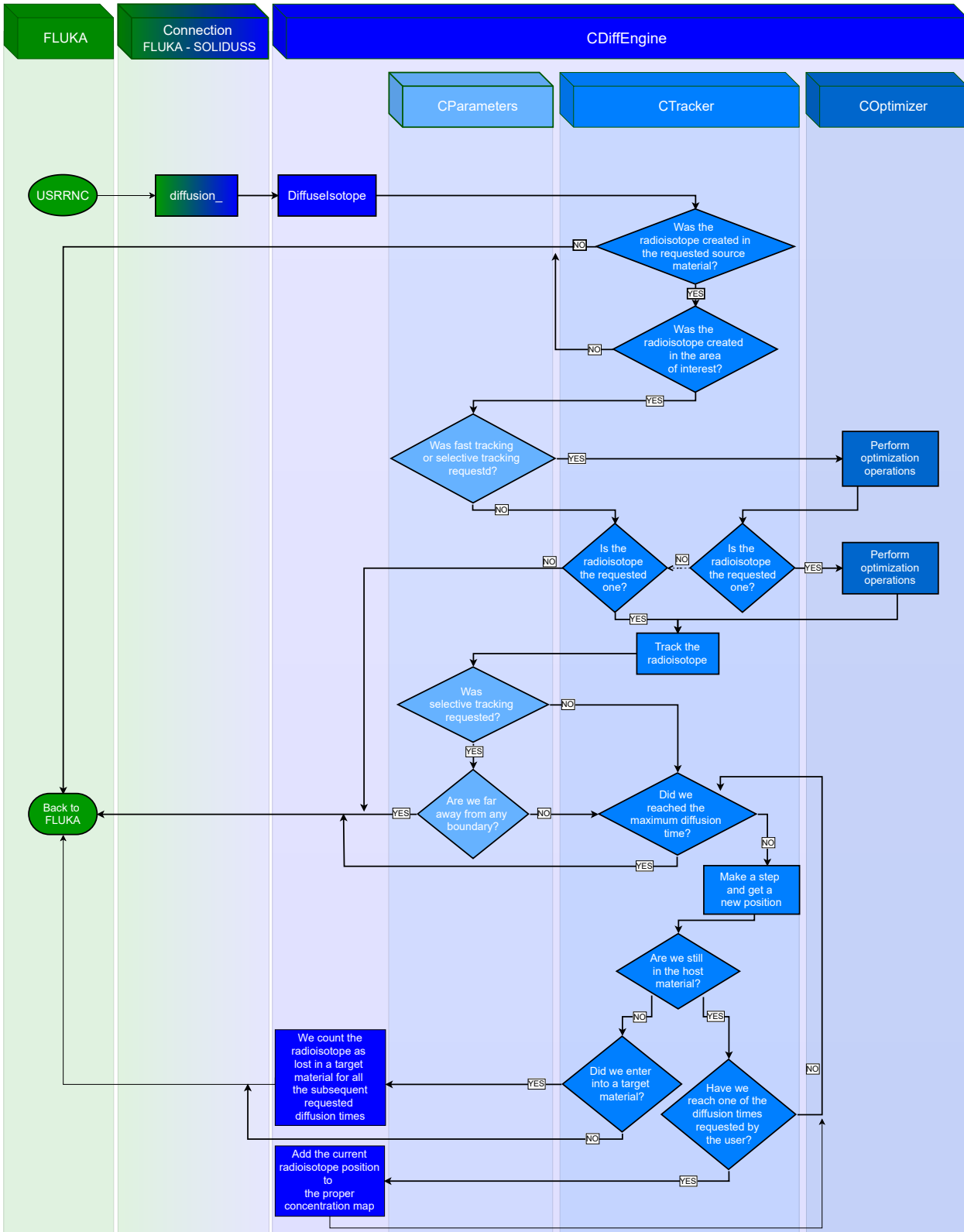


Figure 3.3: Flow chart of the simulation process occurring every time a radionuclide is generated in FLUKA. From the USRRNC routine, the simulation control as well as the characteristics of the new radionuclide are passed to SOLIDUSS. Initially, the program checks whether it is of our interest and, if that is the case, starts tracking it through the host material. Meanwhile, some optimization operations are performed if requested by the user. Every time we reach one of the diffusion times of interest, we save the current position of the radionuclide in order to later obtain the concentration maps. The process finishes when the radionuclide leaves the source material, or the maximum diffusion time requested is reached.

3.3 Further considerations

There are few assumptions in our diffusion model that should be kept in mind by the user. For the sake of clarity and simplicity, we will enumerate them at the risk of being repetitive:

1. We are currently always considering solid and isotropic host materials. This is justified for our applications since diffusion is isotropic in the majority of the materials we are interested in. Extension of the methodology towards anisotropic diffusion is in principle easily possible. However, it would depend on the crystalline structure of the material which generally is not known to the user.
2. Regarding materials that are liquid at typical fire temperatures. Although the numerical treatment should still be valid for static liquids if proper diffusion parameters are provided, the modeled geometry of the originally solid objects would no longer be applicable. Also, for non-static liquids, their flow would significantly impact the out-diffusion fraction in ways that SOLIDUSS cannot predict.
3. It is important to stress the stochastic nature of the tool we are describing and pay attention to the number of histories simulated (amount of nuclides followed for each particular case) as it will be of extreme importance to ensure the statistical significance of the results. The statistical uncertainty associated with each result can be calculated when merging results of different runs (section 3.5).
4. As a general rule, we will assume the isotopic effect on the diffusion coefficient to be negligible, as it is justified in section 2.3. However, this does not prevent the potential users of the software from providing different diffusion coefficients for different isotopes.
5. At this stage we consider as out-diffused every radionuclide reaching the surface of the object that contains it. In later chapters, we will take a closer look to this in order to develop a more realistic approach.
6. After a given diffusion time, the total amount of radionuclides may have been significantly reduced due to decay. This is taken into account by the software, which provides the user with the fraction of radionuclides remaining after the diffusion time by means of a message printed in the output file.
7. Chemical reactions are not simulated by SOLIDUSS and therefore the diffusion of potential compounds containing radioactive elements is not automatically accounted for. Nonetheless, the diffusion of this type of compounds could be simulated by providing its diffusion parameters to SOLIDUSS and requesting the simulation of a given radionuclide as if it was the compound. Note that volatile elements are simulated like any other and their higher diffusivity will be accounted for by using their diffusion coefficient.

3.4 Isotope tracking optimization

The optimization operations executed by SOLIDUSS aim at cutting down the computational time spent in the radioisotope tracking without undermining its correctness or precision. As explained earlier, we sample the position of the radioisotope after a given period of time t , small enough to guarantee a suitable geometrical resolution. However, the calculation time employed in the radioisotope tracking phase strongly depends on the number of simulated steps. From this point of view, $t \rightarrow \infty$ represents the best scenario (computational-wise) since longer time steps imply that less steps are needed to reach the diffusion time requested by the user. Yet, in view of the discussion at the end of section 3.1.1, it follows that we can only increase t without notable influence on the accuracy of the calculations if the radioisotope is sufficiently far from any material boundary, *i.e.* we can assume the host material to be infinitely large.

Let us now imagine a given radioisotope at a distance d from the nearest material boundary, then we could impose a time step that guarantees a 3-D spatial step such as the probability of crossing the boundary is negligible. In such a situation, we can consider the media to be infinitely large. As a consequence of the multivariate normal distribution followed by the radioisotopes position after each simulation step, the distance Δr from their previous position to the new one follows a χ distribution with $k = 3$ degrees of freedom (considering 3-D motion). In general, if X_i are k random variables following $\mathcal{N}(\mu_i, \sigma_i^2)$ distributions, the variable Y (defined below) follows a χ distribution with:

$$Y = \sqrt{\sum_{i=1}^k \left(\frac{X_i - \mu_i}{\sigma_i} \right)^2}, \quad \mu(\chi_k) = \sqrt{2} \frac{\Gamma((k+1)/2)}{\Gamma(k/2)}, \quad \sigma^2(\chi_k) = k - \mu^2, \quad (3.12)$$

Where Γ is the gamma function. Considering our particular case and taking into account that $\mu_i = 0$ and $\sigma_i^2 = 2Dt \forall i$:

$$\Delta r = \sqrt{2Dt} \cdot Y = \sqrt{\Delta x^2 + \Delta y^2 + \Delta z^2}, \quad \mu(\Delta r) = \sqrt{2Dt} \cdot \mu(\chi_{k=3}) = \sqrt{2Dt} \cdot 2\sqrt{\frac{2}{\pi}}, \quad (3.13)$$

$$\sigma^2(\Delta r) = 2Dt \cdot \sigma^2(\chi_{k=3}) = 2Dt \cdot [3 - \mu^2(\chi_{k=3})]. \quad (3.14)$$

We can now impose a probability below $2 \cdot 10^{-7}$ for radioisotope steps larger than the distance d to the nearest boundary⁸, which entails that it is practically impossible for the radioisotope to overtake it. This is true if⁹:

$$d \geq 8.7\sigma(\Delta r) = 8.7 \cdot \sqrt{2Dt \cdot [3 - \mu^2(\chi_{k=3})]}. \quad (3.15)$$

8 The choice of this probability is to some extent arbitrary and can be easily modified. The logic behind the selected value meets two conditions: i) probability below or equal that one of finding values outside the $\mu \pm 5\sigma$ interval for a Normal distribution ($\simeq 5.7 \cdot 10^{-7}$). ii) Return a relatively round scaling factor for eq. (3.15): 8.7 in this case.

9 Note that we are dealing here with a χ distribution, not a Normal.

Hence, the maximum time step that meets the above is:

$$t_{max} = \frac{d^2}{8.7^2 \cdot 2D \cdot [3 - \mu^2 (\chi_{k=3})]} \simeq \frac{d^2}{68.654D}. \quad (3.16)$$

As a result, if we know d , we will be ready to cut down the number of steps that we need to track by extending the interval t up to the maximum given by eq. (3.16). Remember that SOLIDUSS samples step after step until the diffusion time requested by the user is reached or the radioisotope escapes the host material or the area of interest. Eq. (3.16) must then be met in each of those steps prior adjustment of d . This is the approach used by SOLIDUSS when *fast tracking* is requested. The distance d , which is indispensable to take advantage of the procedure, is provided by FLUKA¹⁰ at the beginning of the radioisotope tracking but, unfortunately, it is not always available. In those cases, the tracking cannot be optimized and the software resorts to the original strategy.

If *selective tracking* is requested, a similar but simpler technique is implemented. Let the radioisotope be found at a distance d from the nearest boundary greater than $8.7 \cdot \sqrt{2Dt_T \cdot [3 - \mu^2 (\chi_{k=3})]}$, where t_T is the total diffusion time requested by the user. In this case, the radioisotope motion is not simulated at all since its chances of out-diffusing from the host material are negligible (*i.e.* it is really far away from any boundary). Instead, the simulation control is returned to FLUKA, as we can see in Fig. 3.3.

On the step length

As introduced earlier, the step length of a radioisotope after a diffusion time t is given by a χ distribution with as many degrees of freedom (k) as spatial coordinates we are considering. This may not be obvious at first, since one is often used to discuss in terms of positions instead of distances. To better understand this, let us imagine a large number of radioisotopes initially located at the origin of the 2-D euclidean space. The concentration distribution after one step is shown in Fig. 3.4 and, as expected, it follows a bivariate normal distribution centered in the initial location of the radioisotopes. In the coloured projection of Fig. 3.4 we have drawn few annuli; the radioisotopes inside each of them are approximately at the same distance from the origin (imagine the annuli's width tending to zero). We can estimate the number of radioisotopes at a given distance by weighing the radioisotope concentration inside the appropriate annulus (note its radial symmetry) with its area. It is clear from the figure that annuli's area increase with increasing distance with respect to the origin. As a consequence, even if the concentration is high nearby the center of the normal, the total number of radioisotopes inside a given ring may be small due to a small surface. One can figure out that, for a ring surface tending to 0, the amount of radioisotopes inside it will also tend to 0 (assuming a finite concentration). At the opposite limit, far from the origin, the surface of the rings tends to infinite, but the amount of radioisotopes inside them will tend to 0 once more since the concentration decreases faster (exponentially) than the surface increases (linearly if we consider constant ring widths). As a result of the compromise between these two variables, the distance from the initial radioisotope position to its new location

¹⁰ Most of the times through a variable called DDNEAR.

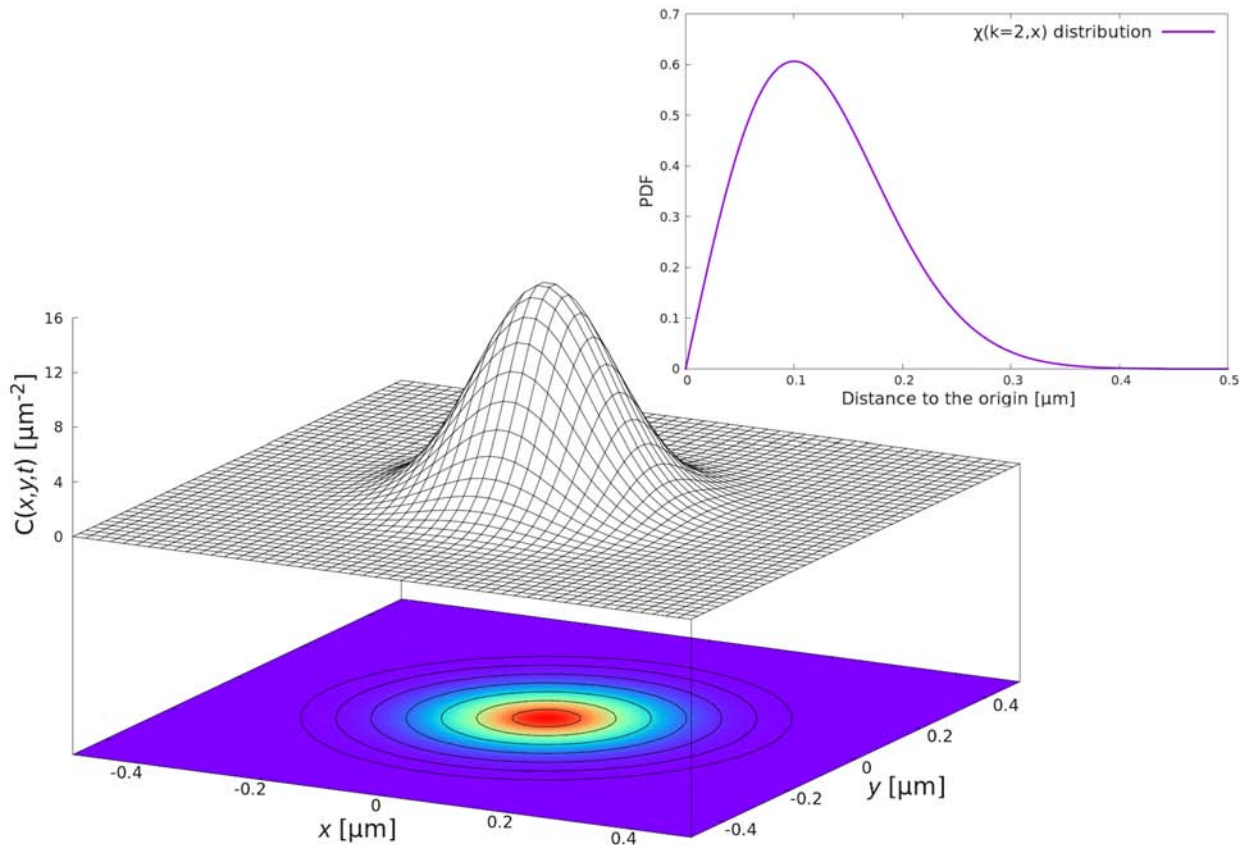


Figure 3.4: The main plot shows the 2-D concentration of radioisotopes initially placed at $x = y = 0$ after a diffusion time t . The inset plot shows the PDF of their distance to the origin after the diffusion time.

after one step follows the aforementioned χ distribution, whose PDF for $k = 2$ (2-D case) is also shown in Fig. 3.4. The same applies to 3-D, but this time one should think in terms of spherical crust volumes instead of ring surfaces.

3.5 Statistical uncertainties calculation

We assume that a diffusion simulation, as any FLUKA simulation, consists of several runs which produce different estimations for a given quantity (*e.g.* the radioisotope concentration in a specific bin of the grid, the fraction of isotopes out-diffused, *etc.*). In order to obtain a more accurate estimation of it, the user should merge the results of the various runs calculating the expected value of every magnitude of interest x , as well as the variance associated to it.

Thanks to the Central Limit Theorem, we know that the estimations provided by each run are normally distributed, but at the same time we have no information about their standard deviations. Since typically we use a limited (and rather small) number of runs, we should rely on the *Student's*

t-distribution [31] to get the desired magnitudes, and thus:

$$\langle x \rangle = \frac{1}{n} \sum_{i=1}^N n_i x_i, \quad s^2(\langle x \rangle) = \frac{1}{N-1} \left[\frac{\sum_{i=1}^N n_i x_i^2}{n} - \langle x \rangle^2 \right], \quad (3.17)$$

where x_i is the value obtained for x in the i -th run, n_i the number of histories simulated in the i -th run, $n = \sum_{i=1}^N n_i$ is the total number of histories, s^2 is the variance and N the number of runs.

3.6 Nonphysical tests

In this section we present results obtained from two FLUKA + SOLIDUSS simulations, which aim to illustrate some of the software capabilities. We describe these tests as nonphysical because we have used extreme temperatures—above the melting point of the simulated materials—to magnify diffusion consequences for instructional reasons.

3.6.1 ^{60}Co from an irradiated Cu cylinder

For this example, a Cu cylinder of 0.2 cm radius and 30 cm long has been irradiated using a 10 GeV proton beam impinging in the center of one of its bases. Radioactive decays are activated using the FLUKA RADDECAY card. Through the diffusion input file, we requested the simulation of the diffusion of ^{60}Co produced inside the Cu cylinder. A temperature gradient inside the cylinder was also provided, sticking to the instructions detailed in appendix B.

In the background of Fig. 3.5 the temperature gradient is shown, which evolves linearly as a function of the z coordinate from 2000 K to 500 K (see the second y axis). Note that the cylinder is parallel to this coordinate, as schematically shown at the bottom of the figure. In this simulation, we are interested in the ^{60}Co distribution along the cable and its evolution after given diffusion times, as well as in the fraction of radionuclides out-diffused from it. All this information is therefore requested using the diffusion input file. As a result, in Fig. 3.5 we can observe several point sets that represent the radionuclide concentration at a given depth in the cylinder for different diffusion times. The shaded regions surrounding them are 1σ confidence intervals. The radionuclide concentration for a diffusion time equal to 0 s is just the initial radionuclide distribution before diffusion, which is a pure FLUKA result. As we can see in the figure, the concentration in those areas with very high temperatures changes fast, while those in low temperatures areas do not experience a visible evolution. The reduction of radionuclides, visible in the left side of the figure is due to the out-diffusion of many of them. In particular, after 10, 30 and 120 minutes of diffusion, SOLIDUSS estimates the out-diffusion of $16.75 \pm 0.12 \%$, $33.0 \pm 0.2 \%$ and $50.0 \pm 0.2 \%$, respectively.

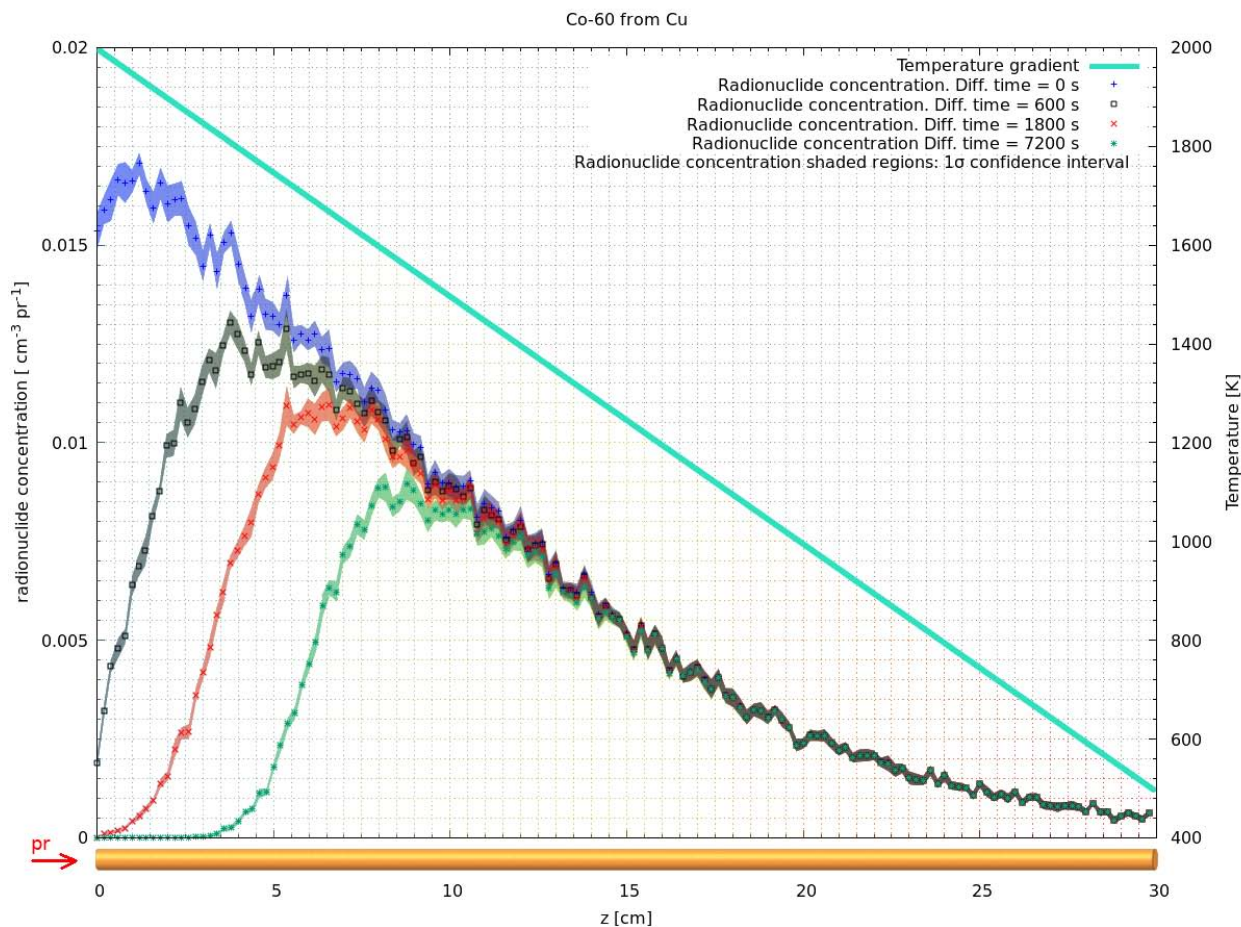


Figure 3.5: Radionuclide concentration along a Cu cylinder irradiated with a 10 GeV proton beam after several diffusion times. The temperature gradient along the cable is also plotted and its values can be found in the right y axis. The reduction of radionuclides due to out-diffusion is clearly visible in those areas with very high temperatures.

3.6.2 ^{54}Mn from a quadrupole yoke

We now consider an LHC quadrupole to study the diffusion of ^{54}Mn produced in its yoke, which we have assumed being made of pure Fe. A cross section of this quadrupole is shown in the upper left image of Fig. 3.6, where we can see the magnet yoke and coils. The temperature gradient is similar to that of the previous example, but this time the maximum temperature is 3000 K, decreasing as the x coordinate increases down to about 1100 K (see upper right image of Fig. 3.6). In this example we have chosen to uniformly distribute the initial position of the radionuclides in the yoke volume and let them diffuse during two hours.

Initial and final distribution maps are shown in the lower images of the previously mentioned figure, where we can appreciate a significant decrease of the radionuclide concentration in those bins with high temperatures and located nearby a yoke surface. As expected, the concentration in those areas far from any surface remains unchanged, on average. The reduction of the concentration in a bin due to radionuclides leaving it is compensated by those arriving from neighboring bins

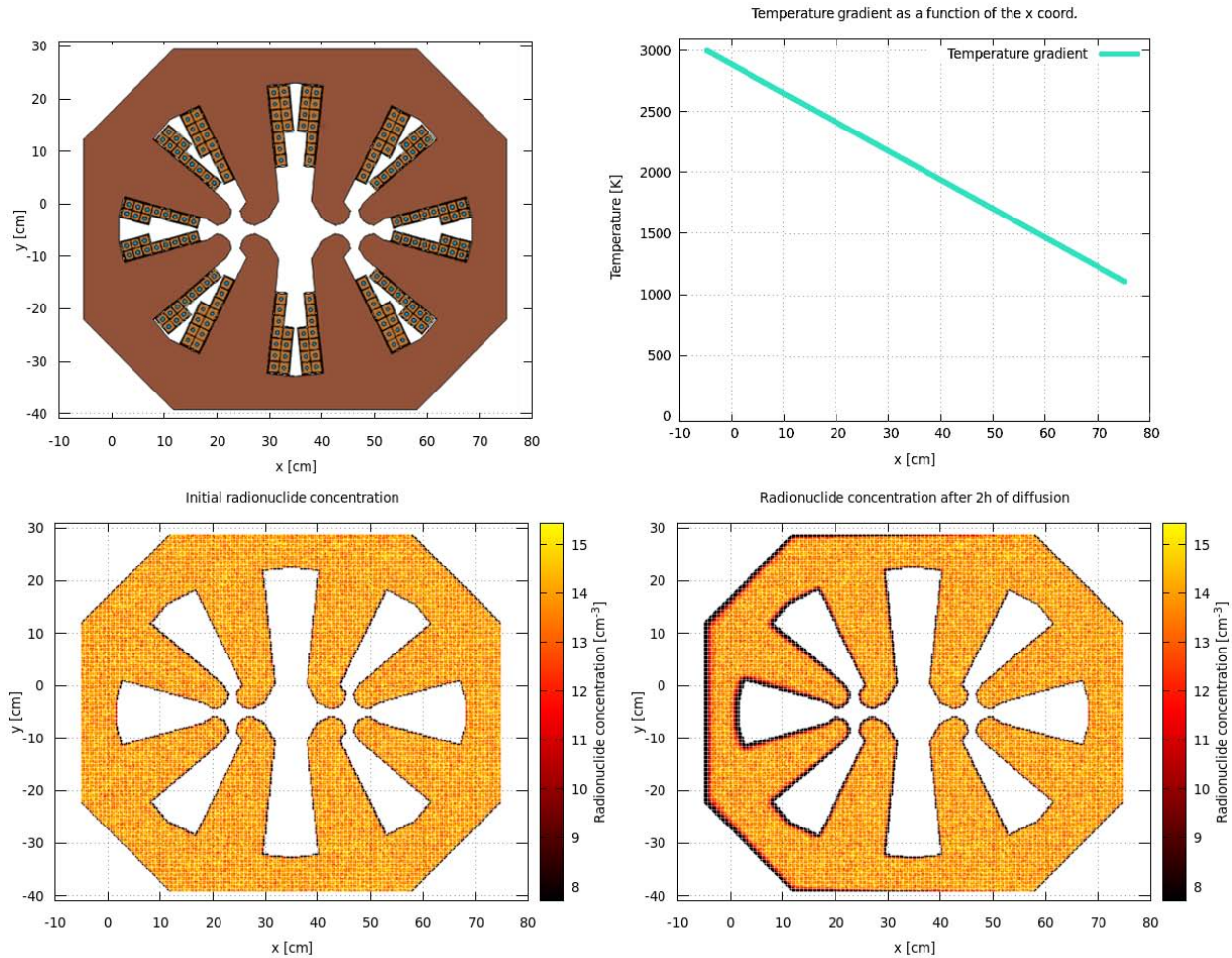


Figure 3.6: Diffusion of ^{54}Mn in an LHC quadrupole yoke (cross section). Upper left: magnet geometry generated using Flair [32]. Upper right: temperature gradient in the simulated volume, it is only a function of the x coordinate. Lower left: initial distribution of radioisotopes as a result of uniform random sampling. Lower right: distribution after two hours of diffusion, the reduction of radioisotopes in high temperature areas nearby the yoke surfaces due to out-diffusion is clearly visible.

in any direction. The only sinks of radionuclides are the yoke surfaces, since we are assuming (as discussed in previous sections) that a radionuclide is out-diffused whenever it reaches a surface.

More detailed information on the concentration variation is shown in Fig. 3.7. In that figure, we can observe those bins with a reduction of the radionuclide concentration above 20 %, 50 % and 80 %, as well as those bins with an increase in the radionuclide concentration (lower right image). Here the reduction of the radionuclide population near the surfaces is clearer and more pronounced the higher the temperature. The increment (and reduction) of the concentration in areas far from surfaces is due to statistical fluctuations, which are also more pronounced the higher the temperature. There is an important detail in the lower right image of Fig. 3.7: two sharp changes in the concentration variation for $x \simeq 50$ and $x \simeq 70$. Coming back to Fig. 3.6, we can see that for these values of x we find temperatures about 1700 K and 1200 K, respectively. The sharp changes are actually due to Fe structural phase transitions at $T \simeq 1667$ K and $T \simeq 1183$ K

that greatly influence diffusion (as mentioned in 2.3). Knowing this, we provided various diffusion coefficients for different temperatures ranges in the diffusion input file (please refer to appendix B for more details) and SOLIDUSS took care of using them properly. The out-diffused fraction of radionuclides after 2 hours of diffusion was estimated to be around $3.658 \pm 0.005 \%$.

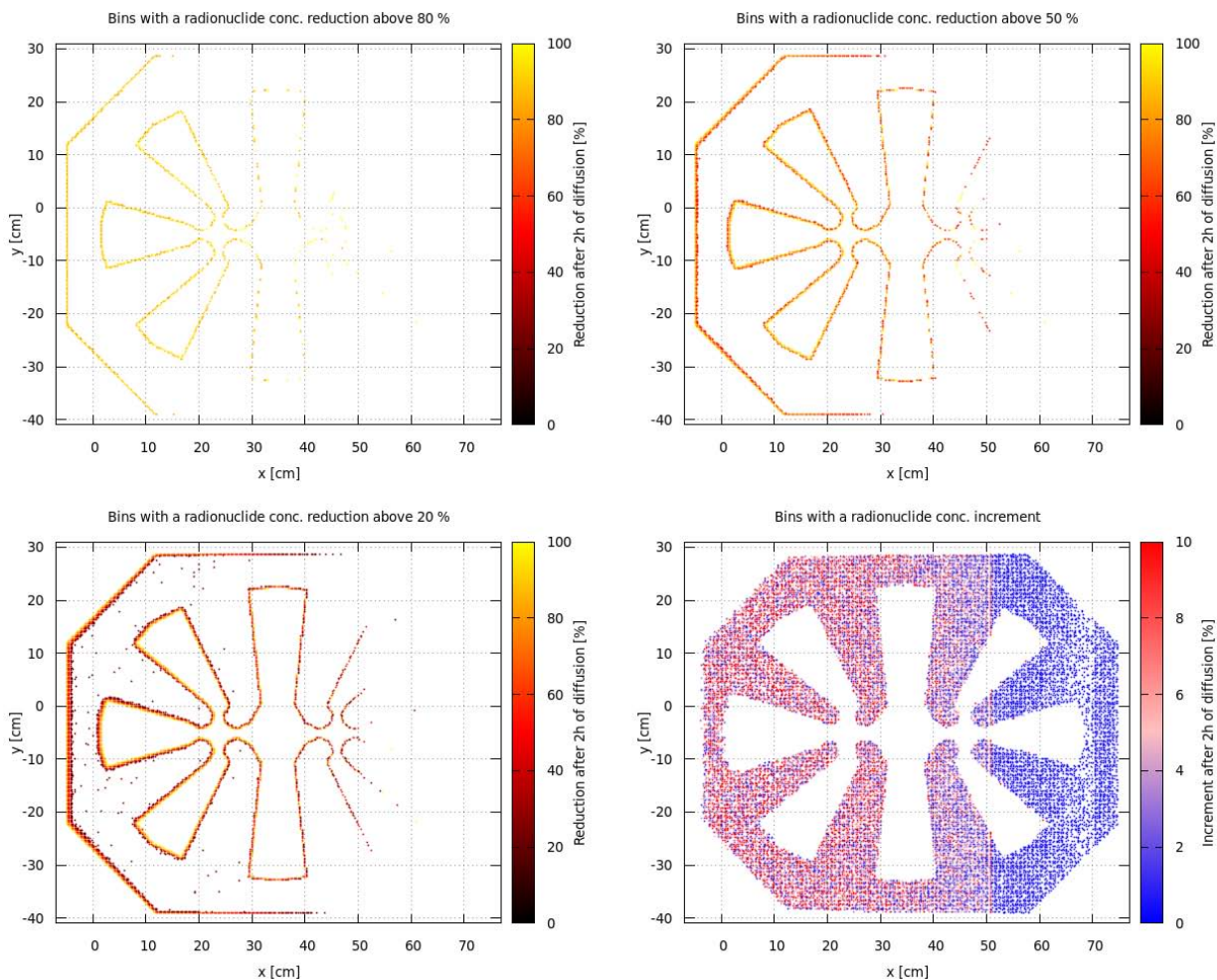


Figure 3.7: Variation of the ^{54}Mn concentration in an LHC quadrupole yoke after two hours of diffusion (cross section). Upper left: only bins with a concentration reduction of above 80 % are shown. Upper right: bins with a reduction above 50 %. Lower left: bins with a reduction above 20 %. Lower right: bins with an increase of the concentration.

Perfect path resolutions

Contents

4.1	Random walk: out-diffusion fraction as a function of the time interval between consecutive position checks	39
4.2	Fitting SOLIDUSS results	40
4.2.1	Different pairs radionuclide - host material	43
4.2.2	Different geometries	44
4.2.3	Different initial distributions	45
4.2.4	Different temperature gradients	46
4.3	Confidence intervals for out-diffusion fraction estimations	47
4.4	Simulation example	48

THESE IS a natural limitation of the simulation approach described in the previous chapter. It is a direct consequence of the use of simulated step lengths greater than real atomic jumps, and entails an underestimation of the out-diffusion of radionuclides. In this chapter we will discuss how to overcome it, obtaining more accurate results while boosting the performance of the software. We will finish looking at a realistic calculation example.

The limitation

The fraction of radionuclides out-diffused from a given object, what we call the *out-diffusion fraction* (ODF), will always be underestimated when calculated using simulated step lengths greater than the real atomic step lengths of the atoms in the solid lattice [29,33]. Note that if a radionuclide reached the surface of an object N_R times during its real path inside of it, its simulation using normal distributions to aggregate a number of atomic jumps in a single simulation step would be able to identify only $N_S < N_R$. This is because even if we check (sample) the position of a radionuclide

often, it may happen that the radionuclide's path would reach a boundary and come back to the host material region between two consecutive position checks. If the final position is known to be inside the material, then we would wrongly consider the radionuclide as not out-diffused. In the limit of simulated steps of the size of real atomic steps we say that the simulation is performed with a *perfect path resolution*. However, this type of simulation is unpractical or even impossible for bulky objects, due to its high consumption of CPU (Central Processing Unit) resources, as mentioned earlier in this document.

The discrepancy between the estimator and the accurate result is therefore influenced by the chosen size of the step lengths (bias), which directly influences the reliability of the final result. A dedicated study showed that the ODF follows a well defined function of the time step used to sample the radioisotopes paths. The extrapolation of this function could be used to obtain a more accurate estimation of the ODF. This behaviour can be observed using a simple random walk simulation, as explained below.

4.1 Random walk: out-diffusion fraction as a function of the time interval between consecutive position checks

Imagine a 1-D crystal lattice and a radionuclide located at the origin ($x = 0$) that can make a jump every second to the right or to the left with same probability. Let us place a boundary at a given position x_b . If at some point we find out that the radionuclide has crossed this boundary, we will consider it as out-diffused from the lattice. Now, we can let the radionuclide move during a time period t and check its position every Δt seconds. By doing this we will see whether the radionuclide is still inside the lattice or, on the contrary, it has traversed the boundary and therefore we must consider it as out-diffused. The radionuclide will keep moving unless we detect it beyond the boundary x_b during one of the checks performed every Δt s. It might very well cross x_b ($x > x_b$) and come back ($x < x_b$) within Δt s. In such a case, it will not be observed beyond the boundary and therefore not accounted for as out-diffused. We performed different simulations for different values of Δt in order to compare the fraction of out-diffused radionuclides that we obtain.

The results considering $N = 2^{20}$ jumps per radionuclide and a boundary placed at $x_b = \sqrt{N} \cdot \Delta s / 2$ (where Δs is the length of a single jump) are shown in Fig. 4.1. This position of x_b was chosen for convenience as explained below. As we can see in the figure, the out-diffusion fraction that we obtained does depend on how often do we check the position of the radionuclides. This dependence perfectly obeys the following function:

$$\text{ODF}(\Delta t) = a \cdot \text{erfc} \left(b \cdot \sqrt{\Delta t} \right) + c, \quad (4.1)$$

where erfc is the *complementary error function* (see Ref. [34] pp. 637-638 for an introduction to this function) and a , b and c are the fit parameters. We know that after N steps, the position of the radionuclide will follow a normal distribution centred on its initial position and with a standard

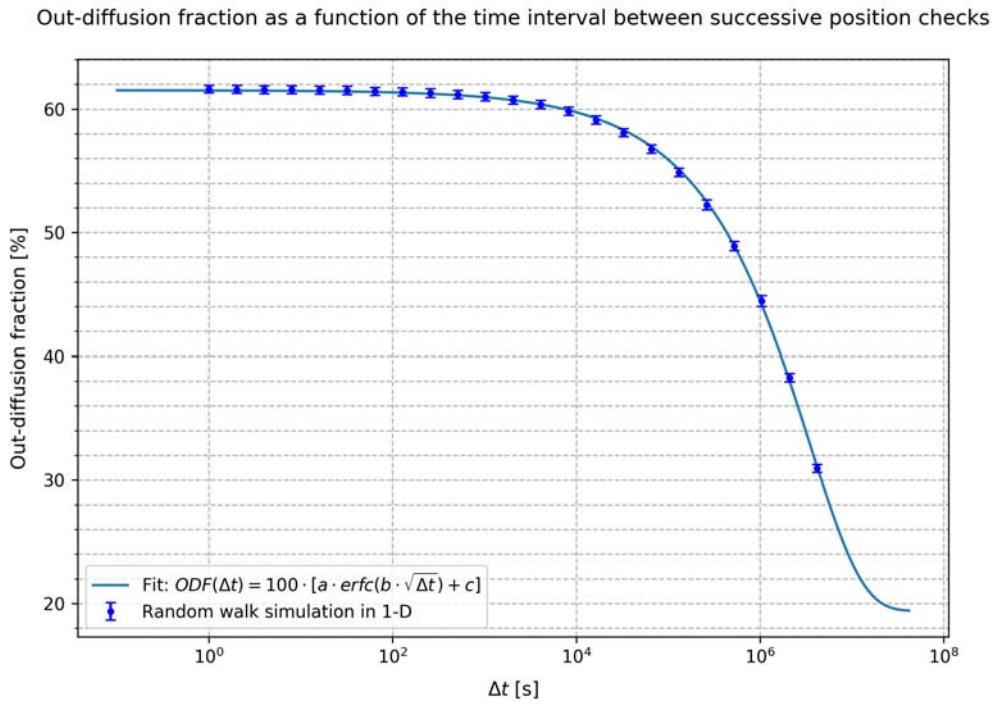


Figure 4.1: Out-diffusion fraction as a function of the time interval Δt between consecutive checks of the radionuclide position for a 1-D random walk considering one jump per second and $N = 2^{20}$ jumps per radionuclide in total. A radionuclide is considered out-diffused if found beyond the position $x_b = \sqrt{N} \cdot \Delta s / 2$, where Δs is the length of a single jump. The fit of these data using eq. (4.1) is also shown.

deviation given by $\sigma = \sqrt{N} \cdot \Delta s$. Therefore, we have located the boundary at a distance of $\sigma/2$ from the initial position of the radionuclides. It can be obtained analytically, using the *reflection principle* for a Wiener process [35, 36], that the out-diffusion fraction (as defined here) would be approximately a 61.8 % of the total number of radionuclides, coinciding with our simulation result for $\Delta t \rightarrow 0$ (see Fig. 4.1).

Eq. (4.1) is a remarkable result since it will allow us to estimate the ODF for tiny time steps just by knowing it for larger ones. In other words, if we have enough data to fit the curve, we can obtain the ODF for any time step, including $\Delta t \rightarrow 0$. The same behaviour has been observed in 2-D and 3-D, as well as for non-trivial boundaries.

4.2 Fitting SOLIDUSS results

Similar results can be observed using SOLIDUSS. Fig. 4.2 shows the ODF of ^{32}P from a Fe cylinder at 1273 K as a function of the time step sizes used when sampling the radionuclides' paths. The initial distribution of radionuclides was considered as uniform within the cylinder and the results are shown for several total diffusion times, which are the duration of the material exposure to high temperatures (*i.e.* to fire). As we can see, the agreement between the fitting function [eq. (4.1)]

and the simulation results is excellent, which corroborates the hypothesis of using it to estimate the real ODF: the one we would obtain for $\Delta t \rightarrow 0$. Nevertheless, using a fitted function for extrapolation purposes should be done with extreme caution; in particular, one should make sure that the tendency of the fitted data in the fit region remains unchanged in the region of interest ([37] pp. 96-99). We are convinced that we should expect nothing else than an asymptotic behaviour of the simulated ODF towards the real value when $\Delta t \rightarrow 0$. To test this assumption, we performed the pure random walk simulation presented earlier, in which this asymptotic tendency has been proven as true down to the minimum time step size possible (that one needed for an isotope to perform a single atomic jump). This is why we believe the use of this fit for extrapolation is justified.

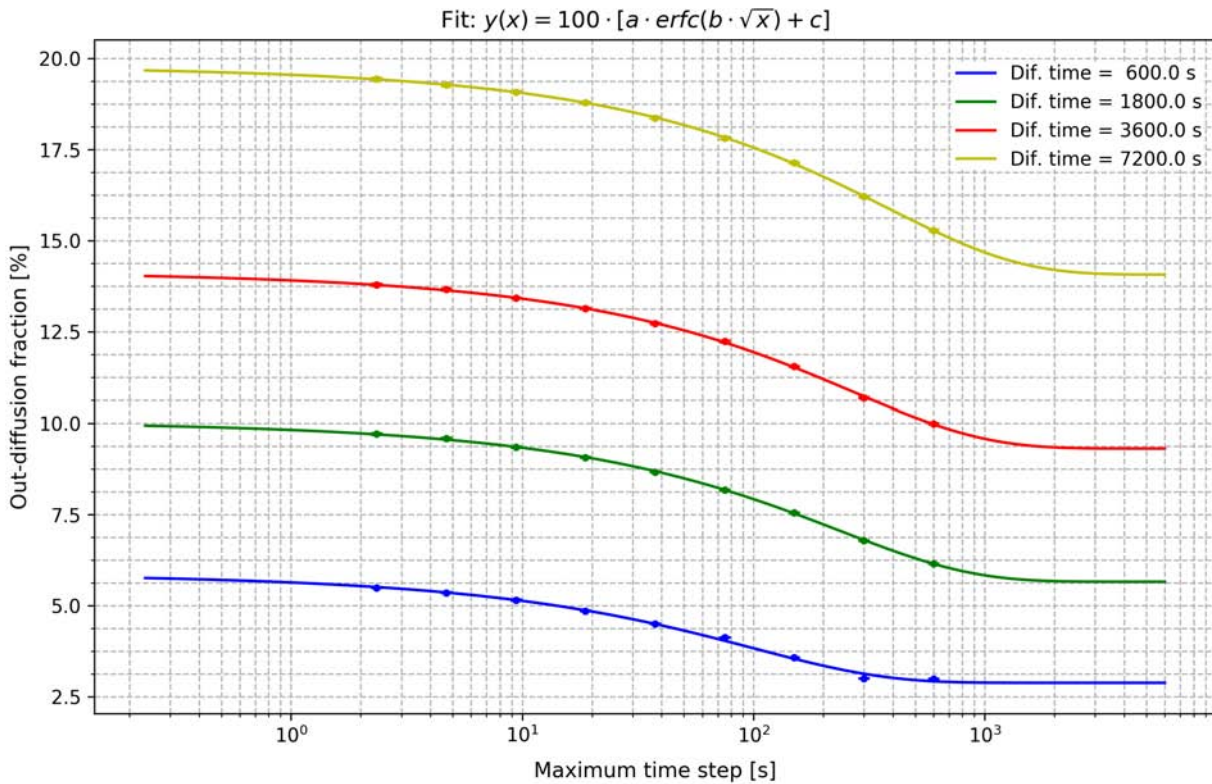


Figure 4.2: Out-diffusion fraction as a function of the time step used in the tracking of the radionuclides for several diffusion times. As expected, the smaller the time step used, the larger the out-diffusion fraction we obtain, saturating as it gets closer to the real value. The curves represent fits to the data obtained using eq. (4.1). The statistical uncertainties of the simulation results are also plotted, but they are too small to be visible.

Once we have obtained the fit parameters, we can estimate the out-diffusion fraction as follows:

$$\text{ODF}(\Delta t \rightarrow 0) = a \cdot \text{erfc}(b \cdot \sqrt{0}) + c = a + c, \quad (4.2)$$

since $\text{erfc}(0) = 1$.

One may suspect that the behaviour shown in Fig. 4.2 is just a consequence of the uniform initial distribution of radionuclides that we have used; or even that this behaviour would be distorted in the presence of non-uniform temperatures. In order to study these hypotheses we have performed a number of tests involving different combinations of radionuclide - host material, geometries,

temperature gradients and non-uniform initial distributions. In the following subsections we will explicitly discuss some of them. The aforementioned behaviour remains present in all of the tests, which allow us to estimate the ODF whenever we have several calculated values for different time steps, even if these values are far from the real fraction. As a consequence, the CPU time needed to estimate an ODF is largely reduced¹, and we obtain a much better approximation of the real ODF. The associated confidence intervals can be estimated using the covariance matrix resulting from the fit and scaling the obtained variance according to the critical values of the Student's t-distribution to account for the small number of data points involved in the fit ([37] pp. 15-16). The post-processing of SOLIDUSS results and the calculations and fits explained here have been automatized by means of C++ and Python² scripts in order to perform accurate estimations of the ODF in a very efficient way, providing plots like Fig. 4.2 that the user can use to judge the quality of the fit and the estimations, as well as the statistical significance of the results. These auxiliary tools would be provided within the SOLIDUSS package.

1 The larger the time step, the smaller the number of steps and hence, the smaller the number of calculations to be performed.

2 In particular, the Python package LMFIT [38] was used.

4.2.1 Different pairs radionuclide - host material

The evolution of the ODF for various diffusion times as a function of the time step sizes for four pairs of radionuclides and host materials can be found in Fig. 4.3. The fit results are shown below each picture, together with the ODF estimation for $\Delta t \rightarrow 0$ obtained using eq. (4.2). Its uncertainty corresponds to a 1σ confidence interval (68.26 % CI) calculated as it will be explained in section 4.3. A cylindrical geometry (cable-like), a uniform initial distribution of radioisotopes and a uniform temperature of 1273 K were considered in the four cases. For all of them, we obtained an almost perfect fit.

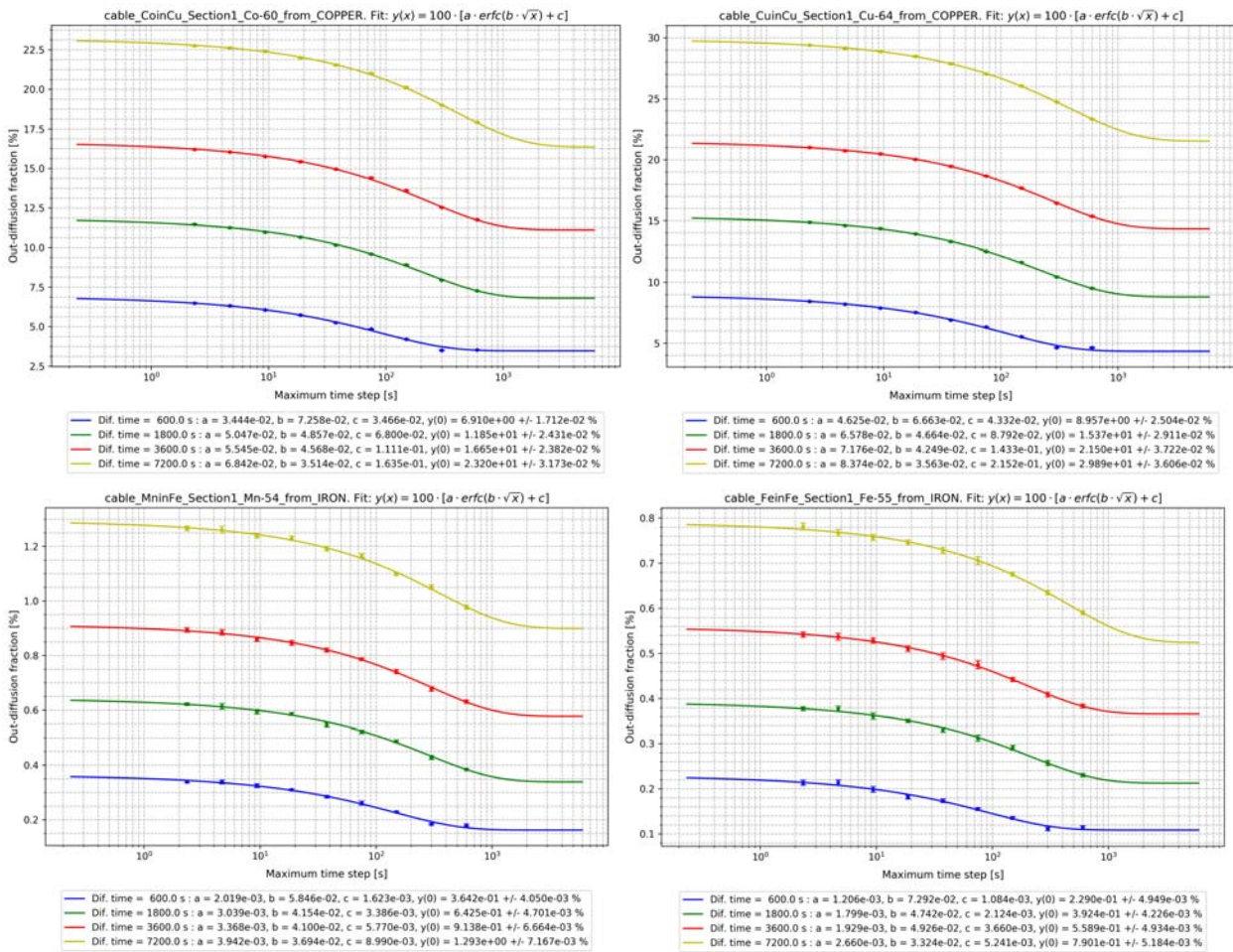


Figure 4.3: ODF obtained with SOLIDUSS as a function of the time step sizes (dots) and the corresponding fits (curves) for ^{60}Co in Cu (top left), ^{64}Cu in Cu (top right), ^{54}Mn in Fe (bottom left) and ^{55}Fe in Fe (bottom right). The fit formula is specified in the picture's titles and the resulting parameters below each plot, together with the ODF estimation for a time step equal to zero. Note that the uncertainties associated with the simulation results are also shown, even if some of them are not visible due to their size.

4.2.2 Different geometries

The ODF for different geometries was also assessed. This time we looked at the ODF of ^{60}Co from Cu for two different objects: a thin plate and a quadrupole's coil cell. In both cases we considered a uniform initial distribution of radioisotopes and a uniform temperature of 1273 K. Results are shown in Fig. 4.4, where we can observe that they still follow the same behaviour discussed previously.

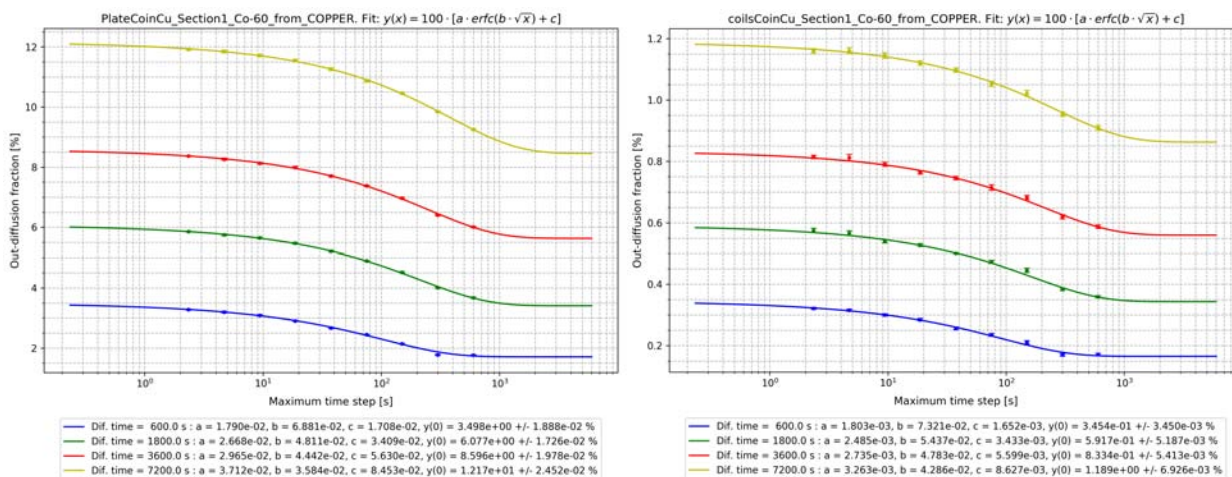


Figure 4.4: ODF obtained with SOLIDUSS as a function of the time step sizes (dots) and the corresponding fits (curves) for ^{60}Co in different Cu objects: a $1 \times 1 \text{ m}^2$ plate of 0.5 mm thickness (left) and a quadrupole's coil cell (right), which in essence is a square cable ($1.7 \times 1.7 \text{ cm}^2$ cross section) with a cylindrical hole in its centre (0.4 cm radius). The fit formula, its parameters and the ODF estimation for a time step tending to zero are provided with each picture. The uncertainties associated with the simulation results are plotted, even if some of them are too small to be visible.

4.2.3 Different initial distributions

Similarly, we have found that a highly non-uniform initial distribution of the radionuclides does not imply a change in the evolution of the ODF as a function of the time steps, as it is shown for a couple of examples in Fig. 4.5. There we can see the initial distribution of radioisotopes considered for each geometry—a sphere and a cylinder—and the obtained results. In both cases, we looked at the diffusion of ^{60}Co in Cu at 1273 K. The initial distribution of radionuclides in the cylinder is that one resulting from the interaction of a 10 GeV proton beam impinging in one of its bases.

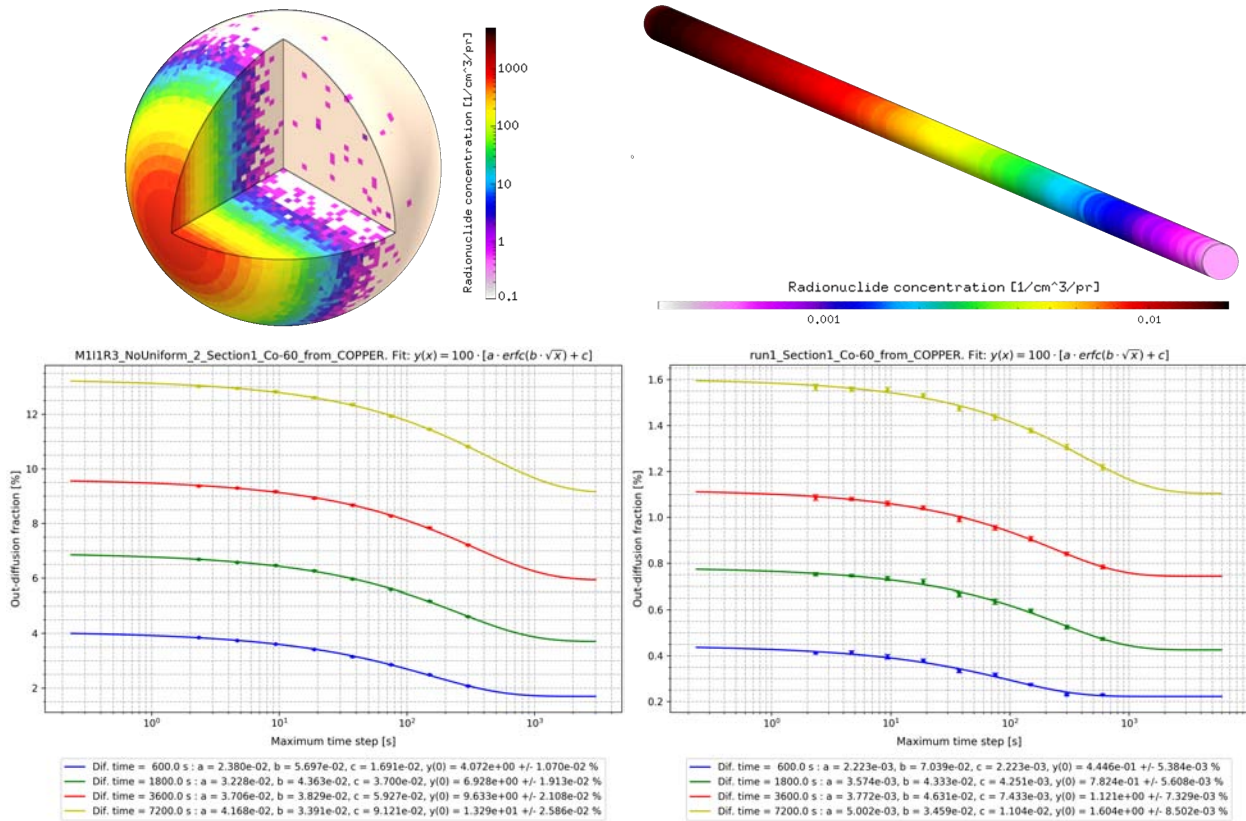


Figure 4.5: ^{60}Co concentration maps in a Cu sphere (top left) and a Cu cylinder (top right). The ODF obtained with SOLIDUSS for both cases as a function of the time step sizes (dots) and the resulting erfc fits (curves) are shown below each concentration map. A uniform temperature of 1273 K has been considered. The uncertainties associated with the simulation results are also shown, although they are very small.

4.2.4 Different temperature gradients

By last, we have considered non-uniform temperature distributions. In these tests, whose results can be found in Fig. 4.6, we look at the out-diffusion of ^{60}Co from a Cu cylinder with a longitudinal gradient of temperature and at the out-diffusion of ^{54}Mn from the Fe yoke of a warm LHC quadrupole. The temperature gradient in the quadrupole is such that the temperature increases as we get closer to its outer surface (temperature maps are also shown in Fig. 4.6). In both cases, we obtained an excellent fit using once more eq. (4.1), so we can conclude that this behaviour is also independent of the temperature gradient. For these tests, we have considered a uniform radionuclide initial distribution.

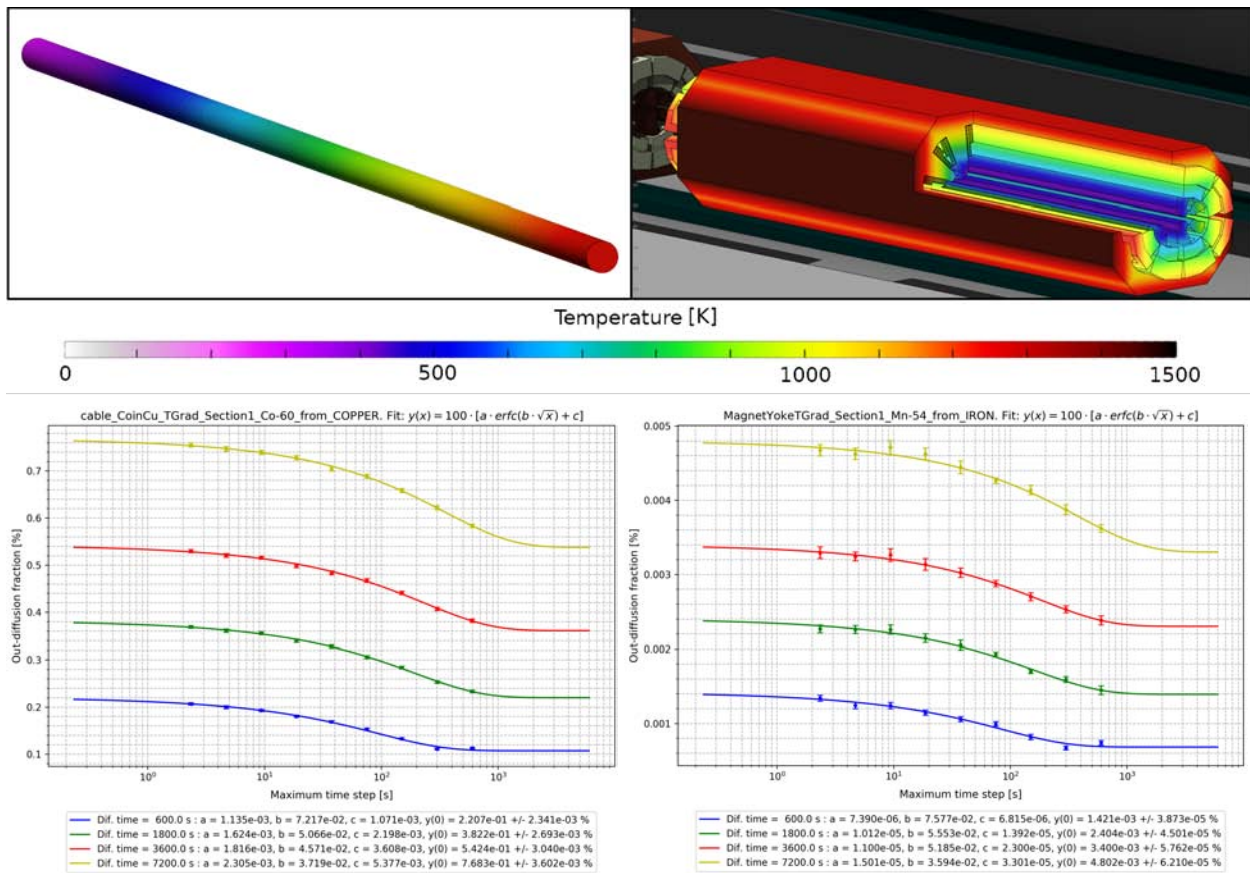


Figure 4.6: Temperature maps considered for a Cu cylinder (top left) and the Fe yoke of a warm LHC quadrupole (top right). Uniform initial distribution of ^{60}Co in the cylinder and of ^{54}Mn in the yoke was assumed. The ODF obtained with SOLIDUSS for both cases as a function of the time step sizes (dots) and the resulting erfc fits (curves) are shown below each temperature map.

4.3 Confidence intervals for out-diffusion fraction estimations

Using the covariance matrix $\mathbf{Cov}[(a, b, c)]$ obtained in the fitting process, we can also calculate confidence intervals for our estimation. The $ODF(\Delta t \rightarrow 0)$ [see eq. (4.2)] is a linear combination of the parameters a, b and c , so we can easily obtain its variance using a simple error propagation:

$$\text{Var} [ODF(\Delta t \rightarrow 0)] = \mathbf{J} \mathbf{Cov} [(a, b, c)] \mathbf{J}^T, \quad (4.3)$$

where \mathbf{J} is the Jacobian of the linear combination (\mathbf{J}^T is its transpose), defined as follow:

$$\mathbf{J} = \begin{bmatrix} \frac{\partial ODF(\Delta t \rightarrow 0)}{\partial a} & \frac{\partial ODF(\Delta t \rightarrow 0)}{\partial b} & \frac{\partial ODF(\Delta t \rightarrow 0)}{\partial c} \end{bmatrix} = \begin{bmatrix} 1 & 0 & 1 \end{bmatrix}. \quad (4.4)$$

Therefore, substituting in eq. (4.3), the variance will be:

$$\begin{aligned} \text{Var} [ODF(\Delta t \rightarrow 0)] &= \begin{bmatrix} 1 & 0 & 1 \end{bmatrix} \begin{bmatrix} \text{Var}(a) & \text{Cov}(a, b) & \text{Cov}(a, c) \\ \text{Cov}(b, a) & \text{Var}(b) & \text{Cov}(b, c) \\ \text{Cov}(c, a) & \text{Cov}(c, b) & \text{Var}(c) \end{bmatrix} \begin{bmatrix} 1 \\ 0 \\ 1 \end{bmatrix} \\ &= \text{Var}(a) + \text{Var}(c) + 2 \text{Cov}(a, c), \end{aligned} \quad (4.5)$$

where we have used that $\text{Cov}(a, c) = \text{Cov}(c, a)$, because every covariance matrix is symmetric by definition. We assume the obtained parameters a, b and c to be a set of values for normally distributed variables with variances and covariances given by the covariance matrix. As a consequence, $ODF(\Delta t \rightarrow 0)$ is also normally distributed. However, one must keep in mind that these values and the covariance matrix have been calculated using a limited data sample (several points of the out-diffusion fraction for different time steps) and therefore, they may not be representative for the whole data population (they would be if the number of points would tend to infinity). In this case and in order to calculate confidence intervals, one must assume the ODF —calculated using a finite and rather small number of data points—to follow a Student's t -distribution and therefore use its cumulative distribution function to estimate them. To do this, we scale the obtained standard deviation using the so-called one-sided critical values $t_{\alpha/2, \nu}$ of the Student's t -distribution for the confidence interval we want to calculate, $(1 - \alpha)CI$, and the degrees of freedom ν of the distribution. The degrees of freedom are given by:

$$\nu = n - p, \quad (4.6)$$

where n is the number of data points used in the fit and p is its number of parameters (3 in our case: a, b and c). Few critical values are shown in Tab. 4.1, but any other can easily be found on the internet or in most probability handbooks. Then, a confidence interval would be given by:

$$(1 - \alpha)CI = t_{\alpha/2, \nu} \cdot \text{Var} [ODF(\Delta t \rightarrow 0)], \quad (4.7)$$

For instance, if we have $n = 6$ and $p = 3$, and we are interested in the 95% confidence interval, we would get the following:

$$0.95 \text{ CI} = t_{0.025,3} \cdot \text{Var} [\text{ODF} (\Delta t \rightarrow 0)] \simeq 3.182 \cdot \text{Var} [\text{ODF} (\Delta t \rightarrow 0)]. \quad (4.8)$$

This is the recommended approach to estimate the confidence intervals of the out-diffusion fraction results obtained using the fit extrapolation.

Table 4.1: Critical values of the Student's t-distribution.

Confidence intervals [%]	50	80	90	95	99	99.9
$\alpha/2$	0.25	0.1	0.05	0.025	0.005	0.0005
ν	$t_{\alpha/2,\nu}$					
1	1.000	3.078	6.314	12.706	63.657	636.6
2	0.816	1.886	2.920	4.303	9.925	31.60
3	0.765	1.638	2.353	3.182	5.841	12.92
4	0.741	1.533	2.132	2.776	4.604	8.610
5	0.727	1.476	2.015	2.571	4.032	6.869
6	0.718	1.440	1.943	2.447	3.707	5.959

4.4 Simulation example

Using the approach explained in the present chapter we have carried out a realistic calculation example. Let us consider a warm quadrupole from the LHC at CERN to investigate the out-diffusion of several radionuclides produced in its yoke and coils. We have assumed the yoke to be made of Fe, and the coils of Cu. A cross section of the quadrupole is shown in the left part of Fig. 4.7, together with a zoom to better observe the coils. These coils consist of rectangular Cu cells with a cylindrical cavity in their center through which cooling water flows. An insulation layer wraps each of those cells.

We assume the temperature map provided in the upper right image of Fig. 4.7, with 1000 °C at the outer surface of the quadrupole and a reduction of the temperature as a function of the distance to this surface. As a consequence, we find the lowest temperatures in the inner part of the quadrupole.

In the lower right image of the same figure, we can see the initial distribution of ^{55}Fe in the magnet yoke. It was produced for this example by simulating the collision of 7 TeV protons with an LHC collimator some meters away from the quadrupole, which generates the particle showers that activate the materials in the magnet. The residual radionuclides produced in this simulation by FLUKA are internally passed to SOLIDUSS, triggering the diffusion calculation according to the user specifications. The isotope ^{55}Fe has been arbitrarily chosen, similar concentration maps are found for other species.

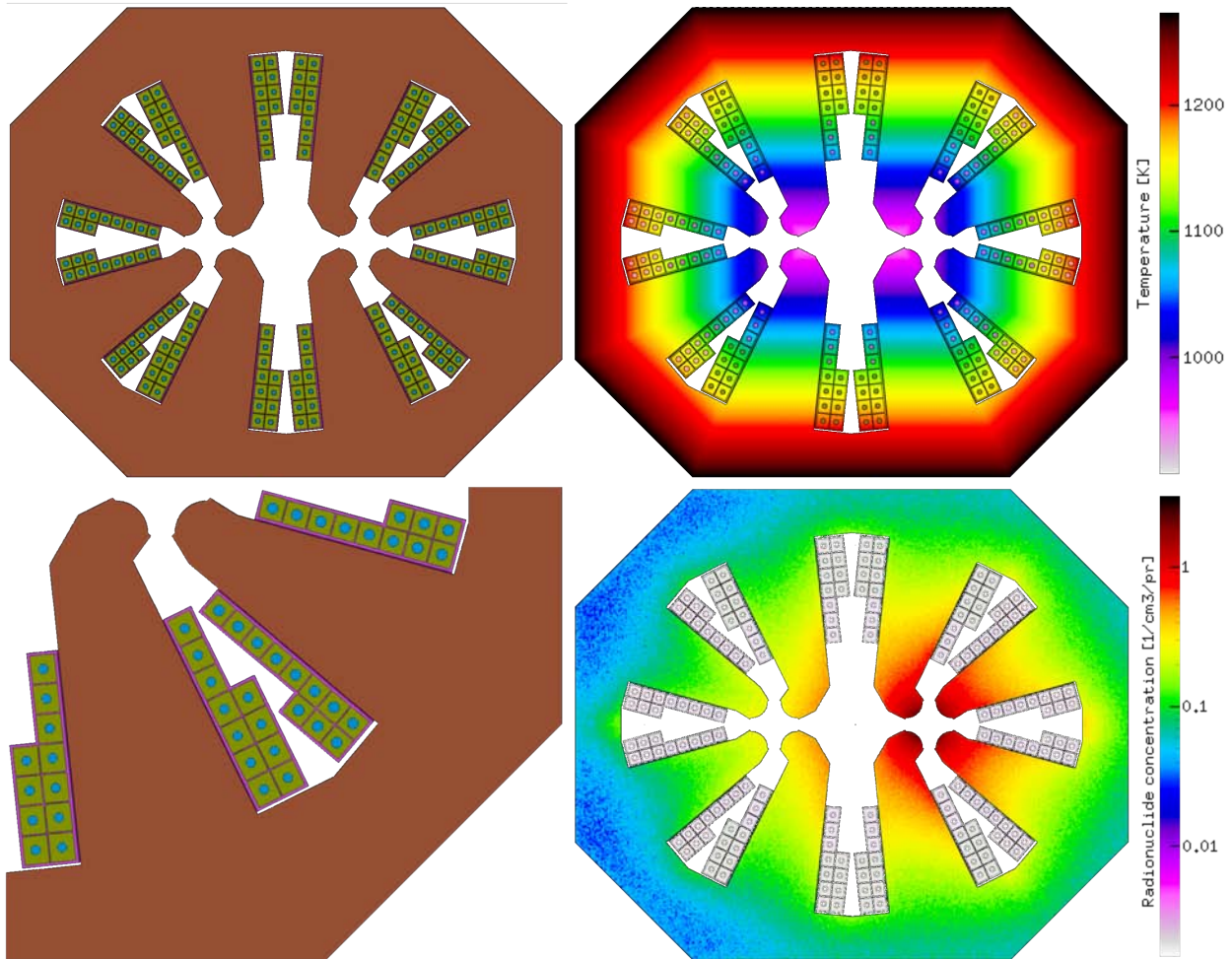


Figure 4.7: Cross section of the simulated geometry of a LHC warm quadrupole (left), together with the assumed temperature map (upper right) and the concentration of ^{55}Fe obtained with FLUKA (lower right). The pictures have been created using Flair [32].

The resulting ODF for different radionuclides from yoke and coils is shown in Table 4.2. The selection of radionuclides for this example is arbitrary. One can perform these calculations for any radionuclides of interest, provided they are produced in the irradiation scheme simulated with FLUKA and the necessary diffusion parameters have been communicated to SOLIDUSS by means of the diffusion input file. In the aforementioned table it can be observed that we have divided the radionuclides out-diffusing from the Cu coils into those entering the insulation and those entering the water cooling. This can be very easily done with SOLIDUSS and may be of interest to assess the portion entering the cooling system and the one potentially released if the coil insulation is burnt during a hypothetical fire in the area. The computational time spent by SOLIDUSS to carry out the presented calculation in a 3.40 GHz Intel Core i7-6700 CPU was 46 hours. Considering 4 CPUs running in parallel, the diffusion calculation could be performed in approximately 11.5 h using a desktop PC (Personal Computer). Note that the example shown here is a highly demanding one in terms of CPU time due to the quadrupole yoke, which is a very bulky object, resulting in very low ODFs. As a consequence, longer run times are needed to achieve sufficiently small uncertainties. The diffusion coefficient parameters used for this simulation has been extracted from [23].

Table 4.2: Out-diffusion fraction for some residual nuclei generated in the quadrupole yoke and coils. Radionuclides are generated in the source material and out-diffused into the target material. We have considered two diffusion times: 30 minutes and 1 hour. Results are provided in parts-per-million (ppm) and its uncertainties correspond to 2σ confidence intervals.

Source material	Target material	Isotope	ODF [ppm]	
			30 min	1 h
Fe	Air	^{55}Fe	$(2.3 \pm 0.4) \cdot 10^1$	$(3.3 \pm 0.4) \cdot 10^1$
		^{54}Mn	$(3.3 \pm 0.4) \cdot 10^1$	$(4.7 \pm 0.4) \cdot 10^1$
		^{48}V	$(3.2 \pm 0.4) \cdot 10^1$	$(4.6 \pm 0.4) \cdot 10^1$
		^{32}P	$(6 \pm 5) \cdot 10^1$	$(9 \pm 5) \cdot 10^1$
Cu	Insulation	^{65}Zn	$(2.52 \pm 0.05) \cdot 10^3$	$(3.61 \pm 0.05) \cdot 10^3$
		^{64}Cu	$(1.48 \pm 0.04) \cdot 10^3$	$(2.11 \pm 0.05) \cdot 10^3$
		^{60}Co	$(9.7 \pm 0.4) \cdot 10^2$	$(1.39 \pm 0.05) \cdot 10^3$
		^{54}Mn	$(2.58 \pm 0.10) \cdot 10^3$	$(3.68 \pm 0.13) \cdot 10^3$
		^{48}V	$(1.8 \pm 0.2) \cdot 10^3$	$(2.6 \pm 0.3) \cdot 10^3$
Cu	Cooling water	^{65}Zn	$(8.5 \pm 0.4) \cdot 10^2$	$(1.23 \pm 0.05) \cdot 10^3$
		^{64}Cu	$(5.0 \pm 0.3) \cdot 10^2$	$(7.1 \pm 0.3) \cdot 10^2$
		^{60}Co	$(3.3 \pm 0.2) \cdot 10^2$	$(4.7 \pm 0.3) \cdot 10^2$
		^{54}Mn	$(8.5 \pm 0.7) \cdot 10^2$	$(1.22 \pm 0.09) \cdot 10^3$
		^{48}V	$(5.2 \pm 1.3) \cdot 10^2$	$(7.8 \pm 1.9) \cdot 10^2$

Modelling desorption

Contents

5.1	Theoretical summary	51
5.2	Monte Carlo desorption model at atomic level	54
5.3	Desorption model for SOLIDUSS	55
5.3.1	Distance to boundary	56
5.3.2	First hitting time	57
5.3.3	Number of atomic jumps	58
5.3.4	Number of surface encounters	59
5.3.5	New position if not desorbed	65

IN PREVIOUS chapters we have discussed how the radionuclides contained in metallic solid objects diffuse inside them when exposed to high temperatures. In the present one we go one step further and discuss one mechanism that become important once they reach the surface of those objects. A theoretical model has been developed to account for this phenomenon and subsequently has been implemented in SOLIDUSS.

5.1 Theoretical summary

If we ignore chemical reactions with surrounding substances (*e.g.* oxidation), a radionuclide reaching an object's surface has three options: diffuse back into the object's bulk matrix, continue its path along the surface or desorb (*i.e.* escape) from it. *Adsorption* is the adhesion of atoms¹ to a surface, and their removal from it is called *desorption*. The nature of the bond between the atoms

¹ We mention only atoms for conciseness but everything discussed in this section is applicable to molecules as well.

and the surface depends on the chemical elements under consideration. However, one generally can divide the adsorbed atoms into two groups: the *physisorbed atoms* and the *chemisorbed atoms*. The latter require the existence of chemical bounds with the surface and the potential well trapping them is typically deeper. Physisorbed atoms are bounded to the surface only by *Van der Waals forces*.

We are interested in assessing the probability of desorption in a general way. In order to do that, let us imagine a surface with a given number of adsorbed atoms, θ_0 . If we assume that the only process these atoms can undergo is first-order desorption (*i.e.* the atom does not need to combine with another one in order to desorb), the number of atoms on the surface will vary with time t as follows [39]:

$$\frac{d\theta}{dt} = -\theta\nu_0 \exp\left(-\frac{E_{des}}{k_B T}\right), \quad (5.1)$$

where E_{des} is the *desorption activation energy*² (*i.e.* energy needed to overcome the potential well and desorb), ν_0 the vibration frequency of the atom, T is the absolute temperature and k_B the Boltzmann's constant. As the reader may have noticed, this law is analogous to that of radioactive decay. Solving the differential equation one obtains that:

$$\theta(t) = \theta_0 \exp\left(-\frac{t}{\tau}\right), \quad (5.2)$$

where τ is the so-called *sojourn time*, which characterizes the desorption process and is given by:

$$\tau = \frac{1}{\nu_0} \exp\left(\frac{E_{des}}{k_B T}\right). \quad (5.3)$$

The vibrations of adsorbed atoms are induced by the vibrations of the adsorbent crystalline lattice. Hence, ν_0 is assumed to be a property of the adsorbent only and supposed to be independent of the temperature [40].

The available experimental data for activation energies of desorption are really scarce. They are commonly approximated using activation energies of adsorption³ by simply inverting its sign, yet also these data are not abundant in literature. In their absence, one may find calculated values for adsorption energies for different adsorbates and adsorbents, which should be taken as rough estimates. For instance, Ref. [41] compiles an extensive list of data calculated by means of the so-called *Eichler-Miedema* model [42]. The approximation of the desorption energy as the negative of the adsorption one should be made with caution. As an example, the adsorption energies obtained with the aforementioned model are a function of the enthalpy of vacancy formation and the solution enthalpy (among others), which we believe should not play a roll in the desorption of an atom already on the object's surface⁴.

2 Also known as desorption enthalpy or desorption energy. Note that we are always assuming ambient pressure.

3 Also known as adsorption enthalpies or simply adsorption energies.

4 On the other hand, it is clear that the adsorption of a given solute would be affected by the number of vacancies in the object's surface as well as by its solubility into the object's material.

The desorption energy can be interpreted as the energy needed to completely break the bounds of an atom on an object's surface with those surrounding it, and become a gas as a consequence. When adsorbate and adsorbent are the same chemical element, we can identify the desorption energy with the *sublimation enthalpy*, which is the energy required to change a substance from solid to gaseous state. When adsorbate and adsorbent are different chemical elements, the strength of their bound will depend of both species. Nonetheless, the adsorption enthalpies of trace amounts of an element are often correlated to the sublimation enthalpy of macro-amounts of the element in question [43,44]. Therefore, one could get a rough indication of how easily the adsorbate will desorb by looking at its vapour pressure or its boiling point. The higher the vapor pressure, the more volatile it is and the more easily it will desorb. The higher the melting point, the less volatile it is and the less it will desorb. In Fig. 5.1 the reader can consult the boiling temperature of a number of chemical elements. Please note that, for elements likely to react with the surrounding atmosphere, the boiling temperature will provide no reliable information regarding their chances to be released. Take for instance C, which has a high boiling temperature but is well known to easily react with oxygen, giving rise to the highly volatile CO and CO₂ [44].

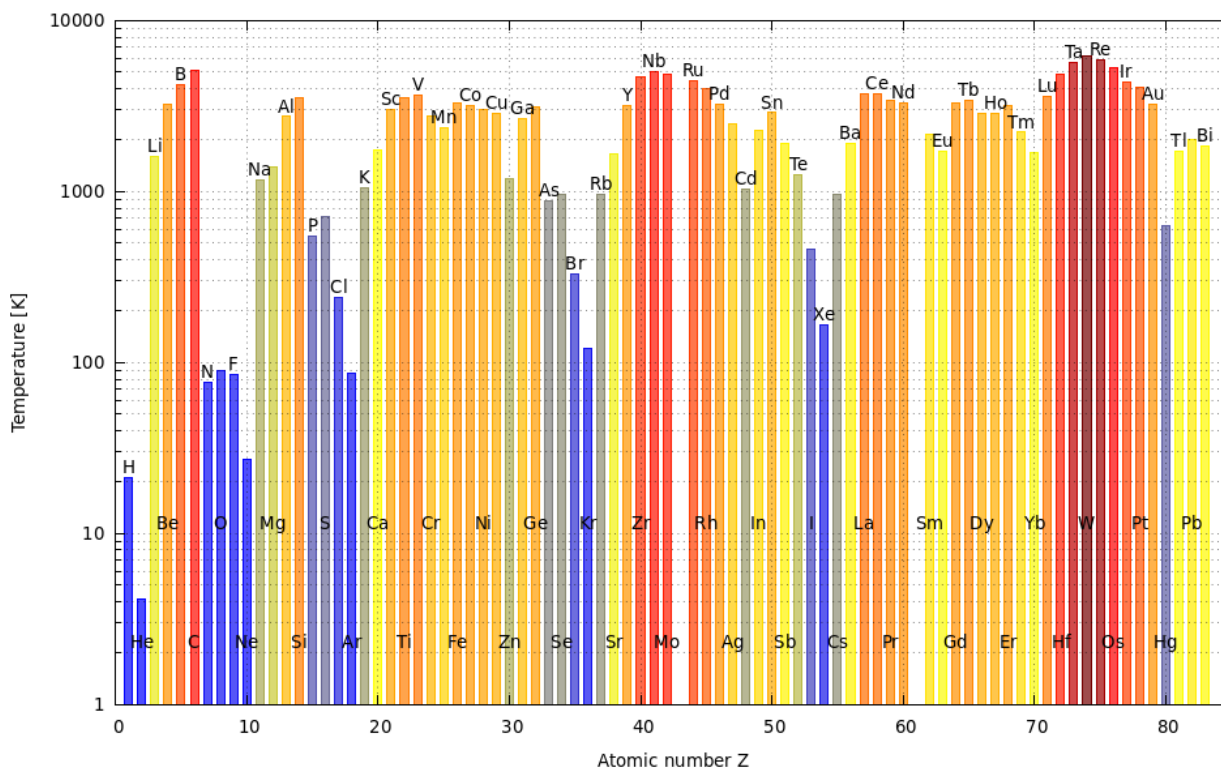


Figure 5.1: Boiling temperature for a number of chemical elements. Source: Ref. [45].

5.2 Monte Carlo desorption model at atomic level

The desorption rate r_{des} can be obtained from eq. (5.3) as follows:

$$r_{des} = \frac{1}{\tau} = \nu_0 \exp\left(-\frac{E_{des}}{k_B T}\right). \quad (5.4)$$

As already mentioned, the atom has further options (apart from desorption) since it could also diffuse back into the object or diffuse along the object's surface. If it diffuses along the object's surface, nothing will change for us as it would still be on the surface and thus, not be accounted for as being out-diffused. Therefore, it only has two mutually exclusive options, either desorb or diffuse back into the solid. The diffusion rate is given by a very similar expression:

$$r_{dif} = \nu_0 \exp\left(-\frac{Q}{k_B T}\right), \quad (5.5)$$

where Q is the activation energy of diffusion. We have assumed that the effective vibration frequency of the atom is equivalent to that of the desorption process. From a Monte Carlo point of view, we can see that whenever a radionuclide reaches a surface there will be a competition between those two processes. The desorption probability would be given by:

$$P_{des} = \frac{r_{des}}{r_{des} + r_{dif}} = \frac{1}{1 + \exp\left(\frac{E_{des}-Q}{k_B T}\right)}. \quad (5.6)$$

In order to decide which process takes place, we could sample a random number ξ from an uniform distribution $U(0, 1)$. If $\xi < P_{des}$, desorption will follow. Otherwise, we shall assume that the radionuclide jumped back inside the solid. In this case, the radionuclide would be extremely close to the surface and the chances of reaching it again are very high. Subsequent surface encounters would need subsequent samplings to decide whether desorption takes place or not. Very likely the situation would be similar to that one shown in Fig. 5.2, in which an atom diffusing in 2-D encounters a boundary multiple times after the first encounter, describing the trajectories drawn in different colours.

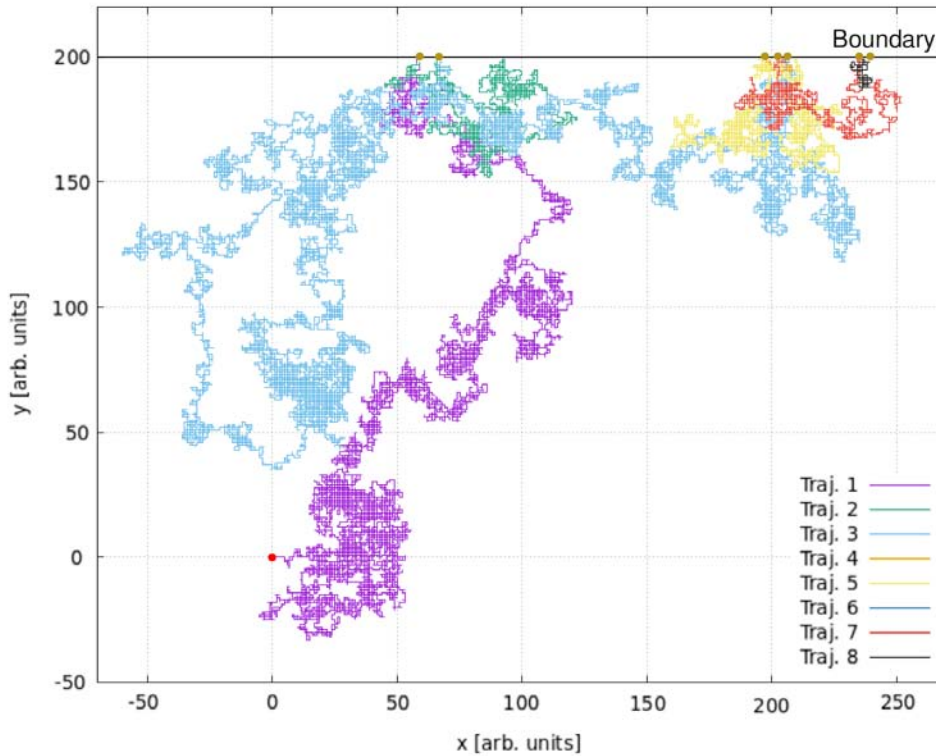


Figure 5.2: Example of a path followed by a random walker diffusing in 2-D. After every encounter with the surface it is forced to jump back inside the lattice (and the colour of the trajectory is changed), reaching the surface again multiple times.

5.3 Desorption model for SOLIDUSS

As detailed earlier, SOLIDUSS simulates the radionuclides' paths through solids at a given scale above the atomic level. It uses adaptive time steps, which condense multiple microscopic steps into a single one. The MC model for desorption described above is therefore not suitable to be implemented in SOLIDUSS as is because one would need to follow each atomic step to decide between desorption and diffusion every time the radionuclide reaches the surface. Nonetheless, it can be adapted to be implemented on top of SOLIDUSS diffusion treatment. The key would be to find out the number of times N_{enc} that a given radionuclide would reach an object's surface during a time step Δt , provided that it does not desorb in any of the encounters. With this data, we can obtain the probability for a radionuclide to desorb in one of those encounters, P_{desT} , as follows:

$$P_{desT} = 1 - (1 - P_{des})^{N_{enc}}, \quad (5.7)$$

where we have used that $(1 - P_{des})$ is the probability that the radionuclide diffuses back into the solid after one encounter with the surface. Knowing this and proceeding analogously as before, we could sample a random number ξ from an uniform distribution $U(0, 1)$ and compare it with P_{desT} . If $\xi < P_{desT}$, the radionuclide desorbed after one of the surface encounters that took place during

the time step. If not, it is still inside the solid and its new position should be properly sampled. This procedure will simplify the simulation from that one in Fig. 5.2 to that one in Fig. 5.3.

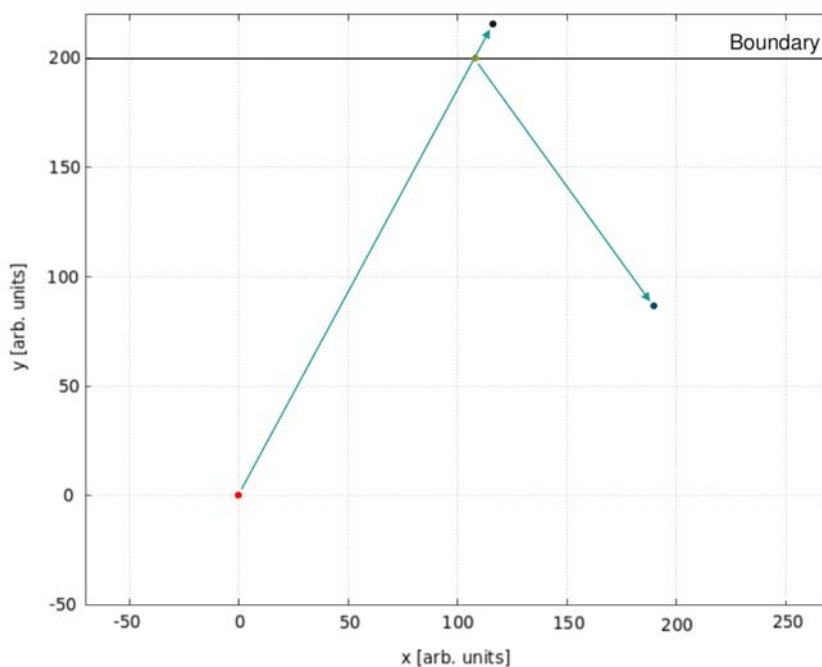


Figure 5.3: Schematic of how SOLIDUSS would deal with the diffusing particle of Fig. 5.2. Instead of simulating each single atomic jump, the intersection point between the next spatial step and the boundary will be determined. Then, the probability of desorption in one of the 8 surface encounters suffered by the particle would be evaluated, and with the help of a single random number it would be decided whether or not desorption had occurred. If it did not, the new position of the particle inside the lattice would subsequently be sampled.

In the rest of this section we will go through the intermediate goals that we need to accomplish in order to finally obtain N_{enc} . In order to determine this quantity, it would be essential to know the number of jumps that the atom would perform within the solid lattice during a time step, as well as the moment at which it hit the surface for the first time. To obtain the latter, we need to estimate the distance from the initial position of the radionuclide to the object's surface (also referred to as boundary in this document).

5.3.1 Distance to boundary

In SOLIDUSS, we have no prior information on the shape of the object of interest, only the intersection point of a ray sampled in a given direction with the object's surface is known. Therefore, we cannot determine the distance d to a boundary in a general way, instead we can estimate it under a reasonable approximation. Given the small time steps used in our simulations and the fact that SOLIDUSS is meant to be used for macroscopic objects, it is justified to assume that the portion of an object's surface that can be reached by a radionuclide in a single time step is well approximated by a plane (see Fig. 5.4).

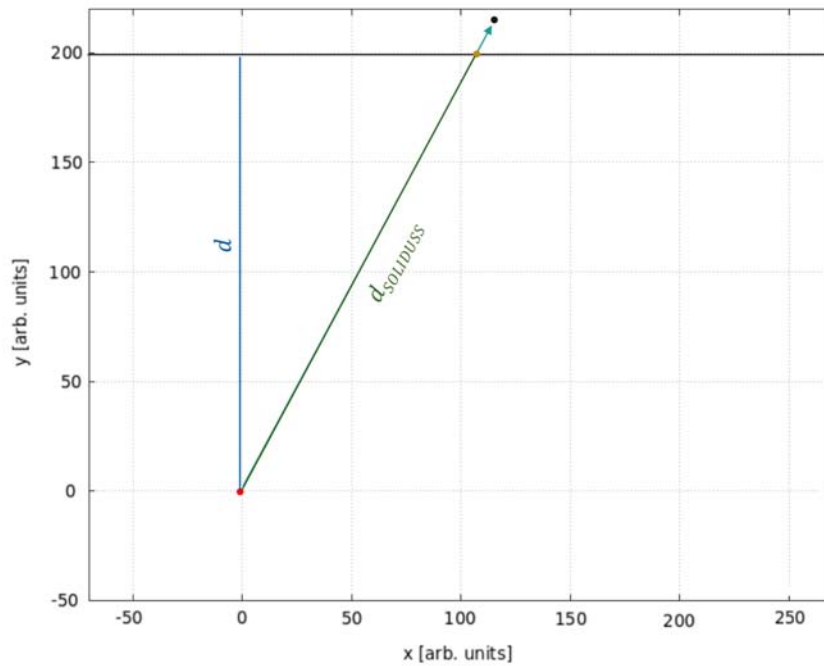


Figure 5.4: Distance $d_{SOLIDUSS}$ from the radionuclide position to the intersection point between the boundary and the vector defining its next spatial step. Using this distance and the normal to the boundary in the intersection point we can calculate the real distance d to the boundary, needed to proceed with the desorption simulation.

If we know the distance from the radionuclide's position to the intersection point between its jump's direction and the surface ($d_{SOLIDUSS}$ in Fig. 5.4), as well as the normal to the latter at the intersection point, the distance d can be easily calculated. The normal can be obtained with the help of the FLUKA subroutine GEONOR.

5.3.2 First hitting time

Once we have a method to estimate the distance to the boundary, we need to sample the time t_0 at which the first hit to the surface takes place. It can be shown that the time at which a 1-D Brownian particle⁵ first reaches a wall-like boundary follows a *Lévy Distribution* [46] given by:

$$f(t_0) = \frac{d}{\sqrt{4\pi Dt_0^3}} \exp\left(-\frac{d^2}{4Dt_0}\right), \quad (5.8)$$

where D is the diffusion coefficient of the radionuclide in the material of interest and t_0 is the time. In Fig. 5.5 we show an example of a distribution obtained using eq. (5.8) together with the results obtained from a random walk simulation. As we can observe, both results are in very good

⁵ Note that we are dealing with 3-D trajectories, but since we have a 2-D boundary, it is the displacement in the remaining dimension that brings the radionuclide closer or farther from the boundary.

agreement. Note that only the normalization was adjusted so that we could properly compare their shape.

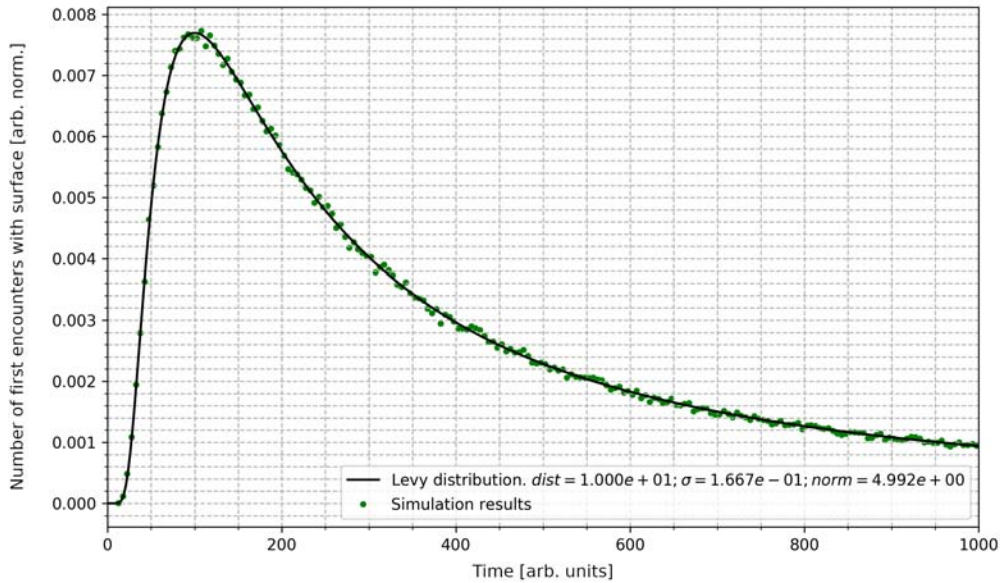


Figure 5.5: Probability distribution of the time at which random walkers initially 10 steps away from a wall-like boundary first hit it. Random walk simulation results are reported together with the curve predicted by eq. (5.8). The normalization has been chosen so the shape of the distributions can be compared.

5.3.3 Number of atomic jumps

After sampling the time at which the radionuclide first hits the surface, we need to find out the number of atomic jumps N that it could perform in the remaining duration⁶ $t = \Delta t - t_0$ of the time step. The number of surface encounters is directly related to the number of jumps, and the latter depends on the diffusion coefficient and the diffusion time of the species of interest. The mean squared distance at which a random walker (*e.g.* a radionuclide) is found after N jumps is given by:

$$\langle dist^2 \rangle_{RW} = N \cdot A^2, \quad (5.9)$$

with A being the jump length. Similarly, if we consider a diffusing Brownian particle, the mean squared distance at which it is found after a time t is:

$$\langle dist^2 \rangle_{Br} = 2mDt, \quad (5.10)$$

where m represents the number of dimensions and D is the diffusion coefficient. We can therefore match both distances in order to obtain the relation between N and t . Since $m = 3$ in our case, we

⁶ Note that the condition $t_0 \leq \Delta t$ should be imposed during the sampling of t_0 .

get the following:

$$\langle dist^2 \rangle_{RW} = \langle dist^2 \rangle_{Br} \Rightarrow N = \frac{6Dt}{A^2}. \quad (5.11)$$

Since atomic migration is in general the result of successive, typically single-atom, jumps of fixed lengths [15], the variable A can often be approximated by the atomic bond length, which is the average distance between nuclei of two bonded atoms. This parameter, together with the desorption activation energy should be provided by the user in the diffusion input file of SOLIDUSS if desorption is to be simulated. Details about how to do it can be found in appendix B.

5.3.4 Number of surface encounters

Once a random walker reaches a boundary for the first time, the average number of times that it will encounter the boundary again is a function of the number of jumps it performs. Now we would like to determine how exactly both are quantities related.

Brownian particle ⁷

Let us first start considering a Brownian particle diffusing in 1-D initially placed at the origin and try to find out the average number of times that it will cross the origin for a given total number of steps. The probability density function for the particle position x after a time t is given by:

$$\phi(x, t) = \frac{1}{\sqrt{4\pi Dt}} e^{-\frac{x^2}{4Dt}}, \quad (5.12)$$

where D is the diffusion coefficient. If we assume that the particle performs one step every time t , the PDF after n steps is:

$$\phi(x, nt) = \frac{1}{\sqrt{4\pi Dnt}} e^{-\frac{x^2}{4Dnt}} = \frac{1}{\sqrt{n}} \phi\left(\frac{x}{\sqrt{n}}, t\right). \quad (5.13)$$

Then, the probability of being at a given position x after n steps and crossing the origin during the next one would be given by:

$$P = \int_{\mathbb{R}} \int_{z \geq |x|} \frac{1}{\sqrt{n}} \phi\left(\frac{x}{\sqrt{n}}, t\right) \phi(z, t) dx dz = \int_{\mathbb{R}} \int_{z \geq |x| \sqrt{n}} \phi(x, t) \phi(z, t) dx dz. \quad (5.14)$$

Note that x represents the position of the particle before the last step, and $\int_{z \geq |x|} \phi(z, t) dz$ the probability of crossing the origin in the next step assuming the particle is currently at x . The right term of eq. (5.14) is the probability for a 2-D Normal distribution to end up in the wedge $(x, z) : z \geq |x| \sqrt{n}$, resulting in:

$$P = \frac{1}{\pi} \arctan\left(\frac{1}{\sqrt{n}}\right). \quad (5.15)$$

⁷ The content of this subsection is heavily based on the online resource [47].

Therefore, the expected number of origin crossings after N steps is:

$$\langle N_c \rangle = \frac{1}{\pi} \sum_{k=1}^N \arctan \left(\frac{1}{\sqrt{k}} \right). \quad (5.16)$$

For an easier handling of the expression we can approximate the summation by an integral⁸, obtaining:

$$\langle N_c \rangle = \frac{1}{\pi} \int_1^N \arctan \left(\frac{1}{\sqrt{k}} \right) dk. \quad (5.17)$$

Finally obtaining that:

$$\langle N_c \rangle = \frac{1}{\pi} \left[\sqrt{N} + N \arctan \left(\frac{1}{\sqrt{N}} \right) - \arctan \left(\sqrt{N} \right) \right] - 1. \quad (5.18)$$

As a consequence of the reflection principle for a Wiener process, we can identify $\langle N_c \rangle$ as $\langle N_{enc} \rangle$, being the total number of encounters with a wall-like boundary placed at the origin, provided that none of the times the particle is able to escape. The subsequent distribution of the particle path is the same regardless the direction that the particle follows after reaching the origin. Therefore the number of crossings is equal to the number of encounters. In Fig. 5.6 we have plotted the number of encounters according to eq. (5.18).

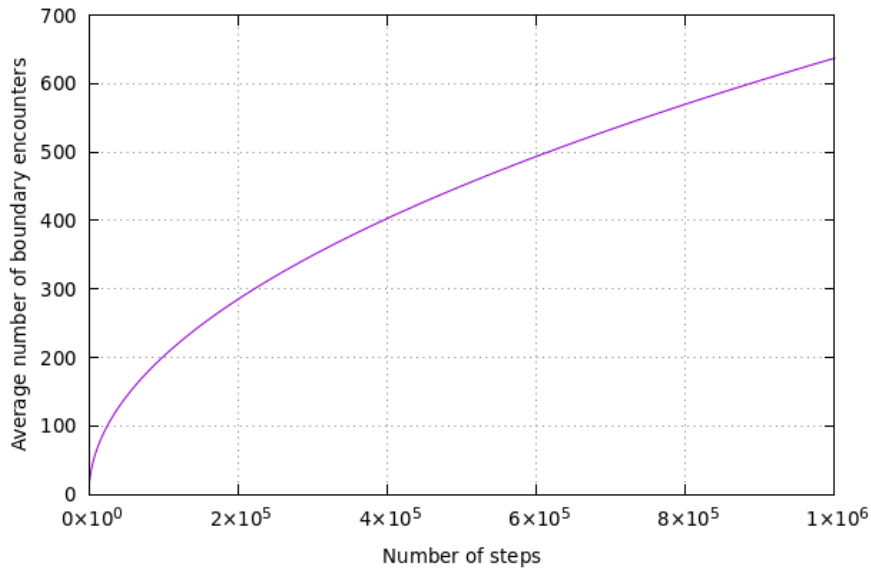


Figure 5.6: Average number of boundary encounters suffered by a Brownian particle as a function of the total number of steps. The particle moves in 1-D and is initially placed at the boundary.

Unfortunately, we cannot make use of this expression since we are interested in the actual description of the atoms movement at the atomic level, and not in the approximation of their path by Brownian motion. Still, we expect the same kind of evolution of the average number of boundary

⁸ It can be shown that the error in which we incur by doing this is negligible for our purposes.

encounters for a random walker, but the absolute values may differ as the lattice structure and its orientation with respect to the boundary should have a significant impact on them.

Random walker⁹

The PDF of the position of a random walker in 1-D after a given number of steps follows a binomial distribution. It can be shown that, if the walker is initially placed at the origin, the probability of being at a position m after N steps is given by:

$$P(m, N) = \frac{N!}{\left(\frac{N+m}{2}\right)! \left(\frac{N-m}{2}\right)!} p^{(N+m)/2} q^{(N-m)/2}, \quad (5.19)$$

where the walker's probability to jump in one direction is p (e.g. right) and in the other (e.g. left) is $q = 1 - p$ as we exclude drift forces. We are interested in the probability of reaching the origin again ($m = 0$), and in our case $p = q$:

$$P(0, N) = \begin{cases} \frac{N!}{\left(\frac{N}{2}\right)! \left(\frac{N}{2}\right)!} p^N, & \text{if } N \text{ is even,} \\ 0, & \text{otherwise.} \end{cases} \quad (5.20)$$

Then, the average number of origin encounters in N steps would be given by:

$$\langle N_e \rangle = \sum_{i=1}^N P(0, i) = \sum_{k=1}^{N/2} \frac{(2k)!}{(k)! (k)!} p^{2k}. \quad (5.21)$$

Similarly to the previous case, we can identify $\langle N_e \rangle$ as $\langle N_{enc} \rangle$. The evolution of the number of encounters is very similar to that one of the expression obtained for a Brownian particle but this time the absolute values are those we are looking for. The evaluation of eq. (5.24) can lead to precision issues very fast for large N since we need to multiply very large number (factorials) by very small ones (p^{2k}). One can avoid this by using *Stirling's approximation* and, in particular, the following expression:

$$n! \simeq \sqrt{2\pi n} \left(\frac{n}{e}\right)^n. \quad (5.22)$$

Using it and taking into account that $p = 1/2$, eq. (5.24) becomes:

$$\langle N_e \rangle \simeq \sum_{k=1}^{N/2} \frac{1}{\sqrt{\pi k}}. \quad (5.23)$$

Similarly to the previous case, we can approximate the summation by an integral, obtaining:

$$\langle N_e \rangle \simeq \sum_{k=1}^{N/2} \frac{1}{\sqrt{\pi k}} \simeq \int_1^{N/2} \frac{1}{\sqrt{\pi k}} dk = \frac{\sqrt{2N} - 2}{\sqrt{\pi}}. \quad (5.24)$$

⁹ The content of this subsection is partially based on the online resource [48].

The expression above meet most of our requirements since it is accurate and quick to evaluate inside the software. Unfortunately, the generalization of this expression for arbitrarily oriented boundaries with respect to the random walker step directions poses a series of difficulties that places it beyond the scope of our studies. We are therefore forced to use a different procedure, which is outlined below.

Power law fit

It was obtained by means of RW simulations that, once a random walker reaches a wall-like boundary for the first time, the average number of times that it will encounter the boundary is well described by the following power law:

$$\langle N_{enc} \rangle = a \cdot N^b, \quad (5.25)$$

where a and b are parameters that depend on the lattice structure and its orientation with respect to the boundary. After each encounter with the boundary, the walker is forced to perform one jump back into the lattice. Fig. 5.7 shows an example case for a simple cubic crystal structure perfectly aligned with the boundary (*i.e.* one of the possible jump directions is perpendicular to the boundary plane and the other two are parallel to it), where we can see the results from the simulation together with the best fit of eq. (5.25) and the results from eq. (5.24).

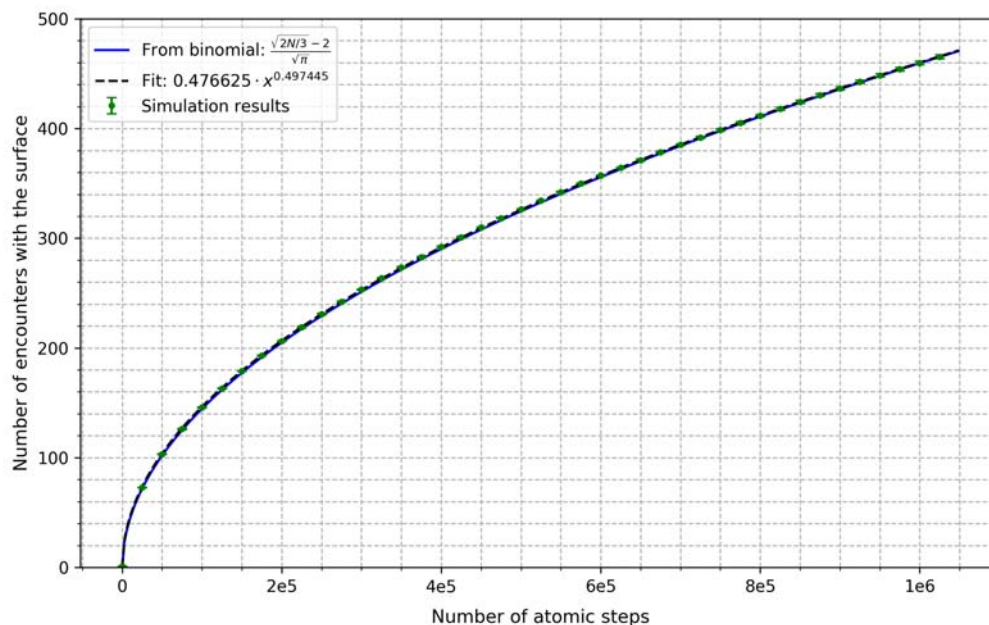


Figure 5.7: Average number of surface encounters suffered by a random walker diffusing in 3-D as a function of the total number of jumps. The boundary is defined by a plane whose normal coincides with one of the three jump directions of the walker. It is initially placed on the boundary and it is obliged to jump once towards the diffusing area every time it reaches the surface. Note that the plot is cumulative (*e.g* after $4 \cdot 10^5$ jumps the walker has reached the boundary approximately 300 times.). Dots are RW simulation results and the dashed curve is the best fit of those results using eq. (5.25). Results from eq. (5.24) are also provided (solid curve), which are in very good agreement with the simulation results. Note that the factor $1/3$ (see legend) takes into account that, in average, only $N/3$ of the total number of jumps are performed in the direction parallel or antiparallel to the normal to the boundary.

Few examples that show the dependence of the number of encounters on the structure and orientation of the lattice are compiled in Fig. 5.8. Nearest-neighbour diffusion was assumed in all cases.

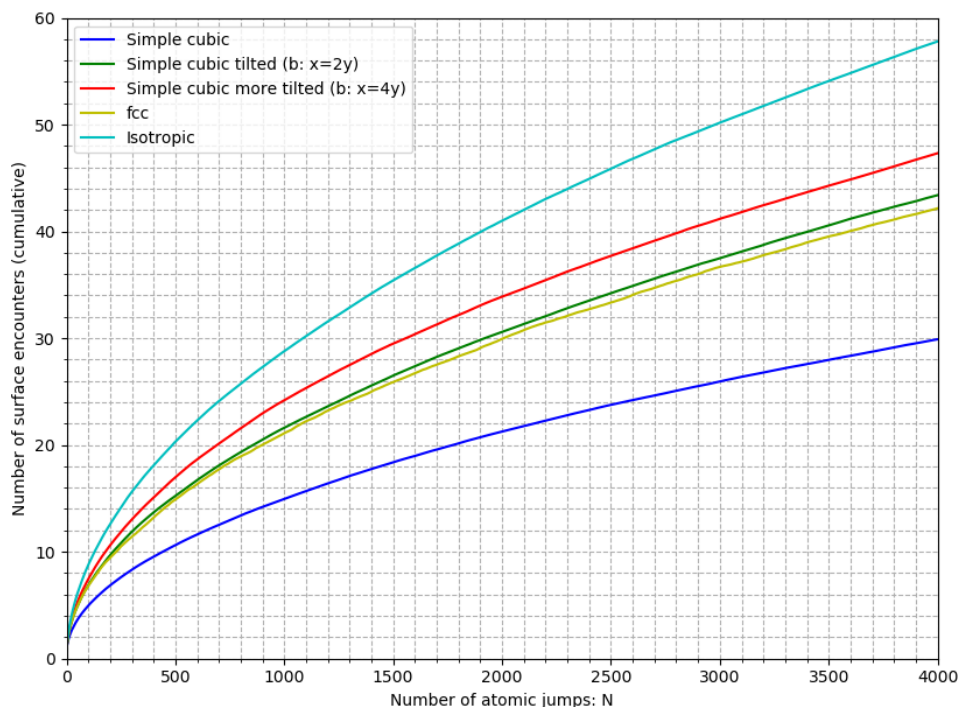


Figure 5.8: Same as Fig. 5.7 for different boundaries and diffusing random walkers. Simple cubic: the random walker has 6 different positions to jump to after each iteration, and every jump is parallel to one of the Cartesian axis. By default, the boundary is a plane whose normal is parallel to one of the Cartesian axis. If “tilted” is specified in the legend, then the boundary is tilted with a given slant. FCC stands for Face-Centered Cubic: in this case the walker has 12 different positions where to jump and none of the jump directions is perpendicular to the boundary. In the isotropic case, the random walker can jump in any direction but with a fixed jump length.

In general, the orientation of the lattice with respect to the object’s surface will be unknown in the scenarios in which SOLIDUSS would be employed to assess the potential out-diffusion of radionuclides. Furthermore, most probably the crystal lattice structure would also be unknown. We must therefore chose a set of values for the parameters a and b to be used as defaults. We deemed it appropriate that, given the radiation protection motivation of this work, we should stay on the safe side and overestimate the number of surface encounters (and as a consequence, the desorption probability) rather than underestimate it. This quantity is maximized when the jumps of the random walker are considered to be isotropic and thus, the amount of positions immediately accessible to it inside the lattice is no longer finite. Nonetheless, we are still considering a fixed jump length. A best fit of the simulation results returned the following function:

$$\langle N_{enc} \rangle = 0.908294 \cdot N^{0.500950}. \quad (5.26)$$

We have also observed that the PDF of the number of surface encounters for a given number of atomic jumps is well approximated by a *half-normal distribution*. Few examples are shown in Fig. 5.9 for different values of N .

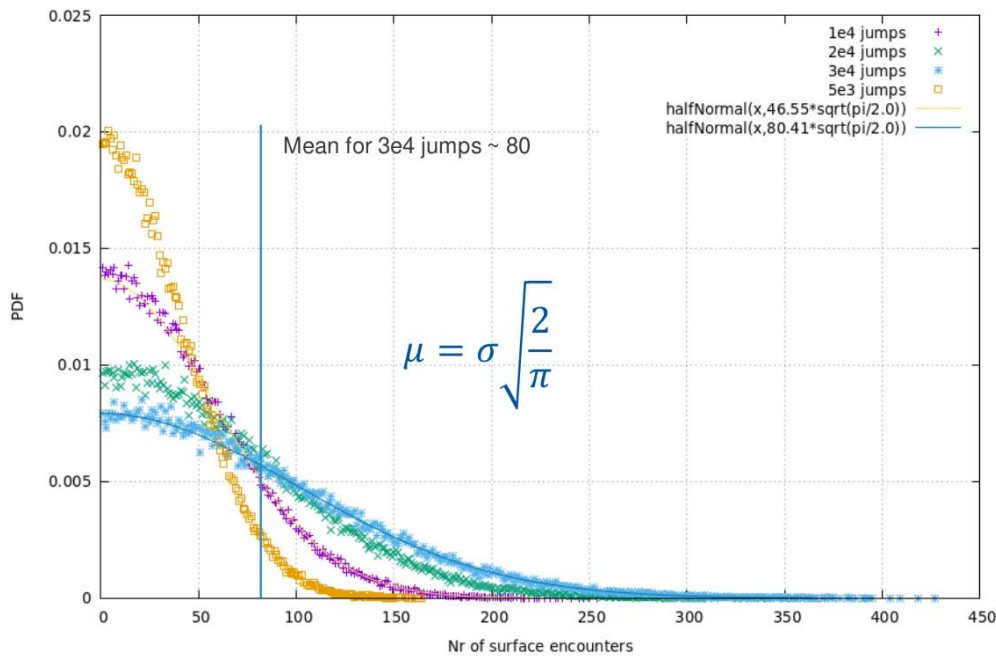


Figure 5.9: Example of the PDFs of the surface encounters suffered by a diffusing random walker for a given total number of jumps (dots). The PDFs are very well approximated by half-normal distributions (lines).

The mean of the half-normal distribution is a function of its standard deviation¹⁰ and therefore one single parameter characterizes the PDF. Since we already have a method to calculate $\langle N_{enc} \rangle$, which is the mean of the PDF, we have everything we need to sample N_{enc} for every time step in which a radionuclide is found to have reached an object's surface. Finally, we can make use of eq. (5.7) to obtain the desorption probability and sample if the radionuclide would desorb or not during the time step under consideration.

5.3.5 New position if not desorbed

If the outcome of the sampling determines that the radionuclide did not desorb, one should keep tracking its diffusion inside the solid. The first step would be to obtain its position back into the object and this can be done sampling a Normal distribution, as it was thoroughly discussed earlier. Naturally, only positions inside the solid would be accepted when sampling. The fact that the distribution of the positions is not distorted by the presence of a wall-like boundary can be seen as a consequence of the reflection principle for a Wiener process.

¹⁰ $\mu = \sigma \sqrt{\frac{2}{\pi}}$

Experimental campaign

Contents

6.1	Methodology	67
6.2	Experimental setup	68
6.2.1	Gas circuit	68
6.2.2	Furnace	71
6.3	Samples	71
6.4	Results and discussion	74
6.4.1	Temperature inside the furnace	74
6.4.2	Non-radioactive Cu in N ₂ atmosphere	79
6.4.3	Radioactive Cu in N ₂ atmosphere	80
6.4.4	Non-radioactive Al in N ₂ atmosphere	82
6.4.5	Radioactive Al in N ₂ atmosphere	82
6.4.6	Non-radioactive Cu in Air: foil and filaments	84
6.5	Acknowledgments	86

AN EXPERIMENTAL campaign was carried out aiming to provide data on the out-diffusion of radionuclides from activated materials when exposed to high temperatures. This data will later be used to better understand the phenomenon and to benchmark SOLIDUSS. In this chapter we will explain how the experiments were conducted, detailing the methodology, setup and samples employed. Their results are also presented and discussed.

6.1 Methodology

The central element of the performed experiments is the heating up of radioactive samples, which is carried out in a controlled oxygen-free atmosphere in order to avoid their combustion. Further tests in an air atmosphere using non radioactive samples were also performed, to simulate conditions more similar to those of a real fire. The gas circuit setup is detailed in section 6.2.1. To guarantee a smooth execution of the experiments involving radioactive isotopes, few tests using non radioactive samples were performed ahead. Few experiments were also carried out to determine the optimal geometrical shape for the samples. The outcome of these experiments is discussed in sections 6.4.2 and 6.4.4.

After the selection of suitable radioactive samples (activated foils of Cu and Al), the procedure followed for each experiment can be summarized in the following steps:

1. Gamma-ray spectrometry measurement to accurately determine the radionuclides present in the sample and their activities. These measurements were performed by the staff of the HSE-RP-CS section at CERN in the gamma-ray spectrometry laboratory placed at CERN's building 24. In particular, the GE5-B10162 detector was employed. See figure 6.1.
2. Heating the sample up to very high temperatures during a certain period of time. This is performed to maximize the ODF, which is the fraction of radionuclides that manages to escape from the material. This has been done in the Solid-State Physics (SSP) labs of ISOLDE [49, 50] using a furnace able to reach temperatures well beyond 1000 °C. The temperature was maximized while keeping it sufficiently low to avoid melting. The temperature gradient inside the furnace used to heat up the samples has been characterized. The procedure and its implications are thoroughly explained in section 6.4.1.
3. Gamma-ray spectrometry of the samples. This second measurement is performed under the same experimental conditions as the first one. Subtraction of both results allows to estimate the ODF.



Figure 6.1: Pictures of the setup used in the gamma-ray spectrometry laboratory in building 24. GE5-B10162 detector open (left), interior of the detector with one of our radioactive samples placed and ready to be measured (centre) and detail of the samples and the support, used for an optimum alignment of the samples and the detector (right).

6.2 Experimental setup

The experimental setup consisted of two main parts: the gas circuit and the furnace. Details on both are provided in the following subsections.

6.2.1 Gas circuit

The gas circuit is made up of the following elements (see Fig. 6.2 for a general overview), which will be enumerated in the order in which the flowing gas encounters them:

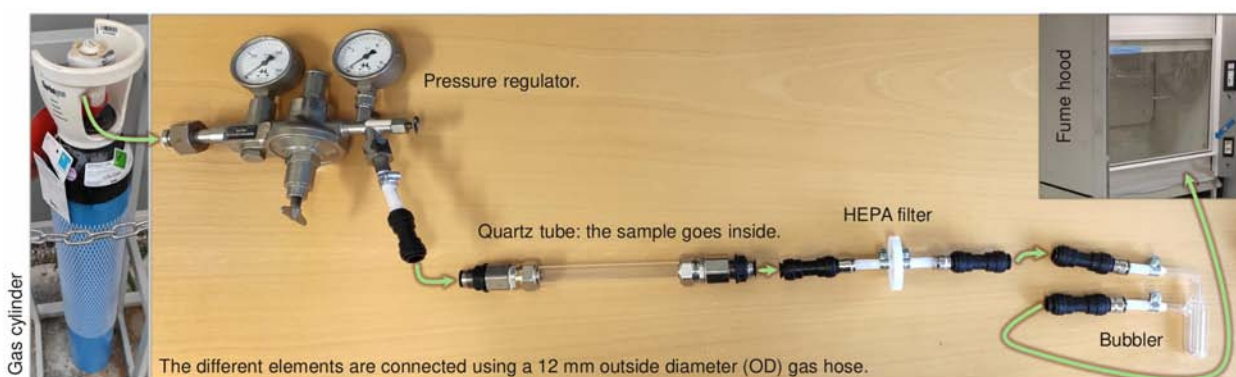


Figure 6.2: Overview of the gas circuit used in the experiments and schematic of the gas flow from the cylinder to the fume hood.

- Gas cylinder: it is the gas source. In our experiments we have used two different gases: N_2 and air. Contrary to our initial estimations, a 10 L (2 m^3)¹ N_2 cylinder was not sufficient to carry out all our experiments. Thus, a 50 L (10 m^3) container eventually had to be employed.
- Pressure regulator: as its name indicates, it provides the means to regulate the gas flux released from the cylinder. It is worth to mention that cylinders containing different gases present different connection threads and therefore pressure regulators specifically targeted for each gas type need to be employed.
- Quartz tube: samples are placed inside the tube, which allows for their immersion in a controlled atmosphere. Quartz is used due to its high melting point, which is a must since the tube is placed inside the furnace for the sample to be heated. The tubes used were approximately 1 m long (the one in Fig. 6.2 is a dummy tube for connection testing purposes) to guarantee that connections and gas hoses were far enough from the furnace, avoiding their exposure to high temperatures. The connection scheme shown in Fig. 6.3 should not be overlooked since finding an optimal and cost-effective way of connecting the quartz tube and the gas hoses was not trivial. The outside diameter (OD) of the quartz tube was 20 mm, which is the biggest one that can be safely introduced in the furnace aperture. Its thickness

¹ Note that the gas is kept at 200 bar pressure inside the cylinder.

was chosen to be 1.5 mm because thinner tubes are too fragile and thicker ones would take away space from our sample.

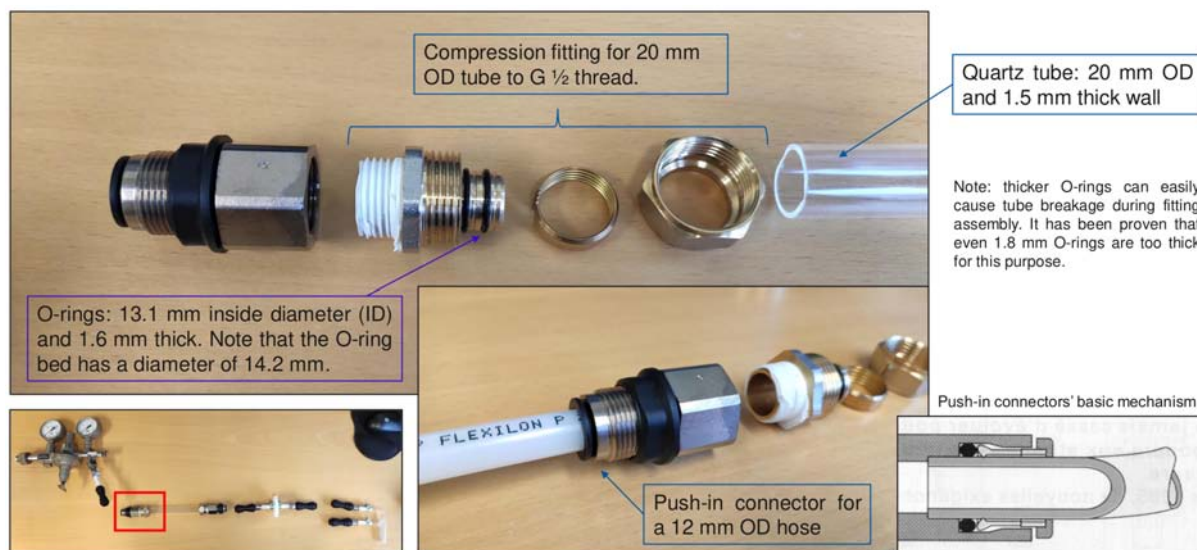


Figure 6.3: Detail of the connection between the quartz tube and the gas hose. Compression fittings with suitable o-rings are used in the tube side, which are then screwed to a push-in connector where the hose is inserted.

- HEPA filter: this inline filter is meant to capture radioactive aerosols that may be released from the samples during the experiments. Formation of volatile radioactive compounds is not expected given the radionuclides' species present in our samples (see section 6.3). In addition to this, their very low activity ruled out the need for using activated charcoal filtration.
- Bubbler: it is used to monitor the gas flux.
- Fume hood: the gas is released inside when exiting the circuit, preventing its liberation in the laboratory.

The different elements are connected using a 12 mm OD gas hose.

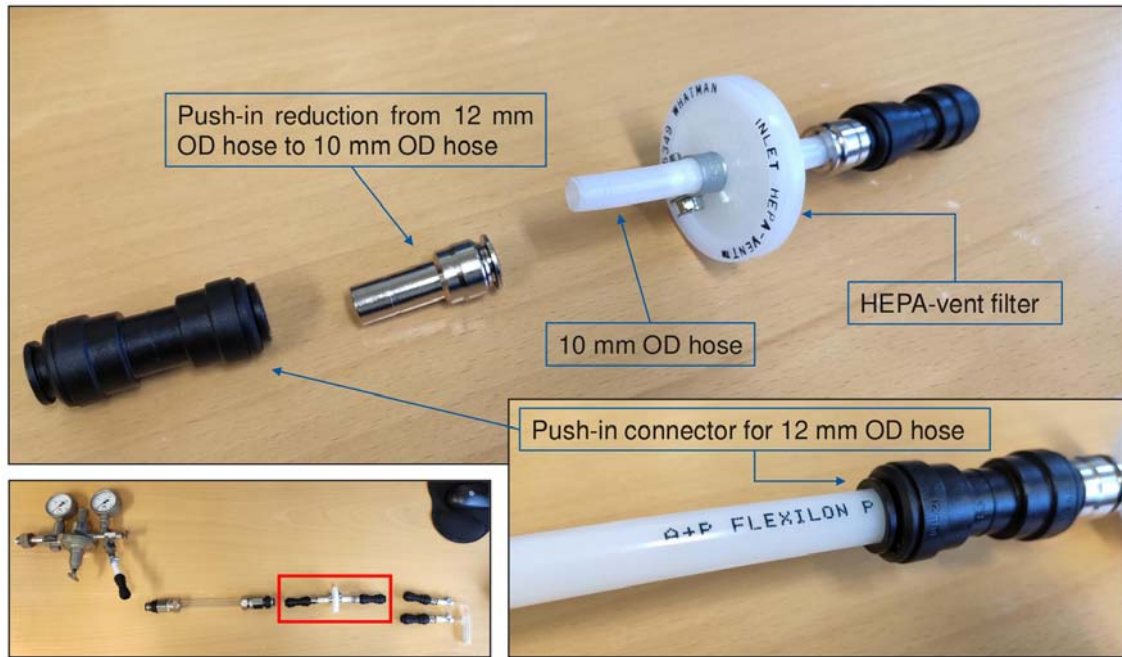


Figure 6.4: Detail of the inline HEPA filter and its connections. Due to the filter connector sizes, a 10 mm hose was needed to guarantee a tight joint. This and the general 12 mm hose were spliced using a push-in reduction and a push-in connector.



Figure 6.5: Detail of the bubbler used to monitor the gas flux. Similarly to the HEPA filter, a 10 mm hose plus connections was used to guarantee tight joints.

6.2.2 Furnace

The furnace used can be seen in Fig. 6.6. It is a HTM Reetz GmbH type LOBA 1100-25-150 and its dimensions are 18.5 cm 16.5 cm x 16.5 cm (l x w x h). The temperature delivered², which can exceed 1000 °C, is tuned by means of a voltage regulator, which controls the voltage provided to the furnace. It should be noted that the temperature needs to be manually stabilized once it has reached the desired value. Fluctuations in the network voltage translate into fluctuations in the furnace voltage³, which can translate into temperature fluctuations. Therefore, it is very important to constantly monitor the temperature evolution during the experiments and to try to minimize the impact of potential fluctuations by continuously fine tuning the voltage regulator's output.

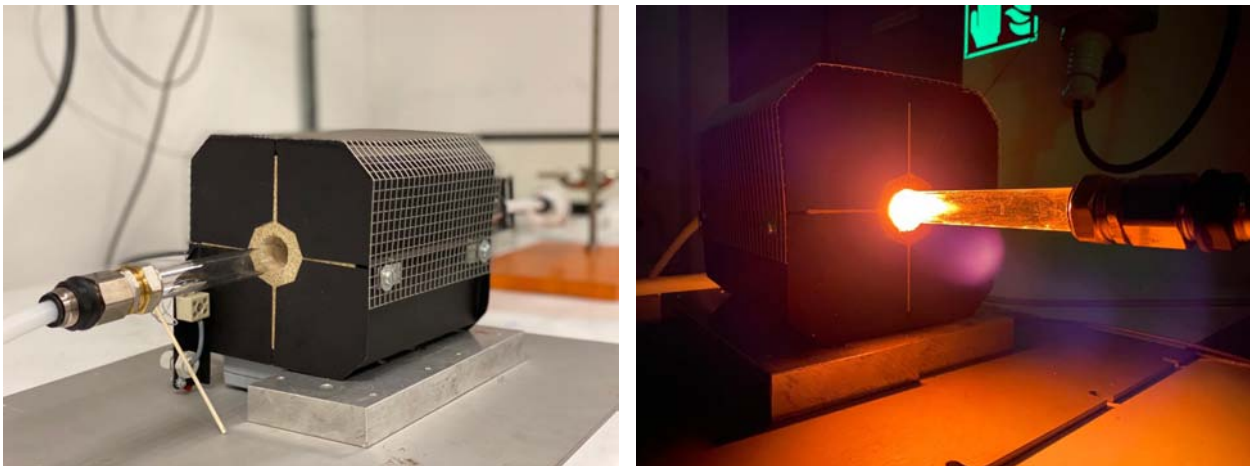


Figure 6.6: Furnace used in the experiments. The metallic blocks under the furnace are used to protect the table in which it is placed from the high temperatures. On the right picture, we can observe the thermal radiation emitted from the furnace aperture, which was at 1000 °C.

6.3 Samples

In this section we present the samples we have used in the different experiments. The radioactive samples were not specifically irradiated and thus activated for these experiments, but they had been exposed previously in the CERN accelerator complex. Given the extended radiation fields they were exposed to in comparison to their sizes as well as the high energies of the impacting particles, it is justified to assume a uniform activation of the samples.

2 The temperature is read using an external thermometer and a K-type thermocouple probe.

3 The output voltage from the regulator is selected as a fraction of the input one.

Non radioactive samples

Non radioactive samples were used prior to performing the experiment with radioactive ones in order to test various aspects such as the structural integrity of the materials to be heated and the optimum shapes to be implemented. These samples were:

- 100 μm thick Cu foils.
- 35 μm thick Cu foils. Extracted from Cu tape.
- 30 μm thick Al foils (*i.e.* two layers of standard Al paper).

Radioactive Cu

The activated Cu foils from where the radioactive Cu samples were extracted are a portion of cable shielding. The cables were placed in the Super-Proton-Synchrotron (SPS) accelerator and got activated as a consequence of its operation.

Given the dimensions of the foils, which can be observed in Fig. 6.7, we prepared three small samples [$(4.0 \pm 0.1) \times (4.8 \pm 0.1) \text{ cm}^2$, $(4.0 \pm 0.1) \times (4.8 \pm 0.1) \text{ cm}^2$ and $(3.0 \pm 0.1) \times (4.8 \pm 0.1) \text{ cm}^2$] in order to get a combined sample of $(11 \pm 0.2) \times (4.8 \pm 0.1) \text{ cm}^2$ and $1.342 \pm 0.001 \text{ g}$. The reasoning behind the use of this particular shape is discussed in section 6.4.2. The foils' thickness is calculated assuming a density of 8.96 g/cm^3 , resulting in $49.3 \pm 1.3 \mu\text{m}$. A total length of 11 cm is chosen to maximize the amount of Cu (which is important in order to minimize the uncertainty of the gamma-ray spectrometry analysis) while confining the sample in the furnace's region with the most uniform temperature (see 6.4.1 for details). The cross-shaped bars that can be observed inside the samples in the top right picture of Fig. 6.7 are made out of non-radioactive Cu (100 μm thick) and they serve two purposes: to improve the structural robustness of the samples and to prevent (up to some extent) that radioactive isotopes escaping from one side of the sample are deposited in another one. The first gamma-ray spectrometry measurement of this sample revealed the presence of ^{57}Co and ^{60}Co (see Tab. 6.1), in agreement with our expectations. As we can observe,

Table 6.1: Results of the first gamma-ray spectrometry measurement of the Cu sample. In addition, the committed effective dose for inhalation (e_{inh}) has been included assuming the inhalation of the total activity for each isotope. MDA stands for Minimum Detectable Activity.

Nuclide	Half life	Activity [Bq]	Activity Unc. [%]	MDA [Bq]	E_{inh} (Adult) [nSv]
^{57}Co	271.79 d	0.0468	21.48	0.0444	0.0281
^{60}Co	5.27 y	0.647	7.79	0.105	11.0

the activation levels of the sample are very low, and even the inhalation of its whole content would provoke a committed effective dose of approximately 11 nSv only (last column of Tab. 6.1). This value has been calculated using the data from the "Ordonnance sur la radioprotection" (ORaP) suisse [51]. Therefore, from a radiological point of view an accidental exposure scenario can be

considered as having negligible health consequences, which was also confirmed with the approval of the responsible Radiation Protection engineer.

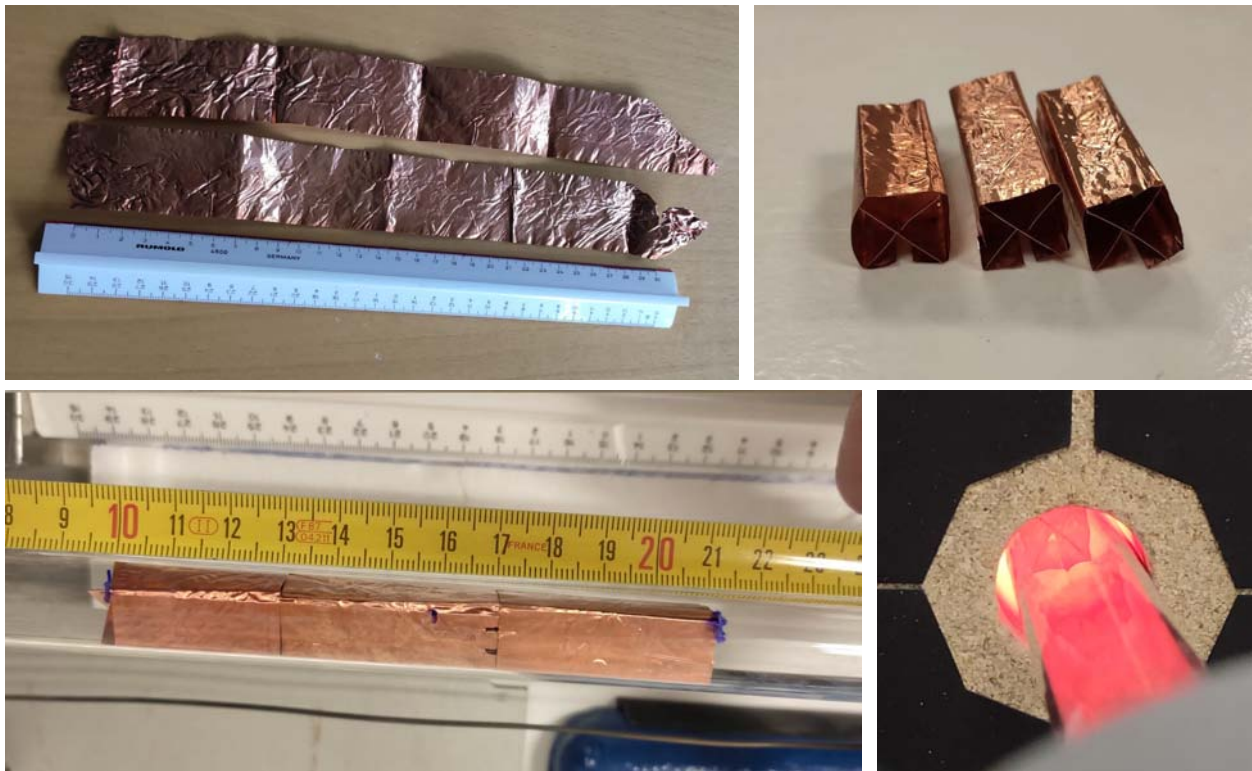


Figure 6.7: Activated Cu foils (upper left), samples ready to be used (upper right), samples inside the quartz tube (lower left) and inside the furnace at high temperature (lower right).

Radioactive Al

The shape and dimensions of the Al sample are similar to those of the Cu one (square-like and $(11.0 \pm 0.1) \times (4.8 \pm 0.1) \text{ cm}^2$) for the same reasons, with the only exception of the thickness. Its mass is $1.342 \pm 0.001 \text{ g}$ and, if we assume a density of 2.70 g/cm^3 , we can obtain its thickness: $94 \pm 2 \text{ }\mu\text{m}$. The full sample is made of a single Al piece (see Fig. 6.8), which comes from the SPS target area TDC2 at CERN. Cross-shaped bars of non radioactive Cu (note that Al has a melting temperature much lower than Cu) are also used to improve robustness and minimize the deposition of radionuclides. The first gamma-ray spectrometry measurement of this sample revealed the results shown in Tab. 6.2. In this case, the activation levels are higher than those of the Cu sample,

Table 6.2: Results of the first gamma-ray spectrometry measurement of the Al sample. In addition, the committed effective dose for inhalation has been included assuming the inhalation of the total activity for each isotope.

Nuclide	Half life	Activity [Bq]	Activity Unc. [%]	MDA [Bq]	E_{inh} (Adult) [nSv]
^{22}Na	2.6 y	17.8	5.48	0.135	35.6
^{54}Mn	312.3 d	0.138	27.49	0.211	0.166

which allows for more accurate measurements of the ^{22}Na activity (see uncertainties). Nonetheless they are still very low and, similarly to the previous one, the complete inhalation of the sample's activity would imply a committed dose of about 36 nSv which can still be considered as a negligible dose.



Figure 6.8: Activated Al foil from TDC2 (upper left), portion to be used to create the sample (upper right), sample ready to be used (lower left) and sample inside the quartz tube (lower right).

X-ray fluorescence spectrometry (XRF) of the Al sample was performed to rule out a significant presence of chemical elements other than Al. The measurement result confirmed the purity of the Al sample (> 99%).

6.4 Results and discussion

In this section we will go through the outcome and discussion of the different experiments we have performed.

6.4.1 Temperature inside the furnace

The temperature inside the furnace is a key parameter of the experiments and its correct determination is of vital importance to extract accurate conclusions from the results. Once stabilized, we assume the temperature inside the furnace to be only a function of the depth inside the furnace's aperture and therefore, for a given depth, the temperature will be considered uniform regardless of the other two spatial coordinates. This may not be entirely true, but it is a reasonable approximation given the lack of a suitable and accurate experimental method to better assess it. The temperature map consequently translates into a longitudinal temperature profile, that has been characterized using two K-type thermocouple probes connected to a thermometer in combination with a standard

ruler to determine the thermocouple position inside the furnace. The second thermocouple is fixed at a chosen position and used to monitor the temperature's stability, so the profile can later be corrected to account for potential fluctuations. Note that this correction may not be perfect because changes in temperature at a given position may not imply exactly the same temperature change at all positions, although this assumption can work well as a first approximation.

There are multiple sources of uncertainty in the experimental procedure that need to be considered:

- Associated with the determination of the thermocouple position:
 - The ruler precision is 1 mm, which introduces a ± 0.5 mm uncertainty to our measurement.
 - Thermocouple bending: the probe is introduced in the furnace outside the quartz tube. Due to the thin aperture available between the tube and the furnace's inner wall, as well as the thermocouple's flexibility, it can be bent very easily when being introduced. This implies an uncertainty in the determination of its position, which is obtained by measuring the displacement of a marked dot in the portion of the probe staying outside the furnace. The quantification of the potential error introduced is not obvious but we can expect to be on the safe side if we assume it to be ± 0.5 cm.
- Associated with the temperature measurement:
 - Thermometer accuracy: ± 0.3 % rdg (reading) $+1$ °C from -50 to 1000 °C and ± 0.5 % rdg $+1$ °C from 1000 to 1300 °C. For those experiments well below 1000 °C we will use the former accuracy, and for those around 1000 °C we will use the latter.
 - Thermocouple accuracy: greater of 2.2 °C or 0.75 %.

It has been observed that measurements of the same temperature profile scanning the furnace in different directions (*i.e.* introducing the thermocouple from right to left and from left to right), return somewhat different results, as shown in Fig. 6.9. The differences are more significant in the extremes and may be explained by a poor performance of the thermocouple probe when its tip is exposed to much lower temperatures than its body. Relying on this assumption, the real profile should be better approximated in the left part of the furnace (position ≤ 11 cm) by the measurement performed from left to right, and by the opposite one in its right part (position > 11 cm). The centres of the profiles are almost identical so we will consider the real profile to be given by the measurement "from left to right" up to position = 11 cm, and by the measurement "from right to left" for position > 11 cm. It is in the furnace's centre where the experimental samples will be placed so that the potential uncertainty associated to this effect is minimized. In the rest of the tests performed we have always measured the temperature profile from left to right and therefore we will use the ratio between the Fig. 6.9 curves to correct the measured temperature for position > 11 cm.

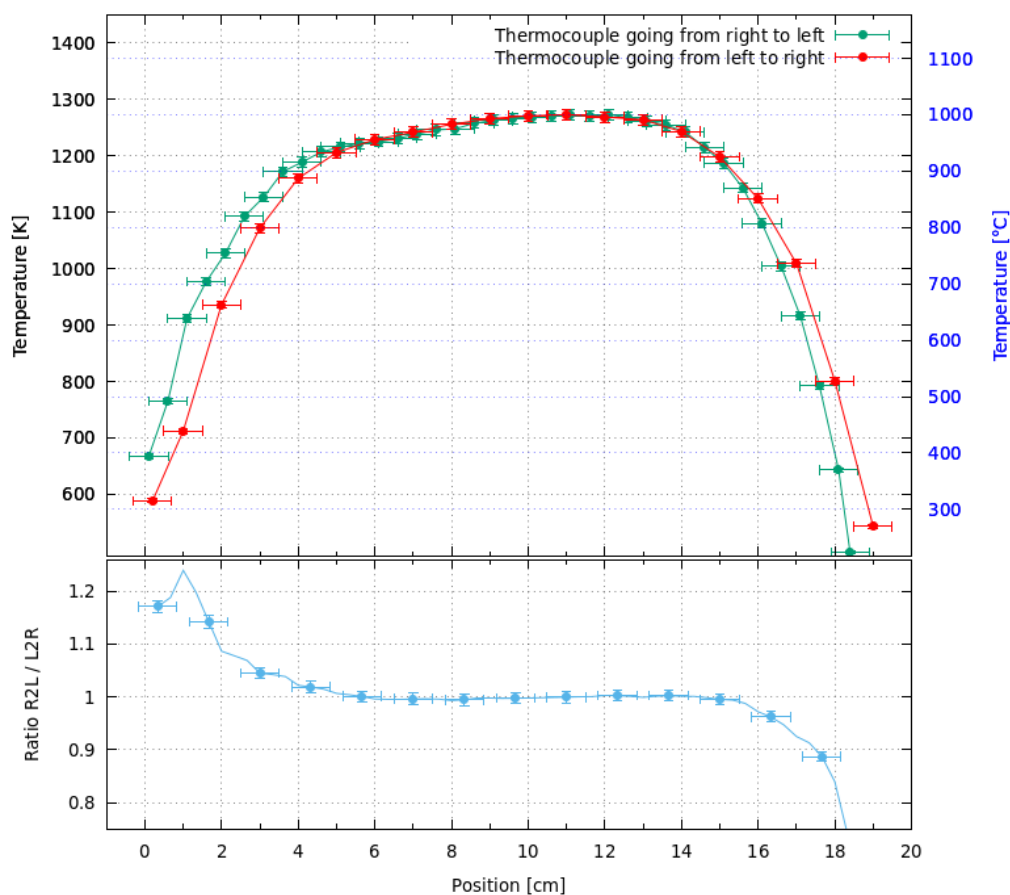


Figure 6.9: Temperature profiles measured scanning the furnace in opposite directions. The ratio between both profiles is also shown. R2L stands for right to left, while L2R stands for left to right.

As mentioned earlier, the thermocouple probe is placed next to the quartz tube but outside of it, which prevents us from provoking potential leaks in the gas circuit. It comes at the cost of not measuring the exact temperature at which our samples are exposed. To clarify whether the temperature inside and outside of the quartz tube are equal or not, we performed another test. The results are shown in Fig. 6.10. To do this test, the left end of the quartz tube was left open in order to introduce the thermocouple inside. The gas (N_2) was flowing from right to left, being released through the open side of the quartz tube. This was done to measure the profiles from left to right, as in the rest of the experiments. One can observe in the figure that the profiles present some differences, in particular, the one inside the quartz tube is smoother than the one outside of it, with lower maximum temperatures. On the other hand, it is also true that the profiles' differences could be explained by the influence of the gas flowing from right to left, transporting heat further to the left. This would result in a reduction of the temperature in the right side of the furnace and an increment in the left one, as observed. Nonetheless, in the central part of the furnace we observe lower temperatures inside the quartz tube than outside, with differences below 2%. In the experiments using samples, the gas flows in the opposite direction and this may affect the temperature profile, as just mentioned. We will use the ratio between both profiles to correct the temperature measured outside of the quartz tube in later experiments to better estimate the

temperature inside of it. However, in case a similar experimental campaign is carried out in the future it may be worth to repeat these measurements with the gas flowing in the opposite direction to study its influence on the temperature gradient.

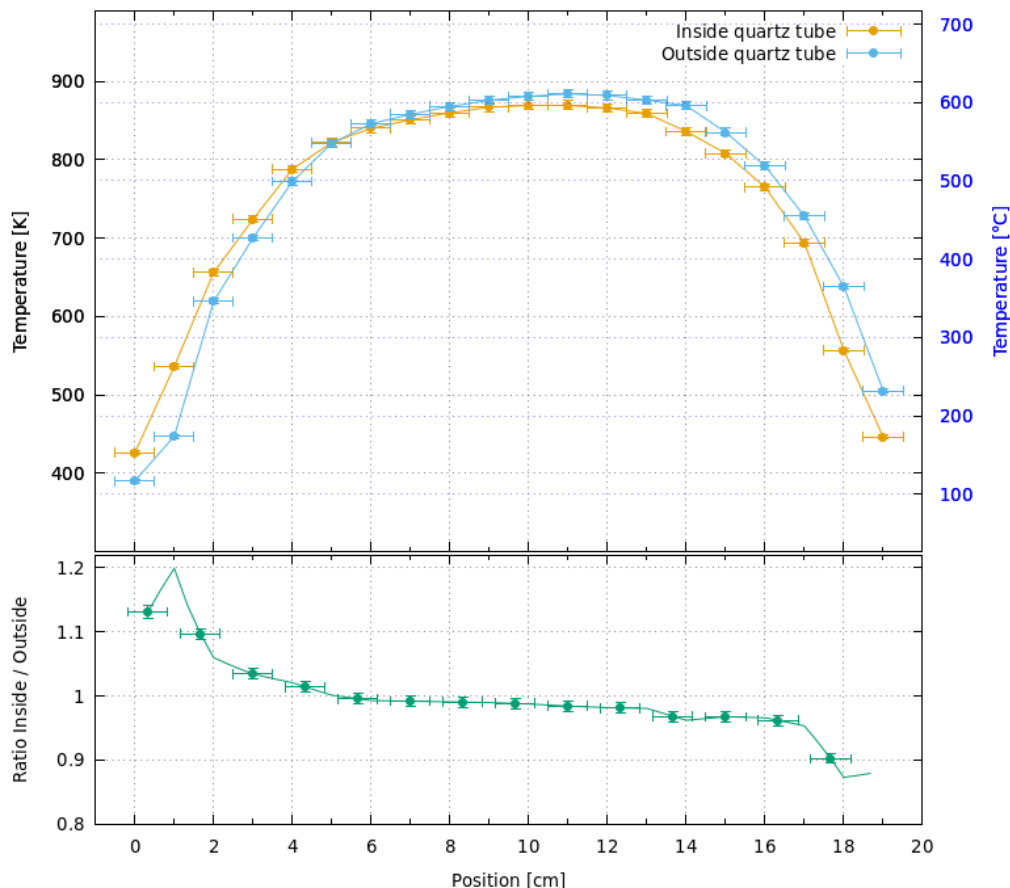


Figure 6.10: Temperature profiles measured outside and inside the quartz tube. In both cases the furnace was scanned from left to right, with the left extreme of the quartz tube open and gas flowing inside it from right to left.

Applying the two corrections discussed above to the measured data we obtain the results shown in Fig. 6.11, where the temperature gradient inside the furnace's aperture is shown for maximum temperatures measured⁴ outside the quartz tube of 1000 °C and 600 °C. The uncertainties also include the temperature fluctuations during the experiments: ± 3 °C. Zooms of the highest temperatures for both profiles are also reported.

⁴ These temperatures are measured by placing the thermocouple in the position at which the maximum temperature was observed during the profile characterization. Then, the obtained value is used to scale the temperature profile accordingly so we can compute the temperature gradient for each experiment. In order to do this correctly, one needs to propagate the uncertainty in the position of the thermocouple and in the temperature reading to the uncertainty of the scaling factor (note that uncertainty in position can lead to uncertainty in temperature, which needs to be accounted for).

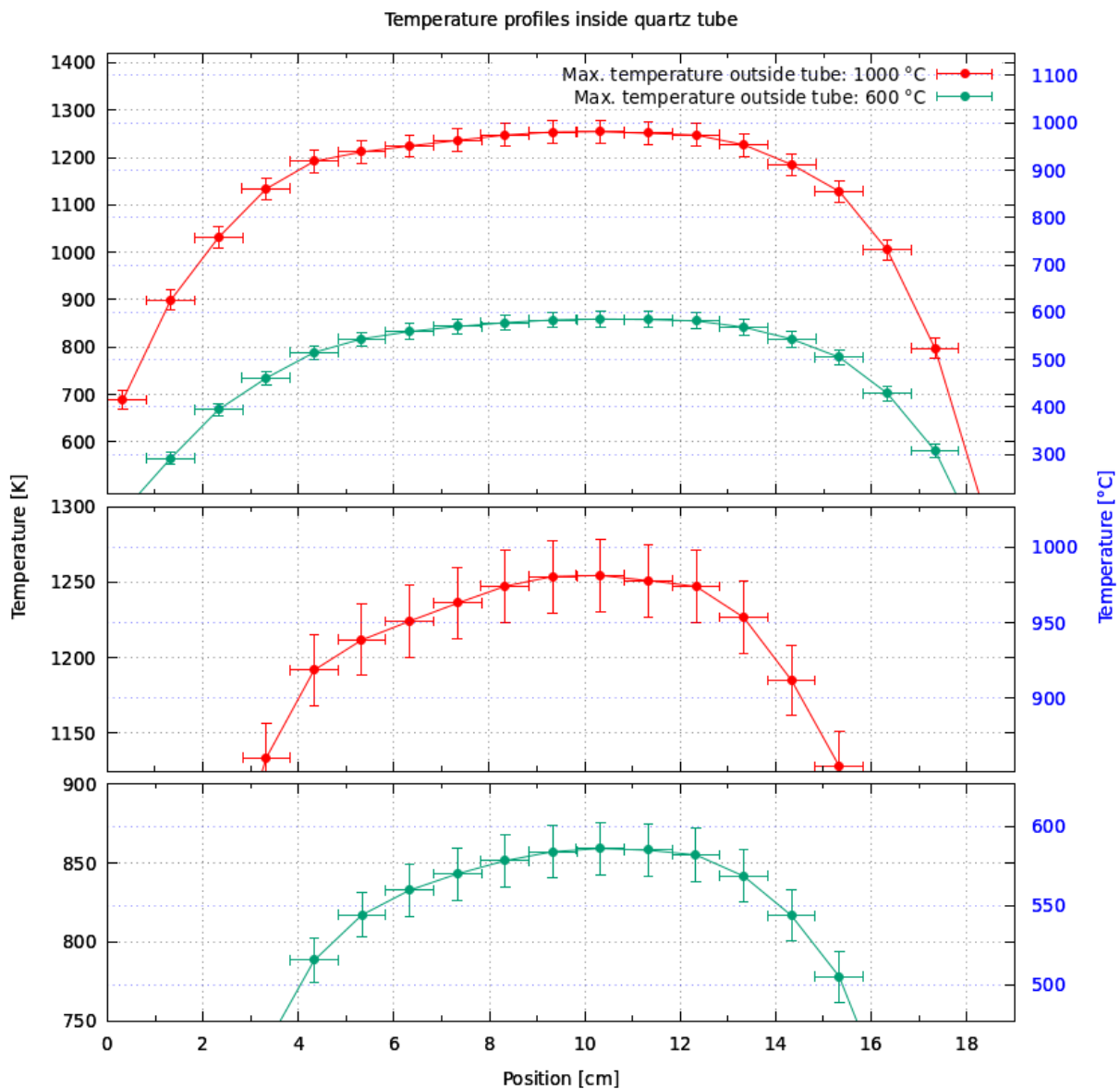


Figure 6.11: Furnace's temperature profiles for two different maximum temperatures. The Cu samples will be exposed to the 1000 °C profile and the Al ones to the 600 °C one. Zooms of the central parts of both profiles are shown.

As discussed in section 6.2.1, the gas flux is monitored using a bubbler, which is crucial for the experiment but cannot provide accurate quantitative data. Therefore, it is likely that the gas flow would not be constant for different experiments and not even during the whole duration of a single one. This is why we performed several tests modifying the gas flow while monitoring the furnace's temperature at its maximum. No significant impact on the temperature was observed for moderate changes in the gas flow. Of course, severe changes could significantly affect the temperature profile, but these changes are sufficiently pronounced to be detected observing the bubbler, being the gas flow interruption the most likely one to happen.

No significant evolution of the temperature gradient was detected during the experiments. In all cases we waited a minimum of 15 minutes after the desired maximum temperature was reached to allow for the gradient's stabilization. Several tests were carried out to check if an appreciable difference was observed, all providing a negative result.

The data shown in Fig. 6.9 and 6.10, the latter used to obtain Fig. 6.11, are the result of the linear interpolation of the raw data obtained during the experiments, which can be consulted in appendix F. This was done to allow for a comparison of results from different experiments, which do not share common ranges and granularity.

6.4.2 Non-radioactive Cu in N₂ atmosphere

Several tests were performed with the goal of testing the structural integrity of the materials to be heated up prior to using radioactive samples. The temperature was maximized in order to maximize the out-diffusion of radionuclides, but preventing the melting of Cu (around 1085 °C). This is why a temperature of 1000 °C during at least 1 h was targeted.

Initially, we performed tests using 100 µm thick Cu foils in a N₂ atmosphere. Several samples were created in order to find an optimum shape, which would maximize the Cu mass, the sample surface and its robustness. Few examples are shown in Fig. 6.12. The spiral shape maximized the Cu mass and the sample surface but unfortunately, after 1 h at 1000 °C, it partially lost its stiffness and some of the spiral walls came into contact. As a consequence, those radionuclides escaping from one surface would immediately be deposited on another one, which would distort our results. On the contrary, the squared and triangular shapes passed the test without major issues, remaining almost unaltered. We chose to proceed with our experiments using the squared shape since the Cu mass and surface are larger than the triangular. In addition, we realised that by introducing a non-radioactive cross-shaped bar inside of the squared sample we could increase its robustness and reduce the chances for a released radionuclide to be deposited again on another part of the sample (lower left picture of Fig. 6.12).

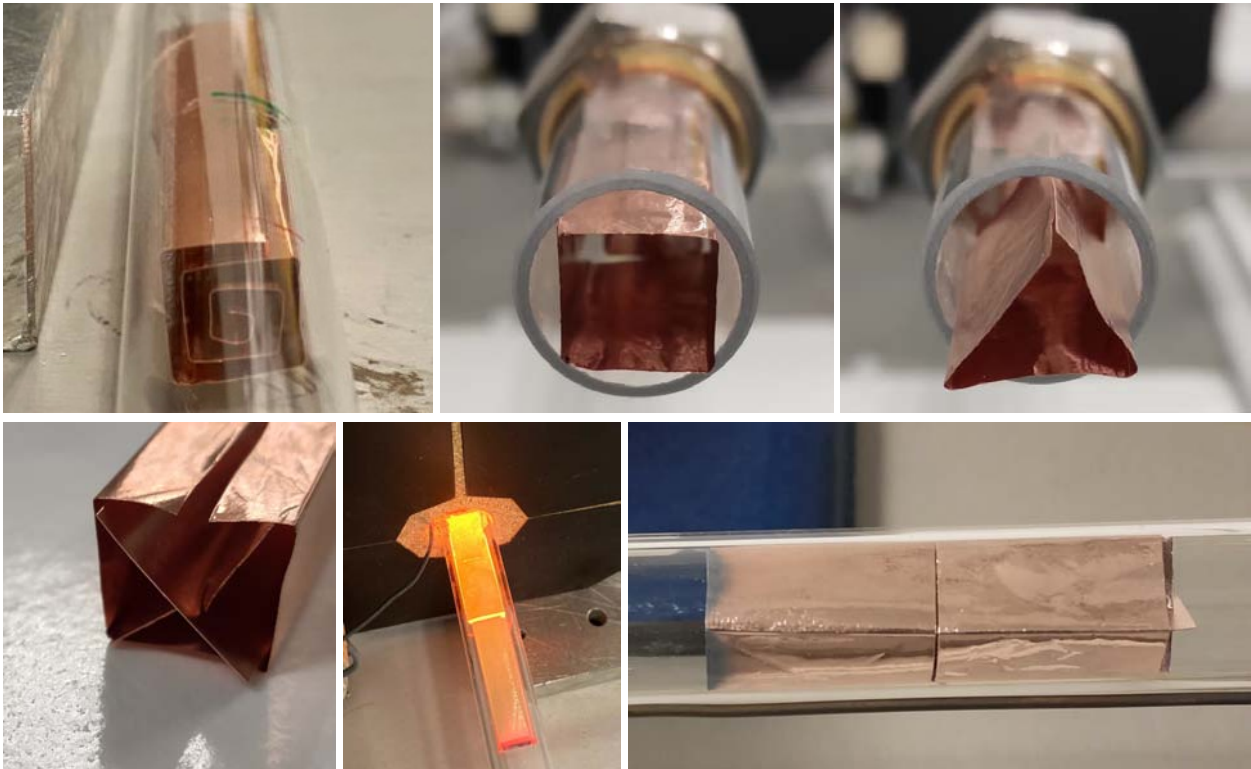


Figure 6.12: Different geometrical shapes tested (upper images), geometry selected for the experiments with radioactive samples (lower left), testing samples immediately after being removed from the furnace (lower centre) and slightly oxidized testing samples (lower right).

Once the sample's shape was selected, further tests were performed using thinner Cu foils of $35\ \mu\text{m}$ thickness to ensure that the radioactive samples (with a thickness of $50\ \mu\text{m}$) would also withstand the temperatures. The experiment was successfully completed without major deformation of the Cu foils, which can be observed in the lower right picture of Fig. 6.12. The reader may notice some darker regions in the left extreme of the sample, which we believe are due to slight oxidation. Most probably some O_2 entered the circuit when the quartz tube was being pulled out from the furnace.

6.4.3 Radioactive Cu in N_2 atmosphere

Several experiments were carried out using the radioactive Cu sample described in section 6.3. The temperature gradient at which the sample was exposed is that one shown in Fig. 6.11 for $1000\ ^\circ\text{C}$ and in particular between position = 4 cm and position = 15 cm. Gamma-ray spectrometry measurements were performed before and after every iteration in order to monitor the radionuclide content of the sample. The results of each measurement are shown in Tab. 6.3.

Table 6.3: Results of the gamma-ray spectrometry measurements of the radioactive Cu sample performed before and after each heating iteration. Activity corr. is the activity of the sample once it has been corrected for its decay in order to be directly comparable to the results of the first spectrometry.

	Nuclide	Activity [Bq]	Activity corr. [Bq]	Activity Unc. [%]	MDA [Bq]
1 st g-spec	⁵⁷ Co	0.0468	0.0468	21.48	0.0444
	⁶⁰ Co	0.647	0.647	7.79	0.105
Heating the sample: 1 h					
2 nd g-spec	⁵⁷ Co	0.0489	0.0491	25.26	0.0566
	⁶⁰ Co	0.615	0.615	8.14	0.117
Heating the sample: 4 h					
3 rd g-spec	⁵⁷ Co	0.0300	0.0323	31.68	0.0451
	⁶⁰ Co	0.630	0.637	7.92	0.091

Acquisition times of 150000 s were employed in all measurements in an effort for reducing their uncertainties. Longer periods are not advisable due to the evolution of the background with time. A large portion of the uncertainty is due to systematic errors that could not be reduced by increasing the measurement time, especially for ⁶⁰Co. The out-diffusion fractions for each heating iteration have been computed and collected in Tab. 6.4.

Table 6.4: Out-diffusion fractions computed using the data in Tab. 6.3 for each heating iteration. Note that since the ODF is given as a percentage, its uncertainty, although absolute, is also given as a percentage.

Total heating time	Nuclide	ODF [%]	ODF Abs. Unc. [%]
1h	⁵⁷ Co	-4.9 ⁵	34.1
	⁶⁰ Co	5.0	11.0
5h	⁵⁷ Co	31.0	31.4
	⁶⁰ Co	1.6	11.0

We shall focus our attention on the results of ⁶⁰Co, since the activities obtained for ⁵⁷Co are too close to (or even below) the MDA, and therefore the actual loss cannot be quantified with sufficient precision. We obtained an ODF of 1.6 ± 11.0 % after 5 h of heating. As a consequence, we cannot assume that any ⁶⁰Co isotopes escaped from the sample; but we can say that the amount that escaped was less than 12.6 % with 1σ certainty.

It is worth to mention that after the second experiment we observed that a previously generated black stain, originating from the deposition of burnt copper during a previous test, changed its color during the experiment, eventually resembling again unoxidized copper. We believe this is due to the deposition of some Cu atoms that managed to escape from the sample. Unfortunately,

⁵ The negative ODF, although not physical, comes simply from subtracting the results of two measurements with high uncertainties. As we can see in Tab. 6.3, the activities obtained for ⁵⁷Co are comparable or below the MDA and therefore they are not reliable results.

even if we had a sufficiently accurate balance, we could not quantify the amount of Cu that escaped from the sample comparing the mass of the sample before and after the experiment because it is increased as a consequence of oxidation. Although the amount of oxygen entering the gas circuit is very small (mainly due to manipulation of the tube to move the samples out of the furnace), it is still enough to slightly increase the mass of our sample, masking any mass change due to other effects.

Note that heating times reported correspond to the time that the sample spent inside the furnace at the maximum temperature. One should keep in mind that several minutes are needed for the sample and the tube to be brought up to this temperature once introduced in the furnace. Similarly, few minutes are needed to cool them down after their extraction. This is true for each and every experiment.

6.4.4 Non-radioactive Al in N₂ atmosphere

Before the experiment using radioactive Al, we carried out a test using a non-radioactive Al foil. We chose the same geometrical shape already used for Cu, introducing cross-shaped Cu bars inside the squared Al sample. It was exposed to the temperature profile shown in Fig. 6.11 for 600 °C during 1 h. After the test, we could not observe any damage of the sample and its structural integrity was preserved, which allowed us to conclude that it was safe to proceed with the radioactive Al. The only difference we could observe was that the sample took on a smoky hue.

6.4.5 Radioactive Al in N₂ atmosphere

Similarly to the experiments carried out with the radioactive Cu foil, we used the Al sample described in section 6.3 with the aim of determining the ODF of (mainly) ²²Na after exposing it to high temperatures during several hours. The temperature profile to which the sample was exposed is the one shown in Fig. 6.11 for 600 °C and in particular between the longitudinal position = 5 cm and position = 16 cm. Three iterations of the experiment were performed and therefore four gamma-ray spectrometry measurements were needed to monitor the evolution of the radioactive content of the sample. The results are shown in Tab. 6.5.

Table 6.5: Results of the gamma-ray spectrometry measurements of the radioactive Al sample performed before and after each heating iteration.

	Nuclide	Activity [Bq]	Activity corr. [Bq]	Activity Unc. [%]	MDA [Bq]
1 st g-spec	²² Na	17.8	17.8	5.48	0.135
	⁵⁴ Mn	0.138	0.138	27.49	0.211
Heating the sample: 2h					
2 nd g-spec	²² Na	15.1	15.2	5.52	0.121
	⁵⁴ Mn	0.130	0.133	28.45	0.112
Heating the sample: 2h10min					
3 rd g-spec	²² Na	13.6	13.8	5.96	0.0110
	⁵⁴ Mn	0.121	0.125	48.95	0.0928
Heating the sample: 2h					
4 th g-spec	²² Na	10.4	10.6	6.39	0.0158
	⁵⁴ Mn	0.100	0.106	36.02	0.0260

As in previously reported experiments, the acquisition time employed was always 150000 s for the same reasons. The ODF for each heating iteration are presented in Tab. 6.6.

Table 6.6: Out-diffusion fractions computed using the data in Tab. 6.5 for each heating iteration.

Total heating time	Nuclide	ODF [%]	ODF Abs. Unc. [%]
2h	²² Na	14.6	7.3
	⁵⁴ Mn	3.6	38.8
4h10min	²² Na	22.5	7.3
	⁵⁴ Mn	9.4	52.2
6h10min	²² Na	40.4	7.0
	⁵⁴ Mn	23.2	39.5

In addition to this analysis, we have carried out combined spectrometry analysis of the cross-shaped Cu bars introduced inside the sample and the HEPA filter used in the experiments. Both elements were replaced by new ones after each iteration. The results are shown in Tab. 6.7.

Table 6.7: Results of the combined gamma-ray spectrometry measurements of the cross-shaped Cu bars and the HEPA filter used in the experiments.

	Nuclide	Activity [Bq]	Activity corr. [Bq]	Activity Unc. [%]	MDA [Bq]
1 st exp.	²² Na	0.946	0.954	30.37	0.155
2 nd exp.	²² Na	0.871	0.881	13.25	0.128
3 rd exp.	²² Na	0.622	0.635	43.26	0.159

Looking at the results for ^{22}Na in Tab. 6.6 it is clear that some of the radioactive content of the sample out-diffused, somewhere in the range of [7.3,21.9] % in 2h and up to [33.4,47.4] % in approximately 6h. These results are also supported by those in Tab. 6.7, which are a second confirmation of the fact that a significant portion of the ^{22}Na escaped from the sample. Of course, the radionuclides deposited on the Cu bars and those captured by the HEPA filter are only a portion of the released ones since many of them would be expected to be deposited in the gas circuit between the sample and the filter (quartz tube, hose and connections).

During visual examination of the sample we noticed the appearance of a small hole (1-2 mm²) after the experiments. Since the temperature was continuously monitored during the process and it stayed at all times well below the Al melting point, we believe it may have been caused by some (momentary or sustained) hot spot inside the furnace.

6.4.6 Non-radioactive Cu in Air: foil and filaments

As previously described, we used oxygen-free atmospheres to carry out out-diffusion experiments with radioactive samples in order to avoid combustion. Nonetheless, we are also interested in what would happen to Cu in a normal air atmosphere in the event of a fire. In particular, we would like to know if part of it and its potential radioactive content could be released to the environment. To shed some light on this, we carried out few tests using non radioactive Cu in a normal air atmosphere. Two different sets of tests were carried out, one using a Cu foil and a second one using the Cu filaments of a standard power cable (from an old laptop power cord).

Foil

A 35 μm thick Cu foil was exposed during 20 min at a maximum temperature⁶ of 800 °C. In Fig. 6.13 one can observe the sample at different moments during the experiment:

- Upper left: sample before heating.
- Upper right: sample once it has been taken out from the furnace after heating. It became very fragile and broke as a consequence of the rapid cooling down.
- Lower left: the sample breaks very easily when extracting it from the quartz tube.
- Lower right: the sample gets completely destroyed during the extraction. The remains are shown.

⁶ It corresponds to the maximum temperature of a profile very similar in shape to those shown in Fig. 6.11

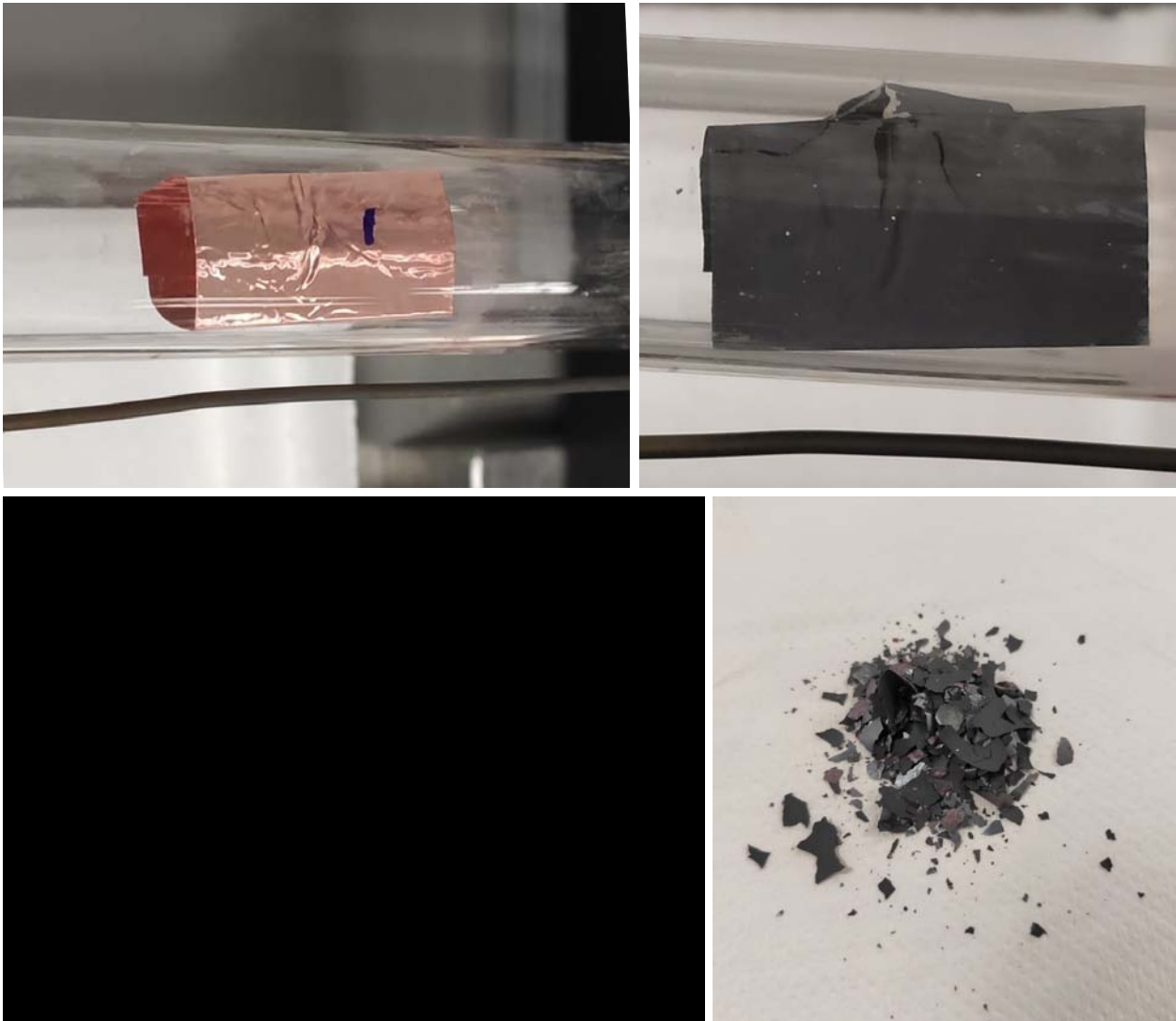


Figure 6.13: Cu foil at 800 °C in an air atmosphere. Sample before heating (upper left), sample after being taken out of the furnace 20 min latter (upper right), sample when being extracted from the quartz tube (lower left) and remains of the sample after its extraction (lower right).

We have used temperatures and heating times likely to be found in accidental fires and, in fact, they may represent an optimistic scenario. The Cu foil, which is very thin, is representative of the typical Cu foils used as cable shielding. And even for thicker objects, we expect a very similar oxidation effect (at least) on their surfaces, which could easily result in the release of material flakes to the environment given the magnitude of turbulence that combustion in a tunnel is expected to cause.

Filaments

Two tests were performed using Cu filaments of 150 μm diameter arranged as shown in the upper picture of Fig. 6.14. During the first test, they were exposed to a maximum temperature of 800 °C for 20 min. The filaments after the experiment are shown in the lower left picture of the same figure.

A significant amount of powder came off as a consequence of a brief manipulation bending them. One could see that some unburnt Cu was left in the most inner part of the filaments. For the second test we got some new Cu filaments and exposed them to a maximum temperature of 1000 °C for 20 min. The result is visible in the lower right picture. This time not much powder came off but instead the filaments became brittle. In the same picture one can also see that some of the filaments melted together.



Figure 6.14: Cu filaments at 800 °C and 1000 °C in an air atmosphere. Filaments before heating (upper picture). Filaments after 20 min at 800 °C; the powder next to them came off after a brief manipulation (lower left). New filaments after 20 min at 1000 °C, they became easily breakable (lower right).

The conclusions of these tests support those of the previous one. In the event of a fire, the outermost part of Cu objects (one could expect similar results for other metals) would burn and may be partially released to the environment in the form of powder or flakes due to fire turbulence. In terms of isotope/material release this effect could outweigh out-diffusion phenomena, due to the associated loss in mass.

6.5 Acknowledgments

The experiments reported in this chapter could be carried out thanks to the assistance of numerous colleagues. In particular, I would like to express my gratitude to:

-
- Guilherme Correia for his invaluable help and advice before and during the experiments.
 - Karl Johnston and Juliana Schell for allowing us to use the SSP labs of ISOLDE.
 - Sebastian Rothe, Jochen Ballof, Thierry Stora and Joachim Vollaire for the discussions that led to these experiments.
 - Reiner Geyer, Yann Pira and Lucie Vitkova for their help in obtaining radioactive and non radioactive samples for our experiments.
 - Alexandre Dorsival for his RP risk assessment and approval of the experiments.
 - Nabil Mena, Aurore Boscher and Giuseppe Prete for their patient assistance regarding the gamma-ray spectrometry analysis.
 - Renaud Charousset for his help with the XRF measurement of the Al sample.
 - Miranda Van Stenis for supplying and cutting the quartz tubes.

SOLIDUSS benchmarking

Contents

7.1	Numerical validation of the diffusion treatment	88
7.2	Experimental benchmarking	93
7.2.1	Simulations	93
7.2.2	Experimental data	98
7.2.3	Discussion	98

EARLIER IN this manuscript we mentioned that Monte Carlo results may be affected by multiple and diverse sources of error. Therefore, a careful check and benchmarking of any Monte Carlo code is, at the very least, highly recommended to assess its reliability. In this chapter we explain how we did it with SOLIDUSS. First, the validation of the diffusion treatment by means of a numerical experiment is detailed. Later, a comparison between the experimental data presented in the previous chapter and the corresponding SOLIDUSS results is shown and discussed.

7.1 Numerical validation of the diffusion treatment

In this section we explain the study carried out to check the implementation of SOLIDUSS' numerical treatment of diffusion [29]. To simulate the diffusion of radionuclides, one of the most important inputs that need to be provided to the code is the diffusion coefficient. This quantity, which is available in the literature for a large variety of species and materials, is usually obtained experimentally [52]. One of the typical procedures to obtain the diffusion coefficient, and in particular the activation parameters A and Q described in section 2.3, is the so-called *tracer diffusion experiment* ([15] pp. 215–223). In such experiments some radioactive isotope—the tracer—of the element whose diffusion coefficient is to be obtained, is deposited on the material of interest. This material

is then heated up to a certain temperature to promote diffusion. The resulting concentration profile of the tracer inside the material is analysed with the aim of extracting the diffusion coefficient. The boundary conditions of the experiment (material geometry, tracer deposition, temperature gradient, *etc.*) are chosen in such a way that the diffusion equation —eq. (2.4)— can be solved analytically and hence, the shape of the tracer's profile inside the host material is known beforehand. One can then obtain the best fit to the experimental results using the analytical solution of the diffusion equation with the diffusion coefficient D as the free parameter of the fit. In this way, D can be determined for a given temperature. Repeating the process, several values of D can be obtained for different temperatures. Since the dependence of the diffusion coefficient with the temperature is given by eq. (2.14) or similar, one can fit the obtained diffusion coefficients using this expression with A and Q as the free parameters of the fit. This way both quantities can be derived from the experimental data.

We can emulate this procedure by replacing the diffusion experiment with a diffusion simulation. The idea is to set up a simple problem that can be solved analytically, give the diffusion coefficient parameters A and Q to SOLIDUSS and simulate the system's evolution. The simulation will return the radionuclide concentration profile after a given diffusion time and we will treat these results as if they were experimental ones. Our goal would be to determine A and Q using those results and compare the obtained values with the ones we provided to SOLIDUSS in the first place. If the resulting values are compatibles with the input ones, we can be fairly confident about the correctness of SOLIDUSS' diffusion implementation and underlying method.

Let us consider a 1-D scenario in which the initial concentration of radionuclides is given by:

$$C(x, 0) = \begin{cases} C_0 & \text{if } x \leq 0, \\ 0 & \text{if } x > 0, \end{cases} \quad (7.1)$$

with x denoting the spatial coordinate. It can be shown (section 3.2.2 of Ref. [15]) that the solution to the diffusion equation for this particular case is the so-called *Grube-Jedele solution*:

$$C(x, t) = \frac{C_0}{2} \operatorname{erfc} \left(\frac{x}{2\sqrt{Dt}} \right), \quad (7.2)$$

where D is the diffusion coefficient and t the diffusion time.

The concentration profiles of ^{48}V after 2 hours of diffusion in Cu at different temperatures have been calculated using SOLIDUSS and reported in Fig. 7.1. Note that the initial concentration of radionuclides for $x \leq 0$ is $C_0 = 2 \cdot 10^{-3} \text{ cm}^{-3}$. In the same figure, we can see the best fits of eq. (7.2) for different temperatures. The free parameter in the fits has been defined as D , and its best fitting values are reported in the figure's legend.

We repeat the process for further temperatures and radionuclides, obtaining the results shown in Fig. 7.2. There we also show the best fits of the diffusion coefficient expression for each pair radionuclide - host material. From each of these fits, we can get A , Q and their uncertainties, which are intrinsic to the stochastic nature of our simulation and to the fitting process. We deemed it convenient to repeat the entire process considering different amounts of tracked radionuclides to

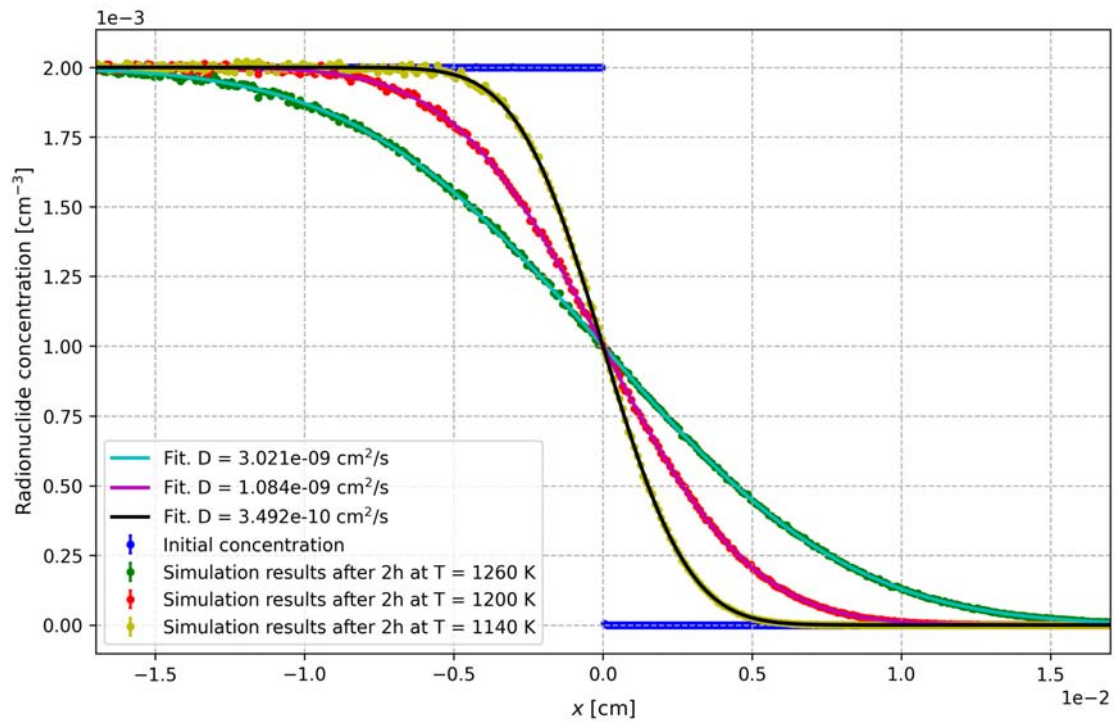


Figure 7.1: Radionuclide concentration profiles returned by SOLIDUSS for ^{48}V in Cu as well as their best fits using eq. (7.2) with D as the free parameter.

verify if the obtained results converge to the input values when the number of histories increase. The extracted values are reported in Fig. 7.3, together with the original activation parameters provided to SOLIDUSS.

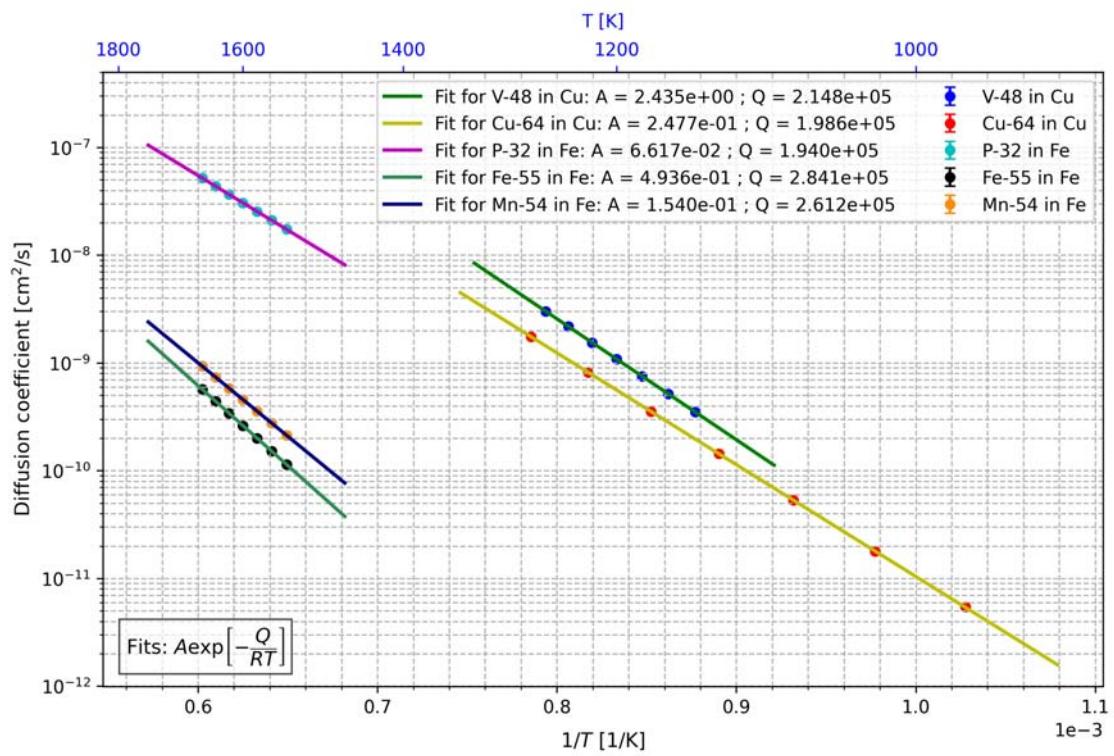


Figure 7.2: Diffusion coefficients for different temperatures and species extracted from SOLIDUSS results, together with the best fits of eq. (2.14) for each pair radionuclide - host material, being A and Q the free parameters.

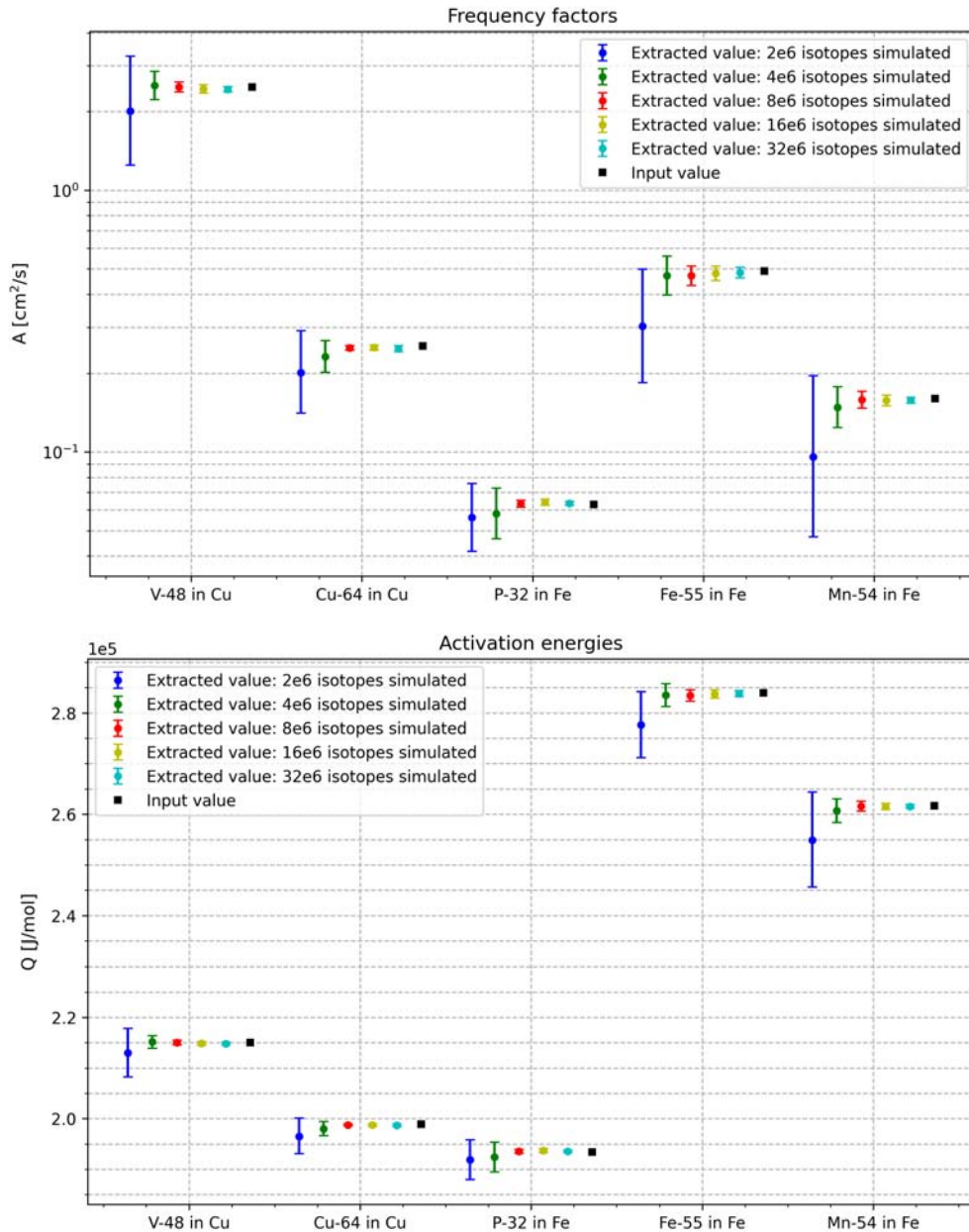


Figure 7.3: Frequency factors (top) and activation energies (bottom) for different radionuclides derived from SOLIDUSS simulations. The results are reported for various number of histories simulated. The original input values given to SOLIDUSS are also shown for comparison. The error bars correspond to 2σ confidence intervals.

We can observe a clear convergence towards the input values in all cases, as well as a good compatibility of input and extracted values within the error bars. Therefore, we conclude that the software implementation and the numerical treatment of diffusion in which it is based work as intended to the best of our knowledge. Note that SOLIDUSS does not make explicit use of the diffusion equation, yet its results are in excellent agreement with those of the diffusion equation.

7.2 Experimental benchmarking

In this section we present the simulations performed with SOLIDUSS with the aim of reproducing those experiments described in chapter 6. A discussion on the agreement of simulation and experimental results will follow.

7.2.1 Simulations

The simulation procedure is as described in previous chapters. A FLUKA geometry has to be created and the generation of the radionuclides that are created in the material of interest has to be simulated. Then, SOLIDUSS will take over and track each one of them, accounting for its potential out-diffusion. For these specific simulations the radionuclides have been uniformly sampled along the material of interest since we are assuming a uniform activation of the experimental samples. We note in passing that the spatial distribution of the radioisotopes can also be determined with FLUKA based on a beam impacting on a material and subsequent generation of radionuclides. To provide the necessary parameters needed to simulate diffusion and desorption, a diffusion input file is provided together with the FLUKA input (see appendix E).

FLUKA models

Two radioactive foils were modelled as those used in the experiments, which were folded in the squared shape that can be observed in Fig. 7.4. Their thicknesses were calculated using their surfaces and masses, which can be measured with better precision than the thickness. The characteristics of the foils are the followings:

- Cu foil. $(11.0 \pm 0.2) \times (4.8 \pm 0.1) \times (0.00493 \pm 0.00013) \text{ cm}^3$, $2.334 \pm 0.001 \text{ g}$. Assumed density: 8.96 g/cm^3 .
- Al foil. $(11.0 \pm 0.1) \times (4.8 \pm 0.1) \times (0.0094 \pm 0.0002) \text{ cm}^3$, $1.342 \pm 0.001 \text{ g}$. Assumed density: 2.70 g/cm^3 .

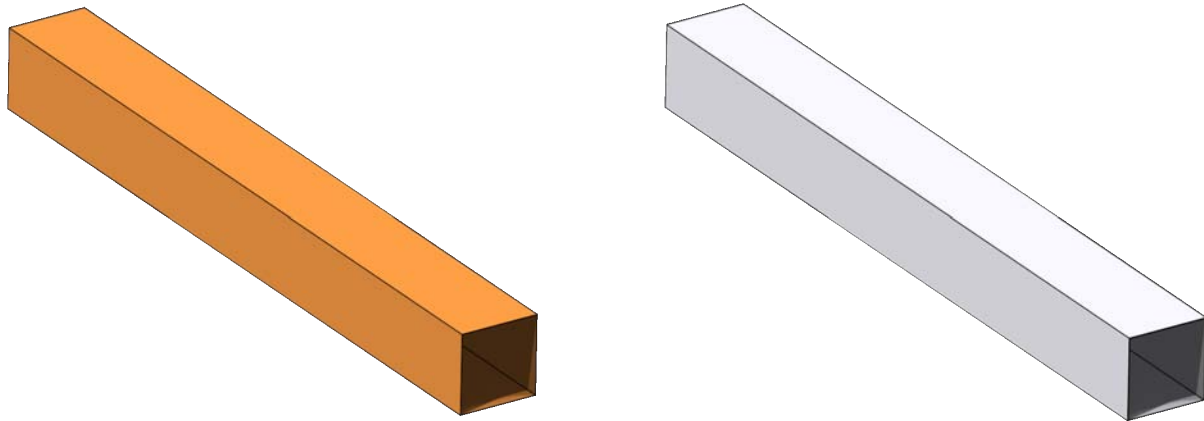


Figure 7.4: Pictures of the FLUKA models of the Cu (left) and Al (right) samples used in out-diffusion experiments.

Temperature profiles

The temperature maps are of key importance in the out-diffusion simulation. We have used those measured in the experimental campaign, but some manipulation has been necessary. The data of the experimental profile have associated uncertainties, both in position and temperature. SOLIDUSS is currently unable to deal with uncertainties in the provided temperature maps and therefore, we need to make different simulations using the extreme cases of the temperature profile in order to find out its impact on the out-diffusion of radionuclides. Please note that the uncertainty in position must be translated into uncertainty in temperature, and this has been done for each temperature bin by scanning those other bins at its reach when considering the position uncertainty and replacing the original temperature maximum and minimum by those of the nearby bins in case they were more extreme. Fig. 7.5 shows the three temperature profiles (upper, lower and mean) used for each case (Cu and Al samples). Note that the original profiles have been interpolated in order to smooth them. The data can be found in appendix F.

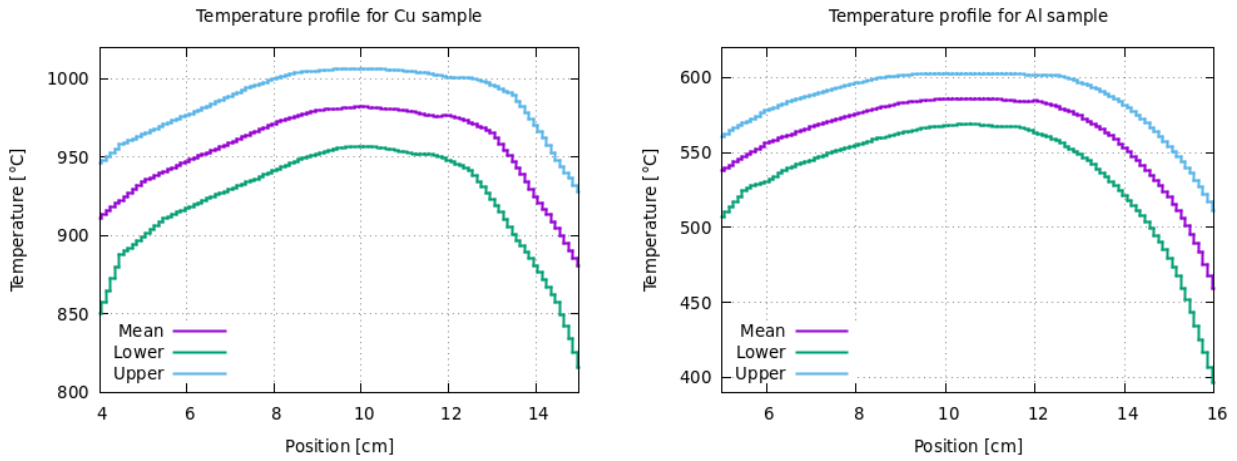


Figure 7.5: Temperature profiles at which the radioactive samples were exposed during out-diffusion experiments. Since the uncertainties of the temperature profiles cannot be fed into SOLIDUSS, three profiles for each sample are used to obtain mean results and their upper and lower limits.

Diffusion and desorption parameters

The diffusion activation energies Q_i and frequency factors A_i need to be provided within the diffusion input files for the program to be able to simulate the diffusion of radionuclides in the host material. As explained earlier, these parameters characterize the diffusion coefficient D for any given temperature T as follows:

$$D = \sum_{i=1}^l A_i \exp\left(-\frac{Q_i}{RT}\right), \quad (7.3)$$

where R is the gas constant. Commonly $l = 1$, but there are often cases in which one single pair of parameters is not enough to properly describe the evolution of D , typically because there are various relevant diffusion mechanisms. This is the case for diffusion of Co in Cu, where on top of monovacancy-mediated diffusion, the contribution of divacancies become important at high temperatures and therefore $l = 2$. Similarly, the desorption activation energies (E_{des}) and distances between nearest atomic neighbours (DNN) are needed to simulate desorption, as explained earlier in this document. The data used in our simulations has been compiled in Tab. 7.1.

Table 7.1: Parameters provided to SOLIDUSS to simulate the out-diffusion of radionuclides of interest (Nuc.) from their host materials (Mat.). A_i and Q_i have been taken from Refs. [23, 53, 54], E_{des} from Ref. [41] and DNN from Ref. [55]. Some uncertainties are not specified because they are not reported in the original references.

Mat.	Nuc.	A_1 [$\text{cm}^2 \text{s}^{-1}$]	Q_1 [kJ mol^{-1}]	A_2 [$\text{cm}^2 \text{s}^{-1}$]	Q_2 [kJ mol^{-1}]	E_{des} [kJ mol^{-1}]	DNN [pm]
Cu	^{60}Co	$0.74^{+0.22}_{-0.17}$	217.2 ± 1.9	$736^{+2.9 \cdot 10^6}_{-735.8}$	312.8 ± 96.5	416.1	256
Al	^{22}Na	$6.7 \cdot 10^{-4}$	97.1 ± 13	-	-	134.5	286

The reader may have noticed the large uncertainties of A_2 and Q_2 for Co in Cu shown in Tab. 7.1. These parameters refer to the divacancy contribution with respect to diffusion and its uncertainties result from the modest contribution of this mechanism to the diffusion coefficient, which makes an accurate determination very difficult [54]. A_i and Q_i are generally obtained by fitting the diffusion coefficients measured at different temperatures using eq. (7.3). Both parameters are strongly correlated and hence, if we are interested in the different out-diffusion results produced when scanning the uncertainties of these parameters, one cannot adjust each of them independently since the obtained D would be completely off from the fitted experimental data (e.g. if we take $A_2 = 736 + 2.9 \cdot 10^6 \text{ cm}^2/\text{s}$ and $Q_2 = 312.8 - 96.5 \text{ kJ/mol}$ we obtain a D seven orders of magnitude above the mean one, which is not at all representative of the experimental uncertainties.). Instead, if we take the upper value of A_i , we must take also the upper value of Q_i and *vice versa*. Nonetheless, the authors are skeptic about the lower limit of A_2 and Q_2 because the resulting contribution of the divacancy mechanism would be large ($\approx 20\%$ of the total D) also for low temperatures and, in fact, it would be larger for lower temperatures (e.g. 900 K) than for higher ones (e.g. 1300 K), which seems unrealistic. As we will see soon, the desorption of Co from Cu is very low, and small variations in the diffusion coefficient would not affect the (ODF) of radionuclides in a significant way.

Results

The simulation results for the two samples are compiled in Tab. 7.2. For comparison, the results are reported with and without activating the desorption model. If it is not activated, every radionuclide reaching the sample's surface is considered as out-diffused, and therefore the ODF is always larger or equal than that one obtained when activating desorption (within statistical fluctuations). We have used three different sets of data with the desorption model activated in order to obtain a mean for the ODF as well as lower and upper limits to it taking into account the uncertainties of the different parameters employed (see Fig. 7.5 and Tab. 7.1):

- Mean: we have used mean foil thicknesses for Cu (49.3 μm) and Al (94 μm), mean temperature profiles and mean diffusion coefficient parameters.
- Lower limit: upper foil thicknesses for Cu (50.6 μm) and Al (96 μm), lower temperature profiles and lower diffusion coefficient parameters.
- Upper limit: lower foil thicknesses for Cu (48.0 μm) and Al (92 μm), upper temperature profiles and upper diffusion coefficient parameters.

Table 7.2: ODF simulation results for both samples and different heating times with and without activating the desorption model. Lower and upper limits have been obtained considering the uncertainties of the different parameters input to SOLIDUSS. The errors reported in this table are purely statistical and correspond to 2σ confidence intervals.

Mat.	Nuc.	Time [min]	ODF [%]			
			Without des. model	With desorption model		
			Mean	Lower limit	Upper limit	
Cu	^{60}Co	60	59.99 ± 0.13	$(1.527 \pm 0.014) \cdot 10^{-2}$	$(6.90 \pm 0.08) \cdot 10^{-3}$	$(1.858 \pm 0.014) \cdot 10^{-2}$
		300	95.88 ± 0.01	$(7.65 \pm 0.03) \cdot 10^{-2}$	$(3.46 \pm 0.02) \cdot 10^{-2}$	$(9.36 \pm 0.02) \cdot 10^{-2}$
Al	^{22}Na	120	34.66 ± 0.20	34.73 ± 0.16	10.69 ± 0.13	90.04 ± 0.16
		250	49.25 ± 0.21	49.17 ± 0.14	15.17 ± 0.12	97.34 ± 0.02
		370	59.82 ± 0.18	59.71 ± 0.16	18.62 ± 0.10	99.26 ± 0.01

The ODF of a given species from its host material will be determined by how easily it diffuses and desorbs. The ODF would be limited by diffusion if the desorption of the nuclides is likely to happen once they reach the surface, or it may be limited by desorption in case it is unlikely and therefore, the radionuclides would not escape even if they reach the surface. From Tab. 7.2 we can easily see (comparing the results with and without diffusion model) that the ODF of Co from Cu is clearly limited by its desorption since a very large fraction of them manages to reach the surface, but very few manage to escape. For these scenarios, the desorption model seems to be a must. On the contrary, we have the case of Na in Al, whose ODF is mostly limited by diffusion since virtually all the nuclides reaching a surface manage to escape. Tab. 7.3 summarizes the results (with desorption model) shown in Tab. 7.2, using the lower and upper limits as the uncertainty ranges for the mean ODF.

Table 7.3: Summary of the simulation results for the ODF obtained with the desorption model active. The uncertainties reported here correspond to the upper and lower limits in Tab. 7.2.

Material	Nuclide	Heating time [min]	ODF [%]
Cu	^{60}Co	60	$1.5^{+0.4}_{-0.9} \cdot 10^{-2}$
		300	$7.7^{+1.7}_{-3.4} \cdot 10^{-2}$
Al	^{22}Na	120	$34.7^{+55.5}_{-24.2}$
		250	$49.2^{+48.2}_{-34.1}$
		370	$59.7^{+39.6}_{-41.3}$

When looking at ODF results, the reader is advised to think in terms of logarithmic scale, rather than linearly. At a first glance, a result like the one for ^{22}Na in Al after 250 min may seem to be covering almost the whole range of values and therefore may be misinterpreted as a poor result when thinking linearly on the [0% – 100%] range. To better understand the reason, let us imagine we are dealing with an activity of 10 TBq, then to say that few TBq would escape if the sample is exposed to a given temperature (case of Na in Al) may be radically different in terms of radiation

protection than an ODF of few MBq (case of Co in Cu), which is still far from zero and could be important, even if the relative amount escaping may be considered as low.

7.2.2 Experimental data

The simulation results presented above should be compared with the experimental data (see Tab. 7.4), obtained by means of the experimental campaign reported in chapter 6.

Table 7.4: ODF results obtained in the experiments that we intend to reproduce using the simulations reported in section 7.2.1. These data have been extracted from Tabs. 6.4 and 6.6.

Material	Nuclide	Heating time [min]	ODF [%]
Cu	^{60}Co	60	5.0 ± 11.0
		300	1.6 ± 11.0
Al	^{22}Na	120	14.6 ± 7.3
		250	22.5 ± 7.3
		370	40.4 ± 7.0

7.2.3 Discussion

The results from the experiments and the simulations are in good agreement within error bars, as shown in Fig. 7.6. Unfortunately, the uncertainties could not be further reduced. In the Co case, this is because of the experimental procedure, which does not allow for establishing a lower limit above zero when the ODF is found to be below few percent (uncertainties linked to the gamma spectrometry analysis). In the case of Na, the larger error bars are those of the simulation's results, since the uncertainties in temperature and the diffusion activation energy have a remarkable impact on the results due to the exponential behaviour of the diffusion coefficient and the desorption rate as functions of these parameters.

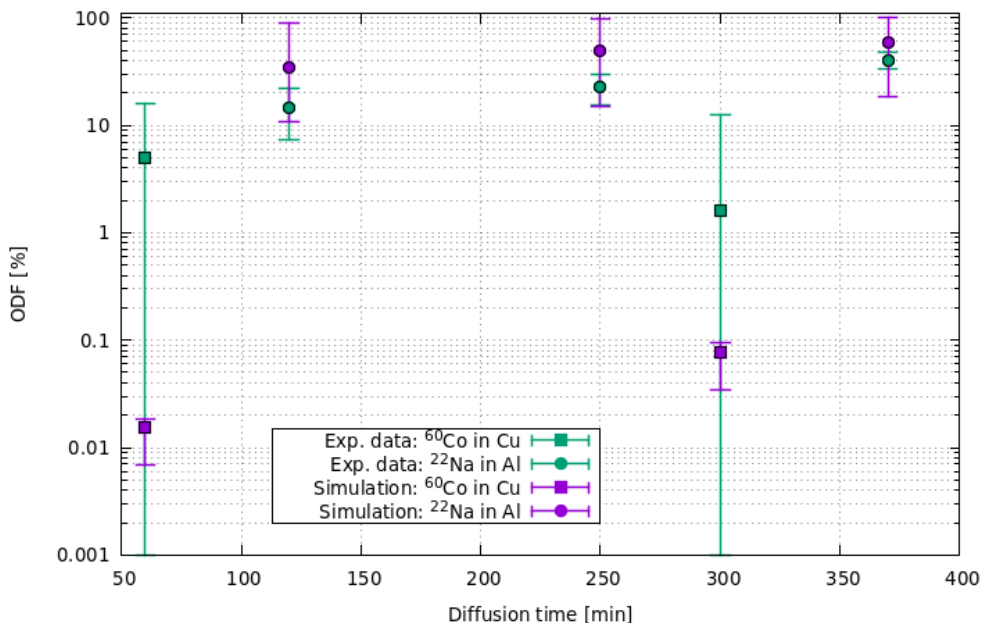


Figure 7.6: Comparison between experimental and simulations results. The plotted data can be found in Tabs. 7.3 and 7.4.

The results clearly support the importance of the implemented desorption model. The ODF simulation results for Co would have been definitely off without it (see Tab. 7.2). This is of especial significance when compared with the Na in Al scenario, in which the desorption model becomes almost transparent (due to the high desorption chances of Na), in both cases returning results in good agreement with the experimental ones.

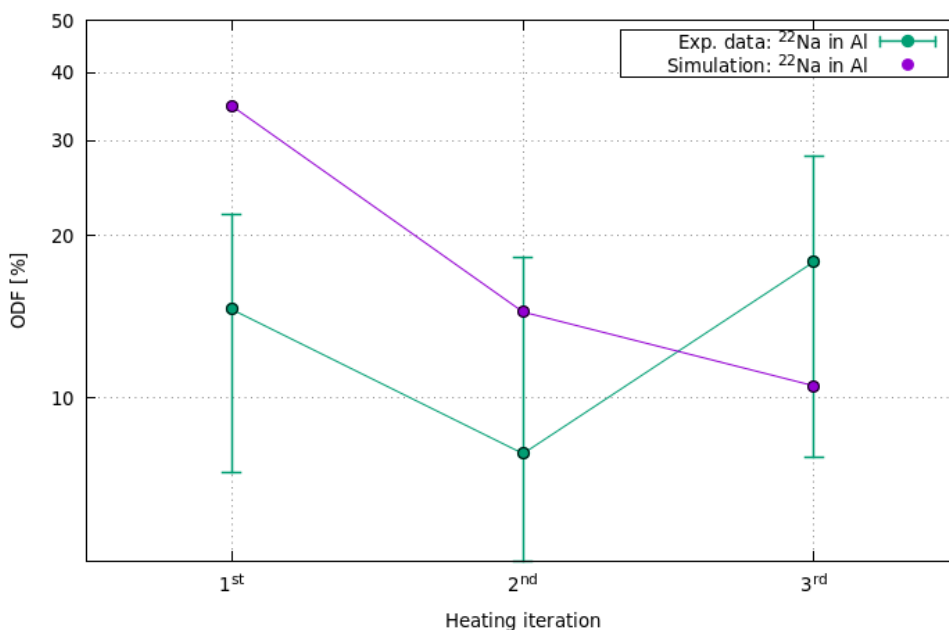


Figure 7.7: Simulated and experimental results for the fraction of radionuclides lost in each heating iteration. The simulation uncertainties are not reported here for the reasons detailed in the text.

As we have seen, three heating iterations of approximately 2 h each were carried out during the experimental campaign to study the out-diffusion of Na from Al. The ODF for each iteration (relative to the initial activity of the sample) is shown in Fig. 7.7 together with the simulation results¹. We do not report the uncertainties of the simulation results in this plot because we are only interested in the data tendency, and this will remain nearly intact even if the actual values would change due to variations in the input parameters. The ODF in successive iterations is expected to behave like that of the simulation results: in every iteration the ODF is smaller than in the previous one, asymptotically decreasing as the sample loses radionuclides. The reason behind is that those radionuclides closer to the sample's surface would manage to out-diffuse in earlier iterations and, as a consequence, the radionuclide's concentration in the outer regions of the sample would decrease. The ODF would then diminish due to the lower probability of deeper radionuclides reaching the surface. This is consistent with the behaviour of the ODF mean that we observe in the 2nd experimental iteration with respect to the 1st, but is clearly not the case for the 3rd one. Although the experimental uncertainties do not allow for a categorical conclusion, the authors suspect there may be indeed a variation in the tendency, which could be related to the potential damage caused to the metal's structure as a consequence of repeated and rapid heating and cooling of the sample. This may have resulted in the creation of significant lattice defects, which would enhance the diffusion of radionuclides inside, modifying the behaviour of the ODF since, as mentioned, it is limited by diffusion in the case of Na in Al. For future potential experiments, some more light could be shed on this by using new samples for each iteration, not reusing already heated ones.

The reader is already aware of the approximations used by SOLIDUSS to perform the calculations. In addition, the calculations can be extremely sensitive to variations of the parameters provided by the user (*e.g.* activation energies, frequency factors, temperature, *etc.*), which are often estimations with important uncertainties. Given the tests performed so far and in absence of further supporting experimental data, the authors consider it as prudent to take SOLIDUSS' results as order-of-magnitude estimations, while encouraging the user to perform accompanying sensitivity analyses.

1 The data is the same reported above in Fig. 7.6 and Tabs. 7.2 and 7.4, but this time we show the amount of radionuclides lost in each 2 h iteration, rather than the total amount after a given diffusion time.

Out-diffusion fraction for simplified scenarios

Contents

8.1	Fraction of atoms Reaching an object's Surface (FRS)	101
8.1.1	Uniform concentration of radionuclides	102
8.1.2	Non-uniform concentration of radionuclides	105
8.2	Global Desorption Probability (GDP)	106
8.3	Out-Diffusion Fraction (ODF)	106

THIS CHAPTER introduces few analytical expressions that we have identified and that can be used to easily estimate the ODF for simplified scenarios. In particular, we can make use of them in cases in which it is reasonable to assume a uniform temperature within the object of interest. In order to do this, we will need to estimate two quantities: the Fraction of atoms Reaching an object's Surface (FRS) and the Global Desorption Probability (GDP). If N_R is the total number of radionuclides inside our object, the total number of radionuclides reaching the object's surface will be given by $N_R \cdot \text{FRS}$. And the fraction of them that will manage to escape the object would be given by the GDP. How to estimate these quantities is explained below.

8.1 Fraction of atoms Reaching an object's Surface (FRS)

In this section, we distinguish between two scenarios: uniform and non-uniform initial concentration of radionuclides. In the former, the FRS can be accurately estimated but, in the later, only rough estimations can be achieved for multiple radionuclides or diffusion times provided that, at least, one single result is known beforehand.

8.1.1 Uniform concentration of radionuclides

There are some cases in which the initial concentration of radionuclides may be assumed to be uniform within the object of interest, either because we know so, or because it is found to be a reasonable assumption in the absence of more specific information. In these cases, if the temperature within the object is also assumed to be uniform, we have found that we can approximate the FRS using the following formula [33]:

$$\text{FRS} \simeq \text{erf} \left(\frac{S}{V} \sqrt{Dt_T} \right), \quad (8.1)$$

where S is the surface of the object and V its volume, D is the diffusion coefficient of interest and t_T is the total diffusion time in consideration. It is worth to highlight few things with respect to this formula:

- It seems intuitive that the radionuclide's chances of reaching the object's surface increase with the ratio S/V . For instance, one would expect a larger FRS for a thin plate of material than for a bulky object.
- Of course, these chances would also increase if the radionuclide can travel further within the object and this is provided by the factor $\sqrt{Dt_T}$.
- For positive arguments (like $\frac{S}{V} \sqrt{Dt_T}$ must always be), erf is naturally bounded between 0 and 1, as it should be for the FRS.
- When using the formula, one should pay attention to its units: the term $\frac{S}{V} \sqrt{Dt_T}$ must be dimensionless and therefore, if the diffusion coefficient is provided in cm^2s^{-1} , time must be provided in s and S/V in cm^{-1} .

We must not forget that the presented formula is just an approximation and should be treated carefully. Fig. 8.1 shows a comparison between the results of a significant number of diffusion calculations for different geometries and radionuclides using SOLIDUSS and those provided by eq. (8.1). The upper picture of the figure is particularly useful to observe the agreement between simulations and formula in the region of low FRS (far from 100 %). On the contrary, in the central picture, we can better appreciate the results for larger FRS. A relatively good agreement is observed in both regions but especially in that of low FRS; this is better visible in the bottom picture, where the ratio between both results is shown. The same ratio is shown in Fig. 8.2, but this time as a function of the FRS itself. From both figures it is clear that for low fractions, below 10 % to be conservative, formula and simulation agree within a 5 % of relative error (the ratio between both FRS stays between 0.95 and 1.05). Outside this region, the agreement evolves differently for different geometries but, for all cases we have tested, the relative error does not surpass 15 %. In this respect, it is important to mention that the FRS for most cases of interest from the radiation protection point of view will fall below few per cent, where we find the best agreement between formula and simulations.

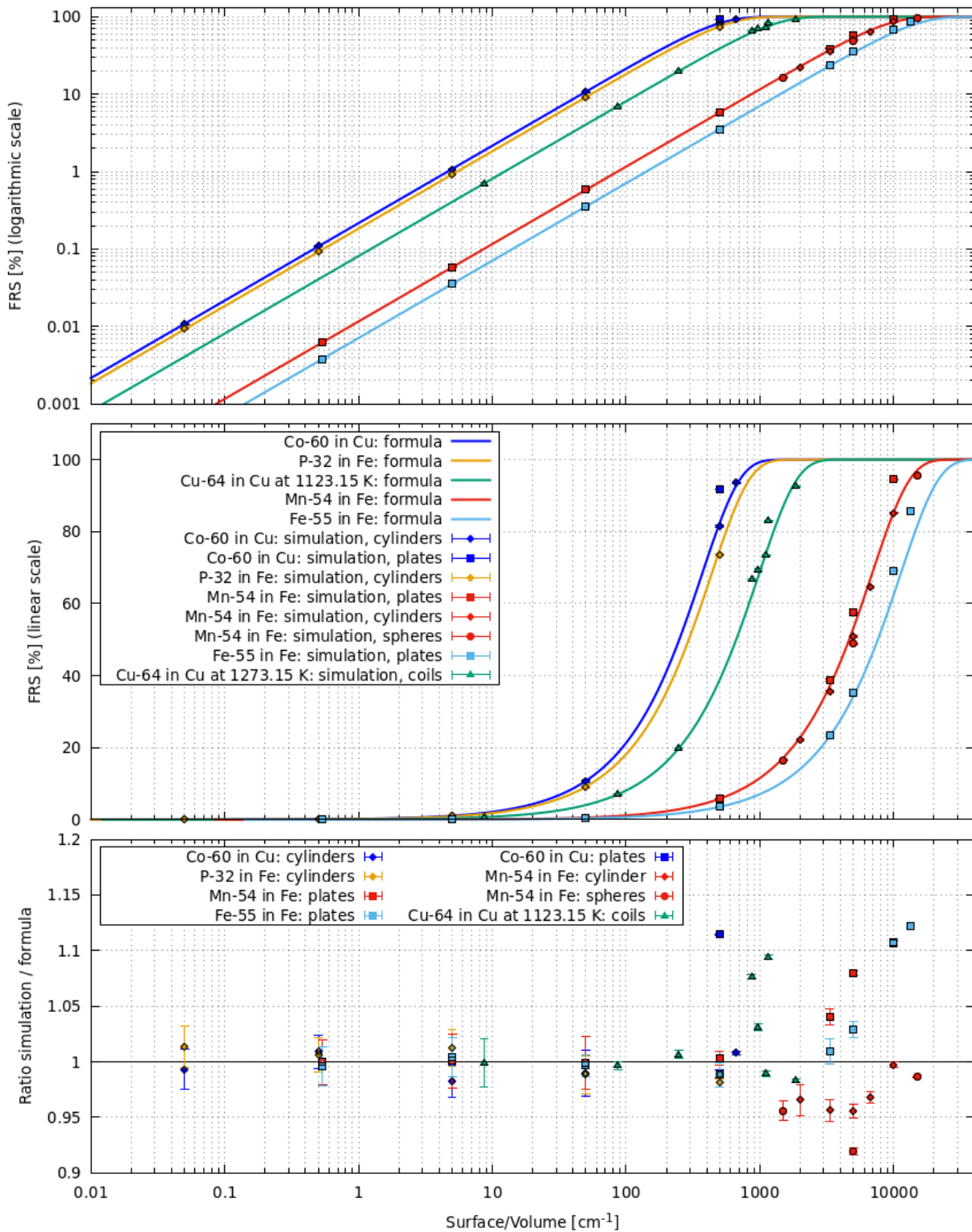


Figure 8.1: Out-diffusion fraction as a function of the surface over volume ratio of the object of interest. The data have been obtained for different geometries and pairs radionuclide-material using SOLIDUSS (dots) and using eq. (8.1) (curves). The top and middle pictures show the results using logarithmic and linear scales respectively, which allow us to better examine them for the entire range of S/V . The ratio between both results is presented in the bottom picture. The temperature considered for all cases is 1273.15 K unless otherwise indicated in the legend. Error bars represent the statistical uncertainties derived from the simulation and, in this case, they encompass 2σ confidence intervals.

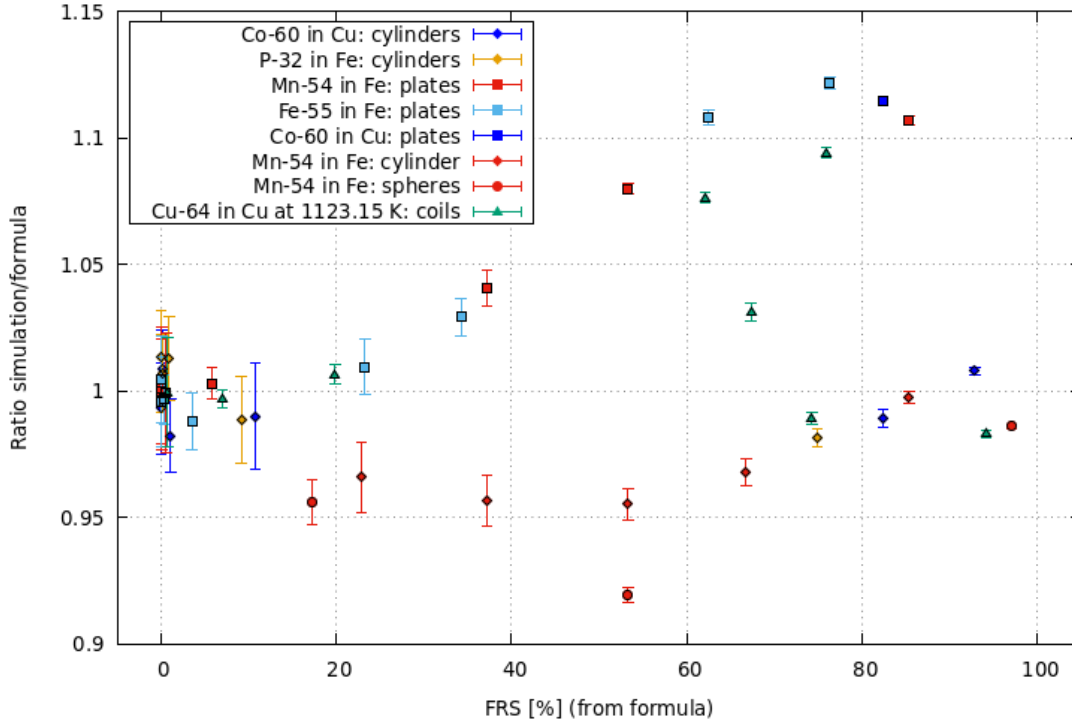


Figure 8.2: Ratio between the out-diffusion fraction for different scenarios obtained using SOLIDUSS and eq. (8.1) as a function of the out-diffusion fraction calculated using the latter. The temperature considered for all cases is 1273.15 K unless otherwise indicated in the legend. Error bars represent the statistical uncertainties derived from the simulations and, in this case, they encompass 2σ confidence intervals.

Pocket calculator formula

The error function is defined as follows:

$$\operatorname{erf}(x) = \frac{2}{\sqrt{\pi}} \int_0^x e^{-t^2} dt. \quad (8.2)$$

The term e^{-t^2} can be written as a power series:

$$e^{-t^2} = \sum_{k=0}^{\infty} \frac{(-t^2)^k}{k!} = 1 - t^2 + \frac{t^4}{2} - \frac{t^6}{6} + \dots \quad (8.3)$$

Restricting ourselves to the first term of the expansion, substituting in eq. (8.2) and integrating:

$$\operatorname{erf}(x) \simeq \frac{2}{\sqrt{\pi}} x. \quad (8.4)$$

Therefore, the FRS can be approximated as below:

$$\operatorname{FRS} \simeq \frac{2}{\sqrt{\pi}} \frac{S}{V} \sqrt{Dt_T}, \quad (8.5)$$

where the different variables are those explained for eq. (8.1). In this case, we are also assuming uniform temperature and uniform radionuclide initial concentration. The equation above can be used to perform quick checks when there are no means to compute the error function at reach. For FRS below 20 % [calculated with eq. (8.5)], the agreement between its result and that one obtained with eq. (8.1) falls within 1 % of relative error (ratio between formulae stays between 0.99 and 1.01); for FRS below 6 %, the relative error drops below 0.1 % and, by last, if the FRS is lower than 2 %, this error goes down to less than 0.01 %. Please note that eq. (8.5) is not bounded and therefore we should not trust FRS results above 20 % as the approximation is no longer accurate.

8.1.2 Non-uniform concentration of radionuclides

One would expect that for non-uniform initial concentrations of radionuclides, a more general formula like the following would still apply for the fraction of atoms reaching the object's surface:

$$\text{FRS} \simeq \text{erf} \left(F \cdot \sqrt{Dt_T} \right), \quad (8.6)$$

where F would not longer be S/V , but a more general factor related to the distances from the radionuclides to the different surfaces of the object of interest. One could think that, for a given geometry and initial distribution, the factor F could be a constant; but in reality, it is a function of $\sqrt{Dt_T}$. To enlighten this, let us consider one simple example. Imagine some radioisotopes being created inside a small cube of material, just next to one of its faces; they will start diffusing inside the material and some of them will reach the surface of the face nearby and out-diffuse. If the diffusion time is short, the radionuclides will not reach other faces. So if using this out-diffusion calculation we estimate F and use it to calculate the FRS for a diffusion time large enough for the radionuclides to reach other faces of the cube, we would underestimate it because the information encoded in the F factor is only taking into account that out-diffusion can take place through one single face: the closest one. On the contrary, we would be overestimating the FRS if F is calculated using a larger diffusion time and then used to estimate it for shorter ones. Similar behaviour would be found for different diffusion coefficients since what matters is the distance $\sqrt{Dt_T}$, which is related to how far can the radioisotopes travel in a given time t_T .

Therefore, if we have a uniform temperature but a non-uniform radionuclide initial concentration inside a given object, and we want to calculate the FRS for different diffusion times or diffusion coefficients; provided that for all of them the distance $\sqrt{Dt_T}$ is comparable, eq. (8.6) could be used to obtain a first approximation of the out-diffusion fraction for all of them if one of the results is already known (so it can be used to estimate F)¹. But, as soon as $\sqrt{Dt_T}$ starts differing from that one used to calculate F , the results may start diverging from the real one, the faster the less uniform the radionuclide concentration within the object and area of interest is. This is why it is recommended to run a dedicated simulation to obtain a reliable result.

¹ Note that by doing this we would assume identical initial concentrations for all cases.

8.2 Global Desorption Probability (GDP)

Although FRS can be used to set a conservative upper limit² for the ODF, there may be cases in which a more accurate estimation is sought. We can get such an estimation by taking the desorption phenomena into account. This can be done by multiplying FRS and GDP. As we saw in chapter 5, the probability of desorption of a particular radionuclide must be calculated taking into account several parameters and, among them, the time when it reached the surface of the object for the first time. This time will be different for every radionuclide and as a consequence, strictly speaking, there is no such a thing as a global desorption probability. Nonetheless, we can assume that every radionuclide reached the surface at t_0 , the beginning of the simulation. This will allow us to estimate a kind of global desorption probability that, although overestimated, allows us to assess the impact of desorption. Similarly to eq. (5.7), we can define GDP as follows:

$$\text{GDP} = 1 - (1 - P_{des})^{\langle N_{enc} \rangle}, \quad (8.7)$$

where we have used the probability of desorption in a single surface encounter P_{des} , as defined by eq. (5.6), and the average number of surface encounters $\langle N_{enc} \rangle$, given by eq. (5.26). In SOLIDUSS we sample N_{enc} for each particular radionuclide according to its probability distribution, but for this analytical calculation we will use its average. Expanding the previous expression we get that³:

$$\text{GDP} = 1 - \left[1 - \frac{1}{1 + \exp\left(\frac{E_{des} - Q}{k_B T}\right)} \right]^{a \left(\frac{6Dt_T}{\text{DNN}^2}\right)^b}, \quad (8.8)$$

where E_{des} is the desorption activation energy, Q is the diffusion activation energy, T is the temperature, k_B is the Boltzmann's constant, DNN is the distance between nearest atomic neighbours in the host material lattice, and a and b are the parameters of eq. (5.25), whose values are given in eq. (5.26).

8.3 Out-Diffusion Fraction (ODF)

Now that we know how to calculate FRS and GDP, we can estimate the ODF as follows:

$$\text{ODF} = \text{FRS} \cdot \text{GDP}. \quad (8.9)$$

2 This value can only be considered as a conservative upper limit assuming that the input data and, in particular the diffusion coefficient, are accurate.

3 Here we have also assumed that diffusion is dominated by one single diffusion mechanism and therefore the diffusion rate (and also the diffusion coefficient) can be obtained using a single diffusion activation energy. If this is not the case, we could assume that the diffusion rate [eq. (5.5)] is instead given by $r_{dif} = \nu_0 \sum_i \exp\left(-\frac{Q_i}{k_B T}\right)$, where i represent each diffusion mechanism.

Provided the input parameters are accurate, eq. (8.9) will overestimate the ODF, as previously discussed. Nonetheless, it may be of great help since there are many cases in which the desorption probability is very low and therefore only a small fraction of the radionuclides reaching an object's surface manage to escape. To assume total desorption in such cases could imply overestimations of several orders of magnitude while using eq. (8.9) should limit them to a factor of a few according to our experience so far.

Table 8.1: ODF for different sets of diffusion and desorption parameters calculated using eq. (8.9) (ODF_{for}) and SOLIDUSS (ODF_{sim}). The ratio between both estimations is also provided. The errors shown only account for the statistical uncertainties of the simulation results. The geometry used in all cases was a plate of $1 \times 1 \text{ m}^2$ of 0.1 mm thick. The values of other parameters of interest are specified in the text.

Q [kJ mol ⁻¹]	E _{des} [kJ mol ⁻¹]	T [K]	FRS	GDP	ODF _{for} [%]	ODF _{sim} [%]	ODF _{for} / ODF _{sim}
200	320	1250	0.739	0.970	71.7	57.7 ± 0.3	1.243 ± 0.006
		1200	0.548	0.765	42.0	25.73 ± 0.19	1.632 ± 0.012
		1150	0.374	0.426	15.9	8.36 ± 0.09	1.90 ± 0.02
		1100	0.238	0.177	4.21	2.10 ± 0.04	2.01 ± 0.04
		1050	0.143	0.0601	0.857	0.413 ± 0.009	2.08 ± 0.05
		1000	0.0808	0.0174	0.141	0.067 ± 0.002	2.09 ± 0.08
		950	0.0429	0.00435	0.0187	0.0089 ± 0.0006	2.11 ± 0.14
	340	380	0.548	0.00354	0.194	0.1020 ± 0.0011	1.90 ± 0.02
		370	0.548	0.00961	0.527	0.276 ± 0.003	1.91 ± 0.02
		360	0.548	0.0260	1.42	0.756 ± 0.008	1.883 ± 0.019
		350	0.548	0.0692	3.79	2.00 ± 0.02	1.90 ± 0.02
		340	0.548	0.177	9.73	5.18 ± 0.05	1.877 ± 0.018
		330	0.548	0.413	22.6	12.45 ± 0.12	1.818 ± 0.017
		320	0.548	0.765	42.0	25.7 ± 0.2	1.634 ± 0.014
250	340	1200	0.0490	0.908	4.45	2.74 ± 0.10	1.62 ± 0.06
		240	0.0808	0.764	6.17	3.47 ± 0.09	1.78 ± 0.05
		230	0.133	0.583	7.76	4.08 ± 0.10	1.90 ± 0.05
		220	0.218	0.412	8.97	4.57 ± 0.07	1.96 ± 0.03
		210	0.352	0.275	9.68	4.92 ± 0.07	1.97 ± 0.03
		200	0.548	0.177	9.73	5.20 ± 0.05	1.872 ± 0.016
		190	0.786	0.112	8.78	5.32 ± 0.03	1.650 ± 0.011

Tab. 8.1 shows a comparison between results returned by eq. (8.9) and by pure SOLIDUSS calculations. The choice of geometry could be particularly important for the calculation of the FRS, but the GDP should be relatively transparent to it if the portion of the object's surface that is reachable by each radionuclide can be reasonably approximated by a plane. For this reason we have employed the same geometry for all cases presented in the table: a plate of $1 \times 1 \text{ m}^2$ of 0.1 mm thick. The value of the chosen diffusion and desorption parameters do not correspond to any particular pair radionuclide - host material. They have been selected to cover a wide range of values for the GDP. In nature, it is very common to find either very low or very high values of the GDP in the temperature range we are interested in. This results either in the depletion of the ODF ($ODF \simeq FRS \cdot 0$) or in a total desorption scenario ($ODF \simeq FRS \cdot 1$), respectively. For all cases shown in Tab. 8.1 we have used a frequency factor A of $1 \text{ cm}^2/\text{s}$, a DNN of 250 pm and a diffusion time of 1 h. As expected, we can

observe that eq. (8.9) systematically overestimates the ODF by approximately a factor of two or less. In this way, we can easily obtain an upper bound for isotope release that can help to quickly identify radiation protection mitigation measures in case of need. Still, small deviations of key input parameters can severely impact ODF estimates, as we will discuss.

Out-diffusion fraction as a function of different parameters

In this subsection we discuss the typical evolution of the ODF as a function of several parameters according to eq. (8.9). To do this, we have selected a set of different pairs of desorption and diffusion activation energies, reported in Tab. 8.2. They have been used to produce the plots in Fig. 8.3. For all different cases, we considered the following values for the rest of parameters: $S/V = 100 \text{ cm}^{-1}$, $A = 1 \text{ cm}^2 \text{ s}^{-1}$, $T = 1273 \text{ K}$, $t_T = 3600 \text{ s}$ and $DNN = 250 \text{ pm}$. Of course, the value of a parameter is not fixed when plotting the ODF as a function of it (*e.g.* when plotting ODF as a function of the temperature, the temperature value is obviously not fixed). We assume a uniform temperature and therefore eq. (8.1) is used to calculate FRS. It should be noted that Q and E_{des} are specific to the

Table 8.2: Diffusion and desorption activation energies used to create Fig. 8.3.

case	Q [kJ mol ⁻¹]	E_{des} [kJ mol ⁻¹]
1	200	400
2	220	380
3	240	360
4	260	340
5	280	320

combination of radionuclide and host material, DNN is specific to the host material lattice, S/V is specific to the object geometry and T and t_T are specific to each (fire) scenario. Looking at the different graphics in Fig. 8.3 we can highlight of a number of significant facts that may be useful to keep in mind when assessing the potential out-diffusion of radionuclides:

- Small variations in temperature may have huge effects on the ODF. As a consequence, an accurate estimation of this parameter is a must to correctly evaluate out-diffusion. A sensitivity analysis is highly recommended to assess the potential impact of the temperature uncertainties.
- Time (duration of the fire or high temperatures) is also an important parameter, but its accurate determination is not as critical as that of the temperature. Small changes in time do not generate very different values of the ODF.
- Accurate estimations of the diffusion and desorption activation energies are of great interest for a good assessment. Unfortunately, the experimental data available is usually not very abundant (especially for desorption), and not always precise. One must be aware of the potentially dramatic impact of small deviations of these parameters. As we can observe in pictures (c) and (d) of the aforementioned figure, there are ranges in which small variations

of the parameters do not entail important consequences, but there are others in which we find the opposite: an overestimation of few percent could result in a ODF underestimation of one order of magnitude. Also, given the wide range of values for Q and E_{des} , one may find very different ODF for different radionuclides hosted in the same object and in the same (fire) scenario.

- The distance between nearest atomic neighbours in different lattices is normally well-known and the impact of small uncertainties on the ODF seems to be limited.
- The geometry of the objects of interest plays a very important role in out-diffusion. It is taken into account in eq. (8.1) by means of the S/V parameter. As shown in Fig. 8.3, the ODF is greatly influenced by this parameter, which should be kept in mind when, for instance, assuming average sizes for cable conductors.

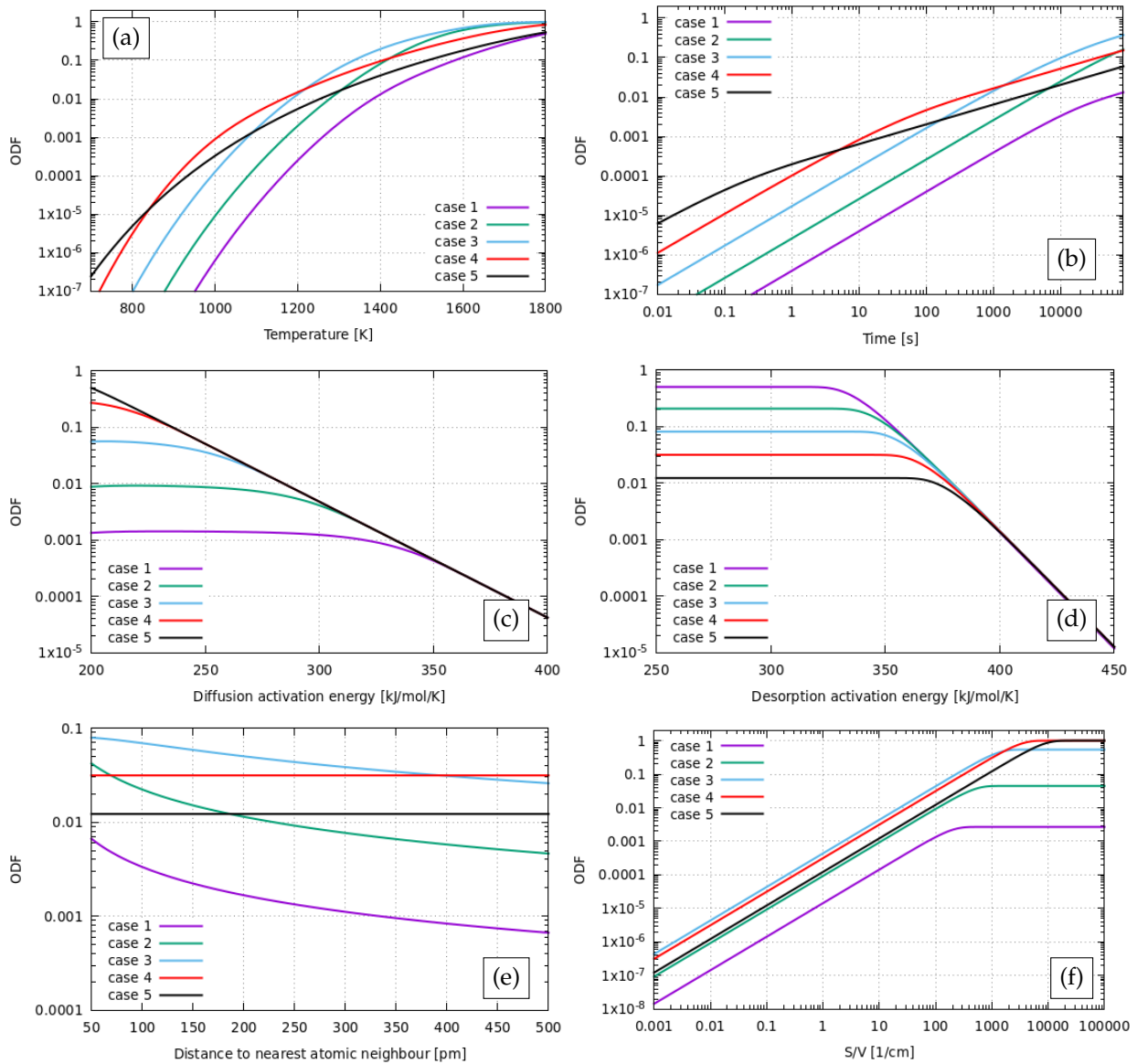


Figure 8.3: Evolution of the ODF as a function of several parameters according to eq. (8.9). For each curve, all but one parameter take constant values that are specified in the text.

The impact of out-diffusion

Contents

9.1	ActiWiz and the generic irradiation scenarios	111
9.2	Radionuclide inventories in few accelerator components	112
9.3	The potential impact of out-diffusion	117
9.3.1	Calculation parameters	118
9.3.2	Results	121
9.3.3	Discussion	125

WITH THE aim of providing some quantitative data on the potential impact of out-diffusion, we will take a look to one scenario of interest. We will use the code ActiWiz to estimate generic radionuclide inventories for a few components of the LHC accelerator. Then, the out-diffusion fraction for each case and radionuclide species will be estimated using the formulae introduced in chapter 8. Results will be put in context by comparing them with the radiological hazard resulting from the combustion of cable insulation, often considered as one of the main contributors to the release of radionuclides in accidental fire scenarios in accelerator facilities.

9.1 ActiWiz and the generic irradiation scenarios

The ActiWiz code [56,57] was initially developed to facilitate the optimization—from a radiation protection standpoint—of the chemical composition of materials used in the accelerator equipment at CERN. To this end, some generic radiation scenarios were chosen because they give rise to radiation environments often encountered along the accelerator chain. These scenarios include, among many others, activation occurring within bulky material (such as magnets) surrounding the beam impact area, activation occurring at 10 cm lateral distance to a target (such as collimators)

and activation close to the concrete tunnel wall around a target (where cables trays are typically placed). Detailed information on the different irradiation scenarios can be found in Ref. [58]). Figure 9.1 shows the geometry used in the aforementioned three cases and the regions where material activation will be assessed (in red). Particle fluences in the regions of interest obtained using FLUKA for each scenario and for each of the accelerators at CERN are used by ActiWiz to compute and return the radiological hazard linked to user-defined materials. These data are used by ActiWiz to compute and return the radiological hazard linked to user-defined materials.

ActiWiz Creator [59] was later developed to extend ActiWiz' capabilities. In particular, the user is free to provide arbitrary particle spectra and choose from numerous reports on different types of hazard (*e.g.* effective dose due to inhalation).

We will use the three generic irradiation scenarios mentioned above and shown in Fig. 9.1 to simulate the radiation environment in which exemplary fictitious accelerator components are placed (see next section). This will allow us to estimate the contribution of out-diffusion to effective inhalation doses following an accidental fire affecting those components. The particle spectra corresponding to these scenarios and used by ActiWiz Creator to compute the radionuclide inventory are shown in Fig. 9.2.

9.2 Radionuclide inventories in few accelerator components

In the present section we will focus our attention on the nuclide inventory found in the following objects:

- Cables typically placed next to the LHC tunnel wall (side-cables). The radiation environment at that location will be simulated using the target-wall scenario. The radionuclide inventory will be obtained for their two components: conductor and insulation.
- An LHC warm quadrupole magnet immersed in the radiation environment described by the bulky object scenario. In this case we will discriminate the contribution of the magnet coil's insulation, the coil's conductor and the magnet yoke.
- An LHC beam collimator vessel, exposed to the particle fluences corresponding to the target-lateral scenario.

In particular, we will take a look at the global committed effective dose E_{50} corresponding to the whole source terms for each material in case of fire. We are interested in relating the potential out-diffusion releases to that one due to the combustion of side-cable insulation. In this sense, absolute values are of no real interest in this study. Nonetheless, somewhat realistic irradiation and cooling times are important to identify the radionuclides of interest. We have considered an irradiation time of 3 years at a rate of $3.5 \cdot 10^7$ protons per second, leading to a total amount

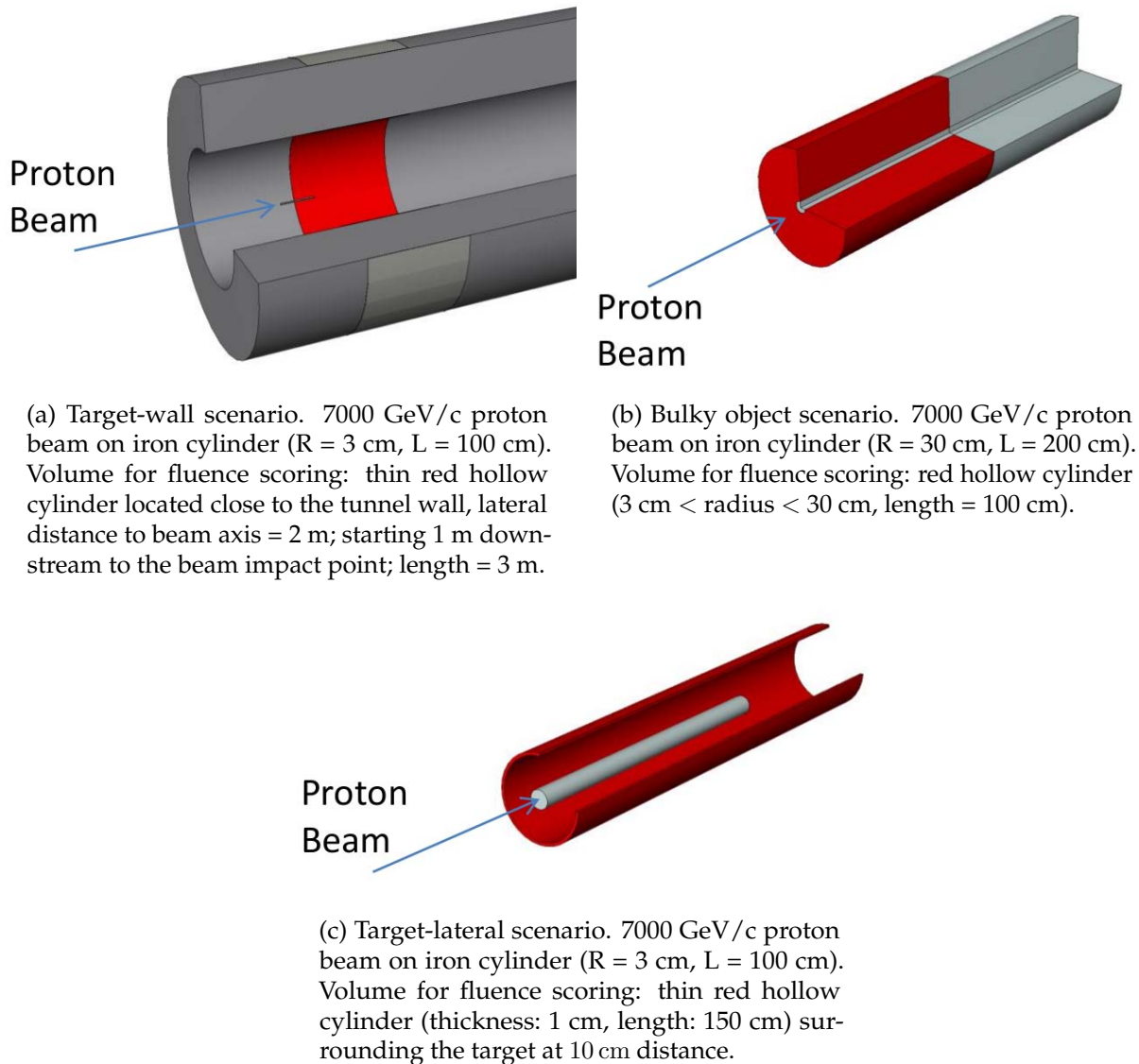


Figure 9.1: Generic irradiation scenarios in the LHC resembling the irradiation of (a) materials located at the tunnel wall in areas where beam with this energy is lost in objects with small lateral extensions, (b) solid massive materials located close to object intercepting protons at this energy (e.g.: iron yoke of magnets) and (c) materials located close to objects with small lateral extension (like targets or collimators) being hit by beam protons. Source: ActiWiz.

of $3.3 \cdot 10^{15}$ protons, approximately coinciding with the total top energy proton losses of LHC beam ¹ in its so-called Betatron Cleaning Insertion (also referred to as IR7) [60] during years 2015–2017 [61]. Cooling time was set at 30 minutes, which we consider to be a reasonable first approximation of the time it could take for smoke from the fire to reach members of the personnel, considering that

¹ There are two beams of protons circulating in opposite directions in the LHC. Some of the protons deviate from the optimal beam trajectory and are intercepted by the LHC collimators, very often in IR7, and are the so-called beam losses. This is done in order to protect the superconducting magnets of the accelerator from quenching that could be triggered by the impact of those protons or their shower of secondary particles. Top energy refers to those protons circulating at LHC's top energy, since they are initially injected into the machine with much lower energies for later acceleration.

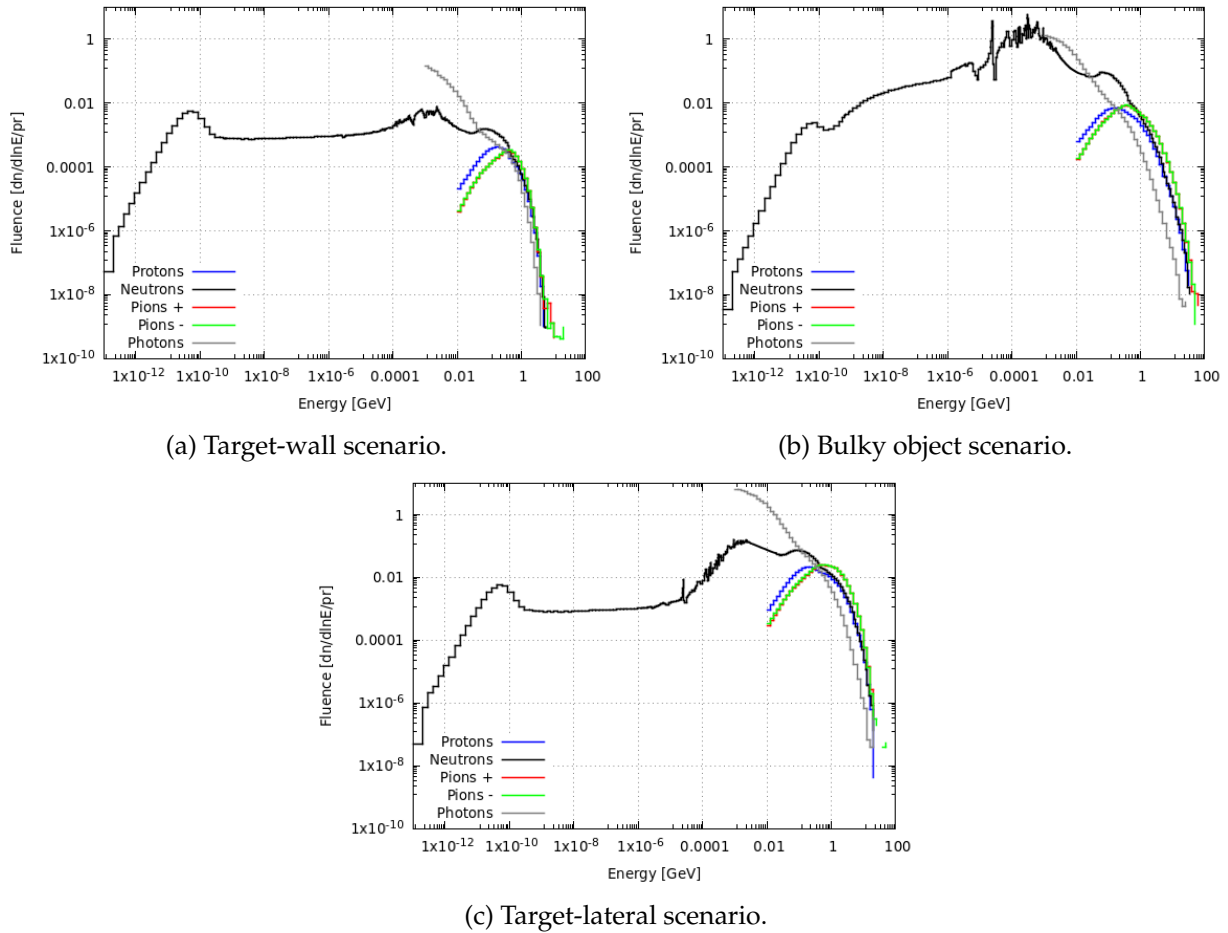


Figure 9.2: Particle fluences for different generic scenarios of interest. They are used by ActiWiz Creator to estimate the radionuclide inventory generated in a user-defined material located in the region of interest. Statistical uncertainties are generally $\pm 1\%$ and have been suppressed for reasons of clarity.

the fire is originated during the operation of the machine. The assumed chemical composition for each of the materials of the aforementioned objects is detailed in Tab. 9.1.

Table 9.1: Assumed chemical composition for the different objects. Natural abundances of isotopes are considered for all elements. Abbreviations: “ins.” means insulation, “cond.” means conductor and “coll.” means collimator.

Scenario →	Target-wall: side-cables		Bulky object: quadrupole			Target-lateral
Object →	Cable ins.	Cable cond.	Coil ins.	Coil cond.	Yoke	Coll. vessel
Material →	Polyethylene	Copper	Glass fiber and epoxy	Copper	ARMCO	SS304L
Density [g cm ⁻³] →	0.94	8.96	2.07	8.96	7.86	8.0
Element ↓	Composition [weight fraction] ↓					
H	0.1437	-	0.0451	-	-	-
B	-	-	0.0106	-	-	-
C	0.8563	-	0.507	-	0.0001	0.0003
N	-	-	-	-	0.00005	-
O	-	-	0.276	-	-	-
Na	-	-	0.000397	-	-	-
Mg	-	-	0.00586	-	-	-
Al	-	-	0.024	-	-	-
Si	-	-	0.0832	-	-	0.01
P	-	-	-	-	0.00005	0.000225
S	-	-	-	-	0.00003	0.00015
K	-	-	0.000674	-	-	-
Ca	-	-	0.0474	-	-	-
Cr	-	-	-	-	-	0.185
Mn	-	-	-	-	0.0006	0.02
Fe	-	-	-	-	0.999	0.671
Co	-	-	-	-	0.00005	0.01
Ni	-	-	-	-	-	0.113
Cu	-	1.00	-	1.00	0.0003	-
Sn	-	-	-	-	0.00005	-

The resulting radionuclide inventories for each component and the contribution of each radionuclide to the total effective E_{50} inhalation dose according to ActiWiz Creator are printed in Tab. 9.2. The main contributors for each component are the following: ^3H , ^7Be and ^{11}C from the side-cables' insulation; ^{60}Co and ^{64}Cu from the cables' conductor; ^3H , ^{22}Na and ^{45}Ca from the magnet coils' insulation, ^{58}Co , ^{60}Co and ^{64}Cu from the coils' conductor; ^{54}Mn and ^{55}Fe from the magnet's yoke; and ^{48}V , ^{54}Mn and ^{56}Co from the collimator's vessel.

Table 9.2: Radionuclide inventories for each component and the contribution of each radionuclide to the total effective E_{50} inhalation dose. Only isotopes contributing above 0.01 % of the total inhalation dose for each component are reported. Those contributing more than 10 % are highlighted in bold. Abbreviations: “ins.” means insulation, “cond.” means conductor and “coll.” means collimator.

Isotope	Effective E_{50} inhalation dose contribution [$\mu\text{Sv cm}^{-3}$]					
	Cable ins.	Cable cond.	Coil ins.	Coil cond.	Yoke	Coll. vessel
^3H	$7.86 \cdot 10^{-3}$	$2.68 \cdot 10^{-2}$	$6.14 \cdot 10^{-1}$	1.14	$8.34 \cdot 10^{-1}$	2.25
^7Be	$4.59 \cdot 10^{-3}$	-	$2.95 \cdot 10^{-1}$	-	$5.95 \cdot 10^{-2}$	$2.45 \cdot 10^{-1}$
^{10}Be	$1.39 \cdot 10^{-6}$	-	-	-	-	-
^{11}C	$1.46 \cdot 10^{-3}$	-	$8.69 \cdot 10^{-2}$	-	-	-

Continuation of Tab. 9.2.

Isotope	Effective E_{50} inhalation dose contribution [$\mu\text{Sv cm}^{-3}$]					
	Cable ins.	Cable cond.	Coil ins.	Coil cond.	Yoke	Coll. vessel
^{14}C	$4.35 \cdot 10^{-7}$	-	$3.02 \cdot 10^{-3}$	-	-	-
^{18}F	-	-	$8.82 \cdot 10^{-3}$	-	-	-
^{22}Na	-	-	$3.80 \cdot 10^{-1}$	$4.93 \cdot 10^{-2}$	$1.07 \cdot 10^{-1}$	$6.58 \cdot 10^{-1}$
^{24}Na	-	-	$1.80 \cdot 10^{-1}$	-	$3.74 \cdot 10^{-2}$	$1.82 \cdot 10^{-1}$
^{28}Mg	-	-	$2.90 \cdot 10^{-3}$	-	-	$7.32 \cdot 10^{-2}$
^{31}Si	-	-	$2.20 \cdot 10^{-2}$	-	-	-
^{32}Si	-	-	$1.35 \cdot 10^{-3}$	$7.02 \cdot 10^{-2}$	$8.43 \cdot 10^{-2}$	$3.31 \cdot 10^{-1}$
^{32}P	-	$2.58 \cdot 10^{-2}$	$2.56 \cdot 10^{-1}$	1.10	2.14	7.93
^{33}P	-	$7.75 \cdot 10^{-3}$	$3.10 \cdot 10^{-2}$	$3.28 \cdot 10^{-1}$	$5.27 \cdot 10^{-1}$	1.96
^{35}S	-	$1.02 \cdot 10^{-2}$	$7.34 \cdot 10^{-2}$	$4.15 \cdot 10^{-1}$	$7.04 \cdot 10^{-1}$	2.50
^{38}Cl	-	-	-	-	-	$1.28 \cdot 10^{-2}$
^{42}K	-	-	-	$2.84 \cdot 10^{-2}$	$5.06 \cdot 10^{-2}$	$1.58 \cdot 10^{-1}$
^{43}K	-	-	$2.61 \cdot 10^{-3}$	-	-	$7.08 \cdot 10^{-2}$
^{45}Ca	-	$1.76 \cdot 10^{-1}$	1.37	6.27	$1.19 \cdot 10^1$	$3.51 \cdot 10^1$
^{47}Ca	-	-	$8.79 \cdot 10^{-3}$	-	-	-
^{43}Sc	-	-	-	-	$8.47 \cdot 10^{-2}$	$2.51 \cdot 10^{-1}$
^{44}Sc	-	$3.71 \cdot 10^{-2}$	$5.76 \cdot 10^{-4}$	1.32	4.10	$1.16 \cdot 10^1$
^{46}Sc	-	$1.48 \cdot 10^{-1}$	$6.38 \cdot 10^{-4}$	5.22	$1.42 \cdot 10^1$	$3.85 \cdot 10^1$
^{47}Sc	-	$8.49 \cdot 10^{-3}$	$3.16 \cdot 10^{-3}$	$2.98 \cdot 10^{-1}$	$6.50 \cdot 10^{-1}$	1.85
^{48}Sc	-	$3.69 \cdot 10^{-3}$	-	$1.30 \cdot 10^{-1}$	$2.54 \cdot 10^{-1}$	$7.32 \cdot 10^{-1}$
^{44}Ti	-	$1.95 \cdot 10^{-2}$	-	$6.97 \cdot 10^{-1}$	2.59	7.43
^{45}Ti	-	-	-	$4.70 \cdot 10^{-2}$	$1.78 \cdot 10^{-1}$	$4.83 \cdot 10^{-1}$
^{47}V	-	-	-	-	$2.62 \cdot 10^{-2}$	$6.45 \cdot 10^{-2}$
^{48}V	-	$1.35 \cdot 10^{-1}$	-	4.61	$2.22 \cdot 10^1$	$5.08 \cdot 10^1$
^{49}V	-	$2.97 \cdot 10^{-3}$	-	$1.02 \cdot 10^{-1}$	$5.37 \cdot 10^{-1}$	1.21
^{48}Cr	-	-	-	-	$6.89 \cdot 10^{-2}$	$1.68 \cdot 10^{-1}$
^{49}Cr	-	-	-	-	$8.48 \cdot 10^{-2}$	$1.94 \cdot 10^{-1}$
^{51}Cr	-	$5.04 \cdot 10^{-3}$	-	$1.74 \cdot 10^{-1}$	1.23	3.23
^{51}Mn	-	-	-	-	$9.25 \cdot 10^{-2}$	$1.38 \cdot 10^{-1}$
^{52}Mn	-	$5.08 \cdot 10^{-2}$	-	1.72	$1.31 \cdot 10^1$	$1.58 \cdot 10^1$
^{54}Mn	-	$2.67 \cdot 10^{-1}$	-	9.95	$1.10 \cdot 10^2$	$8.84 \cdot 10^1$
^{56}Mn	-	$4.50 \cdot 10^{-3}$	-	$1.86 \cdot 10^{-1}$	2.99	2.51
^{52}Fe	-	-	-	-	$2.35 \cdot 10^{-1}$	$3.38 \cdot 10^{-1}$
^{55}Fe	-	$6.92 \cdot 10^{-2}$	-	2.57	$3.78 \cdot 10^1$	$3.48 \cdot 10^1$
^{59}Fe	-	$8.03 \cdot 10^{-2}$	-	3.68	2.62	$5.95 \cdot 10^{-1}$
^{55}Co	-	$7.72 \cdot 10^{-3}$	-	$2.63 \cdot 10^{-1}$	$1.75 \cdot 10^{-1}$	$9.51 \cdot 10^{-1}$
^{56}Co	-	$9.69 \cdot 10^{-1}$	-	$3.53 \cdot 10^1$	7.82	$6.23 \cdot 10^1$
^{57}Co	-	$4.79 \cdot 10^{-1}$	-	$1.91 \cdot 10^1$	$4.18 \cdot 10^{-2}$	$2.72 \cdot 10^1$

Continuation of Tab. 9.2.

Isotope	Effective E_{50} inhalation dose contribution [$\mu\text{Sv cm}^{-3}$]					
	Cable ins.	Cable cond.	Coil ins.	Coil cond.	Yoke	Coll. vessel
^{58}Co	-	1.34	-	$5.89 \cdot 10^1$	$4.57 \cdot 10^{-2}$	$4.43 \cdot 10^1$
^{60}Co	-	3.10	-	$1.57 \cdot 10^2$	3.88	$2.41 \cdot 10^1$
^{61}Co	-	$4.32 \cdot 10^{-3}$	-	$2.08 \cdot 10^{-1}$	-	-
^{56}Ni	-	$1.86 \cdot 10^{-3}$	-	$5.80 \cdot 10^{-2}$	-	$4.54 \cdot 10^{-1}$
^{57}Ni	-	$7.47 \cdot 10^{-3}$	-	$2.51 \cdot 10^{-1}$	-	2.50
^{63}Ni	-	$2.86 \cdot 10^{-2}$	-	1.78	-	$5.36 \cdot 10^{-2}$
^{65}Ni	-	$4.19 \cdot 10^{-3}$	-	$2.39 \cdot 10^{-1}$	-	-
^{60}Cu	-	-	-	$4.77 \cdot 10^{-2}$	-	-
^{61}Cu	-	$5.06 \cdot 10^{-2}$	-	2.28	-	-
^{64}Cu	-	$1.14 \cdot 10^1$	-	$1.20 \cdot 10^2$	$3.16 \cdot 10^{-2}$	-
^{62}Zn	-	$1.05 \cdot 10^{-2}$	-	$2.39 \cdot 10^{-1}$	-	-
^{65}Zn	-	$2.29 \cdot 10^{-2}$	-	$5.48 \cdot 10^{-1}$	-	-
Total	0.01391	18.5	3.34	436.3	241.5	472.4

9.3 The potential impact of out-diffusion

In this section we estimate the fraction of the previous radionuclide inventory that could manage to escape in the event of a fire affecting all presented accelerator components. Nonetheless, we must discuss several points before doing so.

Insulation combustion

We assume that insulation of cables and coils would be burnt if exposed to a fire, releasing all the radioactive content of the incinerated volume. The total effective E_{50} inhalation dose incurred by the inhalation of the whole radioactive content of 1 cm^3 of side-cables insulation will be used as a reference value. This will allow us to put in context the release of radionuclides due to out-diffusion per cm^3 of non-incinerable materials exposed to fire.

Tritium

The diffusion coefficient for tritium is typically very high in the materials we are interested in, even at room temperature. As a consequence, it is probable that some of the tritium created inside an object manages to escape also in the absence of fire. This implies that the amount of tritium present in the object at the time of a fire may be substantially lower than the amount created and estimated, in this case, by ActiWiz Creator. A detailed estimation of the remaining fraction of tritium will not be carried out for this example because it is too case-dependant. Instead, we will assume both

extreme cases: all the tritium remains in the objects at the fire time and all the tritium has escaped prior to the fire.

Cables sizes

The object's surface and volume are important variables to estimate the ODF, as we have seen in chapter 8. Some of the different components that we are looking at in the present chapter have well-defined and standardized sizes (*e.g.* LHC warm quadrupole components). On the contrary, we find a wide range of cable thicknesses in the accelerator tunnels. For thinner cables, their ratio surface over volume is greater, which implies a larger ODF. For a given amount of cable conductor, the release would be more significant the thinner the cables are. In the presence of cables with different sizes, one may think of using their average radius to compute the average ODF. This would not be always accurate, but is a fairly good approximation for small FRS. This comes from the fact that $\overline{\text{FRS}} \simeq \frac{2}{\sqrt{\pi}} \frac{S}{V} \sqrt{Dt_T}$, which can be easily proved. Therefore, the approximation holds true under the conditions discussed in subsection 8.1.1. Whenever possible, the author recommends to compute the FRS separately for different cables sizes since rapidly diffusing isotopes are likely to be present (*e.g.* ^3H). The thickness we have considered in this example for cable conductors is 0.25 cm radius.

9.3.1 Calculation parameters

We will estimate the ODF after 1 h of fire. We will do so by using the analytical expressions introduced in chapter 8, which implies the assumption of uniform temperature and radionuclide distributions. Results will be shown for 800 °C, 900 °C and 1000 °C so we can observe their dependence with temperature. The diffusion and desorption parameters of interest are shown in Tabs. 9.3 and 9.4.

Table 9.3: Diffusion and desorption parameters used to estimate the ODF of different isotopes from a Cu object. In many cases A_2 and Q_2 are not provided, this is simply because the diffusion coefficient follows a simple Arrhenius curve (only one pair is needed).

Host material: Cu. DNN = 256 pm.						
Element	A_1 [$\text{cm}^2 \text{s}^{-1}$]	Q_1 [kJ mol^{-1}]	A_2 [$\text{cm}^2 \text{s}^{-1}$]	Q_2 [kJ mol^{-1}]	E_{des} [kJ mol^{-1}]	Sources
^3H	0.0066	37.337	-	-	-	[52] ^a
Na	-	-	-	-	102.4	[41] ^b
Si	0.007	171.7	-	-	541.8	[41,52]
P	0.00305	136.1	-	-	-	[52] ^a
S	23	206.6	-	-	-	[52] ^a
Ca	-	-	-	-	330.7	[41] ^b
Sc	-	-	-	-	548	[41] ^b
Ti	0.693	196	-	-	574	[41,52]
V	2.48	215	-	-	525.6	[41,52]
Cr	0.1685	195	0.51	224	373	[41,52]
Mn	0.37	195.5	0.71	204.3	290.2	[41,52]
Fe	0.7	216.9	0.505	257.5	451	[41,52]
Co	0.74	217.2	736	312.8	416.1	[41,52]
Ni	0.7	225	250	299.3	423	[41,52]
Cu	0.13	197.8	4.5	237.4	337.4	[52,62] ^c
Zn	0.17	190.9	0.12	188.8	185.3	[41,52]

^a We did not find estimations for the desorption enthalpy from Cu for these species. Nonetheless, at the temperatures we will consider (800 °C–1000 °C) they are gases and therefore, a reasonable approximation would be to assume total desorption for them (all atoms reaching the surface escape from the object).

^b We could not identify experimental data for the diffusion coefficient of these elements in Cu. In the absence of a better approach, we will assume a diffusion coefficient equal to the average diffusion coefficient of the rest of the species in the table except for ^3H , which is a special case diffusing remarkably fast.

^c To account for the desorption of Cu isotopes from Cu we can safely use its sublimation enthalpy as the desorption one as discussed in section 5.1.

Table 9.4: Diffusion and desorption parameters used to estimate the ODF of different isotopes from a Fe object. Two sets of diffusion activation parameters are provided for two temperature ranges of interest. This is needed because of the structural phase transition suffered by Fe at 1183 K. T_i is the initial temperature of the range and T_f is the final.

Host material: Fe. DNN = 248 pm.						
Element	T_i [K]	T_f [K]	A_1 [$\text{cm}^2 \text{s}^{-1}$]	Q_1 [kJ mol^{-1}]	E_{des} [kJ mol^{-1}]	Sources
H	1043	1183	0.00078	7.9	-	[63] ^a
	1183	1667	0.00078	7.9		
Be	1043	1183	5.34	218.1	376	[41,52]
	1183	1667	0.1	241.2		
F	1043	1183	-	-	-	_a, c
	1183	1667	-	-		
Na	1043	1183	-	-	92.7	[41] ^b
	1183	1667	-	-		
Mg	1043	1183	-	-	241.6	[41] ^b
	1183	1667	-	-		
Si	1183	1667	5.35	241.3	611.3	[41,64]
	1043	1183	1.7	229.1		
	1183	1667	0.07	243		
P	1043	1183	287	271	-	[52] ^a
	1183	1667	0.063	193.4		
S	1043	1183	34.6	231.5	-	[52] ^a
	1183	1667	1.7	221.9		
Cl	1043	1183	-	-	-	_a, c
	1183	1667	-	-		
K	1043	1183	-	-	108.7	[41] ^b
	1183	1667	-	-		
Ca	1043	1183	-	-	312.9	[41] ^b
	1183	1667	-	-		
Sc	1043	1183	-	-	473.5	[41] ^b
	1183	1667	-	-		
Ti	1043	1183	2.1	293.2	581.6	[41,64]
	1183	1667	2.1	293.2		
V	1043	1183	124	274	569.7	[41,52]
	1183	1667	0.62	273.5		
Cr	1043	1183	90	271	428.2	[41,52]
	1183	1667	10.8	291.8		
Mn	1043	1183	0.35	219.8	305.2	[41,52]
	1183	1667	0.16	261.7		
Fe	1043	1183	118	281.52	413	[52] ^c
	1183	1667	4.085	311.1		

Continuation of Tab. 9.4

Host material: Fe. DNN = 248 pm.						
Element	T _i [K]	T _f [K]	A ₁ [cm ² s ⁻¹]	Q ₁ [kJ mol ⁻¹]	E _{des} [kJ mol ⁻¹]	Sources
Co	1043	1183	6.38	257.1	452.5	[41,52]
	1183	1667	0.029	247.4		
Ni	1043	1183	1.3	234.5	454.2	[41,52]
	1183	1667	0.77	280.5		
Cu	1043	1183	300	283.9	389	[41,52]
	1183	1667	4.16	305		
Zn	1043	1183	60	262.6	173.5	[41,52]
	1183	1667	60	262.6		

^a We did not find estimations for the desorption enthalpy from Fe for these species. Nonetheless, at the temperatures we will consider (800 °C–1000 °C) they are gases and therefore, a reasonable approximation would be to assume total desorption for them (all atoms reaching the surface escape from the object).

^b We could not identify experimental data for the diffusion coefficient of these elements in Fe. In the absence of a better approach, we will assume a diffusion coefficient equal to the average diffusion coefficient of the rest of the species in the table except for H, which is a special case diffusing remarkably fast.

^c To account for the desorption of Fe isotopes from Fe we can safely use its sublimation enthalpy as the desorption one as discussed in section 5.1.

9.3.2 Results

Using the diffusion and desorption parameters reported in previous sections we can obtain an estimation of the ODF for the different objects and for different temperatures. The results can be found in Tabs. 9.5, 9.6, 9.7 and 9.8.

Table 9.5: Fraction of atoms reaching the object's surface, global desorption probability and out-diffusion fraction for different elements of interest in the side-cables conductors for different temperatures.

Side-cables conductor. S/V = 8.00 cm ⁻¹									
Element	T = 800 °C			T = 900 °C			T = 1000 °C		
	FRS	GDP	ODF	FRS	GDP	ODF	FRS	GDP	ODF
³ H	1.00	1.00	1.00	1.00	1.00	1.00	1.00	1.00	1.00
P	1.46·10 ⁻²	1.00	1.46·10 ⁻²	2.79·10 ⁻²	1.00	2.79·10 ⁻²	4.82·10 ⁻²	1.00	4.82·10 ⁻²
S	2.43·10 ⁻²	1.00	2.43·10 ⁻²	6.52·10 ⁻²	1.00	6.52·10 ⁻²	1.49·10 ⁻¹	1.00	1.49·10 ⁻¹
Ca	6.44·10 ⁻³	8.40·10 ⁻³	5.41·10 ⁻⁵	1.59·10 ⁻²	8.35·10 ⁻²	1.33·10 ⁻³	3.44·10 ⁻²	4.63·10 ⁻¹	1.59·10 ⁻²
Sc	6.44·10 ⁻³	0.00	0.00	1.59·10 ⁻²	1.74·10 ⁻¹¹	2.77·10 ⁻¹³	3.44·10 ⁻²	7.53·10 ⁻¹⁰	2.59·10 ⁻¹¹
Ti	7.64·10 ⁻³	0.00	0.00	1.95·10 ⁻²	0.00	0.00	4.29·10 ⁻²	1.41·10 ⁻¹⁰	6.06·10 ⁻¹²
V	4.98·10 ⁻³	3.81·10 ⁻¹¹	1.90·10 ⁻¹³	1.39·10 ⁻²	2.02·10 ⁻⁹	2.82·10 ⁻¹¹	3.31·10 ⁻²	5.87·10 ⁻⁸	1.94·10 ⁻⁹
Cr	4.21·10 ⁻³	8.61·10 ⁻⁵	3.63·10 ⁻⁷	1.09·10 ⁻²	1.21·10 ⁻³	1.31·10 ⁻⁵	2.43·10 ⁻²	1.11·10 ⁻²	2.69·10 ⁻⁴
Mn	7.52·10 ⁻³	7.34·10 ⁻¹	5.52·10 ⁻³	1.95·10 ⁻²	1.00	1.95·10 ⁻²	4.35·10 ⁻²	1.00	4.35·10 ⁻²

Continuation of Tab. 9.5

side-cables conductor. $S/V = 8.00 \text{ cm}^{-1}$									
Element	T = 800 °C			T = 900 °C			T = 1000 °C		
	FRS	GDP	ODF	FRS	GDP	ODF	FRS	GDP	ODF
Fe	$2.39 \cdot 10^{-3}$	$9.32 \cdot 10^{-8}$	$2.23 \cdot 10^{-10}$	$6.75 \cdot 10^{-3}$	$2.46 \cdot 10^{-6}$	$1.66 \cdot 10^{-8}$	$1.62 \cdot 10^{-2}$	$3.87 \cdot 10^{-5}$	$6.27 \cdot 10^{-7}$
Co	$2.43 \cdot 10^{-3}$	$4.96 \cdot 10^{-6}$	$1.21 \cdot 10^{-8}$	$6.98 \cdot 10^{-3}$	$9.53 \cdot 10^{-5}$	$6.65 \cdot 10^{-7}$	$1.72 \cdot 10^{-2}$	$1.17 \cdot 10^{-3}$	$2.02 \cdot 10^{-5}$
Ni	$1.58 \cdot 10^{-3}$	$3.55 \cdot 10^{-6}$	$5.59 \cdot 10^{-9}$	$4.80 \cdot 10^{-3}$	$7.19 \cdot 10^{-5}$	$3.45 \cdot 10^{-7}$	$1.26 \cdot 10^{-2}$	$9.29 \cdot 10^{-4}$	$1.17 \cdot 10^{-5}$
Cu	$3.55 \cdot 10^{-3}$	$5.50 \cdot 10^{-3}$	$1.95 \cdot 10^{-5}$	$9.73 \cdot 10^{-3}$	$5.56 \cdot 10^{-2}$	$5.41 \cdot 10^{-4}$	$2.30 \cdot 10^{-2}$	$3.40 \cdot 10^{-1}$	$7.83 \cdot 10^{-3}$
Zn	$6.93 \cdot 10^{-3}$	1.00	$6.93 \cdot 10^{-3}$	$1.72 \cdot 10^{-2}$	1.00	$1.72 \cdot 10^{-2}$	$3.69 \cdot 10^{-2}$	1.00	$3.69 \cdot 10^{-2}$

Table 9.6: Fraction of atoms reaching the object's surface, global desorption probability and out-diffusion fraction for different elements of interest in magnet coils conductors for different temperatures.

Magnet coils conductor. $S/V = 3.38 \text{ cm}^{-1}$									
Element	T = 800 °C			T = 900 °C			T = 1000 °C		
	FRS	GDP	ODF	FRS	GDP	ODF	FRS	GDP	ODF
^3H	$9.96 \cdot 10^{-1}$	1.00	$9.96 \cdot 10^{-1}$	$9.99 \cdot 10^{-1}$	1.00	$9.99 \cdot 10^{-1}$	1.00	1.00	1.00
Na	$2.72 \cdot 10^{-3}$	1.00	$2.72 \cdot 10^{-3}$	$6.72 \cdot 10^{-3}$	1.00	$6.72 \cdot 10^{-3}$	$1.45 \cdot 10^{-2}$	1.00	$1.45 \cdot 10^{-2}$
Si	$1.27 \cdot 10^{-3}$	0.00	0.00	$2.87 \cdot 10^{-3}$	0.00	0.00	$5.74 \cdot 10^{-3}$	$8.92 \cdot 10^{-11}$	$5.12 \cdot 10^{-13}$
P	$6.14 \cdot 10^{-3}$	1.00	$6.14 \cdot 10^{-3}$	$1.18 \cdot 10^{-2}$	1.00	$1.18 \cdot 10^{-2}$	$2.04 \cdot 10^{-2}$	1.00	$2.04 \cdot 10^{-2}$
S	$1.03 \cdot 10^{-2}$	1.00	$1.03 \cdot 10^{-2}$	$2.75 \cdot 10^{-2}$	1.00	$2.75 \cdot 10^{-2}$	$6.32 \cdot 10^{-2}$	1.00	$6.32 \cdot 10^{-2}$
K	$2.72 \cdot 10^{-3}$	$9.91 \cdot 10^{-1}$	$2.69 \cdot 10^{-3}$	$6.72 \cdot 10^{-3}$	1.00	$6.72 \cdot 10^{-3}$	$1.45 \cdot 10^{-2}$	1.00	$1.45 \cdot 10^{-2}$
Ca	$2.72 \cdot 10^{-3}$	$8.40 \cdot 10^{-3}$	$2.28 \cdot 10^{-5}$	$6.72 \cdot 10^{-3}$	$8.35 \cdot 10^{-2}$	$5.61 \cdot 10^{-4}$	$1.45 \cdot 10^{-2}$	$4.63 \cdot 10^{-1}$	$6.72 \cdot 10^{-3}$
Sc	$2.72 \cdot 10^{-3}$	0.00	0.00	$6.72 \cdot 10^{-3}$	$1.74 \cdot 10^{-11}$	$1.17 \cdot 10^{-13}$	$1.45 \cdot 10^{-2}$	$7.53 \cdot 10^{-10}$	$1.09 \cdot 10^{-11}$
Ti	$3.22 \cdot 10^{-3}$	0.00	0.00	$8.23 \cdot 10^{-3}$	0.00	0.00	$1.81 \cdot 10^{-2}$	$1.41 \cdot 10^{-10}$	$2.56 \cdot 10^{-12}$
V	$2.10 \cdot 10^{-3}$	$3.81 \cdot 10^{-11}$	$8.01 \cdot 10^{-14}$	$5.87 \cdot 10^{-3}$	$2.02 \cdot 10^{-9}$	$1.19 \cdot 10^{-11}$	$1.40 \cdot 10^{-2}$	$5.87 \cdot 10^{-8}$	$8.20 \cdot 10^{-10}$
Cr	$1.78 \cdot 10^{-3}$	$8.61 \cdot 10^{-5}$	$1.53 \cdot 10^{-7}$	$4.59 \cdot 10^{-3}$	$1.21 \cdot 10^{-3}$	$5.53 \cdot 10^{-6}$	$1.02 \cdot 10^{-2}$	$1.11 \cdot 10^{-2}$	$1.14 \cdot 10^{-4}$
Mn	$3.17 \cdot 10^{-3}$	$7.34 \cdot 10^{-1}$	$2.33 \cdot 10^{-3}$	$8.22 \cdot 10^{-3}$	1.00	$8.22 \cdot 10^{-3}$	$1.84 \cdot 10^{-2}$	1.00	$1.84 \cdot 10^{-2}$
Fe	$1.01 \cdot 10^{-3}$	$9.32 \cdot 10^{-8}$	$9.39 \cdot 10^{-11}$	$2.85 \cdot 10^{-3}$	$2.46 \cdot 10^{-6}$	$7.00 \cdot 10^{-9}$	$6.83 \cdot 10^{-3}$	$3.87 \cdot 10^{-5}$	$2.65 \cdot 10^{-7}$
Co	$1.03 \cdot 10^{-3}$	$4.96 \cdot 10^{-6}$	$5.09 \cdot 10^{-9}$	$2.94 \cdot 10^{-3}$	$9.53 \cdot 10^{-5}$	$2.81 \cdot 10^{-7}$	$7.27 \cdot 10^{-3}$	$1.17 \cdot 10^{-3}$	$8.51 \cdot 10^{-6}$
Ni	$6.65 \cdot 10^{-4}$	$3.55 \cdot 10^{-6}$	$2.36 \cdot 10^{-9}$	$2.03 \cdot 10^{-3}$	$7.19 \cdot 10^{-5}$	$1.46 \cdot 10^{-7}$	$5.31 \cdot 10^{-3}$	$9.29 \cdot 10^{-4}$	$4.94 \cdot 10^{-6}$
Cu	$1.50 \cdot 10^{-3}$	$5.50 \cdot 10^{-3}$	$8.24 \cdot 10^{-6}$	$4.10 \cdot 10^{-3}$	$5.56 \cdot 10^{-2}$	$2.28 \cdot 10^{-4}$	$9.72 \cdot 10^{-3}$	$3.40 \cdot 10^{-1}$	$3.30 \cdot 10^{-3}$
Zn	$2.92 \cdot 10^{-3}$	1.00	$2.92 \cdot 10^{-3}$	$7.25 \cdot 10^{-3}$	1.00	$7.25 \cdot 10^{-3}$	$1.56 \cdot 10^{-2}$	1.00	$1.56 \cdot 10^{-2}$

Table 9.7: Fraction of atoms reaching the object's surface, global desorption probability and out-diffusion fraction for different elements of interest in a magnet yoke for different temperatures.

Magnet yoke. $S/V = 0.22 \text{ cm}^{-1}$									
Element	T = 800 °C			T = 900 °C			T = 1000 °C		
	FRS	GDP	ODF	FRS	GDP	ODF	FRS	GDP	ODF
H	$2.63 \cdot 10^{-1}$	1.00	$2.63 \cdot 10^{-1}$	$2.72 \cdot 10^{-1}$	1.00	$2.72 \cdot 10^{-1}$	$2.81 \cdot 10^{-1}$	1.00	$2.81 \cdot 10^{-1}$
Be	$1.69 \cdot 10^{-4}$	$1.24 \cdot 10^{-3}$	$2.10 \cdot 10^{-7}$	$4.80 \cdot 10^{-4}$	$1.58 \cdot 10^{-2}$	$7.60 \cdot 10^{-6}$	$5.31 \cdot 10^{-5}$	$5.41 \cdot 10^{-2}$	$2.87 \cdot 10^{-6}$
Na	$7.58 \cdot 10^{-5}$	1.00	$7.58 \cdot 10^{-5}$	$2.31 \cdot 10^{-4}$	1.00	$2.31 \cdot 10^{-4}$	$2.37 \cdot 10^{-4}$	1.00	$2.37 \cdot 10^{-4}$
Si	$5.16 \cdot 10^{-5}$	0.00	0.00	$1.54 \cdot 10^{-4}$	0.00	0.00	$4.08 \cdot 10^{-5}$	$1.13 \cdot 10^{-11}$	$4.61 \cdot 10^{-16}$
P	$6.40 \cdot 10^{-5}$	1.00	$6.40 \cdot 10^{-5}$	$2.34 \cdot 10^{-4}$	1.00	$2.34 \cdot 10^{-4}$	$4.03 \cdot 10^{-4}$	1.00	$4.03 \cdot 10^{-4}$
S	$2.03 \cdot 10^{-4}$	1.00	$2.03 \cdot 10^{-4}$	$6.15 \cdot 10^{-4}$	1.00	$6.15 \cdot 10^{-4}$	$5.45 \cdot 10^{-4}$	1.00	$5.45 \cdot 10^{-4}$
K	$7.58 \cdot 10^{-5}$	1.00	$7.58 \cdot 10^{-5}$	$2.31 \cdot 10^{-4}$	1.00	$2.31 \cdot 10^{-4}$	$2.37 \cdot 10^{-4}$	1.00	$2.37 \cdot 10^{-4}$
Ca	$7.58 \cdot 10^{-5}$	1.00	$7.58 \cdot 10^{-5}$	$2.31 \cdot 10^{-4}$	1.00	$2.31 \cdot 10^{-4}$	$2.37 \cdot 10^{-4}$	1.00	$2.37 \cdot 10^{-4}$
Sc	$7.58 \cdot 10^{-5}$	$2.53 \cdot 10^{-7}$	$1.92 \cdot 10^{-11}$	$2.31 \cdot 10^{-4}$	$8.33 \cdot 10^{-6}$	$1.92 \cdot 10^{-9}$	$2.37 \cdot 10^{-4}$	$8.47 \cdot 10^{-6}$	$2.01 \cdot 10^{-9}$
Ti	$1.58 \cdot 10^{-6}$	$5.08 \cdot 10^{-12}$	$8.02 \cdot 10^{-18}$	$6.40 \cdot 10^{-6}$	$3.26 \cdot 10^{-10}$	$2.09 \cdot 10^{-15}$	$2.09 \cdot 10^{-5}$	$1.09 \cdot 10^{-8}$	$2.27 \cdot 10^{-13}$
V	$3.56 \cdot 10^{-5}$	$4.78 \cdot 10^{-11}$	$1.70 \cdot 10^{-15}$	$1.32 \cdot 10^{-4}$	$3.03 \cdot 10^{-9}$	$3.99 \cdot 10^{-13}$	$2.87 \cdot 10^{-5}$	$7.17 \cdot 10^{-9}$	$2.06 \cdot 10^{-13}$
Cr	$3.58 \cdot 10^{-5}$	$2.92 \cdot 10^{-3}$	$1.05 \cdot 10^{-7}$	$1.31 \cdot 10^{-4}$	$3.86 \cdot 10^{-2}$	$5.05 \cdot 10^{-6}$	$5.05 \cdot 10^{-5}$	$4.45 \cdot 10^{-2}$	$2.25 \cdot 10^{-6}$
Mn	$3.94 \cdot 10^{-5}$	1.00	$3.94 \cdot 10^{-5}$	$1.13 \cdot 10^{-4}$	1.00	$1.13 \cdot 10^{-4}$	$2.55 \cdot 10^{-5}$	1.00	$2.55 \cdot 10^{-5}$
Fe	$2.28 \cdot 10^{-5}$	$8.48 \cdot 10^{-2}$	$1.93 \cdot 10^{-6}$	$8.74 \cdot 10^{-5}$	$5.95 \cdot 10^{-1}$	$5.20 \cdot 10^{-5}$	$1.25 \cdot 10^{-5}$	$2.53 \cdot 10^{-1}$	$3.16 \cdot 10^{-6}$
Co	$2.08 \cdot 10^{-5}$	$1.45 \cdot 10^{-6}$	$3.02 \cdot 10^{-11}$	$7.10 \cdot 10^{-5}$	$2.96 \cdot 10^{-5}$	$2.10 \cdot 10^{-9}$	$2.13 \cdot 10^{-5}$	$3.48 \cdot 10^{-5}$	$7.42 \cdot 10^{-10}$
Cu	$3.18 \cdot 10^{-5}$	$6.02 \cdot 10^{-1}$	$1.91 \cdot 10^{-5}$	$1.23 \cdot 10^{-4}$	1.00	$1.23 \cdot 10^{-4}$	$1.68 \cdot 10^{-5}$	$8.82 \cdot 10^{-1}$	$1.48 \cdot 10^{-5}$

Table 9.8: Fraction of atoms reaching the object's surface, global desorption probability and out-diffusion fraction for different elements of interest in a collimator vessel for different temperatures.

Collimator vessel. $S/V = 1.46 \text{ cm}^{-1}$									
Element	T = 800 °C			T = 900 °C			T = 1000 °C		
	FRS	GDP	ODF	FRS	GDP	ODF	FRS	GDP	ODF
H	$9.74 \cdot 10^{-1}$	1.00	$9.74 \cdot 10^{-1}$	$9.79 \cdot 10^{-1}$	1.00	$9.79 \cdot 10^{-1}$	$9.83 \cdot 10^{-1}$	1.00	$9.83 \cdot 10^{-1}$
Be	$1.12 \cdot 10^{-3}$	$1.24 \cdot 10^{-3}$	$1.39 \cdot 10^{-6}$	$3.18 \cdot 10^{-3}$	$1.58 \cdot 10^{-2}$	$5.03 \cdot 10^{-5}$	$3.51 \cdot 10^{-4}$	$5.41 \cdot 10^{-2}$	$1.90 \cdot 10^{-5}$
Na	$5.02 \cdot 10^{-4}$	1.00	$5.02 \cdot 10^{-4}$	$1.53 \cdot 10^{-3}$	1.00	$1.53 \cdot 10^{-3}$	$1.57 \cdot 10^{-3}$	1.00	$1.57 \cdot 10^{-3}$
Mg	$5.02 \cdot 10^{-4}$	1.00	$5.02 \cdot 10^{-4}$	$1.53 \cdot 10^{-3}$	1.00	$1.53 \cdot 10^{-3}$	$1.57 \cdot 10^{-3}$	1.00	$1.57 \cdot 10^{-3}$
Si	$3.41 \cdot 10^{-4}$	0.00	0.00	$1.02 \cdot 10^{-3}$	0.00	0.00	$2.70 \cdot 10^{-4}$	$1.13 \cdot 10^{-11}$	$3.05 \cdot 10^{-15}$
P	$4.24 \cdot 10^{-4}$	1.00	$4.24 \cdot 10^{-4}$	$1.55 \cdot 10^{-3}$	1.00	$1.55 \cdot 10^{-3}$	$2.67 \cdot 10^{-3}$	1.00	$2.67 \cdot 10^{-3}$
S	$1.35 \cdot 10^{-3}$	1.00	$1.35 \cdot 10^{-3}$	$4.07 \cdot 10^{-3}$	1.00	$4.07 \cdot 10^{-3}$	$3.61 \cdot 10^{-3}$	1.00	$3.61 \cdot 10^{-3}$
Cl	$5.02 \cdot 10^{-4}$	1.00	$5.02 \cdot 10^{-4}$	$1.53 \cdot 10^{-3}$	1.00	$1.53 \cdot 10^{-3}$	$1.57 \cdot 10^{-3}$	1.00	$1.57 \cdot 10^{-3}$
K	$5.02 \cdot 10^{-4}$	1.00	$5.02 \cdot 10^{-4}$	$1.53 \cdot 10^{-3}$	1.00	$1.53 \cdot 10^{-3}$	$1.57 \cdot 10^{-3}$	1.00	$1.57 \cdot 10^{-3}$
Ca	$5.02 \cdot 10^{-4}$	1.00	$5.02 \cdot 10^{-4}$	$1.53 \cdot 10^{-3}$	1.00	$1.53 \cdot 10^{-3}$	$1.57 \cdot 10^{-3}$	1.00	$1.57 \cdot 10^{-3}$
Sc	$5.02 \cdot 10^{-4}$	$2.53 \cdot 10^{-7}$	$1.27 \cdot 10^{-10}$	$1.53 \cdot 10^{-3}$	$8.33 \cdot 10^{-6}$	$1.27 \cdot 10^{-8}$	$1.57 \cdot 10^{-3}$	$8.47 \cdot 10^{-6}$	$1.33 \cdot 10^{-8}$
Ti	$1.04 \cdot 10^{-5}$	$5.08 \cdot 10^{-12}$	$5.31 \cdot 10^{-17}$	$4.24 \cdot 10^{-5}$	$3.26 \cdot 10^{-10}$	$1.38 \cdot 10^{-14}$	$1.38 \cdot 10^{-4}$	$1.09 \cdot 10^{-8}$	$1.50 \cdot 10^{-12}$
V	$2.35 \cdot 10^{-4}$	$4.78 \cdot 10^{-11}$	$1.12 \cdot 10^{-14}$	$8.72 \cdot 10^{-4}$	$3.03 \cdot 10^{-9}$	$2.64 \cdot 10^{-12}$	$1.90 \cdot 10^{-4}$	$7.17 \cdot 10^{-9}$	$1.36 \cdot 10^{-12}$

Continuation of Tab. 9.8

Collimator vessel. $S/V = 1.46 \text{ cm}^{-1}$									
Element	T = 800 °C			T = 900 °C			T = 1000 °C		
	FRS	GDP	ODF	FRS	GDP	ODF	FRS	GDP	ODF
Cr	$2.37 \cdot 10^{-4}$	$2.92 \cdot 10^{-3}$	$6.92 \cdot 10^{-7}$	$8.66 \cdot 10^{-4}$	$3.86 \cdot 10^{-2}$	$3.34 \cdot 10^{-5}$	$3.35 \cdot 10^{-4}$	$4.45 \cdot 10^{-2}$	$1.49 \cdot 10^{-5}$
Mn	$2.61 \cdot 10^{-4}$	1.00	$2.61 \cdot 10^{-4}$	$7.46 \cdot 10^{-4}$	1.00	$7.46 \cdot 10^{-4}$	$1.69 \cdot 10^{-4}$	1.00	$1.69 \cdot 10^{-4}$
Fe	$1.51 \cdot 10^{-4}$	$8.48 \cdot 10^{-2}$	$1.28 \cdot 10^{-5}$	$5.78 \cdot 10^{-4}$	$5.95 \cdot 10^{-1}$	$3.44 \cdot 10^{-4}$	$8.27 \cdot 10^{-5}$	$2.53 \cdot 10^{-1}$	$2.10 \cdot 10^{-5}$
Co	$1.38 \cdot 10^{-4}$	$1.45 \cdot 10^{-6}$	$2.00 \cdot 10^{-10}$	$4.70 \cdot 10^{-4}$	$2.96 \cdot 10^{-5}$	$1.39 \cdot 10^{-8}$	$1.41 \cdot 10^{-4}$	$3.48 \cdot 10^{-5}$	$4.92 \cdot 10^{-9}$
Ni	$2.21 \cdot 10^{-4}$	$4.15 \cdot 10^{-5}$	$9.15 \cdot 10^{-9}$	$6.76 \cdot 10^{-4}$	$6.70 \cdot 10^{-4}$	$4.53 \cdot 10^{-7}$	$1.52 \cdot 10^{-4}$	$6.10 \cdot 10^{-4}$	$9.29 \cdot 10^{-8}$

Combining the out-diffusion results with the radionuclide inventories reported earlier in this chapter, we can finally obtain quantitative data on the contribution of the out-diffusion phenomenon to the radiological hazard posed by an accidental fire scenario. Tab. 9.9 shows the effective E_{50} inhalation dose corresponding to the radionuclides released as a consequence of out-diffusion from the different objects under consideration. The results are shown for different temperatures. In the same table we can find the ratio between the out-diffused portion of the hazard per cm^3 for each object and the hazard due to the combustion of 1 cm^3 of side-cable insulation. Two sets of results are provided, one considering ^3H and another one excluding it from the calculations (assuming that all of it was released before the fire). Tab. 9.10 is similar to the previous one, but in this case we consider total desorption, counting as out-diffused every radionuclide reaching the objects' surfaces. The reason behind this second table will be explained in the next section. The unfolded contribution of each radionuclide can be found in appendix G.

Table 9.9: Contribution of the out-diffusion phenomenon to the radiological hazard posed by an accidental fire affecting different objects. A: effective E_{50} inhalation dose corresponding to the radionuclides released as a consequence of out-diffusion from the different objects per cm^3 . B: effective E_{50} inhalation dose corresponding to the entire radionuclide inventory contained in 1 cm^3 of the different objects. C: effective E_{50} inhalation dose corresponding to the entire radionuclide inventory contained in 1 cm^3 of side-cables insulation, which is a combustible material likely to be incinerated in the event of a fire.

Object	T [°C]	Including ^3H			Excluding ^3H		
		A [$\mu\text{Sv cm}^{-3}$]	A/B	A/C	A [$\mu\text{Sv cm}^{-3}$]	A/B	A/C
Side-cables conductor	800	$2.98 \cdot 10^{-2}$	$1.61 \cdot 10^{-3}$	2.14	$2.98 \cdot 10^{-3}$	$1.61 \cdot 10^{-4}$	$4.93 \cdot 10^{-1}$
	900	$4.17 \cdot 10^{-2}$	$2.25 \cdot 10^{-3}$	3.00	$1.49 \cdot 10^{-2}$	$8.05 \cdot 10^{-4}$	2.46
	1000	$1.38 \cdot 10^{-1}$	$7.44 \cdot 10^{-3}$	9.91	$1.11 \cdot 10^{-1}$	$6.00 \cdot 10^{-3}$	$1.84 \cdot 10^1$
Magnet coils conductor	800	1.18	$2.70 \cdot 10^{-3}$	$8.49 \cdot 10^1$	$4.43 \cdot 10^{-2}$	$1.02 \cdot 10^{-4}$	7.33
	900	1.30	$2.99 \cdot 10^{-3}$	$9.37 \cdot 10^1$	$1.63 \cdot 10^{-1}$	$3.75 \cdot 10^{-4}$	$2.71 \cdot 10^1$
	1000	1.87	$4.30 \cdot 10^{-3}$	$1.35 \cdot 10^2$	$7.35 \cdot 10^{-1}$	$1.69 \cdot 10^{-3}$	$1.22 \cdot 10^2$
Magnet yoke	800	$2.25 \cdot 10^{-1}$	$9.33 \cdot 10^{-4}$	$1.62 \cdot 10^1$	$6.28 \cdot 10^{-3}$	$2.61 \cdot 10^{-5}$	1.04
	900	$2.47 \cdot 10^{-1}$	$1.02 \cdot 10^{-3}$	$1.78 \cdot 10^1$	$2.02 \cdot 10^{-2}$	$8.39 \cdot 10^{-5}$	3.34
	1000	$2.42 \cdot 10^{-1}$	$1.00 \cdot 10^{-3}$	$1.74 \cdot 10^1$	$7.68 \cdot 10^{-3}$	$3.19 \cdot 10^{-5}$	1.27
Collimator vessel	800	2.24	$4.75 \cdot 10^{-3}$	$1.61 \cdot 10^2$	$5.41 \cdot 10^{-2}$	$1.15 \cdot 10^{-4}$	8.95
	900	2.38	$5.03 \cdot 10^{-3}$	$1.71 \cdot 10^2$	$1.73 \cdot 10^{-1}$	$3.68 \cdot 10^{-4}$	$2.86 \cdot 10^1$
	1000	2.32	$4.92 \cdot 10^{-3}$	$1.67 \cdot 10^2$	$1.11 \cdot 10^{-1}$	$2.36 \cdot 10^{-4}$	$1.84 \cdot 10^1$

Table 9.10: Contribution of the out-diffusion phenomenon to the radiological hazard posed by an accidental fire affecting different objects. Total desorption has been considered in this case. A: effective E_{50} inhalation dose corresponding to the radionuclides released as a consequence of out-diffusion from the different objects per cm^3 . B: effective E_{50} inhalation dose corresponding to the entire radionuclide inventory contained in 1 cm^3 of the different objects. C: effective E_{50} inhalation dose corresponding to the entire radionuclide inventory contained in 1 cm^3 of side-cables insulation, which is a combustible material likely to be incinerated in the event of a fire.

Object	T [°C]	Including ^3H			Excluding ^3H		
		A [$\mu\text{Sv cm}^{-3}$]	A/B	A/C	A [$\mu\text{Sv cm}^{-3}$]	A/B	A/C
Side-cables conductor	800	$8.89 \cdot 10^{-2}$	$4.80 \cdot 10^{-3}$	6.40	$6.21 \cdot 10^{-2}$	$3.36 \cdot 10^{-3}$	$1.03 \cdot 10^1$
	900	$1.97 \cdot 10^{-1}$	$1.07 \cdot 10^{-2}$	$1.42 \cdot 10^1$	$1.71 \cdot 10^{-1}$	$9.23 \cdot 10^{-3}$	$2.82 \cdot 10^1$
	1000	$4.32 \cdot 10^{-1}$	$2.33 \cdot 10^{-2}$	$3.11 \cdot 10^1$	$4.05 \cdot 10^{-1}$	$2.19 \cdot 10^{-2}$	$6.71 \cdot 10^1$
Magnet coils conductor	800	1.71	$3.91 \cdot 10^{-3}$	$1.23 \cdot 10^2$	$5.71 \cdot 10^{-1}$	$1.31 \cdot 10^{-3}$	$9.45 \cdot 10^1$
	900	2.72	$6.23 \cdot 10^{-3}$	$1.95 \cdot 10^2$	1.58	$3.62 \cdot 10^{-3}$	$2.61 \cdot 10^2$
	1000	4.91	$1.13 \cdot 10^{-2}$	$3.53 \cdot 10^2$	3.77	$8.67 \cdot 10^{-3}$	$6.24 \cdot 10^2$
Magnet yoke	800	$2.29 \cdot 10^{-1}$	$9.47 \cdot 10^{-4}$	$1.65 \cdot 10^1$	$9.72 \cdot 10^{-3}$	$4.04 \cdot 10^{-5}$	1.61
	900	$2.57 \cdot 10^{-1}$	$1.07 \cdot 10^{-3}$	$1.85 \cdot 10^1$	$3.02 \cdot 10^{-2}$	$1.25 \cdot 10^{-4}$	4.99
	1000	$2.48 \cdot 10^{-1}$	$1.03 \cdot 10^{-3}$	$1.78 \cdot 10^1$	$1.37 \cdot 10^{-2}$	$5.68 \cdot 10^{-5}$	2.26
Collimator vessel	800	2.31	$4.89 \cdot 10^{-3}$	$1.66 \cdot 10^2$	$1.19 \cdot 10^{-1}$	$2.53 \cdot 10^{-4}$	$1.97 \cdot 10^1$
	900	2.58	$5.46 \cdot 10^{-3}$	$1.86 \cdot 10^2$	$3.78 \cdot 10^{-1}$	$8.05 \cdot 10^{-4}$	$6.26 \cdot 10^1$
	1000	2.42	$5.13 \cdot 10^{-3}$	$1.74 \cdot 10^2$	$2.10 \cdot 10^{-1}$	$4.47 \cdot 10^{-4}$	$3.48 \cdot 10^1$

9.3.3 Discussion

Let us first highlight few points that are important to properly analyze the results obtained:

- Besides out-diffusion, it is important to note that, according to the ActiWiz results shown in Tab. 9.2, the contribution to the effective E_{50} dose of the radionuclides released by the combustion of 1 cm^3 of magnet coil insulation is 240 times higher than the combustion of the same volume of side-cable insulation. This is due to the higher radiation flux to which magnet coils are exposed as well as to their material composition, less optimized from an RP perspective.
- We have considered uniform temperature and radionuclide concentration. This are approximations allowing us to obtain general results to be used as estimates of the importance of out-diffusion as a radiological source term contributor. The whole versatility of SOLIDUSS is at the user's disposal for more accurate calculations whenever needed.
- When looking at electrical conductors, which are generally wrapped by an insulation layer, we must bear in mind that radionuclides out-diffused from them can be mechanically trapped in the insulation and only be released in the event of its combustion.
- There are two different coil sizes in the warm quadruples that we are considering in this example. The ratio S/V that we have used is the average of the two different ratios (which are reasonably similar. Inside the coil cells there is a cylindrical conduit in which the cooling

water circulates through them. Therefore, approximately a third part of the out-diffused radionuclides will not end up in the air or insulation surrounding the coils but in the cooling water circulating through them.

- As explained in the previous chapter, we expect the GDP to be overestimated by the analytical formula by a factor of a few at most. This overestimation is obviously passed to the ODF (remember that $ODF = FRS \cdot GDP$).
- Chemical reactions are not accounted for by SOLIDUSS, as we already mentioned earlier in this manuscript. This is a clear drawback that could result in the underestimation of the fraction of radionuclides released to the environment in case of fire. The reason is that, besides desorption, a radionuclide reaching an object's surface could undergo chemical reactions with elements in air that could result in its immediate release from the material surface. A typical example is C, whose desorption enthalpy from Fe is huge ($\approx 862 \text{ kJ mol}^{-1}$) and therefore its desorption probability is almost zero. But it reacts very easily with O, giving rise to CO and CO₂, which are highly volatile and would easily escape from the Fe surface. This is why it would be wise to consider $GDP = 1$ for C in order to better estimate the release fraction. We may find further examples of reactions resulting in volatile components, in particular involving O, which is highly reactive. To create a complete compendium of the different possibilities is outside the scope of this thesis, but it is the author's intention to raise awareness on this phenomenon. In the context of this discussion, Tab. 9.10 was produced by considering total desorption for all radionuclides. It is conceived as an upper limit for the real ODF in the unlikely case in which all radionuclides reaching the objects' surfaces manage to escape from them (either by simple desorption or through a chemical reaction).
- For conciseness, we have only considered radionuclides contributing above 0.01 % to the total inhalation dose for each component. This selection was done before computing the out-diffusion fractions, which means that we may have ruled out rapidly diffusing radionuclides with a non-negligible contribution to the final hazard (inhalation dose due to out-diffused radionuclides). ¹¹C may be an example of this.

Looking now at Tab. 9.9, we see that the collimator vessel presents the highest radiological hazard due to out-diffusion per cm³ exposed to fire, closely followed by magnet coils conductor. This is reasonable given the higher flux of energetic particles to which they are exposed in comparison with side-cables, and given their S/V ratio, substantially greater than that one of the magnet yoke.

In general, significantly higher temperatures imply significantly higher ODF, but in the table we can find a common exception, Fe. The structural phase transition suffered by Fe at 1183 K ($\approx 910 \text{ }^\circ\text{C}$) results in a general reduction of the diffusion coefficient of the isotopes inside it, clearly impacting the ODFs. In such a situation, the worst case should be assumed from an RP perspective, since even in the case of a fire above that temperature threshold, the heating up would not be immediate. This is a good example of why sensitivity analysis are recommended, since not always higher temperatures imply higher ODFs.

Let us consider a single quadrupole at 900 °C: according to Tab. 9.9, if we exclude ³H contribution, the contribution to the inhalation dose of the out-diffused radionuclides from a 1 cm³ of yoke equals

the contribution of 3.34 cm^3 of burnt side-cable insulation. Similarly, that one of the out-diffused radionuclides from a 1 cm^3 of magnet coils conductor equals 27.1 cm^3 of burnt side-cable insulation. Approximated volumes for the quadrupole yoke and the coils conductor are 1.08 m^3 and 0.17 m^3 , respectively. Therefore, the radiological hazard posed by the out-diffused radionuclides from the quadrupole is equivalent to the combustion of approximately 8.2 m^3 of side-cable insulation, this is 7708 kg of cable insulation. If we consider all the ^3H to be inside the different components at the time of fire, this value rises to 33 044 kg.

Excluding ^3H and considering normal desorption treatment, we can see that the fraction of the total hazard released because of out-diffusion at the assumed temperatures is of the order of 10^{-3} – 10^{-4} for side-cables and coils insulation, 10^{-4} for the collimator vessel and 10^{-5} for the magnet yoke.

Conclusion and outlook

THE COMPLEXITY of CERN's premises and the nature of its activities give rise to significant safety challenges. In the present manuscript, we have explored the intersection of two types of hazards: fire and radiological. The evaluation of the potential radiological consequences of an accidental fire in the laboratory premises is of the utmost importance to define and implement the measures and protocols necessary to guarantee the safety of the members of the personnel, the public and the environment. CERN launched the FIRIA project in order to reinforce the effort exerted in this direction. The present thesis was carried out as part of this effort, and aims to improve our understanding of a radioactivity release mechanism: thermally promoted out-diffusion of radionuclides. In the early chapters, we have shown how diffusion of radionuclides can be simulated using Monte Carlo methods. The tracking of the path followed by diffusing particles by means of a Wiener process emulates the macroscopic behaviour described by Fick's laws. This process is primarily governed by the diffusion coefficient, which is typically obtained experimentally. It is a function of the diffusing species (*e.g.* ^{60}Co) and its host material (*e.g.* Cu) and exhibits an exponential dependence with temperature.

A brand new software named SOLIDUSS was developed on this foundation. It was conceived as a versatile tool to be used whenever the thermally promoted out-diffusion of radionuclides needs to be assessed. It is internally linked to the general purpose Monte Carlo code FLUKA and profits from this connection to track radionuclides through arbitrarily complex geometries with minimal user intervention. The initial position of radionuclides, obtained as a result of the radiation-matter interaction simulated by FLUKA, is internally provided to SOLIDUSS. The software offers a wide variety of options to suit the user's needs and has been thoroughly tested, proving to be reliable and effective. A remarkably good performance of the code has been achieved. Optional run-time optimizations are combined with an innovative post-processing approach that uses few rough SOLIDUSS calculations to compute a final accurate result. Hence, the CPU time required to perform a fine calculation was greatly reduced.

The diffusion treatment of SOLIDUSS underwent validation through a set of numerical experiments. A series of simulations were performed, and their results treated as if they were experimental. We used them to find out the diffusion coefficient of several species and host materials using Fick's laws. The good agreement between input and obtained diffusion coefficients validated the diffusion model and the implemented algorithm.

When a diffusing radionuclide reaches the host material surface, it can either desorb (*i.e.* escape) or continue its path within the material. We have conceived a model to account for this phenomenon and included it in SOLIDUSS in addition to the diffusion treatment. The desorption probability is mainly dominated by the desorption enthalpy and, depending on its value, the release of radionuclides could be significant or negligible. The inclusion of this effect is therefore of great importance. Unfortunately, the scarcity of experimental data on desorption enthalpies force us to rely on calculated values or rough estimates, such as sublimation enthalpies.

With the aim of benchmarking SOLIDUSS against experimental data, we carried out an experimental campaign that provided valuable insights on the out-diffusion of radionuclides from activated material. The experiments consisted of heating up activated Al and Cu foils (common materials found in accelerators environments) immersed in a N₂ atmosphere and looking at differences in their activation levels before and after the heating using gamma-ray spectrometry analysis. No detectable differences in the ⁶⁰Co content of the Cu samples were obtained. On the contrary, a clear fraction of the ²²Na present in the Al foils out-diffused. Supplementary experiments heating up non-activated metallic foils in an air atmosphere were performed. They showed that a fraction of the foil's material could be released to the environment in the form of flakes and dust in the event of a fire. The data obtained from the experiments allowed for the joint benchmarking of the software's diffusion and desorption treatments. Simulation and experimental results are in good agreement within error bars.

A series of SOLIDUSS simulations helped us come upon two analytical expressions that can be used to assess the out-diffusion of radionuclides under the assumptions of uniform temperature and uniform initial distribution of radionuclides. The first of these expressions returns the fraction of radionuclides reaching an object's surface while diffusing inside it. Its agreement with SOLIDUSS' results is remarkable. The second one is used to estimate the desorption probability for those radionuclides. It might be overestimated since the expression assumes that radionuclides are next to the object's surface from the beginning of the hypothetical fire. The use of these expressions allows for exceptionally time-efficient out-diffusion estimations.

To conclude, we carried out a number of calculations considering generic ActiWiz irradiation scenarios for several LHC components. The analytical expressions were used to estimate the out-diffusion fraction of radionuclide inventories for each component. In the light of the results obtained, we can conclude that the contribution of out-diffusion to radiological source terms may be of considerable significance. The reason is that, even if out-diffused fractions are typically low, releases can be important in absolute terms since fire may affect highly radioactive noncombustible materials.

I would not like to conclude this manuscript without bringing the reader's attention towards a number of potential improvements that could push a little further our current understanding and tools regarding out-diffusion:

- Temperatures maps could be accompanied by their quantitative uncertainties. A method to propagate such uncertainties into SOLIDUSS results could be implemented in a fairly simple way. It would be based on fluctuating temperatures: whenever a radionuclide is produced

inside a certain voxel, the temperature of the voxel is sampled according to a given probability distribution. Typically, it would be a normal distribution with standard deviation equal to the temperature uncertainty. Then, for each radionuclide, the temperature would be different, propagating its uncertainty to the out-diffusion results.

- SOLIDUSS could benefit from the enlargement of the experimental data set obtained in the context of this thesis. Further experimental campaigns using more activated samples and single-heating experiments would provide quality data to extend the software benchmarking as well as our understanding of the out-diffusion phenomenon. Samples containing two or more radionuclides with suitable activation levels would be particularly interesting. It will allow us to compare the out-diffusion of both species for identical experimental conditions and host material. Likewise, heating radioactive samples in an air atmosphere could yield some interesting data provided that the activation levels and the methodology guarantee a safe outcome of the experiments.
- The out-diffusion of ^3H is an important topic for radiation protection. Its high diffusivity makes it significant also in the absence of fire. SOLIDUSS and the presented analytical expressions may be of help whenever it is necessary to assess its release. As a consequence of out-diffusion at room temperature, ^3H abundance in a given object at a particular time could greatly differ from its original abundance. This would affect the accidental fire source term calculations. A dedicated study taking into account the ^3H production temporal profile and its out-diffusion rate would be needed to estimate its abundance at the moment of the fire.
- The accuracy of GDP calculations performed using Eq. (8.8) can be improved by estimating the average time at which the radionuclides of a species in a given object first reach its surface. The improvement may well deserve a closer look in order to find the way to calculate such an average.
- SOLIDUSS does not simulate chemical reactions. This is a point for improvement given their potential impact in facilitating the release of those radionuclides that reach the surface of an object. In particular, it would be important to identify those reactions involving common radionuclides and air elements that give rise to volatile components.
- We explained at the beginning of this manuscript that diffusion of atoms is very often defect-mediated. The abundance of defects has a direct and critical impact on the diffusion coefficient. Materials in heavy radiation environments are damaged as a result of the interaction of energetic particles with their atoms, resulting in the creation of lattice defects. As a consequence, the diffusivity of the radionuclides in such materials may be enhanced. Further investigation on this phenomenon and implications is therefore advisable.
- SOLIDUSS' applications are not limited to the assessment of radionuclides out-diffusion in case of fire. Its flexibility and capabilities related to the use complex geometries, non-uniform concentrations of the diffusing species and non-uniform temperatures make it potentially valuable for other applications in which thermally promoted diffusion of atoms is of interest. The software is designed and built in such a way that allows for an easy introduction of future improvements and, in particular, those related to the underlying physical models.

Bibliography

- [1] Z. Solti, J. Magill, and R. Dreher.
Karlsruhe Nuclide Chart – New 10th edition 2018.
EPJ Nuclear Sci. Technol., 5:6, 2019.
- [2] M.H. Kalos and P.A. Whitlock.
Monte Carlo Methods.
Wiley-VCH, second revised and enlarged edition, 2008.
- [3] CERN.
<https://home.cern/> .
- [4] CERN history: science for peace.
<https://home.cern/about/who-we-are/our-history> .
- [5] CERN accelerators.
<https://home.cern/science/accelerators> .
- [6] CERN experiments.
<https://home.cern/science/experiments> .
- [7] CERN radiation protection mandate.
<https://hse.cern/content/radiation-protection-mandate> .
- [8] *Safety Code F*. Technical Report [EDMS 335729](#), CERN, 2006.
- [9] ICRP.
Recommendations of the International Commission on Radiological Protection.
Pergamon Press, 1991. ICRP Publication 60.
- [10] changes to signage of cern's radiation areas.
<https://home.cern/news/official-news/cern/changes-signage-cerns-radiation-areas> .
Accessed: Sep 2021.
- [11] Facts and figures about the LHC.
<https://home.cern/resources/faqs/facts-and-figures-about-lhc> .
- [12] FIRIA project.
<https://hse.cern/content/firia> .
- [13] G. Gai.
FIRIA Methodology. Technical Report [EDMS 2426715](#), CERN, 2021.
- [14] A. Arnalich.
Introducing FIRIA. Technical Report [EDMS 1976582](#), CERN, 2018.

- [15] H. Mehrer.
Diffusion in Solids.
Springer, 2007.
- [16] H. Föll.
Diffusion in Iron.
https://www.tf.uni-kiel.de/matwis/amat/iss/kap_5/illustr/s5_2.3.html .
Accessed: Jan 2019.
- [17] L. C. Evans.
An introduction to stochastic differential equations. Version 1.2.
<http://ft-sipil.unila.ac.id/dbooks/AN%20INTRODUCTION%20TO%20STOCHASTIC%20DIFFERENTIAL%20EQUATIONS%20VERSION%201.2.pdf> .
Accessed: Sep 2019.
- [18] H. Teichler.
Structural dynamics on the μs scale in molecular-dynamics simulated, deeply undercooled, glass-forming $\text{Ni}_{0.5}\text{Zr}_{0.5}$.
J. Non-Cryst. Solids, 293:339–344, 2001.
- [19] A. Fick.
Ueber Diffusion.
Ann. Phys. (Berl.), 94(1):59–86, 1855.
- [20] J. Crank.
The mathematics of diffusion.
Oxford Science Publications, second edition, 1975.
- [21] A. Einstein.
Über die von der molekularkinetischen Theorie der Wärme geforderte Bewegung von in ruhenden Flüssigkeiten suspendierten Teilchen.
Ann. Phys. (Berl.), 322(8):549–560, 1905.
- [22] C. Theis and H. Vincke.
Development of a computational model for the out-diffusion of radioisotopes from metals. Technical Report [EDMS 1720724](#), CERN, 2016.
- [23] E. A. Brandes and G. B. Brook, editors.
Smithells Metals Reference Book.
Reed Educational and Professional Publishing Ltd, seventh edition, 1992.
- [24] G. Battistoni, T. Boehlen, F. Cerutti, P.W. Chin, L.S. Esposito, A. Ferrari A. Fassò, A. Lechner, A. Empl, A. Mairani, A. Mereghetti, P. Garcia Ortega, J. Ranft, S. Roesler, P.R. Sala, V. Vlachoudis, and G. Smirnov.
Overview of the FLUKA code.
Ann. Nucl. Energy, 82:10–18, 2015.
- [25] T.T. Bohlen, F. Cerutti, M.P.W. Chin, A. Fassò, A. Ferrari, P.G. Ortega, A. Mairani, P.R. Sala, G. Smirnov, and V. Vlachoudis.
The FLUKA Code: Developments and Challenges for High Energy and Medical Applications.
Nuc. Data Sheets, 120:210–214, 2014.
- [26] CERN-FLUKA website.
<https://fluka.cern> .
- [27] S. Lalley.
Brownian Motion.

<https://galton.uchicago.edu/~lalley/Courses/313/BrownianMotionCurrent.pdf> .

Accessed: Sep 2019.

- [28] M. D. Donsker.
An invariance principle for certain probability limit theorems.
Mem. Amer. Math. Soc., 6, 1951.
- [29] F. Ogallar Ruiz, C. Theis, I. Porras, and H. Vincke.
SOLIDUSS: Solid-state diffusion software for radiation protection.
Applied Radiation and Isotopes, 179:109997, 2022.
- [30] C. Theis.
Coding style guide for software written within the RP group using C++ or Java. Technical Report [EDMS 1462696 v.2](#), CERN, 2015.
- [31] Student.
The probable error of a mean.
Biometrika, 6:1–25, 1908.
- [32] V. Vlachoudis.
FLAIR: A Powerful But User Friendly Graphical Interface For FLUKA. In Proc. Int. Conf. on Mathematics, Computational Methods & Reactor Physics (MC 2009).
Saratoga Springs, 2009.
- [33] F. Ogallar Ruiz, Helmut Vincke, and Chris Theis.
On the out-diffusion calculations using SOLIDUSS. Technical Report [EDMS 2446940 v.1.1](#), CERN, 2020.
- [34] H. J. Weber G. B. Arfken and F. E. Harris.
Mathematical methods for physicists.
Academic Press, 7th edition, 2012.
- [35] K. Jacobs.
Stochastic Processes for Physicists.
Cambridge University Press, 2010.
- [36] P. Mörters and Y. Peres.
Brownian Motion.
Cambridge University Press, 2010.
- [37] J. Wolberg.
Data analysis using the method of least squares.
Springer, Berlin Heidelberg New York, 2006.
- [38] M. Newville, T. Stensitzki, R. Otten, et al.
LMFIT: Non-Linear Least-Squares Minimization and Curve-Fitting for Python.
<https://lmfit.github.io/lmfit-py/> .
Accessed: Dec 2020.
- [39] J. Frenkel.
Theorie der Adsorption und verwandter Erscheinungen.
Z. Phys., 26:117–138, 1924.
- [40] I. Zvára.
The Inorganic Radiochemistry of Heavy Elements.
Springer Netherlands, 2008.

- [41] H. Roßbach and B. Eichler.
Adsorption von Metallen auf metallische Oberflächen und Möglichkeiten ihrer Nutzung in der Kernchemie - Ermittlung von AdsorptionSENTHALPIEN mit dem Rechenprogramm AMO. Technical Report [ZfK-527](#), Zentralinstitut für Kernforschung Rossendorf bei Dresden, 1984.
- [42] B. Eichler and H. Rossbach.
Adsorption of Volatile Metals on Metal Surfaces and its Application in Nuclear Chemistry. I. Calculation of Adsorption Enthalpies for Hypothetical Superheavy Elements with Z around 114.
Radiochim. Acta, 33:121–125, 1983.
- [43] M. Schädel.
The chemistry of superheavy elements.
Kluwer Academic Publishers, 2004.
- [44] U. Köster, P. Carbonez, A. Dorsival, J. Dvorak, R. Eichler, S. Fernandes, H. Frånberg, J. Neuhausen, Z. Novackova, R. Wilfinger, and A. Yakushev.
(Im-)possible ISOL beams.
Eur. Phys. J.: Spec. Top., 150(1):285–291, Nov 2007.
- [45] Y. Zhang, J. R. G. Evans, and S. Yang.
Corrected Values for Boiling Points and Enthalpies of Vaporization of Elements in Handbooks.
J. Chem. Eng. Data., 56(2):328–337, 2011.
- [46] O. C. Ibe.
Markov Processes for Stochastic Modeling.
Elsevier, Oxford, second edition, 2013.
- [47] *Expected number of times Random Walk crosses 0 line*.
<https://math.stackexchange.com/questions/1338097/expected-number-of-times-random-walk-crosses-0-line> .
Accessed: Jul 2021.
- [48] L. Sjögren.
Random Walks.
<https://www.google.com/url?sa=t&rct=j&q=&esrc=s&source=web&cd=&cad=rja&uact=8&ved=2ahUKEwiFor2X84XyAhVBzaQKHUaRBGQQFjAOegQIIBAD&url=http%3A%2F%2Fphysics.gu.se%2F~frtbn%2Fjoomla%2Fmedia%2Fmydocs%2FLennartSjogren%2Fkap2.pdf&usg=AOvVaw1yt.Q5H-wLdwDk0z8lg-Iu> .
Accessed: Jul 2021.
- [49] ISOLDE.
<https://home.cern/science/experiments/isolde> .
- [50] Solid-state physics at ISOLDE.
<https://espace.cern.ch/ISOLDE-SSP/> .
- [51] *Ordonnance sur la radioprotection*.
Conseil fédéral suisse, 26 avril 2017.
- [52] E. A. Brandes and G. B. Brook, editors.
Smithells Metals Reference Book.
Reed Educational and Professional Publishing Ltd, seventh edition, 1992.
- [53] S. Sudár, J. Csikai, and M. Buczkó.
Diffusion of ^{24}Na in Polycrystalline Aluminum.
Z. Metallkde., 68:740–741, 1977.

- [54] G. Neumann and V. Tölle.
Monovacancy and divancy contributions to the impurity diffusion in face-centred cubic metals.
Philos. Mag. A, 57(4):621–630, 1988.
- [55] C. Kittel.
Introduction to Solid State Physics.
Eighth edition, 2005.
- [56] H. Vincke and C. Theis.
ActiWiz – Optimizing your Nuclide Inventory at Proton Accelerators with a Computer Code. In Proc. ICRS12 conf., 2012.
Prog. Nucl. Sci. Tech., 2014.
- [57] H. Vincke and C. Theis.
The use of ActiWiz in operational radiation protection. In Proc. SATIF-12 conf., 2014, pages 88–98.
OECD Nuclear Energy Agency (NEA), 2014.
- [58] R. Froeschl, S. Sgobba, C. Theis, F. La Torre, H. Vincke, and N. Walter.
Radiological Hazard classification of material in CERN’s accelerators & the 4 major LHC experiments. Technical Report [EDMS 1184236 v.5](#), CERN, 2021.
- [59] C. Theis and H. Vincke.
ActiWiz 3 – an overview of the concepts, architecture & new features. Technical Report [EDMS 1706010 v.1](#), CERN, 2016.
- [60] O. S. Brüning (ed.), P. Collier (ed.), P. Lebrun (ed.), S. Myers (ed.), R. Ostojic (ed.), J. Poole (ed.), and P. Proudlock (ed.).
LHC Design Report. Technical Report [CERN-2004-003-V-1](#), CERN, 2004.
- [61] E. Skordis.
Radiation impact of collimation beam losses in the LHC and HL-LHC. PhD thesis, Department of Physics, University of Liverpool, 2019.
- [62] D. D. Wagman J.D.Cox and V.A. Medvedev.
CODATA key values for thermodynamics.
Hemisphere Pub. Corp., New York, 1984.
- [63] R.A Oriani.
The diffusion and trapping of hydrogen in steel.
Acta metall., 18(1):147–157, 1970.
- [64] G. Neumann and C. Tuijn.
Self-Diffusion and Impurity Diffusion in Pure Metals: Handbook of Experimental Data.
Pergamon, 1st edition, 2008.

Appendices

A Diffusion in anisotropic media

Anisotropic media have different properties in different directions and, in particular, different diffusion coefficients. As a consequence, the diffusion coefficient, which was found to be a scalar quantity for isotropic media, must now be generalized to a tensor. It is a second-rank symmetric tensor [15] and therefore diagonal when expressed in the basis defined by its three *eigenvectors*, commonly known as the *principal axes*:

$$[\mathbf{D}]_{PA} = \begin{pmatrix} D_1 & 0 & 0 \\ 0 & D_2 & 0 \\ 0 & 0 & D_3 \end{pmatrix}, \quad (\text{A.1})$$

where D_1 , D_2 and D_3 are the *eigenvalues*, so-called *principal diffusion coefficients*. Consequently, Fick's laws can be used normally for anisotropic diffusion if accounting for the tensor nature of \mathbf{D} , which takes its simplest form in the principal axes basis.

In our particular case, making use of the numerical treatment described in section 3.1, the displacement vector defining the radioisotope's step in the principal axes basis will be given by:

$$[\vec{v}]_{PA} = (v_1, v_2, v_3), \quad (\text{A.2})$$

with v_i being scalar variables following $\mathcal{N}(0, 2D_i t)$ distributions. If we know the orientation of the principal axes of diffusion (note that they do not necessarily coincide with the lattice axes), we will be able to obtain the displacement vector in the standard basis $[\vec{v}]_S$, assuming that we prefer to use this one for our tracking purposes.

B Diffusion input file

The diffusion input file is a card-based text file specifying the information necessary to perform the diffusion calculations. It is not case-sensitive and the user can include comment lines using an "*" as first character. Let us divide the different cards in two categories:

- **Mandatory:** those cards providing indispensable data to execute the simulation. They are the following:

- SECTION unused_variable

Example: SECTION 1

Description: as mentioned before, we can perform multiple diffusion calculations while running a single FLUKA simulation. To do this, we must organise the diffusion cards corresponding to different diffusion calculations in different sections. Each of these sections must start with this card.

- RADIOISOTOPE = "chemical element symbol"-"mass number"

Example: RADIOISOTOPE = Mn-54

Description: used to specify the radioisotope whose out-diffusion needs to be assessed.

- HOST_MATERIAL = "FLUKA material name"

Example: HOST_MATERIAL = Iron

Description: it allows us to select the material in which diffusion will take place.

Note: every time a material name has to be provided to SOLIDUSS, we must use the material name used in the FLUKA input.

- DIFFUSION_TIME = Time_1 < Time_2 Time_3 ... >

Example: DIFFUSION_TIME = 600 1800 3600 7200

Description: using this card the user can request an arbitrary number of diffusion times and the program will provide the diffusion results for each of them.

Notes:

- * Time must be positive and provided in seconds.
- * There is no need to request a diffusion time equal to zero in order to obtain the initial distribution of radioisotopes, the program will provide it by default.

- GLOBAL_TEMPERATURE = Temperature

Example: GLOBAL_TEMPERATURE = 1173

Description: the user can select the temperature of the environment where diffusion need to be simulated.

Note: temperatures must be provided in kelvin.

- DIFFUSION_COEFFICIENT = A₁ Q₁ A₂ Q₂ T_i T_f

Example: DIFFUSION_COEFFICIENT = 1.49 233600 0 0 0 1043

DIFFUSION_COEFFICIENT = 0.16 261700 0 0 1043 1667

Description: card used to specify the diffusion coefficient to be used in the simulation. In particular, the user can provide up to two pairs of activation parameters (A₁, Q₁, A₂ and Q₂) for a given range of temperature [T_i, T_f].

Notes:

- * This type of card can be repeated as many times as needed in order to cover the range of temperatures of interest (see example above) when the diffusion coefficient behaviour is not constant over it (maybe due to structural phase transitions). Pay attention not to

provide more than one diffusion coefficient for the same temperature (*i.e.* avoid overlapping temperature ranges).

- * Frequency factors (A_1 and A_2) must be provided in [$cm^2 s^{-1}$], activation energies (Q_1 and Q_2) in [$J \cdot mol^{-1}$], and temperatures in kelvin.

- CONCENTRATION_GRID = MinX MinY MinZ MaxX MaxY MaxZ NrBinsX NrBinsY
NrBinsZ

Example:

```
CONCENTRATION_GRID = -16 -41.5 -17602.4 86 31.5 -17262.4 100 100 20
```

Description: we can define our area of interest specifying the structural characteristics of the radioisotope concentration grid that will be generated by the program using this card. MinX, MinY and MinZ are the minimum coordinates in the X, Y and Z axes respectively, while MaxX, MaxY and MaxZ are the maximum ones. The parameters NrBinsX, NrBinsY and NrBinsZ represent the number of bins into which the delimited volume will be divided in each direction.

Notes:

- * The diffusion simulation will only track those radioisotopes found inside this grid or with non-negligible chances of entering it. So please, make sure the defined grid contains your area of interest. Note also that if a radioisotope leaves the grid, its diffusion will be stopped but it will not be counted as out-diffused unless it is also leaving the host material.
- * This grid is a Cartesian rectangular cuboid. No rotations are supported so far.

- Optional: the user can choose whether to include these cards or not, but they will have an important impact in the simulation execution. Each of them is detailed next:

- FAST_TRACKING = "Yes/No"

Example: FAST_TRACKING = Yes

Description: if selected, we will make use of the optimization procedure explained in section 3.4 to reduce the computation time of the radioisotope tracking whenever possible.

Note: if this card is not present, fast tracking is disabled by default.

- SELECTIVE_TRACKING = "Yes/No"

Example: SELECTIVE_TRACKING = Yes

Description: if activated, the program will only track those radioisotopes with non-negligible probability of out-diffusing from the host material (whenever the necessary information is available).

Notes:

- * If this card is not present, selective tracking is disabled by default.
- * If selective tracking is activated, all concentration maps except the initial one would make no sense. Therefore, only the initial concentration would be exported as a result.

- TEMPERATURE_MAP_FILE = "path to file"

Example: TEMPERATURE_MAP_FILE = ../temperatures_1.dat

Description: we can provide a temperature map by means of an external file. This card enable this option and provide the file path.

- * Please avoid any blank spaces in the file name and path.
- * For any point outside the provided temperature grid, SOLIDUSS will consider the GLOBAL_TEMPERATURE as the material temperature.
- * This grid is also a Cartesian rectangular cuboid and no rotations are supported so far.
- * The temperature file format must stick to the following guidelines:

- Line 2 must contain general structural information about the provided temperature grid. The syntax should be: `# MinX MinY MinZ MaxX MaxY MaxZ NrBinsX NrBinsY NrBinsZ`. `MinX`, `MinY` and `MinZ` are the minimum coordinates in the X , Y and Z axes respectively, while `MaxX`, `MaxY` and `MaxZ` are the maximum ones. `NrBinsX`, `NrBinsY` and `NrBinsZ` are the number of bins into which the delimited volume will be divided in each direction.
- The temperature data should be provided from line 5 on with the following syntax: `bin_Xmin bin_Ymin bin_Zmin Temperature`. Where `bin_Xmin`, `bin_Ymin` and `bin_Zmin` are the lower coordinates of the bin in consideration.
- Every coordinate must be provided in *cm*, and every temperature in *K*.
- Lines 1, 3 and 4 are ignored by the program, but they must be present. It is a good practice to use them to provide helpful information for the reader.

Please take a look to the example provided below concerning the temperature map file syntax:

```
# Xmin[cm] Ymin[cm] Zmin[cm] Xmax[cm] Ymax[cm] Zmax[cm] X.NrBins Y.NrBis Z.NrBins
# -300.0 -300.0 -25000 300.0 300.0 25000.0 10 10 100
# Columns: bin_Xmin[cm] bin_Ymin[cm] bin_Zmin[cm] Temperature[K]
#
-300 -300 -25000 1073
-240 -300 -25000 1095
-180 -300 -25000 1110
...
-300 -240 -25000 1105
...
-300 -300 -24500 950
...
```

- `SELECT_TARGET_MATERIALS = "Material 1" "Material 2" ...`

Example: `SELECT_TARGET_MATERIALS = Air Water`

Description: if desired, the user can select the target materials. If this is the case, the program would only provide the results concerning radioisotopes out-diffused from the host material into the selected target materials (we can provide as many as necessary). In the example above, we would get from the simulation the amount of radioisotopes out-diffused from the host material into Air or Water, and nothing else.

Notes:

- * Not compatible with the `EXCLUDE_TARGET_MATERIALS` card, only one of them can be provided.
- * By default all materials except the host material are target materials unless we use `SELECT_TARGET_MATERIALS` or `EXCLUDE_TARGET_MATERIALS` cards.
- * The concentration maps of the radioisotopes in the host material are not altered by this card.

- `EXCLUDE_TARGET_MATERIALS = "Material 1" "Material 2" ...`

Example: `EXCLUDE_TARGET_MATERIALS = Water`

Description: in the opposite direction of that of the previous card, this one allows us to exclude an arbitrary number of materials from the list of target materials. In the example provided, the program results will tell us the amount of radioisotopes out-diffused from the host material into any material but Water.

Notes:

- * Not compatible with the `SELECT_TARGET_MATERIALS` card.

- * By default all materials except the host material are target materials unless we use `SELECT_TARGET_MATERIALS` or `EXCLUDE_TARGET_MATERIALS` cards.
 - * The concentration maps of the radioisotopes in the host material are not altered by this card.
- `REPLICAS = R`
Example: `REPLICAS = 3`
Description: every time a radionuclide of interest is identified, its statistical weight will be split in R replicas, that will be tracked independently. This feature may help the user to improve statistics.
Note: An integer must be provided as a number of REPLICAS.
- `ADMIT_OTHER_ISOTOPES = Zmin Amin Zmax Amax`
Example: `ADMIT_OTHER_ISOTOPES = 10 20 21 42`
Description: this card provides a range of atomic and mass numbers (Z and A, respectively). Every time an isotope whose Z and A fall within this range, it will be treated as if it was the isotope of interest. This may help the user to increase its statistics but must be used with extreme caution. In particular, one needs to make sure there is a reasonable similarity between the initial spatial distribution of the isotopes in the range and that one of the isotope of interest.
- `DESORPTION_ENTHALPY = Edes`
Example: `DESORPTION_ENTHALPY = 134500`
Description: the desorption enthalpy of the species of interest from the host material is provided with this command. The software will make use of it to compute desorption probabilities.
Notes:
 - * This card is mandatory in order to activate the desorption model.
 - * Desorption enthalpies must be provided in [J/mol].
- `DISTANCE_BETWEEN_ATOMIC_NEIGHBOURS = DNN`
Example: `DISTANCE_BETWEEN_ATOMIC_NEIGHBOURS = 2.86e-8`
Description: the distance between nearest atomic neighbours is provided to the software, which will use it when simulating desorption.
Notes:
 - * This card is mandatory in order to activate the desorption model.
 - * Distances must be provided in [cm].

Next you can find a full diffusion input file example consisting of 2 different sections:

```
SECTION 1
RADIOISOTOPE = Mn-54
HOST_MATERIAL = IRON
DIFFUSION_TIME = 600 1800 3600 7200
GLOBAL_TEMPERATURE = 1173
DIFFUSION_COEFFICIENT = 1.49 233600 0 0 0 1043
DIFFUSION_COEFFICIENT = 0.16 261700 0 0 1043 1667
DIFFUSION_COEFFICIENT = 0.35 219800 0 0 1667 100000
CONCENTRATION_GRID = -16 -41.5 -17602.4 86 31.5 -17262.4 100 100 20
FAST_TRACKING = Yes
SELECTIVE_TRACKING = Yes

* Section 2 will deal with Co-60 coming out from copper, but we only
* want to take into account the amount not out-diffused into water.
SECTION 2
RADIOISOTOPE = Co-60
HOST_MATERIAL = COPPER
DIFFUSION_TIME = 100 500 1000 2000 4000
GLOBAL_TEMPERATURE = 900
DIFFUSION_COEFFICIENT = 0.74 217200 736 312800 0 100000
CONCENTRATION_GRID = 2.84 -20.65 -17617.4 67.16 10.65 -17247.4 50 50 100
FAST_TRACKING = Yes
EXCLUDE_TARGET_MATERIALS = Water
TEMPERATURE_MAP_FILE = ../TempFile
```

C Diffusion outputs

For each diffusion simulation², SOLIDUSS will provide two types of outputs:

- Summary file: groups summarizing results about every diffusion time requested. The file name includes the section number³ as well as the “summary” label.

Example: `IR7_Step2_17001_Section3_Cu-64_from_COPPER_summary.dat`

Inside the output we can find a header providing general information about the simulation (number of primaries simulated, number of radioisotopes followed, host material, global temperature, *etc.*) as well as the following data for each diffusion time requested:

- Relative number of radioisotopes out-diffused from the host material into the target materials (remember that, unless the user requests otherwise, the target materials are all materials except the host).
- Total amount of the requested radioisotope in the concentration grid normalized per primary particle (which refers to the primary particles simulated in FLUKA). Please note that it will be slightly overestimated, for more information on this check section 3.1.1.
- Decay normalization factor, which is the fraction of radioisotopes that remains after the requested diffusion time since some may have decayed during the process.

Next you can find an example of a summary output:

-
- 2 Different sections in the input file are considered different simulations.
 - 3 The section numbering depends strictly on the diffusion input file order: the first section of the input will be Section 1, the second Section 2, and so on.

```

SUMMARY FILE
Number of primaries simulated: 1000000
Host material: COPPER
Diffusion coefficient parameters:
    A1 = 0.1; Q1 = 197150; A2 = 0.155; Q2 = 200689; Ti = 0; Tf = 100000
Fast tracking selected
Radioisotope: Cu-64
    Half life = 45720 s
    The radioisotope may have decayed during diffusion. The normalization factor
    to take this into account is shown below for each diffusion time. If this
    factor is not 1, we recommend to check the radionuclide inventory after the
    diffusion period since you may be interested in the radioisotope's daughters.
    They could be important and you may want to simulate their diffusion as well.
Global temperature (K): 1088
Temperature distribution file: ../TempFire1
Concentration grids structure:
    X-start: -189.1 X-end: -155.1 X-steps: 1
    Y-start: 3 Y-end: 11 Y-steps: 1
    Z-start: -15800 Z-end: -14800 Z-steps: 1
Total weight of nuclides followed: 3358

=====

Diffusion time: 0
Weight of lost nuclides / Weight of followed nuclides (%) = 0
Total weight in the concentration grid per primary particle: 0.03358
Decay normalization factor: 1

=====

Diffusion time: 600
Weight of lost nuclides / Weight of followed nuclides (%) = 0.119119
Total weight in the concentration grid per primary particle: 0.03354
Decay normalization factor: 0.990945

=====

Diffusion time: 1800
Weight of lost nuclides / Weight of followed nuclides (%) = 0.148898
Total weight in the concentration grid per primary particle: 0.03353
Decay normalization factor: 0.97308

=====
    
```

- Isotope concentration maps: one for each diffusion time requested by the user. The output file name includes the diffusion time and the section number.

Example: IR7_Step2_17001_Section6_Cu-64_from_IRON_1800s.dat

This output includes a header with general information that should not be forgotten, as well as the structural characteristics of the grid. The header is followed by the concentration map data, which is presented in lines with syntax:

"Bin number in X" "Bin number in Y" "Bin number in Z" "Data"

Where Data is given in radioisotope weight per primary particle. Please take a look to the following example of a concentration map output:

```

Number of primaries simulated: 1000000
Host material: COPPER
Diffusion coefficient parameters:
  A1 = 0.1; Q1 = 197150; A2 = 0.155; Q2 = 200689; Ti = 0; Tf = 100000
Fast tracking selected
Radioisotope: Cu-64
  Half life = 45720 s
  The radioisotope may have decayed during diffusion. The
  normalization factor to take this into account is shown below.
  If this factor is not 1, we recommend to check the radionuclide inventory after the
  diffusion period since you may be interested in the radioisotope's daughters.
  They could be important and you may want to simulate their diffusion as well.
Decay normalization factor: 0.97308
External temperature (K): 1088
Temperature map file: ../TempFire1
Total weight of nuclides followed: 980894
Diffusion time: 1800
=====
X-start: 1.7 X-end: 68.3 X-steps: 333
Y-start: -33 Y-end: 23 Y-steps: 280
Z-start: -14396.1 Z-end: -14068 Z-steps: 100
=====
X Y Z Data
0 0 0 0
0 0 1 0
0 0 2 0
...
142 266 14 0.002
142 266 15 0.004
...
    
```

D Experimental data: temperature profiles

In the following tables “Temperature ref.” represents the temperature measured using a thermocouple probe fixed at the same position throughout the experiment in order to monitor temperature fluctuations. “From left to right” is used to give some insight on the direction in which the furnace is scanned considering its position in the pictures. Strictly, it means that the furnace was scanned from the smallest to the largest position coordinates. The opposite applies for “from right to left”. When looking at the position coordinate one must keep in mind that the furnace extends from position = 0 cm to position = 18.5 cm.

Table D.1: Raw data of the temperature profile measurement performed from right to left outside the furnace. Maximum temperatures around or above 1000 °C.

Pos. [cm]	T [°C]	T ref. [°C]	Pos. [cm]	T [°C]	T ref. [°C]	Pos. [cm]	T [°C]	T ref. [°C]
0.1	467	1003	6.6	1029	1001	13.1	1064	1005
0.6	560	998	7.1	1035	999	13.6	1056	1004
1.1	706	997	7.6	1041	998	14.1	1043	1004
1.6	773	999	8.1	1049	1004	14.6	1018	1006
2.1	824	1000	8.6	1053	998	15.1	989	1005
2.6	891	1001	9.1	1058	998	15.6	941	1001
3.1	922	998	9.6	1064	1001	16.1	880	1003
3.6	966	997	10.1	1067	1001	16.6	806	1005
4.1	986	1000	10.6	1070	1002	17.1	714	1001
4.6	1005	1001	11.1	1071	1001	17.6	589	1000
5.1	1014	1001	11.6	1070	1002	18.1	439	999
5.6	1018	999	12.1	1070	1000	18.4	293	999
6.1	1022	1000	12.6	1069	1004			

Table D.2: Raw data of the temperature profile measurement performed from left to right. Maximum temperatures around or above 1000 °C.

Pos. [cm]	T [°C]	T ref. [°C]	Pos. [cm]	T [°C]	T ref. [°C]	Pos. [cm]	T [°C]	T ref. [°C]
0.2	315	1000	7.0	970	1001	14.0	970	1000
1.0	440	1001	8.0	984	1001	15.0	926	1001
2.0	665	1002	9.0	994	1001	16.0	853	1002
3.0	801	1002	10.0	1002	1004	17.0	738	1002
4.0	888	1001	11.0	1004	1004	18.0	529	1001
5.0	934	1001	12.0	998	1002	19.0	268	998
6.0	957	1001	13.0	991	1000			

Table D.3: Raw data of the temperature profile measurement performed inside the quart tube (Temperature in) while the temperature is monitored outside it at a given position (Temperature out).

Pos. [cm]	T [°C]	T ref. [°C]	Pos. [cm]	T [°C]	T ref. [°C]	Pos. [cm]	T [°C]	T ref. [°C]
0.0	150	601	7.0	578	604	14.0	562	603
1.0	262	603	8.0	587	604	15.0	534	603
2.0	382	603	9.0	594	604	16.0	491	603
3.0	450	603	10.0	597	604	17.0	419	602
4.0	514	603	11.0	597	604	18.0	282	602
5.0	548	603	12.0	593	604	19.0	171	602
6.0	566	603	13.0	586	604			

Table D.4: Raw data of the temperature profile measurement performed outside the quart tube (Temperature out) while the temperature is monitored inside it at a given position (Temperature in).

Pos. [cm]	T [°C]	T ref. [°C]	Pos. [cm]	T [°C]	T ref. [°C]	Pos. [cm]	T [°C]	T ref. [°C]
0.0	596	116	7.0	597	585	14.0	597	596
1.0	596	173	8.0	597	595	15.0	597	562
2.0	596	345	9.0	597	603	16.0	597	519
3.0	596	426	10.0	597	608	17.0	597	455
4.0	596	498	11.0	597	611	18.0	597	365
5.0	596	547	12.0	597	609	19.0	597	232
6.0	597	573	13.0	597	603			

E Diffusion input files of benchmarking simulations

Below you can find the diffusion input files used in the simulation of the experiments. For conciseness only the cases in which we use the mean values for the different parameters is shown.

```
SECTION 1
Radioisotope = Co-60
Host_Material = COPPER
Diffusion_Coefficient = 0.74 217200 736 312800 0 100000
Diffusion_Time = 3600 18000
Global_temperature = 1273.15
Temperature_map_file = ../temp.dat
Concentration_Grid = -10 -10 -10 10 10 30 1 1 1
Fast_Tracking = Yes
DESORPTION_ENTHALPY = 416100
DISTANCE_BETWEEN_ATOMIC_NEIGHBOURS = 2.56e-8
```

```
SECTION 1
Radioisotope = Na-22
Host_Material = ALUMINUM
Diffusion_Coefficient = 0.00067 97100 0 0 0 100000
Diffusion_Time = 3600 7200 10800
Global_temperature = 873.15
Temperature_map_file = ../temp.dat
Concentration_Grid = -10 -10 -10 10 10 30 1 1 1
Fast_Tracking = Yes
DESORPTION_ENTHALPY = 134500
DISTANCE_BETWEEN_ATOMIC_NEIGHBOURS = 2.86e-8
```

F Temperature profiles for benchmarking simulations

Table F.1: Temperature profiles used to simulate out-diffusion from the Cu sample. Temp stands for temperature, Pos for position, Low for lower limit and Up for upper limit.

Pos. [cm]	Temp. [K]			Pos. [cm]	Temp. [K]			Pos. [cm]	Temp. [K]		
	Mean	Low.	Up.		Mean	Low.	Up.		Mean	Low.	Up.
3.95	1184.19	1123.18	1219.09	7.75	1242.04	1211.95	1271.04	11.55	1249.70	1224.97	1276.38
4.05	1186.52	1130.54	1221.41	7.85	1243.31	1213.18	1271.90	11.65	1249.37	1224.24	1275.80
4.15	1188.85	1137.97	1223.77	7.95	1244.58	1214.40	1272.76	11.75	1249.47	1223.50	1275.23
4.25	1191.18	1145.57	1226.19	8.05	1245.44	1215.62	1273.61	11.85	1249.57	1222.47	1274.70
4.35	1193.49	1153.17	1228.62	8.15	1246.30	1216.85	1274.46	11.95	1249.66	1221.31	1274.18
4.45	1195.79	1160.77	1231.04	8.25	1247.17	1218.12	1275.33	12.05	1248.93	1220.15	1273.65
4.55	1198.09	1163.07	1232.35	8.35	1248.02	1219.38	1276.21	12.15	1248.19	1218.94	1273.61
4.65	1200.42	1165.38	1233.67	8.45	1248.86	1220.64	1277.08	12.25	1247.46	1217.60	1273.60
4.75	1202.82	1167.68	1234.98	8.55	1249.70	1221.50	1277.30	12.35	1246.43	1216.26	1273.60
4.85	1205.22	1169.97	1236.27	8.65	1250.55	1222.35	1277.53	12.45	1245.27	1214.91	1273.59
4.95	1207.62	1172.24	1237.55	8.75	1251.41	1223.21	1277.75	12.55	1244.11	1211.25	1272.84
5.05	1208.91	1174.53	1238.82	8.85	1252.28	1224.05	1277.97	12.65	1242.89	1207.58	1272.10
5.15	1210.19	1176.84	1240.10	8.95	1253.14	1224.88	1278.19	12.75	1241.54	1203.92	1271.35
5.25	1211.48	1179.23	1241.42	9.05	1253.36	1225.72	1278.40	12.85	1240.19	1200.13	1270.31
5.35	1212.75	1181.62	1242.73	9.15	1253.58	1226.57	1278.61	12.95	1238.84	1196.30	1269.14
5.45	1214.00	1184.00	1244.05	9.25	1253.79	1227.43	1278.83	13.05	1235.16	1192.48	1267.95
5.55	1215.26	1185.28	1245.23	9.35	1254.00	1228.30	1279.05	13.15	1231.48	1188.35	1266.71
5.65	1216.52	1186.55	1246.41	9.45	1254.21	1229.16	1279.27	13.25	1227.81	1183.48	1265.33
5.75	1217.83	1187.83	1247.60	9.55	1254.42	1229.37	1279.27	13.35	1224.01	1178.62	1263.95
5.85	1219.13	1189.08	1248.76	9.65	1254.63	1229.59	1279.27	13.45	1220.17	1173.76	1262.57
5.95	1220.43	1190.32	1249.91	9.75	1254.85	1229.80	1279.27	13.55	1216.32	1170.04	1258.86
6.05	1221.60	1191.56	1251.06	9.85	1255.06	1230.01	1279.28	13.65	1212.16	1166.32	1255.16
6.15	1222.77	1192.82	1252.21	9.95	1255.28	1230.14	1279.28	13.75	1207.27	1162.60	1251.44
6.25	1223.94	1194.11	1253.39	10.05	1255.05	1229.91	1279.28	13.85	1202.38	1158.39	1247.61
6.35	1225.09	1195.41	1254.57	10.15	1254.82	1229.68	1279.28	13.95	1197.49	1153.95	1243.73
6.45	1226.22	1196.70	1255.75	10.25	1254.59	1229.45	1279.28	14.05	1193.74	1149.51	1239.85
6.55	1227.36	1197.86	1257.03	10.35	1254.36	1229.23	1279.28	14.15	1189.99	1144.99	1235.66
6.65	1228.51	1199.02	1258.31	10.45	1254.13	1229.00	1279.27	14.25	1186.24	1140.25	1230.74
6.75	1229.68	1200.17	1259.59	10.55	1253.91	1228.43	1279.04	14.35	1181.99	1135.52	1225.81
6.85	1230.85	1201.31	1260.84	10.65	1253.68	1227.85	1278.81	14.45	1177.52	1130.79	1220.88
6.95	1232.02	1202.44	1262.08	10.75	1253.45	1227.28	1278.58	14.55	1173.05	1122.97	1217.10
7.05	1233.29	1203.56	1263.32	10.85	1253.22	1226.75	1278.35	14.65	1168.49	1115.14	1213.31
7.15	1234.56	1204.70	1264.58	10.95	1252.99	1226.23	1278.12	14.75	1163.72	1107.32	1209.52
7.25	1235.83	1205.86	1265.86	11.05	1252.42	1225.72	1277.89	14.85	1158.96	1098.52	1205.23
7.35	1237.07	1207.02	1267.14	11.15	1251.85	1225.39	1277.66	14.95	1154.19	1089.30	1200.72
7.45	1238.30	1208.18	1268.42	11.25	1251.27	1225.39	1277.42	15.05	1146.33	1080.10	1196.19
7.55	1239.52	1209.43	1269.29	11.35	1250.74	1225.40	1277.19				
7.65	1240.77	1210.69	1270.17	11.45	1250.22	1225.40	1276.95				

Table F.2: Temperature profiles used to simulate out-diffusion from the Al sample. Temp stands for temperature, Pos for position, Low for lower limit and Up for upper limit.

Pos. [cm]	Temp. [K]			Pos. [cm]	Temp. [K]			Pos. [cm]	Temp. [K]		
	Mean	Low.	Up.		Mean	Low.	Up.		Mean	Low.	Up.
4.85	807.716	777.004	832.198	8.65	854.029	833.866	873.454	12.45	853.31	830.894	874.32
4.95	811.15	780.328	833.972	8.75	854.736	834.566	873.764	12.55	852.26	829.099	873.55
5.05	812.968	783.656	835.742	8.85	855.443	835.252	874.067	12.65	851.17	827.305	872.78
5.15	814.786	787.015	837.528	8.95	856.15	835.932	874.368	12.75	849.98	825.512	872.01
5.25	816.605	790.444	839.351	9.05	856.453	836.615	874.666	12.85	848.79	823.616	871.03
5.35	818.385	793.873	841.174	9.15	856.756	837.303	874.967	12.95	847.61	821.677	869.97
5.45	820.15	797.303	842.997	9.25	857.059	838.006	875.274	13.05	845.80	819.743	868.91
5.55	821.915	799.116	844.114	9.35	857.356	838.71	875.58	13.15	844.00	817.595	867.80
5.65	823.695	800.693	845.466	9.45	857.65	839.413	875.886	13.25	842.20	814.945	866.59
5.75	825.514	801.721	847.367	9.55	857.944	839.713	875.89	13.35	840.29	812.296	865.39
5.85	827.332	802.712	849.245	9.65	858.241	840.013	875.893	13.45	838.34	809.648	864.18
5.95	829.15	803.686	851.114	9.75	858.544	840.313	875.896	13.55	836.39	806.797	862.36
6.05	830.261	805.442	852.201	9.85	858.847	840.606	875.9	13.65	834.22	803.948	860.54
6.15	831.372	807.214	853.298	9.95	859.15	840.897	875.903	13.75	831.56	801.103	858.71
6.25	832.484	809.023	854.418	10.05	859.15	841.19	875.904	13.85	828.89	797.91	856.78
6.35	833.572	810.832	855.539	10.15	859.15	841.485	875.905	13.95	826.23	794.568	854.81
6.45	834.65	812.64	856.659	10.25	859.15	841.787	875.907	14.05	823.36	791.23	852.83
6.55	835.728	813.742	857.578	10.35	859.15	842.089	875.908	14.15	820.49	787.827	850.64
6.65	836.816	814.843	858.498	10.45	859.15	842.391	875.909	14.25	817.62	784.275	847.95
6.75	837.928	815.943	859.418	10.55	859.15	842.069	875.91	14.35	814.40	780.726	845.25
6.85	839.039	817.019	860.32	10.65	859.15	841.746	875.911	14.45	811.04	777.178	842.56
6.95	840.15	818.086	861.214	10.75	859.15	841.424	875.912	14.55	807.67	772.562	839.66
7.05	841.059	819.155	862.105	10.85	859.15	841.128	875.91	14.65	804.24	767.946	836.76
7.15	841.968	820.235	863.004	10.95	859.15	840.844	875.91	14.75	800.67	763.332	833.86
7.25	842.877	821.337	863.922	11.05	858.83	840.562	875.91	14.85	797.09	758.008	830.61
7.35	843.768	822.44	864.839	11.15	858.51	840.41	875.91	14.95	793.51	752.381	827.21
7.45	844.65	823.544	865.756	11.25	858.19	840.412	875.91	15.05	788.86	746.764	823.81
7.55	845.532	824.445	866.471	11.35	857.89	840.415	875.90	15.15	784.22	740.467	820.34
7.65	846.423	825.348	867.184	11.45	857.61	840.417	875.90	15.25	779.57	732.582	816.72
7.75	847.332	826.253	867.895	11.55	857.32	840.096	875.58	15.35	774.22	724.702	813.09
7.85	848.241	827.139	868.592	11.65	857.17	839.336	875.26	15.45	768.56	716.823	809.46
7.95	849.15	828.017	869.283	11.75	857.32	838.573	874.94	15.55	762.90	707.663	804.77
8.05	849.857	828.891	869.978	11.85	857.46	837.609	874.64	15.65	756.56	698.507	800.07
8.15	850.564	829.772	870.68	11.95	857.61	836.558	874.36	15.75	748.63	689.362	795.36
8.25	851.271	830.672	871.395	12.05	856.85	835.515	874.35	15.85	740.71	679.806	789.94
8.35	851.964	831.572	872.112	12.15	856.08	834.431	874.34	15.95	732.78	670.073	784.22
8.45	852.65	832.471	872.829	12.25	855.32	833.251	874.34	16.05	723.57	660.351	778.49
8.55	853.336	833.168	873.142	12.35	854.36	832.072	874.33				

G Out-diffused radionuclide inventories for IR7 objects

In this appendix we show the results obtained after combining the radionuclide inventories produced in the non-combustible materials of IR7 under consideration in chapter 9 with the out-diffusion fraction obtained for each object and chemical element. Therefore, in the following table we detail the global effective inhalation dose due to out-diffusion for each object and radionuclide for different temperatures.

Table G.1: Out-diffused radionuclide inventories for each component and the contribution of each radionuclide to the total effective E_{50} inhalation dose due to out-diffusion.

Isotope	Effective E_{50} inhalation dose contribution due to out-diffusion [$\mu\text{Sv cm}^{-3}$]											
	Cable conductor			Magnet coil conductor			Magnet Yoke			Collimator vessel		
	800 °C	900 °C	1000 °C	800 °C	900 °C	1000 °C	800 °C	900 °C	1000 °C	800 °C	900 °C	1000 °C
^3H	$2.68 \cdot 10^{-2}$	$2.68 \cdot 10^{-2}$	$2.68 \cdot 10^{-2}$	1.14	1.14	1.14	$2.19 \cdot 10^{-1}$	$2.27 \cdot 10^{-1}$	$2.34 \cdot 10^{-1}$	2.19	2.20	2.21
^7Be	-	-	-	-	-	-	$1.25 \cdot 10^{-8}$	$4.52 \cdot 10^{-7}$	$1.71 \cdot 10^{-7}$	$3.41 \cdot 10^{-7}$	$1.23 \cdot 10^{-5}$	$4.66 \cdot 10^{-6}$
^{22}Na	-	-	-	$1.34 \cdot 10^{-4}$	$3.31 \cdot 10^{-4}$	$7.15 \cdot 10^{-4}$	$8.11 \cdot 10^{-6}$	$2.47 \cdot 10^{-5}$	$2.54 \cdot 10^{-5}$	$3.30 \cdot 10^{-4}$	$1.01 \cdot 10^{-3}$	$1.03 \cdot 10^{-3}$
^{24}Na	-	-	-	-	-	-	$2.83 \cdot 10^{-6}$	$8.63 \cdot 10^{-6}$	$8.87 \cdot 10^{-6}$	$9.13 \cdot 10^{-5}$	$2.78 \cdot 10^{-4}$	$2.86 \cdot 10^{-4}$
^{28}Mg	-	-	-	-	-	-	-	-	-	$3.67 \cdot 10^{-5}$	$1.12 \cdot 10^{-4}$	$1.15 \cdot 10^{-4}$
^{32}Si	-	-	-	-	-	$3.59 \cdot 10^{-14}$	-	-	$3.88 \cdot 10^{-17}$	-	-	$1.01 \cdot 10^{-15}$
^{32}P	$3.76 \cdot 10^{-4}$	$7.19 \cdot 10^{-4}$	$1.24 \cdot 10^{-3}$	$6.76 \cdot 10^{-3}$	$1.29 \cdot 10^{-2}$	$2.24 \cdot 10^{-2}$	$1.37 \cdot 10^{-4}$	$5.00 \cdot 10^{-4}$	$8.63 \cdot 10^{-4}$	$3.36 \cdot 10^{-3}$	$1.23 \cdot 10^{-2}$	$2.12 \cdot 10^{-2}$
^{33}P	$1.13 \cdot 10^{-4}$	$2.16 \cdot 10^{-4}$	$3.74 \cdot 10^{-4}$	$2.01 \cdot 10^{-3}$	$3.86 \cdot 10^{-3}$	$6.68 \cdot 10^{-3}$	$3.37 \cdot 10^{-5}$	$1.23 \cdot 10^{-4}$	$2.12 \cdot 10^{-4}$	$8.31 \cdot 10^{-4}$	$3.03 \cdot 10^{-3}$	$5.23 \cdot 10^{-3}$
^{35}S	$2.48 \cdot 10^{-4}$	$6.65 \cdot 10^{-4}$	$1.52 \cdot 10^{-3}$	$4.26 \cdot 10^{-3}$	$1.14 \cdot 10^{-2}$	$2.62 \cdot 10^{-2}$	$1.43 \cdot 10^{-4}$	$4.33 \cdot 10^{-4}$	$3.84 \cdot 10^{-4}$	$3.37 \cdot 10^{-3}$	$1.02 \cdot 10^{-2}$	$9.02 \cdot 10^{-3}$
^{38}Cl	-	-	-	-	-	-	-	-	-	$6.42 \cdot 10^{-6}$	$1.96 \cdot 10^{-5}$	$2.01 \cdot 10^{-5}$
^{42}K	-	-	-	$7.64 \cdot 10^{-5}$	$1.91 \cdot 10^{-4}$	$4.12 \cdot 10^{-4}$	$3.83 \cdot 10^{-6}$	$1.17 \cdot 10^{-5}$	$1.20 \cdot 10^{-5}$	$7.93 \cdot 10^{-5}$	$2.41 \cdot 10^{-4}$	$2.48 \cdot 10^{-4}$
^{43}K	-	-	-	-	-	-	-	-	-	$3.55 \cdot 10^{-5}$	$1.08 \cdot 10^{-4}$	$1.11 \cdot 10^{-4}$
^{45}Ca	$9.52 \cdot 10^{-6}$	$2.34 \cdot 10^{-4}$	$2.80 \cdot 10^{-3}$	$1.43 \cdot 10^{-4}$	$3.52 \cdot 10^{-3}$	$4.21 \cdot 10^{-2}$	$9.02 \cdot 10^{-4}$	$2.75 \cdot 10^{-3}$	$2.82 \cdot 10^{-3}$	$1.76 \cdot 10^{-2}$	$5.36 \cdot 10^{-2}$	$5.51 \cdot 10^{-2}$
^{43}Sc	-	-	-	-	-	-	$1.63 \cdot 10^{-12}$	$1.63 \cdot 10^{-10}$	$1.70 \cdot 10^{-10}$	$3.19 \cdot 10^{-11}$	$3.19 \cdot 10^{-9}$	$3.33 \cdot 10^{-9}$
^{44}Sc	-	$1.03 \cdot 10^{-14}$	$9.59 \cdot 10^{-13}$	-	$1.54 \cdot 10^{-13}$	$1.44 \cdot 10^{-11}$	$7.88 \cdot 10^{-11}$	$7.88 \cdot 10^{-9}$	$8.23 \cdot 10^{-9}$	$1.48 \cdot 10^{-9}$	$1.48 \cdot 10^{-7}$	$1.54 \cdot 10^{-7}$
^{46}Sc	-	$4.10 \cdot 10^{-14}$	$3.83 \cdot 10^{-12}$	-	$6.10 \cdot 10^{-13}$	$5.70 \cdot 10^{-11}$	$2.73 \cdot 10^{-10}$	$2.73 \cdot 10^{-8}$	$2.85 \cdot 10^{-8}$	$4.90 \cdot 10^{-9}$	$4.90 \cdot 10^{-7}$	$5.12 \cdot 10^{-7}$
^{47}Sc	-	$2.35 \cdot 10^{-15}$	$2.20 \cdot 10^{-13}$	-	$3.48 \cdot 10^{-14}$	$3.25 \cdot 10^{-12}$	$1.25 \cdot 10^{-11}$	$1.25 \cdot 10^{-9}$	$1.30 \cdot 10^{-9}$	$2.35 \cdot 10^{-10}$	$2.35 \cdot 10^{-8}$	$2.46 \cdot 10^{-8}$

Continuation of Tab. G.1.

Isotope	Effective E ₅₀ inhalation dose contribution due to out-diffusion [$\mu\text{Sv cm}^{-3}$]											
	Cable conductor			Magnet coil conductor			Magnet Yoke			Collimator vessel		
	800 °C	900 °C	1000 °C	800 °C	900 °C	1000 °C	800 °C	900 °C	1000 °C	800 °C	900 °C	1000 °C
⁴⁸ Sc	-	1.02·10 ⁻¹⁵	9.54·10 ⁻¹⁴	-	1.52·10 ⁻¹⁴	1.42·10 ⁻¹²	4.88·10 ⁻¹²	4.88·10 ⁻¹⁰	5.10·10 ⁻¹⁰	9.31·10 ⁻¹¹	9.32·10 ⁻⁹	9.73·10 ⁻⁹
⁴⁴ Ti	-	-	1.18·10 ⁻¹³	-	-	1.78·10 ⁻¹²	2.08·10 ⁻¹⁷	5.41·10 ⁻¹⁵	5.87·10 ⁻¹³	3.94·10 ⁻¹⁶	1.03·10 ⁻¹³	1.12·10 ⁻¹¹
⁴⁵ Ti	-	-	-	-	-	1.20·10 ⁻¹³	1.43·10 ⁻¹⁸	3.72·10 ⁻¹⁶	4.04·10 ⁻¹⁴	2.56·10 ⁻¹⁷	6.68·10 ⁻¹⁵	7.25·10 ⁻¹³
⁴⁷ V	-	-	-	-	-	-	4.45·10 ⁻¹⁷	1.05·10 ⁻¹⁴	5.40·10 ⁻¹⁵	7.26·10 ⁻¹⁶	1.70·10 ⁻¹³	8.80·10 ⁻¹⁴
⁴⁸ V	2.56·10 ⁻¹⁴	3.81·10 ⁻¹²	2.62·10 ⁻¹⁰	3.69·10 ⁻¹³	5.48·10 ⁻¹¹	3.78·10 ⁻⁹	3.77·10 ⁻¹⁴	8.86·10 ⁻¹²	4.58·10 ⁻¹²	5.71·10 ⁻¹³	1.34·10 ⁻¹⁰	6.93·10 ⁻¹¹
⁴⁹ V	5.64·10 ⁻¹⁶	8.37·10 ⁻¹⁴	5.77·10 ⁻¹²	8.17·10 ⁻¹⁵	1.21·10 ⁻¹²	8.36·10 ⁻¹¹	9.12·10 ⁻¹⁶	2.14·10 ⁻¹³	1.11·10 ⁻¹³	1.36·10 ⁻¹⁴	3.20·10 ⁻¹²	1.65·10 ⁻¹²
⁴⁸ Cr	-	-	-	-	-	-	7.20·10 ⁻⁹	3.48·10 ⁻⁷	1.55·10 ⁻⁷	1.16·10 ⁻⁷	5.62·10 ⁻⁶	2.50·10 ⁻⁶
⁴⁹ Cr	-	-	-	-	-	-	8.87·10 ⁻⁹	4.28·10 ⁻⁷	1.91·10 ⁻⁷	1.34·10 ⁻⁷	6.49·10 ⁻⁶	2.89·10 ⁻⁶
⁵¹ Cr	1.83·10 ⁻⁹	6.60·10 ⁻⁸	1.36·10 ⁻⁶	2.66·10 ⁻⁸	9.62·10 ⁻⁷	1.98·10 ⁻⁵	1.29·10 ⁻⁷	6.21·10 ⁻⁶	2.77·10 ⁻⁶	2.24·10 ⁻⁶	1.08·10 ⁻⁴	4.81·10 ⁻⁵
⁵¹ Mn	-	-	-	-	-	-	3.64·10 ⁻⁶	1.04·10 ⁻⁵	2.36·10 ⁻⁶	3.60·10 ⁻⁵	1.03·10 ⁻⁴	2.33·10 ⁻⁵
⁵² Mn	2.80·10 ⁻⁴	9.90·10 ⁻⁴	2.21·10 ⁻³	4.00·10 ⁻³	1.41·10 ⁻²	3.16·10 ⁻²	5.16·10 ⁻⁴	1.48·10 ⁻³	3.34·10 ⁻⁴	4.12·10 ⁻³	1.18·10 ⁻²	2.67·10 ⁻³
⁵⁴ Mn	1.47·10 ⁻³	5.20·10 ⁻³	1.16·10 ⁻²	2.32·10 ⁻²	8.18·10 ⁻²	1.83·10 ⁻¹	4.33·10 ⁻³	1.24·10 ⁻²	2.80·10 ⁻³	2.31·10 ⁻²	6.59·10 ⁻²	1.49·10 ⁻²
⁵⁶ Mn	2.48·10 ⁻⁵	8.77·10 ⁻⁵	1.96·10 ⁻⁴	4.33·10 ⁻⁴	1.53·10 ⁻³	3.41·10 ⁻³	1.18·10 ⁻⁴	3.37·10 ⁻⁴	7.62·10 ⁻⁵	6.55·10 ⁻⁴	1.87·10 ⁻³	4.24·10 ⁻⁴
⁵² Fe	-	-	-	-	-	-	4.54·10 ⁻⁷	1.22·10 ⁻⁵	7.44·10 ⁻⁷	4.32·10 ⁻⁶	1.16·10 ⁻⁴	7.08·10 ⁻⁶
⁵⁵ Fe	1.54·10 ⁻¹¹	1.15·10 ⁻⁹	4.34·10 ⁻⁸	2.41·10 ⁻¹⁰	1.80·10 ⁻⁸	6.80·10 ⁻⁷	7.30·10 ⁻⁵	1.96·10 ⁻³	1.20·10 ⁻⁴	4.45·10 ⁻⁴	1.20·10 ⁻²	7.29·10 ⁻⁴
⁵⁹ Fe	1.79·10 ⁻¹¹	1.33·10 ⁻⁹	5.04·10 ⁻⁸	3.46·10 ⁻¹⁰	2.57·10 ⁻⁸	9.74·10 ⁻⁷	5.06·10 ⁻⁶	1.36·10 ⁻⁴	8.29·10 ⁻⁶	7.60·10 ⁻⁶	2.05·10 ⁻⁴	1.25·10 ⁻⁵
⁵⁵ Co	9.31·10 ⁻¹¹	5.14·10 ⁻⁹	1.56·10 ⁻⁷	1.34·10 ⁻⁹	7.38·10 ⁻⁸	2.24·10 ⁻⁶	5.29·10 ⁻¹²	3.67·10 ⁻¹⁰	1.30·10 ⁻¹⁰	1.90·10 ⁻¹⁰	1.32·10 ⁻⁸	4.67·10 ⁻⁹
⁵⁶ Co	1.17·10 ⁻⁸	6.45·10 ⁻⁷	1.95·10 ⁻⁵	1.80·10 ⁻⁷	9.91·10 ⁻⁶	3.00·10 ⁻⁴	2.36·10 ⁻¹⁰	1.64·10 ⁻⁸	5.81·10 ⁻⁹	1.25·10 ⁻⁸	8.66·10 ⁻⁷	3.06·10 ⁻⁷
⁵⁷ Co	5.78·10 ⁻⁹	3.19·10 ⁻⁷	9.66·10 ⁻⁶	9.72·10 ⁻⁸	5.36·10 ⁻⁶	1.62·10 ⁻⁴	1.26·10 ⁻¹²	8.78·10 ⁻¹¹	3.10·10 ⁻¹¹	5.44·10 ⁻⁹	3.78·10 ⁻⁷	1.34·10 ⁻⁷
⁵⁸ Co	1.62·10 ⁻⁸	8.92·10 ⁻⁷	2.70·10 ⁻⁵	3.00·10 ⁻⁷	1.65·10 ⁻⁵	5.01·10 ⁻⁴	1.38·10 ⁻¹²	9.59·10 ⁻¹¹	3.39·10 ⁻¹¹	8.87·10 ⁻⁹	6.16·10 ⁻⁷	2.18·10 ⁻⁷
⁶⁰ Co	3.74·10 ⁻⁸	2.06·10 ⁻⁶	6.25·10 ⁻⁵	7.99·10 ⁻⁷	4.41·10 ⁻⁵	1.34·10 ⁻³	1.17·10 ⁻¹⁰	8.15·10 ⁻⁹	2.88·10 ⁻⁹	4.82·10 ⁻⁹	3.35·10 ⁻⁷	1.18·10 ⁻⁷
⁶¹ Co	5.21·10 ⁻¹¹	2.87·10 ⁻⁹	8.71·10 ⁻⁸	1.06·10 ⁻⁹	5.84·10 ⁻⁸	1.77·10 ⁻⁶	-	-	-	-	-	-
⁵⁶ Ni	1.04·10 ⁻¹¹	6.42·10 ⁻¹⁰	2.18·10 ⁻⁸	1.37·10 ⁻¹⁰	8.45·10 ⁻⁹	2.86·10 ⁻⁷	-	-	-	4.16·10 ⁻⁹	2.06·10 ⁻⁷	4.22·10 ⁻⁸
⁵⁷ Ni	4.18·10 ⁻¹¹	2.58·10 ⁻⁹	8.74·10 ⁻⁸	5.92·10 ⁻¹⁰	3.66·10 ⁻⁸	1.24·10 ⁻⁶	-	-	-	2.29·10 ⁻⁸	1.13·10 ⁻⁶	2.32·10 ⁻⁷

Continuation of Tab. G.1.

Isotope	Effective E ₅₀ inhalation dose contribution due to out-diffusion [$\mu\text{Sv cm}^{-3}$]											
	Cable conductor			Magnet coil conductor			Magnet Yoke			Collimator vessel		
	800 °C	900 °C	1000 °C	800 °C	900 °C	1000 °C	800 °C	900 °C	1000 °C	800 °C	900 °C	1000 °C
⁶³ Ni	1.60·10 ⁻¹⁰	9.87·10 ⁻⁹	3.35·10 ⁻⁷	4.20·10 ⁻⁹	2.59·10 ⁻⁷	8.79·10 ⁻⁶	-	-	-	4.91·10 ⁻¹⁰	2.43·10 ⁻⁸	4.98·10 ⁻⁹
⁶⁵ Ni	2.34·10 ⁻¹¹	1.45·10 ⁻⁹	4.90·10 ⁻⁸	5.64·10 ⁻¹⁰	3.48·10 ⁻⁸	1.18·10 ⁻⁶	-	-	-	-	-	-
⁶⁰ Cu	-	-	-	3.93·10 ⁻⁷	1.09·10 ⁻⁵	1.57·10 ⁻⁴	-	-	-	-	-	-
⁶¹ Cu	9.89·10 ⁻⁷	2.74·10 ⁻⁵	3.96·10 ⁻⁴	1.88·10 ⁻⁵	5.20·10 ⁻⁴	7.53·10 ⁻³	-	-	-	-	-	-
⁶⁴ Cu	2.23·10 ⁻⁴	6.16·10 ⁻³	8.92·10 ⁻²	9.89·10 ⁻⁴	2.74·10 ⁻²	3.96·10 ⁻¹	6.04·10 ⁻⁷	3.89·10 ⁻⁶	4.68·10 ⁻⁷	-	-	-
⁶² Zn	7.28·10 ⁻⁵	1.80·10 ⁻⁴	3.87·10 ⁻⁴	6.99·10 ⁻⁴	1.73·10 ⁻³	3.72·10 ⁻³	-	-	-	-	-	-
⁶⁵ Zn	1.59·10 ⁻⁴	3.93·10 ⁻⁴	8.45·10 ⁻⁴	1.60·10 ⁻³	3.97·10 ⁻³	8.53·10 ⁻³	-	-	-	-	-	-

List of Figures

1.1	The chart of nuclides.	3
1.2	Calculation of π using Monte Carlo methods.	4
1.3	Statistical uncertainty evolution of the π estimation.	5
1.4	Layout of CERN's accelerators and experiments.	6
1.5	Radiation signage at CERN.	8
1.6	LHC tunnel at CERN.	8
2.1	Different diffusion mechanisms in solids.	13
2.2	Diffusion coefficients as a function of the inverse of temperature.	18
3.1	Schematic example of a sampled radionuclide's path.	24
3.2	Schematic example of the path of a radionuclide in presence of a boundary.	25
3.3	Flow chart of SOLIDUSS tracking a radionuclide.	29
3.4	Concentration of radioisotopes after diffusion and distance to their initial position.	33
3.5	Radionuclide concentration along a Cu cylinder irradiated with a 10 GeV protons.	35
3.6	Diffusion of ^{54}Mn in an LHC quadrupole yoke at extremely high temperatures	36
3.7	Variation of the ^{54}Mn concentration in an LHC quadrupole yoke	37
4.1	ODF as a function of the time interval between consecutive checks using RWs.	40
4.2	ODF as a function of the time interval between consecutive checks using SOLIDUSS.	41
4.3	SOLIDUSS ODFs as a function of the time steps for different radionuclides.	43
4.4	SOLIDUSS ODFs as a function of the time steps for different geometries.	44
4.5	SOLIDUSS ODFs as a function of the time steps for different concentrations.	45
4.6	SOLIDUSS ODFs as a function of the time steps for different temperatures.	46
4.7	Cross section, temp. map and radionuclide concentration for a LHC quadrupole	49
5.1	Boiling temperature for a number of chemical elements.	53
5.2	Example of a path followed by a random walker in 2-D encountering a boundary.	55
5.3	Schematic of how SOLIDUSS would deal with the diffusing particle of Fig. 5.2.	56
5.4	Distance from the nuclide position to its intersection point with the boundary.	57
5.5	Probability distribution of the time at which RWs will hit a boundary	58
5.6	Average number of boundary encounters suffered by a Brownian particle.	60
5.7	Average number of surface encounters suffered by a random walker.	63
5.8	Same as Fig. 5.7 for different boundaries and diffusing random walkers.	64
5.9	Example of the PDFs of the surface encounters suffered by a random walker.	65
6.1	Pictures of the setup used in the gamma-ray spectrometry laboratory.	67
6.2	Overview of the gas circuit used in the experiments.	68
6.3	Detail of the connection between the quartz tube and the gas hose.	69
6.4	Detail of the inline HEPA filter and its connections.	70
6.5	Detail of the bubbler used to monitor the gas flux.	70
6.6	Furnace used in the experiments.	71

6.7	Activated Cu samples used in the experiments.	73
6.8	Activated Al samples used in the experiments.	74
6.9	Temperature prof. measured scanning the furnace in opposite directions.	76
6.10	Temperature profiles measured outside and inside the quartz tube.	77
6.11	Furnace's temperature profiles for two different maximum temperatures.	78
6.12	Different geometric shapes tested for the samples.	80
6.13	Cu foil at 800 °C in an air atmosphere.	85
6.14	Cu filaments at 800 °C and 1000 °C in an air atmosphere.	86
7.1	Radionuclide concentration profiles for ⁴⁸ V and best fits.	90
7.2	Diffusion coef. extracted from SOLIDUSS results for different temp. and species.	91
7.3	A and Q for different radionuclides derived from SOLIDUSS simulations.	92
7.4	Pictures of the FLUKA models of the Cu and Al samples	94
7.5	Temp. profiles at which the samples were exposed during the experiments.	95
7.6	Comparison between experimental and simulations results.	99
7.7	Simulated and experimental results for the ODF in each iteration.	99
8.1	ODF as a function of the surface over volume ratio of the object.	103
8.2	Ratio between the ODF obtained using SOLIDUSS and eq. (8.1).	104
8.3	Evolution of the ODF as a function of several parameters.	110
9.1	Generic irradiation scenarios in the LHC.	113
9.2	Particle fluences for different generic scenarios.	114

List of Tables

1.1	MC estimation of π for different number of sampled points.	5
2.1	Experimental values of diffusion activation parameters for Cu in Al.	17
2.2	Experimental values of diffusion activation parameters for several elements in Fe.	17
4.1	Critical values of the Student's t-distribution.	48
4.2	ODFs for some residual nuclei generated in a quadrupole yoke and coils.	50
6.1	Results of the first gamma-ray spectrometry measurement of the Cu sample.	72
6.2	Results of the 1st gamma-ray spectrometry measurement of the Al sample.	73
6.3	Results of the gamma-ray spectrometry measurements of the radioactive Cu.	81
6.4	Experimental ODFs fractions for the Cu sample.	81
6.5	Results of the gamma-ray spectrometry measurements of the radioactive Al.	83
6.6	Experimental ODFs fractions for the Al sample.	83
6.7	Results of the gamma-ray spectrometry of the Cu bars and the HEPA filter.	83
7.1	Parameters provided to SOLIDUSS to simulate the out-diffusion of radionuclides.	95
7.2	ODF simulation results for both samples.	97
7.3	Summary of the simulation results for the ODF obtained using the desorption model.	97
7.4	Reminder of ODF results obtained in the experiments.	98
8.1	ODF for simplified scenarios: analytical expression <i>vs.</i> SOLIDUSS.	107
8.2	Q and E_{des} used to create Fig. 8.3.	108
9.1	Assumed chemical composition for different IR7 objects.	115
9.2	Radionuclide inventories for IR7 objects.	115
9.3	Diffusion and desorption parameters for isotopes in a Cu object.	119
9.4	Diffusion and desorption parameters for isotopes in a Fe object.	120
9.5	FRS, GDP and ODF for elements in side-cable conductors.	121
9.6	FRS, GDP and ODF for elements in magnet coils conductors.	122
9.7	FRS, GDP and ODF for elements in a magnet yoke.	123
9.8	FRS, GDP and ODF for elements in a collimator vessel.	123
9.9	Contribution of the ODF to the radiological hazard.	124
9.10	Contribution of the ODF to the radiological hazard. Total desorption.	125
D.1	Raw data of the temp. profile measured from right to left.	146
D.2	Raw data of the temp. profile measured from left to right.	146
D.3	Raw data of the temp. profile measured inside the tube.	147
D.4	Raw data of the temp. profile measured outside the tube.	147
F.1	Temp. profiles used to simulate out-diffusion from the Cu sample.	149
F.2	Temp. profiles used to simulate out-diffusion from the Al sample.	150
G.1	Out-diffused radionuclide inventories for IR7 objects.	151

List of Abbreviations

- ALARA As Low As Reasonably Achievable. 7
- CAD Computer-Aided Design. 21
- CERN European Organization for Nuclear Research. 5
- CPU Central Processing Unit. 39
- CSG Constructive Solid Geometry. 21
- DNN Distance Nearest Neighbour. 106
- FCC Face Centered Cubic. 64
- FIRIA Fire Induced Radiological Integrated Assessment. 8
- FLUKA FLUktuierende KAskade. 21
- FRS Fraction Reaching Surface. 101
- GDP Global Desorption Probability. 101
- HEPA High-Efficiency Particulate Air. 69
- HSE Occupational Health & Safety and Environmental Protection Unit. 8
- ICRP International Commission on Radiological Protection. 7
- IR7 Interaction Region around point 7 in the LHC ring. 113
- LHC Large Hadron Collider. 8
- MC Monte Carlo. 3
- MDA Minimum Detectable Activity. 72
- ODF Out Diffusion Fraction. 38
- OD Outside Diameter. 68
- ORaP Ordonnance sur la radioprotection. 72
- PC Personal Computer. 49
- PDF Probability Density Function. 23

- ROI** Region Of Interest. [26](#)
- RP** Radiation Protection. [6](#)
- SI** International System of Units. [2](#)
- SOLIDUSS** SOLID-state diffUSion Software. [26](#)
- SPS** Super Proton Synchrotron. [72](#)
- SSP** Solid-State Physics. [67](#)
- TDC2** Tunnel, Divider (splitter) Cave 2. [73](#)
- XRF** X-ray fluorescence. [74](#)

List of Terms

- activation** Artificial induction of radioactivity. [2](#)
- ActiWiz** Software that facilitates the optimization of the chemical composition of materials used in the accelerator equipment at CERN from a radiation protection standpoint. [111](#)
- ActiWiz Creator** Software extending ActiWiz capabilities. [112](#)
- adsorption** Adhesion of atoms to a surface. [51](#)
- allotropy** Property of some chemical elements to exist in more than one structural form in the same physical state (*e.g.* carbon: graphite and diamond). [17](#)
- beam collimator** Device used to intercept certain particles of a beam in order to improve it in some aspect. [112](#)
- Brownian particle** Particle moving according to Brownian motion. [57](#)
- chemisorbed atoms** Atoms attached to a surface by chemical bonds. [52](#)
- continuous limit** Approximation of a discrete process by a continuous one carried out under adequate limit conditions. [15](#)
- decay constant** Proportionality constant between the number of unstable nuclei of a given species and the rate at which it decreases due to radioactive decay. [1](#)
- desorption** Release of a substance from a surface. [51](#)
- desorption activation energy** Energy required for an atom to desorb. [52](#)
- diffusion** Movement of anything, in particular radionuclides, from higher concentration regions to lower concentration ones. [11](#)
- diffusion activation energy** One of the parameters that characterise the temperature dependence of the diffusion coefficient. It is related to the energy required by an atom species placed in a solid to successfully jump to a different position on the lattice. [16](#)
- diffusion activation parameters** Frequency factor and diffusion activation energy. [17](#)

- diffusion coefficient** Proportionality constant of the diffusion equation. It is a measure of how quickly a given species diffuses in the medium that contains it. [14](#)
- diffusion equation** Fick's second law. [14](#)
- diffusion input file** Text file containing all the information necessary to simulate diffusion according to the user preferences (e.g. radionuclide of interest, host material, activation parameters, diffusion times, temperature maps, concentration mesh boundaries). [27](#)
- Fick's laws** Laws describing diffusion. Fick's first law relates the diffusion particle flux to the particle concentration gradient. Fick's second law relates the particle concentration evolution to its gradient divergence. [14](#)
- frequency factor** One of the parameters that characterise the temperature dependence of the diffusion coefficient. It is related to how the atoms vibrate in the solid lattice. [16](#)
- furnace** Device used to heat materials to very high temperatures. [67](#)
- half-life** Period of time required for half of the radionuclides in a given sample to decay. [2](#)
- ionising radiation** Particles and electromagnetic waves sufficiently energetic to ionise atoms or molecules. [2](#)
- migration energy** Energy required for an atom to overcome the potential well that holds it in position in the solid lattice. [13](#)
- Monte Carlo methods** Numerical techniques based on the use of random numbers to solve mathematical problems. [3](#)
- out-diffusion** Release of anything, in particular radionuclides, after diffusion to the surface of the object containing it. [9](#)
- perfect path resolution** A simulation is said to be performed with perfect path resolution if the simulated spatial steps are of the size of the real atomic steps. [39](#)
- physisorbed atoms** Atoms bounded to the surface only by Van der Waals forces. [52](#)
- proton losses** Protons leaving the ideal trajectory of the beam and colliding with the surrounding material. [113](#)
- radioactive activity** Rate at which radioactive decay takes place. [2](#)
- radioactive decay** Natural process that unstable atomic nuclei undergo releasing energy and gaining stability. It results in the ejection of particles carrying some of the released energy and often also in the transmutation of the nucleus. [1](#)
- random walks** Stochastic process describing the path followed by an object that moves randomly in a given space. [15](#)

sojourn time Expected amount of time an atom will spend on a surface before desorbing. [52](#)

source term inventory of radionuclides —species and quantities— that is released as a consequence of an accident. [9](#)

sublimation enthalpy Heat required to convert one mole of solid into gas. [53](#)

tracer diffusion experiment Experiments that benefit from the radioactive decay of isotopes to study diffusion, typically to obtain the diffusion coefficient dependence of a given chemical element in certain material. [88](#)

warm quadrupole Non-superconducting quadrupole operating at room temperature. [112](#)

Wiener process Real valued continuous-time stochastic process with normally distributed and independent increments. Also called Brownian motion. [23](#)

CORRIGENDUM

EVALUATION AND CRITICALITY ASSESSMENT OF RADIOLOGICAL SOURCE TERMS TO BE USED FOR FIRE RISK STUDIES AT ACCELERATOR FACILITIES

Thesis by
Francisco Ogallar Ruiz

UNIVERSIDAD DE GRANADA
Granada, Spain

Corrigendum applicable to document with ISBN 78-84-1117-231-8 published by the University of Granada in <https://digibug.ugr.es/handle/10481/72879>.

Most of the corrections are related to the misuse of term *gradient* or the use of both 1σ and 2σ uncertainties. Since it could lead to confusion, corrections are introduced to consistently use 1σ uncertainties.

Page	Reads	Should read
viii	geometries, temperature gradients and	geometries, temperature maps and
ix	from Cu of 1.6 ± 11 % after 5 h	from Cu of 1.5 ± 5.5 % after 5 h
ix	less than 12.6 % with 1σ certainty	less than 7.0 % with 1σ certainty
ix	obtained was 14.6 ± 7.3 % after 2 h	obtained was 14.6 ± 3.3 % after 2 h
ix	and up to 40.4 ± 7.0 % after	and up to 40.4 ± 2.5 % after
x	of 10 TBq , then to say that few TBq	of 10 GBq then to say that few GBq
xiv	$C(\vec{r}, t)/t = D\nabla^2 C(\vec{r}, t)$	$\partial C(\vec{r}, t)/\partial t = D\nabla^2 C(\vec{r}, t)$
xv	así como gradientes de temperatura	así como mapas de temperatura
xvi	en Cu de 1.6 ± 11 % tras 5 h	en Cu de 1.5 ± 5.5 % tras 5 h
xvi	menos del 12.6 % con 1σ de certeza	menos del 7.0 % con 1σ de certeza
xvi	obtenida fue 14.6 ± 7.3 %	obtenida fue 14.6 ± 3.3 %
xvi	subió hasta 40.4 ± 7.0 % después	subió hasta 40.4 ± 2.5 % después
xvii	de 10 TBq , si obtenemos que unos pocos TBq	de 10 GBq , si obtenemos que unos pocos GBq
7	specified on its Recommendation 60	specified on its Recommendation 103
34	A temperature gradient inside	The temperature map inside
34	In the background of Fig. 3.5 the temperature gradient	In Fig. 3.5 the temperature map
35	The temperature gradient along	The temperature map along
35	The temperature gradient is similar	The temperature map is similar
36	Upper right: temperature gradient	Upper right: temperature map
42	temperature gradients and non-uniform	temperature maps and non-uniform
46	Different temperature gradients	Different temperature distributions
46	a longitudinal gradient	a longitudinal map
46	The temperature gradient in the	The temperature map in the

Page	Reads	Should read
46	independent of the temperature gradient	independent of the temperature distribution
77	The temperature gradient inside	The temperature map inside
72	0.0468 21.48 0.0444	0.0468 10.74 0.0444
72	0.647 7.79 0.105	0.647 3.90 0.105
73	17.8 5.48 0.135	17.8 2.74 0.135
73	0.138 27.49 0.211	0.138 13.75 0.211
77	on the temperature gradient	on the temperature profile
77	the temperature gradient inside	the temperature profile inside
77	compute the temperature gradient	compute the temperature profile
79	evolution of the temperature gradient	evolution of the temperature distribution
79	allow for the gradient's stabilization	allow for the profile's stabilization
80	temperature gradient at which	temperature profile at which
81	0.0468 21.48 0.0444	0.0468 10.74 0.0444
81	0.647 7.79 0.105	0.647 3.90 0.105
81	0.0491 25.26 0.0566	0.0491 12.63 0.0566
81	0.615 8.14 0.117	0.615 4.07 0.117
81	0.0323 31.68 0.0451	0.0323 15.84 0.0451
81	0.637 7.92 0.091	0.637 3.96 0.091
81	⁵⁷ Co -4.9 34.1	⁵⁷ Co -4.9 17.4
81	⁶⁰ Co 5.0 11.0	⁶⁰ Co 4.9 5.4
81	⁵⁷ Co 31.0 31.4	⁵⁷ Co 31.0 13.2
81	⁶⁰ Co 1.6 11.0	⁶⁰ Co 1.5 5.5
81	an ODF of 1.6 ± 11.0 % after	an ODF of 1.5 ± 5.5 % after
81	less than 12.6 % with 1σ certainty	less than 7.0 % with 1σ certainty
83	17.8 5.48 0.135	17.8 2.74 0.135
83	0.138 27.49 0.211	0.138 13.75 0.211
83	15.2 5.52 0.121	15.2 2.76 0.121
83	0.133 28.45 0.112	0.133 14.23 0.112
83	13.8 5.96 0.0110	13.8 3.20 0.0110
83	0.125 48.95 0.0928	0.125 24.48 0.0928
83	10.6 6.39 0.0158	10.6 3.20 0.0158
83	0.106 36.02 0.0260	0.106 18.01 0.0260
83	²² Na 14.6 7.3	²² Na 14.6 3.3
83	⁵⁴ Mn 3.6 38.8	⁵⁴ Mn 3.6 19.1
83	²² Na 22.5 7.3	²² Na 22.5 3.1
83	²² Na 40.4 7.0	²² Na 40.4 2.5
83	⁵⁴ Mn 23.2 39.5	⁵⁴ Mn 23.2 17.4
83	0.954 30.37 0.155	0.954 15.19 0.155
83	0.881 13.25 0.128	0.881 6.63 0.128
83	0.635 43.26 0.159	0.635 21.63 0.159
84	in the range of [7.3,21.9] %	in the range of [11.3,17.9] %
84	and up to [33.4,47.4] %	and up to [37.9,42.9] %
98	5.0 ± 11.0	4.9 ± 5.4
98	1.6 ± 11.0	1.5 ± 5.5
98	14.6 ± 7.3	14.6 ± 3.3
98	22.5 ± 7.3	22.5 ± 3.1
98	40.4 ± 7.0	40.4 ± 2.5